A CONTRIBUTION TO THE THEORY OF HIGH FREQUENCY ELASTIC WAVES, WITH APPLICATIONS TO THE SHADOW BOUNDARY OF THE EARTH'S CORE

Thesis by

Paul Granston Richards

In Partial Fulfillment of the Requirements

For the Degree of

Doctor of Philosophy

California Institute of Technology

Pasadena, California

1970

(Submitted January 29, 1970)

ACKNOWLEDGMENTS

The author appreciates the advice given by Prof. C. B. Archambeau throughout the development of this study. Many useful discussions were held with past and present staff members of the Seismological Laboratory at the California Institute of Technology, and in particular with Prof. J. N. Brune (now at the University of California at San Diego).

Prof. T. L. Teng of the University of Southern California worked with the author on a preliminary numerical study of the solution presented in Chapter 2, section 2, and its geophysical consequences. The author was fortunate in being able to spend four weeks during 1969 at Princeton, where he learned of the recent work done by Prof. R. A. Phinney of Princeton University and Mr. C. H. Chapman (then visiting from the University of Cambridge): their contributions to the present study are acknowledged in the text below.

Mr. David P. Hill has given the author valuable assistance, particularly on computational problems.

Mrs. Barbara Sloan typed the manuscript, and Mr. Laszlo Lenches drafted the figures.

This research was supported by the Air Force Office of Scientific Research, Office of Aerospace Research, United States Air Force, under AFOSR contract (F44620-69-C-0067).

ABSTRACT

The diffraction of P and S waves by various obstacles is studied theoretically, in order to evaluate frequency dependent corrections to ray theory for elastic waves which travel nearly along the Earth's core shadow boundary.

Most of the properties of this scattering process are conveniently illustrated by a simple Earth model, which gives rise to a problem in plane strain. This model is an infinite homogeneous elastic solid in which a steady state plane body wave (of the type P, SV, or SH) is incident on a circular cylindrical cavity. A Poisson summation is used for the scattered elastic potentials, and contributions from waves diffracted at least once around the cylinder are neglected. Simple approximation formulae are developed to examine the behavior of P, SV, and SH waves on and near their geometrical shadow boundary behind the fluid. Computed numerical results are believed to be valid for frequencies above 0.03 Hz.

The solution method, which may be regarded as a corrected Fresnel theory, is taken through four successive stages of generalization to study increasingly realistic Earth models: (i) diffraction of cylindrical waves from a line source. For this problem our solution is in excellent agreement with the results of

an ultrasonic model experiment conducted by Teng and Wu (1968). (ii) Diffraction by a fluid cylinder of cylindrical waves from a line source. (iii) Diffraction by a spherical fluid of spherical waves from a point source. Here we find good agreement between numerical results from our approximate method, and computation of the exact Poisson line integral.

The final stage of generalization, to study (iv) diffraction by a spherical fluid/solid discontinuity in a realistic radially heterogeneous Earth, is obtained by methods similar to (iii), but after an extensive revision of Hook's (1961) discussion of elastic potentials in general media. In our approach, we recognize that the designation of P and S displacements is somewhat arbitrary in heterogeneous elastic media, but becomes precise in the high frequency limit of ray theory (in which P and two S components are decoupled). These facts are used for radially heterogeneous isotropic Earth models to establish three potentials (P,S,T) with the properties (a) that $T(\underset{\sim}{r},t)$ is decoupled from P and S, and is a potential for SH motion, (b) the coupling of P and SV waves is reflected in a system of coupled scalar equations for $P(\underset{\sim}{r},t)$ and $S(\underset{\sim}{r},t)$, and (c) in the high frequency limit we have $P(\underset{\sim}{r},t)$ and $S(\underset{\sim}{r},t)$ satisfying canonical uncoupled wave equations with the respective velocities $\left(\frac{\lambda+2\mu}{\rho}\right)^{\frac{1}{2}}$, $\left(\frac{\mu}{\rho}\right)^{\frac{1}{2}}$.

Many possibilities are suggested by the coupled equations for $P(\underset{\sim}{r},t)$ and $S(\underset{\sim}{r},t)$, apart from their use in the solution of (iv) above. They lead to a statement of conditions on the Earth model under which P and SV waves can propagate independently (at any frequency). We also use them to obtain approximate reflection coefficients for upper mantle transition regions which generate observed precursors to the phase PKPPKP, finding that the extent of velocity gradient anomaly in such regions must be less than about 4 km, in order to observe short period (1 sec) reflections.

Our numerical study of core diffraction provides an explanation for the observed polarization towards SH of diffracted S waves, and also shows that there is a slight dispersion effect on $\frac{dT}{d\Delta}$ data, obtained for P in the range beyond 90°, which can and must be allowed for in accurate Herglotz-Wiechert inversion studies. The numerical methods developed for discussion of (iv) are expected to have wider applications in seismological studies of the Earth's core, mantle, and crust.

TABLE OF CONTENTS

Chapter 1

General Introduction

Improvements during the 1960's in both the quality and quantity of seismic data have concurrently stimulated considerable interest in an improvement of the theory for elastic waves. The immediate goal of such new theory and data is a more accurate estimation of the longitudinal and shear wave velocities, and density, everywhere within the Earth.

The achievement of this goal is in turn crucial to that most basic aim of geological science, a full statement of the constitution and evolution of the Earth, because it appears that from data now available there is a potential for assigning the seismic parameters with great precision. This potential has indeed been realized already throughout most of the Earth, and we may cite for example the longitudinal velocity distributions of Gutenberg and Jeffreys which had been established by 1939, each distribution differing between depths of 900 and 2800 km by less than 1% from the recent study of Hales, Cleary and Roberts (1968). However, the importance of further data analysis lies in the fact that diagnostic clues to composition are principally contained in regions of high velocity gradient, or of velocity contrast, and such regions are just those for which the classical interpretive theories of seismology are least reliable. Perhaps the major example of this difficulty is the wide class of upper mantle models which fit experimental

travel time data (see Gerver and Markushevich, 1966, for a theoretical discussion), and it is necessary to use other phenomena such as surface wave dispersion (see Brune and Dorman, 1963) or the amplitude of body waves (see Julian and Anderson, 1968) to discriminate further between velocity models.

This study is directed towards improvements of classical ray theory, and, while several new and quite general results are presented for homogeneous and inhomogeneous elastic media, we emphasize the particular problems of analyzing core-diffracted body waves near the shadow boundary.

The geophysical community has seen a large number of publications reporting theoretical and observed properties of core diffraction (for a review, see our Introduction to Chapter 2 below), and there are several reasons why the core-mantle boundary remains the subject of widespread current research. In summary we may mention here that theoretical departures from ray methods are suggested by Johnson (1969) for rays which nearly graze the boundary, so standard methods for inverting seismic data are suspect. Yet the determination of present core-mantle boundary parameters is important both to our knowledge of the present density distribution throughout the Earth, and to the historical study of core differentiation. A large amount of relevant seismic data is available, partly because arrivals in the distance range 85°-115° cover a disproportionately large surface area of the Earth.

Alexander and Phinney (1966) have pointed out that comparison of arrivals in the core shadow which are along the same great circle path can be used to study lateral heterogeneities at the bottom of the mantle. A final and basic reason for our examination of the core-mantle boundary is that it appears to be a simple example within the Earth of a region of varying velocity, bounded by a velocity discontinuity. This combination is possibly present in several other regions of the Earth (see Archambeau, Flinn and Lambert, 1969), and also in planetary atmospheres which have been subjected to occultation experiments, and so our new theoretical and numerical methods may be expected to find applications considerably wider than the present study. Our results are summarized below in this Introduction, but first we briefly survey the standard wave propagation theories now used in seismology.

Ray theory itself (see Bullen's 1963 text for a summary, and applications), with its underlying assumption that P, SV, and SH waves separately obey the laws of geometrical optics, is an approximation which can provide a basic guide to more exact methods. This must be true, because the bi-characteristics of the general equations for elastic displacement are identifiable precisely as rays (see Section (3.2) below). Before developing new methods, we should thus be aware of two types of problems for which ray theory is essentially exact:

(i) It is exact for problems of plane waves, incident on plane boundaries, in homogeneous media. (Although there are

some exceptional problems concerned with grazing and critical incidence. See Goodier and Bishop, 1952, and Hudson, 1962.) The case of a curved wavefront can be expressed as an integral over plane waves, and the evaluation of such integrals has led to a vast catalogue of solved problems, for different source-receiver-boundary geometries (for an extensive review, see Miklowitz, 1966).

(ii) Robinson (1957) and Vlaar (1968) have shown for heterogeneous media that a ray theory, based on the concept of a wavefront as the carrier of a discontinuity in particle velocity, can give exact results for the propagating wavefront itself. Discontinuities in P, SV, and SH are shown to propagate independently - but behind the wavefront, these displacement fields are, of course, coupled in ways which ray theory cannot exactly interpret.

It is often claimed that ray theory is accurate for a medium in which the changes in such physical properties as velocity, and velocity gradient, are small over a wavelength (see Officer, 1958, and Archambeau, Flinn and Lambert, 1969). While such criteria can be useful in some particular applications, they must be insufficient in general, since the total path length within the heterogeneity is not taken into account - if this path length is sufficiently long, we intuitively expect that ray theory must become arbitrarily bad. But note from (ii) above that we also should expect ray theory to be arbitrarily good for a spatially fixed source and receiver, and inhomogeneity (however bad, provided

the elementary equation for displacement is valid) if the source frequency is sufficiently high. Further breakdown of ray theory occurs in the neighborhood of caustics (i.e. the envelope of a system of rays), and of the geometrical boundaries of shadows cast by discontinuities within the elastic media.

It is clear then that the approximate solutions of ray theory in seismological applications need checking against exact solutions, wherever this is possible, in order to assess the accuracy of the former method. To this end, we give in Chapter 2 below the exact solution for elastic displacement in simple Earth models, near the shadow boundary due to the core-mantle discontinuity, and compare it with ray theory and other approximations. In this case we can show by example how the assumption of uncorrected ray theory may consistently bias the conclusions of inversion for mantle velocities just above the core.

The device of approximating the Earth by welded layers of homogeneous plates (or concentric homogeneous shells) has led to much successful work. Methods initiated by Thomson (1950), Haskell (1953, 1960, 1962), and Knopoff (1964) are particularly useful in studies of surface wave dispersion, and of course this type of model is particularly suited to the geophysical problems of inversion.

But there are some strong objections to modelling the Earth by homogeneous plates.

One type of objection is that these models have spurious

properties not common in general media. Thus, a calculation of the travel times in layered models often reveals small triplications induced by the layering - an inconvenience which usually can be avoided by using, for example, a Mohorovičić law of inhomogeneity (i.e. velocity proportional to an irrational power of radius). A more interesting, but still somewhat spurious, property leads to the fascinating problem of headwaves; the travel time for a head-wave arrival indicates a travel path of critical incidence at one of the boundaries, together with grazing boundary ray transmission in the faster medium, and this special property is the basis of special methods for the evaluation of headwave displacement. Typically, these are the branch line discussions of, for example, Berry and West (1966), or the less well-known operational methods of Jeffreys (1926), or studies of wavefront curvature by Yanovskaya (1968). But even a small velocity gradient destroys the simple property of critical incidence - grazing transmission; the theoretical approach to "headwaves" (in so far as this energy may be isolated) is then either a diffraction study of scattering poles (if velocity decreases with depth: see Hill, 1970) or a multi-ray study of saddle points and scattering poles (if the velocity increases with depth: see Červený, 1966, Chekin, 1965, and also Chapman, 1969, for the related problem of SKK...KS within a simple Earth model). It appears that Runge's Theorem (Hille, 1962) provides a theoretical link between these different methods for

positive and negative gradients (as the gradient becomes smaller), and the branch line method in the limiting case of two homogeneous media.

The second type of objection is part practical, part aesthetic. We have considerable evidence (e.g. Johnson, 1967) for regions of high velocity gradient within the upper mantle, but the number of homogeneous layers needed to model such a region accurately for body waves is so large that reflection data (Adams, 1968, and Whitcomb and Anderson, 1970) cannot yet be related accurately to the velocity gradient (although Teng and Tung (1969) have recently reported some success). And so far as we know, the Earth is not composed of homogeneous layers, and the coupling between P and SV is not accomplished by discontinuous boundaries; it is accomplished intrinsically in the equations of motion.

It seems that the only method which both accepts this last fact, and calculates its effect, is that initiated by Epstein (1930), which for certain velocity gradients in acoustic media can furnish an exact solution for the reflection and transmission coefficients. This method, which transforms the equations of motion into a form satisfied by hypergeometric functions, and then uses the connection formulae between different pairs of solutions, is available for a theoretical study of SH waves. And a conclusion of our Chapter 3 below is that the same method may possibly be used, with an approximate equation for P waves, to study longitudinal-longitudinal reflection

coefficients for the precursors to PKPPKP.

The methods of Phinney and Alexander (1966) and Phinney and Cathles (1969) have guided several sections of our Chapter 2 below. Their procedure is to represent the displacement potentials, for elastic waves in a simple Earth model, in a standard way as complex line integrals, and to evaluate the integrals numerically. Such an approach has been slow in finding seismological applications, since a similar break-through was achieved in 1946, in a study by Fock of electromagnetic waves - and see also Wait and Conda (1959). Recent work of Chapman (1969) has further extended the method in seismology by incorporating a scheme for direct numerical integration of the equations of motion through the turning point at the bottom of a ray path.

The study below is presented in two chapters, which are almost independent. (Just one conclusion of Chapter 3 is used in Chapter 2.)

In Chapter 2 we solve a simple shadow boundary problem in elastic plane strain. In several stages we generalize the solution method to investigate the shadow boundary set up by a point source in a simple Earth model composed of separately homogeneous mantle and core. Exact displacements are calculated (by Phinney's method) for P, SV, and SH sources, and are compared with the approximations of ray theory in the lit region, and a corrected Fresnel theory near the geometrical shadow boundary (see Rubinow and Keller, 1961).

We find that the latter approximation (which is found to be quite accurate in the simple Earth models) can successfully be generalized to examine more general Earth models (with radial heterogeneity), giving the combination P + PcP from distances where they begin to interact, out to (and including) the shadow boundary. And a numerical method is given for evaluation of diffracted arrivals in the shadow, back to (and including) the shadow boundary. Both these methods are quite simple to use in realistic Earth models; the corrected Fresnel method is expressed as a factor multiplying the ray approximation for the direct P wave field, and successfully matches the numerical shadow region method on the shadow boundary. Several implications of our results are described, and include (a) showing that the grazing reflection coefficient for elementary waves at a spherical discontinuity is, for our geophysical parameters, substantially different from the corresponding coefficient with a plane discontinuity, (b) explanation of the observed polarizing effect, on S waves, of core diffraction, and (c) an evaluation of Johnson's (1969) caveat, that velocities obtained at the bottom of the mantle, by standard Herglotz-Wiechert inversion of observed $\frac{dT}{d\Delta}$ values, are too low.

In Chapter 3 we attack the problem of finding potentials for elastic displacement in spherically symmetric isotropic media. The study of wave propagation has led physicists and applied

mathematicians to take advantage of many similarities to be found between the different problems. The similarities arise because equations of wave propagation (be they for a magnetic intensity, for a stress tensor, or for particle scattering) may often be transformed to and from certain "canonical forms" of wave equation. The widely studied properties of canonical forms may then be simply related to our particular problem, provided we can establish the necessary transformation. Hook (1961) and Singh and Ben-Menahem (1969) have studied the equation for elastic deformation, but our approach differs from these authors in using a slightly simpler potential representation by which (we prove) all possible displacement solutions can be studied. We are able to see, from our final choice of potentials, the theoretical reasons why P and SV body waves in the Earth are observed to propagate almost independently, and the generality of our final coupling equations permits a survey of many possible applications. For example, we show the relevance to seismology of some canonical wave solutions in certain standard kinds of inhomogeneity, and are able to see that all experimentally identifiable reflection horizons in the Earth's mantle must be highly localized.

The new work presented in this dissertation includes our study of amplitudes near a shadow boundary in homogeneous elastic media, and the methods of generalization needed to study radially

heterogeneous Earth models, their core shadow boundary and shadow region. The generalizations are examined numerically for a realistic Earth model. We also place Hook's method of potentials on a firm and simpler foundation.

The conclusions of our Chapters 2 and 3 may briefly be summarized by remarking that ray theory, a basic pillar for many years of seismological research, has now guided us to more accurate practical approximations, which can improve our interpretation of existing data.

Chapter 2

Diffracted P, SV, and SH Waves, and Their Shadow Boundary Amplitudes

2.1 Introduction

Since the installation of the World-Wide Standardized Seismograph Network, rapid accumulation of seismic data on diffracted body-wave amplitudes has given us hope of better determination of the radius and nature of the Earth's core-mantle boundary. There has been, however, a lack of appropriate diffraction theory for the interpretation of these recorded amplitudes, particularly for observations made near the shadow boundary. This chapter develops a solution for the displacement of body waves which closely graze the core, and the theory is examined in relation to some observed data. It is found that the phenomenon of SH polarization in diffracted S waves, reported by Cleary et al (1968), is qualitatively explained. It is also found that the departure from ray theory in the shadow boundary region may be very simply allowed for when using Herglotz-Wiechert inversion to set up models of the lower mantle (see Johnson (1969): a frequency dependent correction is made to the observed $\frac{dT}{d\Delta}$, to allow for the interference effect of PcP).

Displacement solutions that are valid only in limited regions have previously been obtained for some problems with simple configurations; for example, a spherical cavity in a homogeneous elastic medium (Nagase, 1956), a fluid sphere in a homogeneous

elastic solid (Scholte, 1956; Duwalo and Jacobs, 1969; Knopoff and Gilbert, 1961), and scattering from a rigid cylinder or sphere (Gilbert and Knopoff, 1959). Some of these solutions are for impulsive elastic waves, and so are unsuited to the interpretation of spectra. All of these solutions are valid only within the "illuminated" region (that is, the region accessible to direct body waves from the source), or within the shadow boundary, and they fail for regions near the geometrical shadow boundary. The failure of these theories in the critical region of core-grazing rays has hindered meaningful discussion of the observed diffraction data - for presumably it is just these rays which provide the best information we have on core-mantle structure.

Recent progress in acoustics and electromagnetics has provided solutions valid in the neighborhood of the geometrical shadow boundary, for scatterers of various simple geometrical shapes (Rice, 1954; Rubinow and Wu, 1956; Rubinow and Keller, 1951; Nussenzveig, 1965). Although these results are not immediately applicable to the study of elastic waves, the gross structure of the solutions and the general conclusions are expected to be common to all wave-scattering problems: typically, their findings are

(1) a broadening of the transition zone (that is, the region between illumination and shadow) with lower frequency,

(2) a dependence of the extent and position of the transition zone on the boundary condition at the surface of the scatterer, and

(3) strong similarity among solutions for spherical, cylindrical, and paraboloidal scatterers with the same boundary condition.

The theory of this chapter is an extension to seismology of the solution techniques developed in acoustics and electromagnetics, and we examine the amplitude behavior of P and S-waves near the geometrical shadow boundary. This extension involves the study of more general boundary conditions that couple two potentials and their derivatives, as opposed to the Dirichlet or Neumann conditions considered in acoustic and electromagnetic problems. A substantial extension to the theory of radially heterogenous media is also given.

We are fortunate in having two independent checks on the theory of this chapter. An ultrasonic seismic model experiment (Teng and Wu, 1968) has been conducted, which measured transition amplitudes of P and SV behind a circular hole cut in a thin plate. Also, a method of Phinney and Alexander (1966), and further described in Phinney and Cathles (1969), has given transition amplitudes of a P-wave potential due to a fluid spherical core. The method of Phinney and his co-workers, which involves extensive numerical integration, is described below. The results of both the above projects are in accord with our theory.

Plan of Theoretical Development

The simplest geophysically relevant problem of elastic wave diffraction is a problem in plane strain: a steady state plane wave of displacement is incident upon a circular cylindrical cavity, and it is required to evaluate displacements near the geometrical shadow boundary. This basic problem is solved in section (2.2). The generalization to diffraction of waves from a line source, and a comparison of theory with the results of Teng and Wu (1968), is given in (2.3). In (2.4), we generalize to the case of a fluid cylindrical scatterer, and in (2.5) we solve the parallel problem of a point source, with waves scattered by a spherical fluid, and compare the results of Phinney and Cathles (1969). The generalization to a radially heterogeneous Earth is made in section (2.6). In (2.7) we apply our new results to observed phenomena.

2.2 Theoretical Development of a Simple Model of Diffraction

Statement of Elasticity Problem

A steady-state plane wave of unit displacement is incident from the left on a circular cylindrical cavity of radius a (see Figure 1(a)). This is a problem of plane strain, and we wish to evaluate the scattered displacement field.

We use polar coordinates (r,θ,z) centered on the cylinder axis, and shall consider the cases of

1. Diffraction of P-waves with a plane P-wave incidence:

$$\underset{\sim}{u}_i = (\cos\theta,-\sin\theta,0)\ e^{i(hr\cos\theta - \omega t)}$$

2. Diffraction of SV-waves with a plane SV-wave incidence:

$$\underset{\sim}{u}_i = (\sin\theta,\ \cos\theta,0)\ e^{i(kr\cos\theta - \omega t)}$$

3. Diffraction of SH-waves with a plane SH-wave incidence:

$$\underset{\sim}{u}_i = (0,0,1)\ \ e^{i(kr\cos\theta-\omega t)}$$

For the P-wave due to SV-wave incidence, and the SV-wave due to P-wave incidence, formulae are given in Appendix I.

In the first two cases, our problem can be reduced to a two-dimensional one involving two scalar potentials ϕ and ψ, which are related to the displacement field $\underset{\sim}{u}$ by

$$\underset{\sim}{u} = \left(\frac{\partial\phi}{\partial r} + \frac{1}{r}\frac{\partial\psi}{\partial\theta}\ ,\ \frac{1}{r}\frac{\partial\phi}{\partial\theta} - \frac{\partial\psi}{\partial r}\ \ ,\ 0\right) \qquad (2.2.1)$$

The total displacement $\underset{\sim}{u}$ is a solution under the conditions

(i) that $(\nabla^2 + h^2)\phi = (\nabla^2 + k^2)\psi = 0$, where (h,k) are the wave numbers for (P,S) waves,

(ii) that the scattered waves $\underset{\sim}{u}_s \equiv \underset{\sim}{u} - \underset{\sim}{u}_i$ are outgoing, and

(iii) that there is neither tangential nor normal stress on the boundary $r = a$.

Scattering of P

The incident wave clearly may be represented by

$$\phi_i = \frac{1}{ih} \, e^{i(hr\cos\theta - \omega t)}, \text{ and } \psi_i = 0.$$

The conditions (i) and (ii) allow us to write scattered potentials as

$$\phi_s = \frac{1}{ih} \sum_{n=-\infty}^{\infty} (i)^n \, A_n H_n^{(1)}(hr) \, e^{i(n\theta - \omega t)} ,$$

$$\psi_s = \frac{1}{ih} \sum_{n=-\infty}^{\infty} (i)^n \, B_n \, H_n^{(1)}(kr) \, e^{i(n\theta - \omega t)} \qquad (2.2.2).$$

We can evaluate A_n and B_n by using condition (iii), together with the relation

$$e^{i \, hr\cos\theta} = \sum_{n=-\infty}^{\infty} (i)^n \, J_n(hr) \, e^{in\theta}$$

This procedure is straightforward, but lengthy, and gives

$$A_n = -\frac{1}{2}\left[1 + \frac{\Omega_1 H_n^{(2)}(ha)}{\Omega_1 H_n^{(1)}(ha)}\right], \quad B_n = -\frac{1}{2}\left[\frac{\Omega_2 J_n(ha)}{\Omega_1 H_n^{(1)}(ha)}\right], \tag{2.2.3}$$

where for convenience we have defined operators

$$\Omega_1 H_n^{(\ell)}(ha) \equiv S^{(1)} P^{(\ell)} + Q^{(1)} R^{(\ell)}, \qquad \ell = 1,2$$

$$\Omega_2 J_n(ha) \equiv i\left[R^{(2)} P^{(1)} - R^{(1)} P^{(2)}\right]$$

where

$$\begin{aligned} P^{(\ell)} &\equiv 2ha\, H_n^{(\ell)'}(ha) + \left[k^2a^2 - 2n^2\right] H_n^{(\ell)}(ha) \\ Q^{(\ell)} &\equiv -2n\left(ka\, H_n^{(\ell)'}(ka) - H_n^{(\ell)}(ka)\right) \\ R^{(\ell)} &\equiv 2n\left(ha\, H_n^{(\ell)'}(ha) - H_n^{(\ell)}(ha)\right) \\ S^{(\ell)} &\equiv 2ka\, H_n^{(\ell)'}(ka) + \left[k^2a^2 - 2n^2\right] H_n^{(\ell)}(ka). \end{aligned} \tag{2.2.4}$$

Each of the A_n and B_n may now be evaluated, for specific values of ω, a, α and β: the unique solution for $\underset{\sim}{u}_s$ follows from equations (2.2.2) and (2.2.1).

Discussion of ϕ_s (i.e. P-P Scattering)

It is unfortunate that the series solutions (2.2.2) converge so slowly that they are of little direct use. It is clear from the form of (2.2.3) and (2.2.4) that, if there is convergence, it must be slow, for A_n is small in general only for $n >> ha$. For a simple model of the Earth's core-mantle boundary, we find for body waves with period 1 to 50 seconds that ha varies between 1600 and 30 (and ka between 3000 and 60).

However, if we wish to find ϕ_s for values of (r,θ) in the illuminated zone, and for an incident wave of frequency high enough for us to expect a reflection effect, we can make an estimate of the values of n which we expect physically to be most significant. These values are integers which most nearly satisfy the relation (see Figure 2)

$$n = - \frac{\omega \, r \sin i(r)}{\alpha} \qquad (2.2.5)$$

(The corresponding relation for a spherically symmetric body is $n + \frac{1}{2} = - \frac{\omega \, r \sin i}{\alpha}$; see Bremmer (1949), Ben-Menahem (1964).)

A simple way to obtain (2.2.5) is to use the factor $e^{(in\theta - \omega t)}$ in the n-th term of the series (2.2.2). This factor indicates that each term of the series represents a wave travelling around the cavity with phase velocity $v_n = \frac{\omega r}{n}$ in the direction of increasing θ.

The summation ϕ_s represents an interference effect of all these different phase velocities, and the reflected-ray phase velocity is (see Figure 2) $-\alpha/\sin i$ in the direction of increasing θ. The interference is thus constructive only when $v_n = \frac{\omega r}{n} \approx \frac{-\alpha}{\sin i}$, i.e. when (2.2.5) is nearly satisfied. For (r,θ) near the shadow boundary, we have $r \sin i \approx a$, so the significant terms are $n \approx -ha$. The quantity $\frac{r \sin i}{\alpha}$ in (2.2.5) is the familiar seismic ray parameter, and part of the above theory has a generalization to radially heterogeneous models (see section (2.6)).

We now proceed to an evaluation of ϕ_s for large values of ha, using the Poisson sum formula. Our development has been guided substantially by the methods of Rubinow and Keller (1961), who discuss a problem with only one potential and with a different boundary condition on r = a. A factor $\exp(-i\omega t)$ is understood in some of the expressions below.

If we define

$$A(r,\theta) \equiv \int_{-\infty}^{\infty} e^{i\nu\left(\theta + \frac{\pi}{2}\right)} \left[1 + \frac{\Omega_1 H_n^{(2)}(ha)}{\Omega_1 H_n^{(1)}(ha)} \right] H_\nu^{(1)}(hr)\, d\nu$$

and use the Poisson sum formula (Morse and Feshbach, 1953)

$$\sum_{n=-\infty}^{\infty} F(n) = \sum_{m=-\infty}^{\infty} \left(\int_{-\infty}^{\infty} F(\nu)\, e^{2i\nu m\pi}\, d\nu \right)$$

with

$$F(n) = \frac{1}{ih}\, e^{in\pi/2}\, A_n\, H_n^{(1)}(hr)\, e^{in\theta} \quad ,$$

we see that

$$\phi_s = -\frac{1}{2ih} \sum_{m=-\infty}^{\infty} A(r,2m\pi + \theta) \qquad (2.2.6).$$

In this exact formula for ϕ_s we wish to identify waves that travel around the cylinder and are then summed to give the scattered field. For example, we note that, for large ha and $m \geq 1$, $A(r,2m\pi + \theta)$ has a phase $ha(2m\pi + \theta)$ and hence represents a wave that has travelled m times around in the direction of increasing θ. To make further identification it is helpful to rearrange the terms in equation (2.2.6), to reveal also (1) which waves travel around in the direction of decreasing θ, (2) which wave just grazes the cavity for a field point near the upper shadow boundary, and (3) which wave is diffracted around the lower part of the cavity. We are guided towards the correct rearrangement by noting that physically we expect $\phi_s(r,\theta) = \phi_s(r,-\theta)$ and in particular that the upper and lower shadow boundaries are symmetrical.

Using the relations

$$\Omega_1 H_{-\nu}^{(1)}(ha) = e^{2\pi i\nu}\, \Omega_1 H_{\nu}^{(1)}(ha)$$

and

$$\Omega_1 H_{-\nu}^{(2)}(ha) = \Omega_1 H_{\nu}^{(2)}(ha) \quad ,$$

(2.2.6) becomes

$$\phi_s = -\frac{1}{2ih}\left[\left\{ \sum_{m=1}^{\infty} \left(A(r,2m\pi+\theta) + A(r,2m\pi-\theta)\right)\right\}\right.$$

$$+\left\{\int_0^{\infty} e^{i\nu\left(\theta+\frac{\pi}{2}\right)}\, H_{\nu}^{(1)}(hr)\,d\nu + \int_{-\infty}^{\infty} e^{i\left(\theta+\frac{\pi}{2}\right)}\, H_{\nu}^{(1)}(hr)\, \frac{\Omega_1 H_{\nu}^{(2)}(ha)}{\Omega_1 H_{\nu}^{(1)}(ha)}\, d\nu\right\}$$

$$\left.+\left\{\int_0^{\infty} e^{i\nu'\left(-\theta+\frac{\pi}{2}\right)}\, H_{\nu'}^{(1)}(hr)\,d\nu' + \int_{-\infty}^{\infty} e^{i\nu'\left(-\theta+\frac{\pi}{2}\right)}\, H_{\nu'}^{(1)}(hr)\, \frac{\Omega_1 H_{\nu'}^{(2)}(ha)}{\Omega_1 H_{\nu'}^{(1)}(ha)}\, d\nu'\right\}\right]$$

(2.2.7)

Evaluation of ϕ_s Near the Upper Shadow Boundary

The first infinite sum in (2.2.7) represents waves that, from their phase, we identify as having travelled m times ($m \geq 1$) completely around the cylinder. These waves attenuate with distance at a rate proportional to $(ha)^{\frac{1}{3}}$ and arrive much later, outside the time-window we are interested in, so we may ignore them. The integrals in the remaining two brackets { } represent waves which have not travelled completely around the cylinder.

From the interference argument mentioned above, we expect to get contributions for the integrals in (2.2.7) from those regions near $\nu' = -ha$ and (since in fact $\nu' = -\nu$) $\nu' = ha$. Near the upper boundary of the shadow, the second bracket { } is then seen to be negligible relative to the third. Just the opposite is true when we consider the lower boundary of the shadow (but with contributions still coming from $\nu = -ha$, $\nu' = +ha$). Our interpretation is thus that the second bracket describes the wave travelling via the bottom of the cylinder, and the third bracket that via the top. For our evaluation, the diffracted contribution via the bottom of the cylinder is negligible, and we may take just the third bracket { } in (2.2.7), writing it now as

$$\phi_s = \frac{-1}{2ih}\left\{\int_0^\infty e^{i\nu\left(-\theta+\frac{\pi}{2}\right)} H_\nu^{(1)}(hr)\,d\nu + \int_{-\infty}^{\infty} e^{i\nu\left(-\theta+\frac{\pi}{2}\right)} \frac{\Omega_1 H_\nu^{(2)}(ha)}{\Omega_1 H_\nu^{(1)}(ha)} H_\nu^{(1)}(hr)\,d\nu\right\}$$

for $(ha)^{\frac{1}{3}} >> 1$, near the upper shadow boundary.

Following Rubinow and Keller (1961), we use

$$\phi_s = -\frac{1}{2ih}\left[a_1(r,-\theta) + a_2(r,-\theta)\right] \qquad \text{where}$$

$$a_1(r,-\theta) \equiv \int_0^{ha} e^{i\nu\left(-\theta+\pi/2\right)} H_\nu^{(1)}(hr)\,d\nu$$

$$a_2(r,-\theta) \equiv \int_{-\infty}^{ha} e^{i\nu\left(-\theta+\pi/2\right)} \frac{\Omega_1 H_\nu^{(2)}(ha)}{\Omega_1 H_\nu^{(1)}(ha)} H_\nu^{(1)}(hr)\,d\nu$$

$$+ \int_{ha}^{\infty} e^{i\nu\left(-\theta+\pi/2\right)}\left[1 + \frac{\Omega_1 H_\nu^{(2)}(ha)}{\Omega_1 H_\nu^{(1)}(ha)}\right] H_\nu^{(1)}(hr)\,d\nu \quad .$$

To evaluate a_1, we may use the Debye formula for $H_\nu^{(1)}(hr)$ (since hr > ha and ha is large) to obtain

$$a_1(r,-\theta) \sim \sqrt{\frac{2}{\pi}} \cdot e^{-i\pi/4} \int_0^{ha} \frac{1}{(h^2r^2-\nu^2)^{\frac{1}{4}}} \exp i\left[(h^2r^2-\nu^2)^{\frac{1}{2}} + \nu \sin^{-1}\frac{\nu}{hr} - \nu\theta\right] d\nu$$

(2.2.8).

This integrand has just one stationary phase point, given by a value $\nu = \nu_s$ such that

$$\sin^{-1}\left(\frac{\nu_s}{hr}\right) = \theta \quad , \text{ i.e.} \quad \nu_s = hy.$$

For $P(r,\theta)$ near the upper shadow boundary (see Figure 1), this stationary phase point is near the upper limit of integration in (2.2.8). Making the definition

$$\xi = \frac{1}{\sqrt{2hx}} \left(\nu-\nu_s\right) \quad ,$$

and expanding the phase within (2.2.8) as powers of ξ, we find

$$a_1(r,-\theta) \sim e^{ihx} \cdot \frac{2}{\sqrt{\pi}} \cdot e^{-i\pi/4} \cdot \int_{-\left(\frac{h}{2x}\right)^{\frac{1}{2}} y}^{\left(\frac{h}{2x}\right)^{\frac{1}{2}} (a-y)} e^{i\xi^2} \, d\xi \, .$$

The upper limit is small near the shadow boundary, and the lower limit is large for high frequencies; so this Fresnel integral may be approximated by

$$a_1(r,-\theta) \sim e^{ihx}\left[1 + e^{-i\pi/4}\cdot\left(\frac{2h}{\pi x}\right)^{\frac{1}{2}}(a-y)\right] \qquad \text{if both}$$

$$\left(\frac{h}{2x}\right)^{\frac{1}{2}} y >> 1 \qquad \text{and} \qquad \left(\frac{h}{2x}\right)^{\frac{1}{2}} |\, a-y \,| << 1 \quad .$$

For regions in which the second condition is invalid, $a_1(r,-\theta)$ may be found from a table of Fresnel integrals.

To evaluate $a_2(r,-\theta)$, we may still use the Debye expressions for $H_\nu^{(1)}(hr)$, and find near $\nu = ha$ that

$$e^{i\nu(-\theta + \pi/2)}\, H_\nu^{(1)}(hr) \sim e^{i(hx - \pi/4)}\cdot\left(\frac{2}{\pi hx}\right)^{\frac{1}{2}} \quad .$$

But, for $H_\nu^{(\ell)'}(ha)$ and $H_\nu^{(\ell)}(ha)$ ($\ell = 1,2$), the simple Debye approximations are useless. Since argument and order are nearly equal, some form of Langer approximation is necessary (see "Higher Transcendental Functions" by staff of the Bateman Manuscript Project, 1953, Vol. II, p. 89), and we discuss this below in the section on numerical results.

Then

$$a_2(r,-\theta) \sim \left(\frac{2}{\pi hx}\right)^{\frac{1}{2}} e^{i\left(hx-\pi/4\right)} (ha)^{\frac{1}{3}} C_p(\omega) \qquad \text{where}$$

$$C_p(\omega) \equiv \frac{1}{(ha)^{\frac{1}{3}}}\left[\int_{-\infty}^{ha} \frac{\Omega_1 H_\nu^{(2)}(ha)}{\Omega_1 H_\nu^{(1)}(ha)} \cdot d\nu + \int_{ha}^{\infty} \left(1 + \frac{\Omega_1 H_\nu^{(2)}(ha)}{\Omega_1 H_\nu^{(1)}(ha)} \right) \cdot d\nu \right]$$

(2.2.9)

and $C_p(\omega)$ is evaluated below, numerically.

In summary: we have for $\phi = \phi_i + \phi_s$ that

$$\phi \sim \frac{e^{i(hx-\omega t)}}{ih}\left\{ \frac{1}{2} - \left(\frac{1}{2\pi hx} \right)^{\frac{1}{2}} e^{-i\pi/4}\left[h(a-y) + (ha)^{\frac{1}{3}} C_p(\omega) \right] \right\}$$

(2.2.10).

Scattering of SV

The incident wave may be represented by

$$\phi_i = 0 \quad , \qquad \psi_i = -\frac{1}{ik} e^{i(krcos\ \theta-\omega t)}$$

The conditions (i) and (ii) allow us to write

$$\phi_s = -\frac{1}{ik} \sum_{n=-\infty}^{\infty} (i)^n C_n H_n^{(1)}(hr) e^{i(n\theta-\omega t)} , \qquad (2.2.11)$$

$$\psi_s = -\frac{1}{ik} \sum_{n=-\infty}^{\infty} (i)^n D_n H_n^{(1)}(kr) e^{i(n\theta-\omega t)}$$

and condition (iii) then gives

$$C_n = -\frac{1}{2}\left[\frac{\Omega_4 J_n(ka)}{\Omega_3 H^{(1)}(ka)}\right], \quad D_n = -\frac{1}{2}\left[1 + \frac{\Omega_3 H_n^{(2)}(ka)}{\Omega_3 H_n^{(1)}(ka)}\right] \tag{2.2.12}$$

where we have defined the operators

$$\Omega_3 H_n^{(\ell)}(ka) \equiv S^{(\ell)}P^{(1)} + Q^{(\ell)}R^{(1)} \quad , \ell = 1,2$$

$$\Omega_4 J_n(ka) \equiv -i\left[S^{(2)}Q^{(1)} - S^{(1)}Q^{(2)}\right] \tag{2.2.13}$$

and $P^{(\ell)}$, $Q^{(\ell)}$, $R^{(\ell)}$, $S^{(\ell)}$ are defined in (2.2.4).

Discussion of ψ_s (i.e. SV-SV scattering)

We use a Poisson sum formula, just as before. Thus, defining

$$\mathcal{D}(r,\theta) \equiv \int_{-\infty}^{\infty} e^{i\nu(\theta+\pi/2)}\left[1 + \frac{\Omega_3 H_\nu^{(2)}(ka)}{\Omega_3 H_\nu^{(1)}(ka)}\right] H_\nu^{(1)}(kr)\, d\nu$$

we have

$$\psi_s = + \frac{1}{2ik} \sum_{m=-\infty}^{\infty} \mathcal{D}(r, 2m\pi+\theta).$$

We find that this sum may be rewritten and interpreted term by term just as we interpreted equation (2.2.7), so that for an evaluation near the upper boundary of the shadow we have

$$\psi_s = + \frac{1}{2ik} \left\{ \int_0^{\infty} e^{i\nu\left(-\theta+\pi/2\right)} H_\nu^{(1)}(kr)\, d\nu \right.$$

$$\left. + \int_{-\infty}^{\infty} e^{i\nu\left(-\theta+\pi/2\right)} \frac{\Omega_3 H_\nu^{(2)}(ka)}{\Omega_3 H_\nu^{(1)}(ka)} H_\nu^{(1)}(kr)\, d\nu \right\}$$

for $(ka)^{\frac{1}{3}} >> 1$. We expect the major contribution to come from near $\nu = ka$, and so we write

$$\psi_s = \frac{1}{2ik} \left[d_1(r,-\theta) + d_2(r,-\theta) \right]$$

where

$$d_1(r,-\theta) \equiv \int_0^{ka} e^{i\nu(-\theta+\pi/2)} H_\nu^{(1)}(kr)\, d\nu$$

$$d_2(r,-\theta) \equiv \int_{-\infty}^{ka} e^{i\nu(-\theta+\pi/2)} \frac{\Omega_3 H_\nu^{(2)}(ka)\, d\nu}{\Omega_3 H_\nu^{(1)}(ka)}$$

$$+ \int_{ka}^{\infty} e^{i\nu(-\theta+\pi/2)} \left[1 + \frac{\Omega_3 H_\nu^{(2)}(ka)}{\Omega_3 H_\nu^{(1)}(ka)} \right] H_\nu^{(1)}(kr)\, d\nu \,.$$

d_1 corresponds to a_1 above, and so

$$d_1(r,-\theta) \sim e^{ikx} \left[1 + e^{-i\pi/4} \left(\frac{2k}{\pi x} \right)^{\frac{1}{2}} (a-y) \right]$$

if both $\left(\frac{k}{2x} \right)^{\frac{1}{2}} y >> 1$ and $\left(\frac{k}{2x} \right)^{\frac{1}{2}} | a-y | << 1.$

To evaluate d_2 near the upper boundary, we may again use the Debye expansion

$$e^{i\nu(-\theta+\pi/2)}\ H_\nu^{(1)}(kr) \sim e^{i(kx-\pi/4)} \cdot \left(\frac{2}{\pi kx}\right)^{\frac{1}{2}} \quad \text{near } \nu = ka.$$

For $H_\nu^{(\ell)'}(ka)$ and $H_\nu^{(\ell)}(ka)$ $(\ell = 1,2)$, we shall use the Langer approximation. Then

$$d_2(r,-\theta) \sim \left(\frac{2}{\pi kx}\right)^{\frac{1}{2}} \cdot e^{i(kx-\pi/4)} \cdot \left(ka\right)^{\frac{1}{3}} C_{SV}(\omega)$$

where

$$C_{SV}(\omega) = \frac{1}{(ka)^{\frac{1}{3}}}\left[\int_{-\infty}^{ka} \frac{\Omega_3 H_\nu^{(2)}(ka)}{\Omega_3 H_\nu^{(1)}(ka)}\, d\nu + \int_{ka}^{\infty}\left(1 + \frac{\Omega_3 H_\nu^{(2)}(ka)}{\Omega_3 H_\nu^{(1)}(ka)}\right) d\nu\right]$$

(2.2.14)

The function $C_{SV}(\omega)$ is evaluated below, numerically.

In summary: we have for $\psi = \psi_i + \psi_s$ that

$$\psi \sim -\frac{e^{i(kx-\omega t)}}{ik}\left\{\frac{1}{2} - \left(\frac{1}{2\pi kx}\right)^{\frac{1}{2}} e^{-i\pi/4}\left[k(a-y) + (ka)^{\frac{1}{3}} C_{SV}(\omega)\right]\right\}$$

(2.2.15)

Scattering of SH

The incident wave has its displacement $\underset{\sim}{u}_i = (0,0,1)\ e^{i(kr\cos\theta-\omega t)}$ parallel to the axis of the cylinder. The z component of the displacement satisfies the scalar Helmholtz equation

$$\left(\nabla^2 + k^2\right) u_z = 0$$

and the stress-free boundary condition on the cylindrical boundary r = a,

$$\mu \frac{\partial}{\partial r}\ u_z = 0$$

This boundary condition has been studied by Rubinow and Keller (1961), and from their results we have

$$\underset{\sim}{u} = \underset{\sim}{u}_i + \underset{\sim}{u}_s$$

$$\approx \left(0,0, \frac{1}{2} - \left(\frac{1}{2\pi kx}\right)^{\frac{1}{2}}\ e^{-i\pi/4}\left[\ k(a-y) + \left(ka\right)^{\frac{1}{3}}\ C_{SH}\ \right]\right) e^{i(kx-\omega t)} \qquad (2.2.16)$$

where

$$C_{SH} = -\ 0.4321\ x\ \left(1 + \sqrt{3}\ i\right)$$

This asymptotic solution is valid for

$$\left(\frac{k}{2x}\right)^{\frac{1}{2}} y >> 1 \quad , \quad \left(\frac{k}{2x}\right)^{\frac{1}{2}} | a-y | << 1 \quad .$$

The Shift of Shadow Boundaries

Using Cartesian coordinates, we see from equations (2.2.1) and (2.2.10) that the total P-wave displacement field near the upper shadow boundary for P-P scattering is

$$\underset{\sim}{u} \sim \left(\frac{1}{2} - \frac{e^{-i\pi/4}}{(2\pi hx)^{1/2}} \left[h(a-y) + (ha)^{1/3} C_p(\omega) \right] , \frac{e^{-3i\pi/4}}{(2\pi hx)^{1/2}} , 0 \right) e^{i(hx-\omega t)}$$

From this expression, we see that on the geometrical boundary y = a we have

$$\underset{\sim}{u} \to \left(\frac{1}{2},0,0\right) e^{i(hx-\omega t)} = \frac{1}{2} \underset{\sim}{u}_i \quad \text{as} \quad \omega \to \infty$$

Therefore, following the method of several other authors [for example, Rubinow and Keller (1961), Nussenzveig (1965)], we make the practical definition that the shadow boundary for finite frequencies is the curve on which $|\underset{\sim}{u}| = \frac{1}{2}$. It is then a simple matter to show that,

if $\left(ha\right)^{1/3} >> 1$, the shadow boundary is $y = a + s_p$, where s_p is the "shadow boundary shift," and

$$s_p = \left[\text{Re } C_p(\omega) + \text{Im} C_p(\omega) \right] \left(ha\right)^{-2/3} a. \qquad (2.2.17)$$

Similarly, for SV-SV scattering, we have

$$\underset{\sim}{u} \sim \left(\frac{e^{i\pi/4}}{\left(2\pi kx\right)^{\frac{1}{2}}} , \frac{1}{2} - \frac{e^{-i\pi/4}}{\left(2\pi kx\right)^{\frac{1}{2}}} \left[k(a-y) + (ka)^{1/3} \; C_{SV}(\omega) \right] , 0 \right) e^{i(kx-\omega t)}$$

and $$s_{SV} = \left[\text{Re } C_{SV}(\omega) + \text{Im } C_{SV}(\omega) \right] \left(ka\right)^{-\frac{2}{3}} a. \qquad (2.2.18)$$

For SH-SH scattering $\underset{\sim}{u}$ is given by equation (2.2.16)

and $$s_{SH} = -1.1806 \left(ka\right)^{-\frac{2}{3}} a \qquad (2.2.19)$$

Numerical Method and Results

Method

We present here the evaluation of $C_p(\omega)$ and $C_{SV}(\omega)$ (see equations (2.2.9) and (2.2.14)), and of amplitudes near the shadow boundary.

The elastic medium was assumed to have a P-wave velocity

α of 13.6 km/sec, and an S-wave velocity β of 7.5 km/sec, and embedded in it a cylindrical cavity of radius a = 3480 km. These assumptions make the computational results also comparable to previously obtained model-experiment data (Teng and Wu, 1968). Although the theory is valid for $(ha)^{\frac{1}{3}} >> 1$, $(ka)^{\frac{1}{3}} >> 1$, the computation was made over the frequency range 0.01 Hz $\leq f \leq$ 5 Hz, which corresponds to intervals $16 < ha < 8000$, and $30 < ka < 15000$. A general Hankel subroutine described by Berry (1964) was modified and incorporated into the program.

Inspection of the integrands for $C_P(\omega)$ and $C_{SV}(\omega)$ shows that three types of numerical evaluation of Hankel functions are required.

(i) For $C_P(\omega)$ we need $H_\nu^{(1)}(ka)$ and $H_\nu^{(1)'}(ka)$ for ν near ha. These two functions are oscillatory.

(ii) For $C_{SV}(\omega)$ we need $H_\nu^{(1)}(ha)$ and $H_\nu^{(1)'}(ha)$ for ν near ka. These two functions are exponentially large.

(iii) For both $C_P(\omega)$ and $C_{SV}(\omega)$ we need $H_\nu^{(k)}(z)$, $H_\nu^{(k)'}(z)$ (k=1,2) for order ν varying in value near fixed z. (z = ha or ka.)

In fact, in cases (i) and (ii) it is only the ratio $H_\nu^{(1)'}(z)/H_\nu^{(1)}(z) = R(\nu,z)$ (say) which is needed, with ν not near z. R satisfies exactly the Riccati equation

$R' = -\frac{R}{z} - \left(1 - \frac{\nu^2}{z^2}\right) - R^2$, and R varies slowly. So approximately

$$R(\nu, ka) = -\frac{1}{2ka} + i\left[1 - \frac{\nu^2}{k^2a^2} - \frac{1}{4k^2a^2}\right]^{\frac{1}{2}} \quad \text{for } \nu \text{ near } ha$$

$$R(\nu, ha) = -\frac{1}{2ha} - \left[-1 + \frac{\nu^2}{h^2a^2} + \frac{1}{4h^2a^2}\right]^{\frac{1}{2}} \quad \text{for } \nu \text{ near } ka.$$

Calculation of R by these formulae is correct to within 1%, when checked against values returned by the HANKEL package. So this approximation is used in cases (i) and (ii).

For cases (iii), the HANKEL package uses Langer approximation in the form

$$H_\nu^{(k)}(z) \approx \exp\left[(-1)^{k-1}\, i\pi/6\right] \sqrt{1 - \eta \coth \eta}\; H_{\frac{1}{3}}^{(k)}(-i\zeta) \quad , k = 1,2,$$

where $\zeta = \nu(\tanh \eta - \eta)$ and $\eta = \cosh^{-1} \nu/z$. A subroutine for Hankel functions of order 1/3 is included, and $H_\nu^{(k)'}(z)$ is found from the recurrence relation $H_\nu^{(k)'}(z) = H_\nu^{(k)}(z) - (\nu/z)\, H_\nu^{(k)}(z)$.

The numerical evaluation of case (iii) was checked against two constants referred to in Rubinow and Keller (1951), namely

$$C_1 \equiv \frac{1}{z^{\frac{1}{3}}}\left[\int_{-\infty}^{z} \frac{H_\nu^{(2)}(z)}{H_\nu^{(1)}(z)}\, d\nu + \int_{z}^{\infty}\left(1 + \frac{H_\nu^{(2)}(z)}{H_\nu^{(1)}(z)}\right) d\nu\right]$$

$$C_2 \equiv \frac{1}{z^{\frac{1}{3}}}\left[\int_{-\infty}^{z} \frac{H_\nu^{(2)'}(z)}{H_\nu^{(1)'}(z)}\, d\nu + \int_{z}^{\infty}\left(1 + \frac{H_\nu^{(2)'}(z)}{H_\nu^{(1)'}(z)}\right) d\nu\right] \quad . \qquad (2.2.20)$$

Rubinow and Wu (1956) show that it is only the region of Langer approximation which contributes to the integral, and after path deformation and residue summation obtain

$$C_1 \approx 0.49808 \times (1 + \sqrt{3}\, i) \quad , \quad C_2 \approx -0.4321\, (1 + \sqrt{3}\, i). \qquad (2.2.21)$$

Using our HANKEL package, together with a Simpson integration method, we find C_1 and C_2 are indeed almost independent of z, for the range $16 < z < 10{,}000$, since Rubinow and Wu's values are returned to within $\frac{1}{2}$ %.

The integration path for $C_P(\omega)$ and $C_{SV}(\omega)$ in equations (2.2.9) and (2.2.14) is the real order axis. Although this is an adequate path for numerical evaluation, a better path is that shown in Figure 3. Whenever a complex path might involve extra contributions, from complex poles not near A, the real axis integration was evaluated as a check. The advantage of the complex path shown is that the

integrand decays exponentially on either side of the point A, where order equals argument, and a path length of about $4z^{\frac{1}{3}}$ or $5z^{\frac{1}{3}}$ is all that contributes. For a real axis integration, the integrand to the left of A oscillates with slowly decreasing contributions as the frequency of oscillation increases, and a path length of about $15z^{\frac{1}{3}}$ or $20z^{\frac{1}{3}}$ must be taken.

Results

We first present in Figure 4 the computed complex functions $C_P(\omega)$ and $C_{SV}(\omega)$, for the frequency range 0.01 Hz - 5 Hz. The computation becomes less relevant near the low-frequency end - because then $(ha)^{\frac{1}{3}} \sim 2$. Nevertheless, some values are presented for these low frequencies, and the theory is believed to be good for frequencies above 0.03 Hz.

It is interesting to compare the results for elastic waves with the results for acoustic waves. Figure 5 shows the quantity $H = [\text{Re } C + \text{Im } C]$, which is proportional to the shift s of shadow boundaries. H is a negative constant for a hard cylinder (on which the normal derivative of the field vanishes) and is a positive constant for a soft cylinder (on which the field itself vanishes) (see Rice (1964); Rubinow and Keller (1961). In fact, for a soft cylinder $H = \text{Re } C_1 + \text{Im } C_1$ (see equation (2.2.21)), and for a hard cylinder $H = \text{Re } C_2 + \text{Im } C_2$)). Thus we see that for our SH-wave we have exactly the hard cylinder acoustic problem. For P- or SV-wave

incidence, H becomes frequency dependent, tending with high frequencies to the acoustic soft cylinder value - a fact we can expect by seeing directly from (2.2.9) and (2.2.14) that $C_P(\omega)$ and $C_{SV}(\omega)$ both tend to the integral for C_1 (see (2.2.20)) as $\omega \to \infty$.

The shifts of the shadow boundary are shown in Figure 6. At a given frequency, incident P- and SV- waves would "feel" an effectively larger scatterer than its true size, whereas SH waves would "feel" a smaller one. At high frequencies, all shifts correctly approach zero (i.e. the shadow boundary approaches its geometrical limit). At lower frequencies, the amounts of shadow shift for different wave types diverge. For long period body waves, e.g. with period 20 seconds, the cylindrical scatterer of radius a = 3480 km would seem to be 90 km (2.6%) larger to P-waves, and 290 km (8.3%) larger to SV-waves, but 150 km (4.3%) smaller to SH-waves.

Further discussion of these results is deferred to the following sections, in which we develop (1) the generalization to a line source, and can thus compare our theory with the results of Teng and Wu (1968), and (2) the generalization to point source and spherical scatterer, permitting comparison with Phinney and Cathles (1969).

2.3 Diffraction of Cylindrical Waves by a Cylindrical Cavity

The nature of the diffraction of a cylindrical wave by a cylinder is qualitatively different, in the far field, from the nature of the

diffraction of a plane wave (see Shenderov (1962)). This is because the amplitudes of incident and scattered waves decay with distance according to the same law, for cylindrical incidence, but a plane wave does not decay at all. However, we shall see below that for the intermediate distances of geophysical interest, the field set up by cylindrical incidence can be quantitatively derived in a very simple way from the plane wave cases considered in Section 2.2.

Statement of Elasticity Problem

A steady-state cylindrical wave of displacement, emanating from a line source at distance b from a circular cylindrical cavity of radius a (see Figure 7), is incident from the left on the cavity. We wish to evaluate displacements near the shadow boundary.

Scattering of P-Waves

In order to obtain the simple form $\frac{e^{ihR}}{\sqrt{R}}$ for the incident displacement (at high frequencies), we choose the displacement potentials

$$\phi_i = \sqrt{\frac{\pi}{2h}}\ e^{-i\pi/4}\ H_o^{(1)}(hR)\ e^{-i\omega t} \quad , \quad \psi_i = 0.$$

An application of Graf's addition theorem (Watson, 1958) gives

$$\phi_i = \sqrt{\frac{\pi}{2h}}\, e^{-i\pi/4} \sum_{n=-\infty}^{\infty} H_n^{(1)}(hb)\, e^{in\pi/2}\, J_n(hr)\, e^{in\pi/2}\, e^{i(n\theta-\omega t)} \quad (\text{for } r < b).$$

So we take

$$\begin{pmatrix} \phi_s \\ \psi_s \end{pmatrix} = \sqrt{\frac{\pi}{2h}}\, e^{-i\pi/4} \sum_{n=-\infty}^{\infty} H_n^{(1)}(hb)\, e^{in\pi/2} \begin{pmatrix} A_n H_n^{(1)}(hr) \\ B_n H_n^{(1)}(kr) \end{pmatrix} e^{in\pi/2} e^{i(n\theta-\omega t)} \qquad (2.3.1)$$

The boundary conditions of zero normal and tangential stress on $r = a$ then give the forms (2.2.3) for A_n and B_n, i.e.

$$A_n = -\frac{1}{2}\left[1 + \frac{\Omega_1 H_n^{(2)}(ha)}{\Omega_1 H_n^{(1)}(ha)}\right], \qquad B_n = -\frac{1}{2}\frac{\Omega_2 J_n(ha)}{\Omega_1 H_n^{(1)}(ha)}$$

where Ω_1 and Ω_2 are defined in (2.2.4).

Hence we see that the step by step methods of section (2.2) may be duplicated for the problem of a line source. After identification and rejection of waves which travel around the cavity, and the contribution from the lower half-cylinder, we may drop the restriction $r < b$ (by an appeal to reciprocity), and obtain

$$\phi_s = -\frac{1}{2}\sqrt{\frac{\pi}{2h}}\; e^{-i\pi/4}\left[a_1(r,-\theta) + a_2(r,-\theta)\right]$$

where now

$$a_1(r,-\theta) = \int_0^{ha} e^{i\nu(-\theta+\pi/2)}\, H_\nu^{(1)}(hb)\, e^{i\nu\pi/2}\, H^{(1)}(hr)\, d\nu$$

$$a_2(r,-\theta) = \int_{-\infty}^{ha} e^{i\nu(-\theta+\pi/2)}\, H_\nu^{(1)}(hb)\, e^{i\nu\pi/2}\, \frac{\Omega_1 H_\nu^{(2)}(ha)}{\Omega_1 H_\nu^{(1)}(ha)}\, H_\nu^{(1)}(hr)\, d\nu$$

$$+ \int_{ha}^{\infty} e^{i\nu(-\theta+\pi/2)} H_\nu^{(1)}(hb)\, e^{i\nu\pi/2}\left[1 + \frac{\Omega_1 H_\nu^{(2)}(ha)}{\Omega_1 H_\nu^{(1)}(ha)}\right] H_\nu^{(1)}(hr)\, d\nu.$$

Evaluation of $a_1(r,-\theta)$

Since hr, hb are bigger than ν throughout the integration, we may use Debye expansions to see

$$a_1(r,-\theta) \sim \frac{2}{\pi}\, e^{-2i\pi/4} \int_0^{ha} \left(h^2r^2-\nu^2\right)^{-1/4} \left(h^2b^2-\nu^2\right)^{-1/4} \quad X$$

$$\exp i\left[\left(h^2r^2-\nu^2\right)^{\frac{1}{2}} + \left(h^2b^2-\nu^2\right)^{\frac{1}{2}} + \nu \sin^{-1}\frac{\nu}{hr} + \nu \sin^{-1}\frac{\nu}{hb} - \nu\theta\right] d\nu$$

This integrand has just one stationary phase point, given by a value $\nu = \nu_s$ such that

$$\sin^{-1}\left(\frac{\nu_s}{hr}\right) + \sin^{-1}\left(\frac{\nu_s}{hb}\right) = \theta \qquad \text{i.e.} \quad \nu_s = hy \text{ (see Figure 7).}$$

For $P(r,\theta)$ near the upper shadow boundary, this stationary phase point is near the upper limit of integration. Making the definition

$$\xi = \sqrt{\frac{R}{2hR_1R_2}}\,(\nu-\nu_s) \text{ and expanding the phase in powers of } \xi,$$

we find

$$a_1(r,-\theta) \sim e^{ihR} \cdot \frac{2}{\pi}\, e^{-2i\pi/4} \cdot \sqrt{\frac{2}{hR}} \cdot \int_{-\sqrt{\frac{hR}{2R_1R_2}}\,y}^{\sqrt{\frac{hR}{2R_1R_2}}\,(a-y)} e^{i\xi^2}\, d\xi$$

$$\sim \sqrt{\frac{2}{\pi hR}}\, e^{i(hR-\pi/4)} \left[\, 1 + e^{-i\pi/4} \sqrt{\frac{2hR}{\pi R_1R_2}}\,(a-y) \,\right] \quad \text{if both}$$

$$\left(\frac{hR}{2R_1R_2}\right)^{\frac{1}{2}} y >> 1, \qquad \left(\frac{hR}{2R_1R_2}\right)^{\frac{1}{2}} |a-y| << 1.$$

Evaluation of $a_2(r,-\theta)$

We may still use the Debye expressions for $H_\nu^{(1)}(hr)$, $H_\nu^{(1)}(hb)$, and so near $\nu = ha$

$e^{i\nu(-\theta+\pi/2)} H_\nu^{(1)}(hb)\ e^{i\nu\pi/2}\ H_\nu^{(1)}(hr) \sim \frac{2}{\pi h} \frac{e^{-i\pi/4}}{\sqrt{R_1 R_2}}\ e^{i(hR-\pi/4)}$. Then

$$a_2(r,-\theta) \sim \frac{2}{\pi}\ \frac{e^{-i\pi/4}\ e^{i(hR-\pi/4)}}{h\sqrt{R_1 R_2}} \cdot (ha)^{\frac{1}{3}}\ C_p(\omega),$$

where $C_p(\omega)$ is the function defined above for plane incidence, in equation (2.2.9).

In summary: we have for $\phi = \phi_i + \phi_s$ that

$$\phi \sim \frac{1}{h\sqrt{R}}\ e^{i(hR-\pi/2)} \left\{ \frac{1}{2} - e^{-i\pi/4} \sqrt{\frac{R}{2\pi h R_1 R_2}} \left[h(a-y) + (ha)^{\frac{1}{3}}\ C_p(\omega) \right] \right\} \tag{2.3.2}.$$

Discussion

We see from (2.3.2) that in the neighborhood of the geometrical shadow boundary (which is given by $y = a$) the P-wave displacement due to a line source is still directed along a ray from the source, and is

$$\frac{e^{ihR}}{\sqrt{R}} \left\{ \frac{1}{2} - e^{-i\pi/4} \sqrt{\frac{R}{2\pi h R_1 R_2}} \left[h(a-y) + (ha)^{\frac{1}{3}} \; C_p(\omega) \right] \right\} \tag{2.3.3}$$

We still have the result

$$\underset{\sim}{u} \to \frac{1}{2} \underset{\sim}{u}_i \text{ on the geometrical shadow boundary, as } \omega \to \infty,$$

so we may still define the shadow boundary shift as the distance from geometrical shadow boundary to the half amplitude line. From (2.3.3) we see that the half amplitude line still has the equation $y = a + s_p$, where s_p is the shift for plane waves (see 2.2.17). But this line is radial to the source, and hence diverges from the geometrical shadow boundary. In fact, we see

$$\text{SHIFT}\Big|_{\text{P-wave, line source}} = \frac{R}{R_1} \times \text{SHIFT}\Big|_{\text{P-wave, plane source}}$$

$$= \frac{R}{R_1} \times \left[\text{Re}C_p(\omega) + \text{Im}C_p(\omega) \right] \; (ha)^{-\frac{2}{3}} \; .a \tag{2.3.4}$$

The simple geometrical relation between the shifts for a line source and a plane source is illustrated in Figure 8.

Theoretical consideration of SV and SH line sources yields the same geometrical relation as (2.3.4) and Figure 8 (although the SH shift is negative).

Numerical Results

A model experiment described by Teng and Wu (1968) gives several measurements of the shadow boundary shift for P- and SV-waves. Their Model I and Model II, illustrated in Figure 9, were thin sheets of aluminum with a "pulse" of one dominant frequency, and with a circular hole as the scatterer. The velocity of P-waves in such a plate is given by

$$\alpha = \sqrt{\frac{4\mu(\lambda+\mu)}{(\lambda+2\mu)\rho}} \quad \text{(for Lamé constants } \lambda \text{ and } \mu\text{, and density } \rho\text{)},$$

since we can assume this is a system in plane stress (see Love, 1944, p. 208). Table 1 shows the shifts calculated from our theory (equation (2.3.4)), and Teng and Wu's experimental values. Also in this table is the geophysical body-wave period for which the model is scaled.

The methods of this chapter receive encouraging confirmation from the agreement in Table 1 between theory and experiment. But direct application of our theory to diffracted seismic waves still requires additional generalization, given in the following sections.

2.4 Diffraction by a Fluid Cylinder

The effect on shadow boundaries of a fluid scatterer (as opposed to scatter by a cavity) is difficult to estimate, even qualitatively.

The boundary conditions become much more complex, and we must allow for internally reflected waves. But solution of this problem is important in geophysics, since we have seen that we expect the location of the shadow boundary to be dependent on physical properties at the core-mantle interface. We shall see below that our theory requires very little extension to accommodate the case of fluid scatterers.

Statement of Elasticity Problem

A steady-state cylindrical wave of displacement, emanating from a line source at distance b from a circular cylindrical fluid of radius a (see Figure 7) is incident from the left on the fluid. We wish to evaluate displacements near the shadow boundary. We take ρ, h, k as the density, and P and SV wave numbers in the solid, and ρ', h' as density and wave number in the fluid.

Scattering of P-waves

As in section (2.3), we take $\phi_i = \sqrt{\frac{\pi}{2h}}\, e^{-i\pi/4} H_o^{(1)}(hR)\, e^{-i\omega t}$, $\psi_i = 0$. Clearly, we may solve for the total scattered field by writing three potentials in the form

$$\begin{pmatrix} \phi_s^T \\ \psi_s^T \\ \phi_s'^T \end{pmatrix} = \sum_{n=-\infty}^{\infty} \begin{pmatrix} a_n H_n^{(1)}(hr) \\ b_n H_n^{(1)}(kr) \\ a_n' J_n(h'r) \end{pmatrix} \cdot e^{i(n\theta-\omega t)} \qquad \begin{matrix} \text{P-wave } r > a \\ \text{SV-wave in } r > a \\ \text{P-wave in } r < a \end{matrix} \tag{2.4.1}$$

and then solving for (a_n, b_n, a_n') from the continuity of radial displacement, and tangential and normal stress, across $r = a$. But for a source emitting waves with high frequency energy, it is standard seismological practice to separate a record into P, PP, PcP, PKKP, etc., and to think of these phases as having different ray paths. The potential ϕ_s^T of (2.4.1) includes all such contributions (except the types PP, PcPPKP, etc., which involve reflection from the free surface), and the problem of splitting ϕ_s^T for these phases is quite well understood (see Bremmer, 1948, Chap. III; Scholte, 1956; Duwalo and Jacobs, 1959, for solutions in spherical geometry). Since we are concerned with the interaction of P and PcP at and near grazing incidence, we wish to set up scattered wave potentials ϕ_s, ψ_s in the region $r > a$ which ignore phases transmitted through $r < a$.

This is done by showing that the solution for each a_n, b_n in (2.4.1) can be written as a geometric progression in the form

$$a_n = -\frac{1}{2} + \frac{1}{2}\,\frac{H_n^{(2)}(ha)}{H_n^{(1)}(ha)}\left\{(LL) + (LL')\cdot\sum_{N=0}^{\infty}(L'L')^N\left(\frac{H_n^{(1)}(h'a)}{H_n^{(2)}(h'a)}\right)^{N+1}\cdot(L'L)\right\}$$

$$b_n = \frac{1}{2}\,\frac{H_n^{(2)}(ha)}{H_n^{(1)}(ka)}\left\{(LT)+(LL')\cdot\sum_{N=0}^{\infty}(L'L')^N\left(\frac{H_n^{(1)}(h'a)}{H_n^{(2)}(h'a)}\right)^{N+1}\cdot(L'T)\right\}$$

where the symbols (LL), (LL'), (L'L'), (L'L), (LT), (L'T) (of Scholte, 1956) may be identified as reflection and transmission coefficients in the following way: the term with index N represents (when summed over n in (2.4.1)) an arrival which approximately has the phase appropriate to a ray path made up by N internal reflections within the core. That is, PKK...KP (for a_n), and PKK...KS (for b_n), with N + 1 K's in each case. The initial terms,

$$-\frac{1}{2}\left[1 - \frac{H_n^{(2)}(ha)}{H_n^{(1)}(ha)}(LL)\right] \equiv A_n \qquad \text{and}$$

$$\frac{1}{2}\,\frac{H_n^{(2)}(ha)}{H_n^{(1)}(ha)}(LT) \equiv B_n \quad \text{(say)}$$

represent arrivals with the respective phases of PcP and PcS, so these are the terms which we wish to study. (Note that since we have a steady state source, the signals coming along all the different possible paths are superimposed. So the identification of specified modes of propagation is performed by studying their phase, and not their travel time).

The manipulative procedure for obtaining the above expansions of (a_n, b_n) is quite lengthy, and so an alternative method is given below for the introduction and calculation of the required (A_n, B_n). It may be shown that the same result is reached by either method.

Potentials for PcP and PcS

The n-th partial wave component within the fluid is chosen in equation (2.4.1) to have the factor $J_n(h'r)$. This choice must be made to avoid any singularity at $r = 0$. But $J_n(h'r)$ is a sum of ingoing and outgoing waves, although the system of a P-wave source and conversion to PcP, PcS requires only an ingoing wave within the fluid. (The outgoing wave within the fluid may then be thought of as generated by reflection in the origin: upon reaching $r = a$, it generates PKP, PKS, and another ingoing component in the fluid.) Hence, for our examination of PcP, it is necessary to ignore $H_n^{(1)}(h'r)$ terms within the fluid, and we use potentials (cf equation (2.3.1))

$$\begin{pmatrix} \phi_s \\ \psi_s \\ \phi_s' \end{pmatrix} = \sqrt{\frac{\pi}{2h}}\, e^{-i\pi/4} \sum_{n=-\infty}^{\infty} H_n^{(1)}(hb)\, e^{in\pi/2} \begin{pmatrix} A_n H_n^{(1)}(hr) \\ B_n H_n^{(1)}(kr) \\ A'_n H_n^{(2)}(h'r) \end{pmatrix} e^{in\pi/2}\, e^{i(n\theta-\omega t)} \qquad (2.4.2)$$

The boundary conditions on r = a then give

$$A_n = -\frac{1}{2}\left[1 + \frac{\Omega_5 H_n^{(2)}(ha)}{\Omega_5 H_n^{(1)}(ha)}\right] \qquad B_n = -\frac{1}{2}\,\frac{\Omega_6 J_n(ha)}{\Omega_5 H_n^{(1)}(ha)}$$

where

$$\Omega_5 H_n^{(\ell)}(ha) \equiv S^{(1)}\left[P^{(\ell)} - \frac{P'^{(2)}}{U'^{(2)}}\,U^{(\ell)}\right] + \left[Q^{(1)} - \frac{P'^{(2)}}{U'^{(2)}}\,V^{(1)}\right] R^{(\ell)}$$

$$\Omega_6 J_n(ha) \equiv +i\left(R^{(2)}\left[P^{(1)} - \frac{P'^{(2)}}{U'^{(2)}}\,U^{(1)}\right] - R^{(1)}\left[P^{(2)} - \frac{P'^{(2)}U^{(2)}}{U'^{(2)}}\right]\right).$$

$P^{(\ell)}$, $Q^{(\ell)}$, $R^{(\ell)}$, $S^{(\ell)}$ are defined in (2.2.4) and

$$P'^{(2)} \equiv \frac{k^2a^2}{\rho}\,\rho' H_n^{(2)}(h'a) \qquad U'^{(2)} \equiv h'a\, H_n^{(2)'}(h'a)$$

$$U^{(\ell)} \equiv ha\, H_n^{(\ell)'}(ha) \qquad V^{(\ell)} \equiv nH_n^{(\ell)}(ka).$$

(2.4.3)

Since the operator Ω_5 obeys the same reflection rules as Ω_1, namely $\Omega_5 H_{-\nu}^{(1)}(ha) = e^{2\pi i\nu}\, \Omega_5 H_{\nu}^{(1)}(ha)$, $\Omega_5 H_{-\nu}^{(2)}(ha) = \Omega_5 H_{\nu}^{(2)}(ha)$, the methods of section (2.3) for scattering by a cavity may now be applied for the present problem of scattering by a fluid. We find the asymptotic solution for P-wave displacement is still directed along the ray from the source (see Figure 10), and is given by

$$\frac{e^{ihR}}{\sqrt{R}} \left\{ \frac{1}{2} - e^{-i\pi/4} \sqrt{\frac{R}{2\pi h R_1 R_2}} \left[h(a-y) + (ha)^{1/3}\, C_P^{FLUID}(\omega) \right] \right\} ,$$

and the shadow boundary shift is

$$\text{SHIFT}\Big|_{\substack{\text{P-wave, line-source,} \\ \text{fluid scatterer}}} = \frac{R}{R_1} \left[\text{Re}C_P^{FLUID}(\omega) + \text{Im}C_P^{FLUID}(\omega) \right] (ha)^{-2/3} \cdot a$$

(2.4.4)

where

$$C_P^{FLUID}(\omega) \equiv \frac{1}{(ha)^{1/3}} \left[\int_{-\infty}^{ha} \frac{\Omega_5 H_{\nu}^{(2)}(ha)\, d\nu}{\Omega_5 H_{\nu}^{(1)}(ha)} + \int_{ha}^{\infty} \left(1 + \frac{\Omega_5 H_{\nu}^{(2)}(ha)}{\Omega_5 H_{\nu}^{(1)}(ha)} \right) d\nu \right]$$

Theoretical consideration of an SV source leads to a result just like (2.4.4), but with $C_P^{FLUID}(\omega)$ replaced by

$$C_{SV}^{FLUID}(\omega) \equiv \frac{1}{(ka)^{\frac{1}{3}}}\left[\int_{-\infty}^{ka} \frac{\Omega_7 H_\nu^{(2)}(ka)\,d\nu}{\Omega_7 H_\nu^{(1)}(ka)} + \int_{ka}^{\infty} \left(1 + \frac{\Omega_7 H_\nu^{(2)}(ka)}{\Omega_7 H_\nu^{(1)}(ka)} \right) d\nu\right] \tag{2.4.5}$$

$$\Omega_7 H_n^{(\ell)}(ka) = S^{(\ell)}\left[P^{(1)} - \frac{P'^{(2)}}{U'^{(2)}} U^{(1)}\right] + \left[Q^{(\ell)} - \frac{P'^{(2)}}{U'^{(2)}} V^{(\ell)} \right] R^{(1)} \tag{2.4.6}$$

where $S^{(\ell)}, \ldots\ldots, R^{(1)}$ are given above in (2.2.4) and (2.4.3).

The SH scattering is of course unaffected by a fluid core.

Numerical Results

In order to estimate the effect of a fluid scatterer, C_P^{FLUID} and C_{SV}^{FLUID} were computed from formulae (2.4.5) and (2.4.6), for the model with a = 3480 km, α = 13.6 km/sec, β = 7.5 km/sec, ρ = 5.5 gm/cc, α' = 8.3 km/sec, and ρ' = 9.5 gm/cc. The real and imaginary parts of these functions are displayed in Figure 10, plotted as functions of frequency. The shadow boundary shifts were then calculated (using (2.4.4)) for both source and receiver at radius 6350 km, and our results are shown in Figure 11. A convenient way of describing the shift is to give the distance $\Delta_{\frac{1}{2}}$, in degrees, from the source to the half-ray-amplitude point on the arc with radius 6350 km. This method is used in Figure 11, and for reference we note that the geometrical shadow boundary is at Δ = 113.54°. Also shown in this Figure are the shifts due to scattering by a cavity, in the same model.

From these numerical results, we see that in the frequency range of geophysical interest (corresponding to periods between $\frac{1}{2}$ sec and 20 sec) the different boundary conditions of cavity and fluid give rise to substantially different shifts, particularly for P-waves. The shadow shift for P-waves scattered by the fluid is very small - as we might expect, since the solid and fluid are acoustically matched ($\rho\alpha \sim \rho'\alpha'$) and the PcP reflection coefficient is small. But the shifts for S-waves are quite large, about 2° at 10 sec period, with SH and SV being affected in opposite senses.

We expect the shadow shifts for line source/cylindrical scatterer and point source/spherical scatterer to be very similar, because they have been shown (Rubinow and Keller, 1961; Rice, 1954; Nussenzveig, 1965) to be similar for more simple boundary conditions. So the numerical results above may be directly relevant to the geophysical problem of core-scattered body waves. However, the theory may be simply extended to the case of point source and spherical core, and in next section below we develop numerical results for this model.

2.5 Diffraction of Spherical Waves by a Spherical Fluid.

Statement of Elasticity Problem

A steady-state spherical wave of displacement, emanating in an elastic solid from a point source at distance b from a spherical fluid of radius a (see Figure 7), is incident from the left. We wish to evaluate displacements near the shadow boundary. We take ρ, h, k as the density, and P and SV wave numbers in the solid, and ρ', h' as the density and wave number in the fluid.

Scattering of P-Waves

In order to obtain the simple form $\frac{e^{ihR}}{R}$ for the incident displacement (directed radially from the source), we choose the displacement potentials

$\phi_i = \frac{e^{ihR}}{ihR}$, $\psi_i = 0$. We use spherical coordinates (r,θ,Φ), in which the displacement components are related to potentials by

$\underset{\sim}{u}$ = grad ϕ + curl curl $(r\psi,0,0)$.

We have an additional formula in the form

$$\phi_i = \sum_{n=0}^{\infty} (2n+1)\, h_n^{(1)}(hb)\, j_n(hr)\, P_n(\cos(\pi-\theta)) \quad \text{for } r < b$$

(see Abramowitz and Stegun, 1964, p. 440, 6th printing or later) where $h^{(1)}$ and j are spherical Hankel/Bessel functions, and P_n is a Legendre function of the first kind. Following the reasoning of section (2.4), we set up potentials ϕ_s, ψ_s, and ϕ_s' for respectively PcP, PcS and the ingoing component of core body waves, and then solve for coefficients a_n, b_n, a_n' in

$$\begin{pmatrix} \phi_i \\ \phi_s \\ \psi_s \\ \phi_s' \end{pmatrix} = \sum_{n=0}^{\infty} (2n+1)\, h_n^{(1)}(hb) \begin{pmatrix} j_n(hr) \\ a_n h_n^{(1)}(hr) \\ b_n h_n^{(1)}(kr) \\ a_n' h_n^{(2)}(h'r) \end{pmatrix} P_n(\cos(\pi-\theta)). \qquad (2.5.1)$$

The solutions for (a_n, b_n), found with a_n' from the requirements of continuous stresses and normal displacement across r = a, may be written in the form

$$a_n = -\frac{1}{2}\left[1 + \frac{\Omega_5 h_n^{(2)}(ha)}{\Omega_5 h_n^{(1)}(ha)}\right], \quad b_n = -\frac{1}{2}\,\frac{\Omega_6 j_n(ha)}{\Omega_5 h_n^{(1)}(ha)} \qquad \text{where}$$

$$\Omega_5 h_n^{(\ell)}(ha) \equiv s^{(1)}\left[p^{(\ell)} - \frac{p'^{(2)}}{u'^{(2)}}\,u^{(\ell)}\right] + \left[q^{(1)} - \frac{p'^{(2)}}{u'^{(2)}}\,v^{(1)}\right] r^{(\ell)}$$

$$\Omega_6 j_n(ha) \equiv -r^{(2)}\left[p^{(1)} - \frac{p'^{(2)}}{u'^{(2)}}\,u^{(1)}\right] + r^{(1)}\left[p^{(2)} - \frac{p'^{(2)}}{u'^{(2)}}\,u^{(2)}\right] \quad \text{and}$$

$$p^{(\ell)} \equiv 4\,ha\,h_n^{(\ell)'}(ha) + \left[k^2a^2 - 2n(n+1)\right] h_n^{(\ell)}(ha)$$

$$q^{(\ell)} \equiv -2n(n+1)\left(ka\,h_n^{(\ell)'}(ka) - h_n^{(\ell)}(ka)\right)$$

$$p'^{(2)} \equiv \frac{k^2a^2\rho'}{\rho}\,h_n^{(2)}(h'a) \qquad\qquad r^{(\ell)} \equiv 2\left(ha\,h_n^{(\ell)'}(ha) - h_n^{(\ell)}(ha)\right)$$

$$s^{(\ell)} \equiv + \left\{ 2kah_n^{(\ell)'}(ka) + \left[k^2a^2 + 2-2n(n+1) \right] h_n^{(\ell)}(ka) \right\}$$

$$u^{(\ell)} \equiv ha\, h_n^{(\ell)'}(ha)$$

$$v^{(\ell)} \equiv n(n+1)\, h_n^{(\ell)}(ka) \qquad u'^{(2)} \equiv h'a\, h_n^{(2)'}(h'a)$$

(2.5.2)

We separate in ϕ_s those waves which travel more than once around the core by using a Poisson sum formula. In our case, this takes the form

$$\phi_s = -\frac{1}{2} \sum_{n=0}^{\infty} f\left(n + \tfrac{1}{2}\right) = -\frac{1}{2} \sum_{m=-\infty}^{\infty} (-1)^m \int_0^{\infty} f(\nu)\, e^{2i\pi m\nu}\, d\nu \qquad (2.5.3)$$

with

$$f(\nu) \equiv 2\nu h^{(1)}_{\nu-\frac{1}{2}}(hb) \left[1 + \frac{\Omega_5 h^{(2)}_{\nu-\frac{1}{2}}(ha)}{\Omega_5 h^{(1)}_{\nu-\frac{1}{2}}(ha)} \right] h^{(1)}_{\nu-\frac{1}{2}}(hr)\, P_{\nu-\frac{1}{2}}\left(\cos(\pi-\theta)\right).$$

The terms from m = 0 may be split by using

$$P_n(\cos\Delta) = \frac{1}{2}\left[P_n(\cos\Delta) + \frac{2i}{\pi} Q_n(\cos\Delta) \right] + \frac{1}{2}\left[P_n(\cos\Delta) - \frac{2i}{\pi} Q_n(\cos\Delta) \right]$$

$$\equiv Q_n^{(1)}(\cos\Delta) + \qquad\qquad Q_n^{(2)}(\cos\Delta), \text{ say,}$$

where Q_n is a Legendre function of the second kind, and $Q_n^{(1)}$ and $Q_n^{(2)}$ may be shown to represent travelling waves (see Nussensveig, 1965, p. 96), in respectively the negative and positive Δ directions.

Hence, we may use near the upper shadow boundary the formula

$$\phi_s(r,\theta) = -\frac{1}{2}\int_0^\infty 2\nu h^{(1)}_{\nu-\frac{1}{2}}(hb)\left[1+\frac{\Omega_5 h^{(2)}_{\nu-\frac{1}{2}}(ha)}{\Omega_5 h^{(1)}_{\nu-\frac{1}{2}}(ha)}\right] h^{(1)}_{\nu-\frac{1}{2}}(hr)\; Q^{(2)}_{\nu-\frac{1}{2}}\left(\cos(\pi-\theta)\right)d\nu \qquad (2.5.4)$$

The basic method of section (2.2) is still completely appropriate. Noting the result

$$Q^{(2)}_{\nu-\frac{1}{2}}\left(\cos(\pi-\theta)\right) \sim \left(\frac{1}{2\pi\nu\sin\theta}\right)^{\frac{1}{2}} e^{i[\nu(\pi-\theta)-\pi/4]}$$, we can obtain

$$\phi = \phi_i + \phi_s \sim \frac{e^{ihR}}{ihR}\left\{\frac{1}{2} - e^{-i\pi/4}\sqrt{\frac{R}{2\pi hR_1R_2}}\left[h(a-y)+(ha)^{\frac{1}{3}}\; C_p(\omega)\right]\right\}$$

near the shadow boundary, where now

$$C_p(\omega) \equiv \frac{1}{(ha)^{\frac{1}{3}}}\left[\int_0^{ha}\frac{\Omega_5 h^{(2)}_{\nu-\frac{1}{2}}(ha)\,d\nu}{\Omega_5 h^{(1)}_{\nu-\frac{1}{2}}(ha)} + \int_{ha}^{\infty}\left(1+\frac{\Omega_5 h^{(2)}_{\nu-\frac{1}{2}}(ha)}{\Omega_5 h^{(1)}_{\nu-\frac{1}{2}}(ha)}\right)d\nu\right] \qquad (2.5.5)$$

Scattering of SV-Waves

Similarly, for a SV-wave source with potentials $\phi_i = 0$, $\psi_i = \frac{e^{ikR}}{ikR}$, the total SV-wave potential near the shadow boundary is

$$\psi = \psi_i + \psi_s \sim \frac{e^{ikR}}{ikR}\left\{\frac{1}{2} - e^{-i\pi/4}\sqrt{\frac{R}{2\pi kR_1R_2}}\left[k(a-y)+(ka)^{1/3}C_{SV}(\omega)\right]\right\} ,$$

with

$$C_{SV}(\omega) \equiv \frac{1}{(ka)^{1/3}}\left[\int_0^{ka}\frac{\Omega_7 h^{(2)}_{\nu-\frac{1}{2}}(ka)\,d\nu}{\Omega_7 h^{(1)}_{\nu-\frac{1}{2}}(ka)} + \int_{ka}^{\infty}\left(1 + \frac{\Omega_7 h^{(2)}_{\nu-\frac{1}{2}}(ka)}{\Omega_7 h^{(1)}_{\nu-\frac{1}{2}}(ha)}\right)d\nu\right] \quad \text{and}$$

$$\Omega_7 h_n^{(\ell)}(ka) \equiv s^{(\ell)}\left[p^{(1)} - \frac{p'^{(2)}}{u'^{(2)}}u^{(1)}\right] + \left[q^{(\ell)} - \frac{p'^{(2)}}{u'^{(2)}}v^{(\ell)}\right] r^{(1)}$$

(2.5.6)

Scattering of SH-Waves

The SH-wave in spherical coordinates may be expressed as $\underset{\sim}{u} = \text{curl}(r\chi,0,0)$ where the potential χ satisfies $\nabla^2\chi + k^2\chi = 0$. Using the boundary condition of zero tangential stress on $r = a$, with an SH source potential $\chi_i = \frac{e^{ikR}}{ikR}$, we find the total SH-wave potential near the shadow boundary is

$$\chi = \chi_i + \chi_s \sim \frac{e^{ikR}}{ikR}\left\{ \frac{1}{2} - e^{-i\pi/4}\sqrt{\frac{R}{2\pi kR_1R_2}}\left[k(a-y) + (ka)^{1/3}\, C_{SH}(\omega)\right]\right\} \quad ,$$

with

$$C_{SH}(\omega) \equiv \frac{1}{(ka)^{1/3}}\left[\int_0^{ka} \frac{kah^{(2)'}_{\nu-\frac{1}{2}}(ka) - h^{(2)}_{\nu-\frac{1}{2}}(ka)}{kah^{(1)'}_{\nu-\frac{1}{2}}(ka) - h^{(1)}_{\nu-\frac{1}{2}}(ka)}\, d\nu \right.$$

$$\left. + \int_{ka}^{\infty}\left(1 + \frac{kah^{(2)'}_{\nu-\frac{1}{2}}(ka) - h^{(2)}_{\nu-\frac{1}{2}}(ka)}{kah^{(1)'}_{\nu-\frac{1}{2}}(ka) - h^{(1)}_{\nu-\frac{1}{2}}(ka)}\right) d\nu\right] \qquad (2.5.7)$$

Numerical Results

We first present in Figure 12 the computed functions $C_P(\omega)$ and $C_{SV}(\omega)$ for the frequency range 0.01 Hz - 5 Hz, for the model with a = 3480 km, α = 13.6 km/sec, β = 7.5 km/sec, ρ = 5.5 gm/cc, α' = 8.3 km/sec, and ρ' = 9.5 gm/cc. The results are also given for a spherical cavity. It may be seen from a comparison of Figure 12 with Figures 4 and 6 that a change from cylindrical to spherical scatterer makes very little difference to the $C_P(\omega)$ and $C_{SV}(\omega)$. This is then direct confirmation of a result (mentioned in Section (2.1)) which we would expect from a survey of the solutions published for simpler boundary

conditions (Rubinow and Keller, 1961; Nussenzveig, 1965). Namely, that there is a strong similarity among solutions for cylindrical and spherical scatterers with the same boundary conditions.

The function $C_{SH}(\omega)$ may be calculated from equation (2.5.7), and it is found to be essentially independent of frequency for $f > 0.1$ Hz, taking the value C_2 (see Equation (2.2.20)) which arises in a discussion of the cylindrical scatterer. The slight frequency dependence of $C_{SH}(\omega)$ at lower frequencies is such that the relation $ReC_{SH}(\omega) + ImC_{SH}(\omega) \sim ReC_2 + ImC_2$ is maintained. But this is the combination of real and imaginary parts which appears in our formula for shadow boundary shift (see e.g. (2.2.18) and (2.2.19)), and so there is confirmation of the similarity among cylindrical and spherical solutions for the boundary conditions of SH waves also.

An interesting feature of the computation for $C_{SV}(\omega)$ is the effect of what may be described as a "head-wave" at the core mantle boundary. Since we have taken $\alpha' = 8.3$ km/sec, and $\beta = 7.5$ km/sec, the diffracted SV time path from the source to receiver in the geometrical shadow (i.e. travelling part way with velocity β on the mantle side of the core/mantle boundary) is longer than the combination (a) source to core/mantle boundary at critical incidence $\sin^{-1} \frac{7.5}{8.3}$, (b) travel at velocity α' on the core side of the core/mantle boundary, and (c) departure at critical transmission from core/mantle boundary to receiver.

In ray theoretical terms, this latter "head-wave" may be thought of as a contribution to SV which has a ray parameter $h'a/\omega$. The numerical effect is observed in equation (2.5.6) as a small contribution to $C_{SV}(\omega)$ from values of the integrand near $\nu = h'a$, and by deforming the path of integration to separate the contribution of poles near $\nu = h'a$ from the contribution of poles near $\nu = ka$ we have a device for separating the "head-wave" from the diffracted SV wave. Even at low frequencies, $f \sim 0.02$ Hz, the head wave amplitude is then only 1% of diffracted SV amplitudes (in the transition zone), so the effect is completely negligible in our model. But the numerical method of separating "head wave" contributions will work for models of a spherical boundary between two media in which a head-wave is more prominent. A complete discussion of such a boundary must of course include waves like SKS, SKKKKS which have horizontal phase velocities approaching that of the head wave (see e.g. Chekin, 1969).

A method of finding the accuracy of our transition region formula, equations (2.5.5) - (2.5.7), is suggested by the methods of Phinney and Alexander (1966) and Phinney and Cathles (1969), in which exact formulae for P-wave potential (e.g. our equation(2.5.4)) are evaluated numerically. Phinney and his co-workers, and Nussenzveig (1965), show that the total P-wave may be evaluated by a complex path

integration in the complex ν-plane. For a receiver in the lit zone, the path may be chosen to pass through two saddles (at $\nu = \nu_1$, $\nu = \nu_2$, say) on the real ν-axis, and $\nu_1 (< ha)$ and $\nu_2 (> ha)$ correspond to the horizontal phase velocities of PcP and P. As the receiver moves towards the geometrical shadow boundary, the saddle points ν_1 and ν_2 move together so that $\nu_1 = ha = \nu_2$. Beyond the geometrical shadow boundary, the complex path integral for the potential is regarded as a summation of the residues from a series of poles of the integrand, these poles lying near a line in the ν plane which starts out from $\nu = ha$ at an angle of $\frac{\pi}{3}$ with the real ν-axis. Phinney and Cathles (1969) show that for source-receiver distances of several degrees on either side of the geometrical shadow boundary, the same path in the ν-plane may be used in numerical evaluation of the field.

We have used this exact method for the evaluation of scattered fields, using the FORTRAN program described in Appendix IV. The results of such computation (which are given below for P-P, SV-SV, and SH-SH scattering) have obvious merit, in that they are the exact solutions for our simple Earth model. But the exact results have a double purpose, in that the success or failure of approximate formulae - which exhibit source-receiver geometry explicitly - may also be judged.

In order that our results may be more relevant to seismic data, we in fact calculate displacement components, rather than potentials (ϕ, ψ, χ). Thus, for example, we see that the exact formula for total radial displacement in P-P scattering from a source with potential

$\phi_i = \frac{e^{ihR}}{ihR}$ is the radial derivative of potential $\phi = \phi_i + \phi_s$.

Comparing Section VI of Nussenzveig (1965), we have

$$\phi = -\frac{1}{2}\int_{\Gamma} 2\nu h^{(1)}_{\nu-\frac{1}{2}}(hb)\, h^{(1)}_{\nu-\frac{1}{2}}(hr)\, \frac{\Omega_5 h^{(2)}_{\nu-\frac{1}{2}}(ha)}{\Omega_5 h^{(1)}_{\nu-\frac{1}{2}}(ha)}\, Q^{(2)}_{\nu-\frac{1}{2}}(\cos\Delta)\, d\nu$$

where Γ is the complex path discussed in our Appendix IV, and so the radial displacement is calculated from a numerical evaluation of

$$u_r = -\int_{\Gamma} \nu h^{(1)}_{\nu}(hb)\, hh^{(1)\prime}_{\nu}(hr)\, \frac{\Omega_5 h^{(2)}_{\nu-\frac{1}{2}}(ha)}{\Omega_5 h^{(1)}_{\nu-\frac{1}{2}}(ha)}\, Q^{(2)}_{\nu-\frac{1}{2}}(\cos\Delta)\, d\nu \quad .$$

The model used for our computation is the same as that used above for the evaluation of C_P, C_{SV}, C_{SH} (fluid core). We have also to specify the source and receiver radii (since the exact method of computation does not give any simple explicit dependence on source-receiver geometry), and take b = r = 6350 km.

Our model is then the model 1 of Phinney and Cathles (1969) - with the exception of a S-wave velocity of 0.001 km/sec in their "core." However, a part of Phinney and Cathles' conclusions is that this non-zero shear velocity has a negligible effect on the scattered field. Our program may also be used to find the potentials (ϕ,ψ,χ), and as a check we have obtained the P-P total potential at 0.03 Hz and 0.3 Hz: Phinney and Cathles (1969) results for periods 32 sec and 3.2 sec are then accurately reproduced.

P-P Results

Figure 13 displays the amplitude of total radial P-wave displacement due to a P-wave point source, with scattering from a spherical fluid core. The displacement is calculated in three different ways, using the formulae listed in Table 2, and the calculations are done for the two frequencies 0.1 Hz and 1.0 Hz.

A few degrees into the lit region, the exact solution is seen to oscillate slightly about the direct P-wave values.

In the transition region, our approximate formula is verified. (This formula is plotted only for values of Δ such that

$$\left(\frac{hR}{2R_1R_2}\right)^{\frac{1}{2}} \mid a-y \mid < \frac{1}{2} \quad : \text{ see}$$

our derivation of potentials in Section (2.3) above.)

Beyond the geometrical shadow boundary, the decay with distance becomes exponential. At 125°, the P-wave with frequency 0.1 Hz has decreased slowly to about 1/6 th of its amplitude at 105° and the shadow of the core is not very sharp. But for the 1.0 Hz P-wave, the amplitude decreases at 118° to 1/10 of its amplitude at 110°, and the shadow is very pronounced. Note that the shadow boundary shift is very small (i.e. the amplitude at the geometrical shadow boundary is almost exactly one-half the amplitude of the incident P-wave), a result we noted in section (2.4) above for the cylindrical problem.

SV-SV results

Figure 14 displays a normalized amplitude of total horizontal SV-wave displacement due to a SV-wave point source, with scattering from a spherical fluid core. The displacement is calculated in three different ways, using the formulae listed in Table 3, and the calculations are done for the two frequencies 0.03 Hz and 0.2 Hz.

A few degrees into the lit region, the exact solution is seen to oscillate about the direct SV-wave values, ranging up to 30% above and below the ray theory amplitudes.

In the transition region, our approximate formula is verified.

Beyond the geometrical shadow, the decay with distance becomes exponential. At 125°, the SV-wave with frequency 0.03 Hz has decreased to about 1/11 of its amplitude at 105° - so at this

low frequency, SV is more effectively shadowed than P-waves of half the wavelength. For the 0.2 Hz SV-wave, the amplitude decreases at 118° to 1/10 of its amplitude at 110°, and the shadow is thus as sharp as for P-waves of about one third the wavelength. Note that the shadow boundary is 111.3° at 0.03 Hz, and 112.3° at 0.2 Hz.

SH-SH Results

Figure 15 displays a normalized amplitude of total horizontal SV-wave displacement due to a SH-wave point source, with scattering from a spherical fluid core (or spherical cavity). The displacement is calculated in three different ways, using the formulae listed in Table 4, and the calculations are done for the two frequencies 0.03 Hz and 0.2 Hz.

A few degrees into the lit region, the exact solution is seen to oscillate slightly about the direct SH-wave values.

In the transition region, our approximate theory is again verified.

Beyond the geometrical shadow, the decay with distance becomes exponential. At 125°, the SH-wave with frequency 0.03 Hz has decreased to about $\frac{1}{4}$ of its amplitude at 105°, and the shadow is not sharp at all. Even for the 0.2 Hz SH wave, the amplitude only decreases at 118° to 1/3½ of its amplitude at 110°, so for a whole range of frequencies we may expect SH to be observable in the shadow

region. Note that the shadow boundary is 120.0° at 0.03 Hz, and 114.5° at 0.2 Hz. This is very different from the SV values at these frequencies.

In order that these numerical results may be compared to observable body wave amplitudes, we must first obtain the theoretical generalization of our basic method for transition regions to a model with radial heterogeneity. This generalization is obtained below in Section (2.6), but we first conclude the present section with a remark on amplitudes beyond the transition region.

Amplitude within the Shadow

The theoretical aspects of solutions in this region have been well understood for over fifty years (Watson, 1919), and we may briefly summarize by quoting, in our notation for the P-P scattering problem, the results of Scholte (1956) or of Duwalo and Jacobs (1959):

with source potential $\phi_i = \frac{e^{ihR}}{ihR}$ at the point (b,0), the total potential within the shadow is

$$\phi(r,\Delta) = \frac{1}{2}\sqrt{\pi}\, e^{-i\pi/4}\, \frac{e^{ih\left[\left(b^2-a^2\right)^{1/2} + a\left(\Delta-\cos^{-1}\frac{a}{b} - \cos^{-1}\frac{a}{r}\right)+\left(r^2-a^2\right)^{1/2}\right]}_{(ha)^{5/6}}}{\left(br\sin\Delta\right)^{1/2} h^2 \left(b^2-a^2\right)^{1/4} \left(r^2-a^2\right)^{1/4}} X$$

$$\sum_{n=0}^{\infty} \delta_n^{-\frac{1}{2}} \exp\left[i\,\delta_n \left(\Delta - \cos^{-1}\frac{a}{b} - \cos^{-1}\frac{a}{r}\right) (ha)^{\frac{1}{3}} \right] \qquad (2.5.8)$$

(Note that $\Delta > \cos^{-1}\frac{a}{b} + \cos^{-1}\frac{a}{r}$ for stations within the shadow.) The quantities $\{\delta_j\}$ in equation (2.5.8) are defined by their relation to the zeros $\{\nu_j\}$ of $\Omega_5 h^{(1)}_{\nu-\frac{1}{2}}(ha)$, as ν varies near ha in the complex order plane,

$$\nu_j = ha + (ha)^{1/3}\,\delta_j \,.$$

The problems associated with any practical use of equation (2.5.8) are that the complex numbers $\{\delta_j\}$ have not been easy to obtain. We give here a simple method for the evaluation, which relies on the expansion of Hankel functions, in the region $|\text{ORDER-ARGUMENT}| \sim |\text{ORDER}|^{1/3}$, in terms of Airy functions. Thus (Abramowitz and Stegun, 1964, p. 367)

$$h^{(1)}_{\nu-\frac{1}{2}}(ha) = \left(\frac{\pi}{2ha}\right)^{\frac{1}{2}}\left[\left(\frac{2}{\nu}\right)^{1/3}\left\{2e^{-i\pi/3}\ \mathrm{Ai}\left(ue^{2i\pi/3}\right)\right\}\right.$$

$$+\frac{2}{\nu}\left\{\frac{u}{5}\,e^{-i\pi/3}\ \mathrm{Ai}\left(ue^{2i\pi/3}\right)+\frac{3u^2}{10}\,e^{i\pi/3}\ \mathrm{Ai}'\left(ue^{2i\pi/3}\right)\right\}$$

$$\left.+\ 0\left\{\left(\frac{2}{\nu}\right)^{5/3}\right\}\right]$$

$$h^{(1)'}_{\nu-\frac{1}{2}}(ha) = \left(\frac{\pi}{2ha}\right)^{\frac{1}{2}}\left[\left(\frac{2}{\nu}\right)^{2/3}\left\{-\,2e^{i\pi/3}\ \mathrm{Ai}'\left(ue^{2i\pi/3}\right)\right\}+0\left\{\left(\frac{2}{\nu}\right)^{4/3}\right\}\right]$$

where $u \equiv \left(\frac{2}{\nu}\right)^{1/3}\left(\nu-ha\right)$

(2.5.9)

These standard formulae are not quite suited to our purpose, since we wish to study $\Omega_5 H^{(1)}_{\nu-\frac{1}{2}}(ha)$ for varying ν near fixed ha - and then ν as a function of varying u in (2.5.9) is difficult to obtain. So we define instead the variable

$$t \equiv \left(\frac{2}{ha}\right)^{1/3}\left(\nu-ha\right) ,$$

and then

$$h^{(1)}_{\nu-\frac{1}{2}}(ha) = \left(\frac{\pi}{2ha}\right)^{\frac{1}{2}}\left[\left(\frac{2}{ha}\right)^{\frac{1}{3}} 2e^{-i\pi/3}\,\mathrm{Ai}\left(te^{2i\pi/3}\right)\right.$$

$$\left. + \frac{2}{ha}\left\{-\frac{2t}{15}\,e^{-i\pi/3}\,\mathrm{Ai}\left(te^{2i\pi/3}\right) - \frac{t^2 e^{i\pi/3}}{30}\,\mathrm{Ai}'\left(te^{2i\pi/3}\right)\right\} + O\left\{\left(\frac{2}{ha}\right)^{5/3}\right\}\right]$$

$$h^{(1)'}_{\nu-\frac{1}{2}}(ha) = \left(\frac{\pi}{2ha}\right)^{\frac{1}{2}}\left[\left(\frac{2}{ha}\right)^{2/3}\left\{-2e^{i\pi/3}\,\mathrm{Ai}'\left(te^{2i\pi/3}\right)\right\} + O\left\{\left(\frac{2}{ha}\right)^{4/3}\right\}\right].$$

Also,

$$h^{(1)'}_{\nu-\frac{1}{2}}(ka)\Big/h^{(1)}_{\nu-\frac{1}{2}}(ka) = i\left(1 - \nu^2/k^2a^2\right)^{\frac{1}{2}} + O\left(\frac{2}{ha}\right)$$

$$h^{(2)'}_{\nu-\frac{1}{2}}(h'a)\Big/h^{(2)}_{\nu-\frac{1}{2}}(h'a) = -i\left(1 - \nu^2/h'^2a^2\right)^{1/2} + O\left(\frac{2}{ha}\right) .$$

These expansions may be used to write $\Omega_5 h^{(1)}_{\nu-\frac{1}{2}}(ha)$ as an asymptotic series in increasing powers of $\left(\frac{2}{ha}\right)^{1/3}$. The first three terms may be written explicitly, giving

$$\Omega_5 h^{(1)}_{\nu-\frac{1}{2}}(ha) = \left(\frac{\pi}{2ha}\right)^{1/2} h^{(1)}_{\nu-\frac{1}{2}}(ka)\,(k^2a^2-2h^2a^2)^2 \left(\frac{2}{ha}\right)^{1/3} 2e^{-i\pi/3}\left[F(z) + 0\left(\frac{2}{ha}\right)\right]$$

where $z \equiv te^{-i\pi/3}$ and

$$F(z) \equiv Ai(-z) + \left(\frac{2}{ha}\right)^{1/3} M_1 e^{7i\pi/6}\, Ai'(-z) -$$

$$\left(\frac{2}{ha}\right)^{2/3}\left\{\left(\frac{1}{15} + M_2\right) ze^{i\pi/3}\, Ai(-z) + \frac{z^2 e^{4i\pi/3}}{60}\, Ai'(-z)\right\}$$

with model constants

$$M_1 = \left[\frac{4\beta^3}{\alpha^3}\left(1-\frac{\beta^2}{\alpha^2}\right)^{1/2} + \frac{\alpha'\rho'}{\alpha\,\rho}\left(1-\frac{\alpha'^2}{\alpha^2}\right)^{-1/2}\right]\left(1-\frac{2\beta^2}{\alpha^2}\right)^{-2}$$

$$M_2 = \frac{4\beta^2}{\alpha^2}\left(1-\frac{\beta^2}{\alpha^2}\right)^{-1}$$

We assume that the problem of finding zeros, in the ν-plane, of $\Omega_5 h^{(1)}_{\nu-\frac{1}{2}}(ha)$ reduces to finding zeros $\{z_j\}$, in the complex z-plane, of F(z). And then we may use equation (2.5.8) with $\delta_j = z_j\, e^{i\pi/3}/2^{1/3}$. But F(z) is simple to evaluate for real values z = 0.0, 0.1, 0.2, - since Airy functions are tabulated for these values. The zeros in fact have a small imaginary part, and if x_j^o is a real value near the zero z_j, we take Newton's rule $z_n \sim x_j^o - F(x_j^o)/F'(x_j^o)$ as our approximation. Note that $F'(x_j^o)$ is also simple to evaluate, since we may use the relation $\frac{d}{dz}\ Ai'(-z) = z\ Ai(-z)$. We find below in Section (2.6) that zeros may also be found in this way for media which are radially heterogeneous, and we defer computation of the $\{\delta_j\}$ until this generalization has been obtained.

The above method is certainly simple to use, and is probably more accurate than the existing methods for homogeneous media of

(i) Scholte (1956), who essentially has a graphical method of solving $F_1(z) = 0$, in which $F_1(z)$ is obtained from our F(z) by ignoring the terms in $0\left\{\left(\frac{2}{ha}\right)^{2/3}\right\}$.

(ii) Duwalo and Jacobs (1959), who first assume that the $\{\nu_j\}$ are near the zeros which arise in a study of the "soft" boundary condition, $\phi = 0$ on $r = a$. But in fact, for geophysical parameters, the $\{\nu_j\}$ are near the zeros which arise in a study of the "hard" boundary condition, $\phi' = 0$ on $r = a$.

(iii) Phinney and Alexander (1966), who use a numerical search directly in the ν-plane, but with a Hankel function evaluation which ignores the term $\left(\frac{\pi}{2ha}\right)^{\frac{1}{2}} \left(\frac{2}{\nu}\right) \{\}$ in our expansion (2.5.9).

In section (2.7) below, we examine the relation of the real part of δ_1 to observable array measurements $\frac{dT}{d\Delta}$, and of the imaginary part of δ_1 to amplitude decay in the shadow. But we first extend the results of this section to a study of spherically symmetric inhomogeneous Earth models.

2.6 Body Waves in Radially Heterogeneous Media, Scattered by one Solid/Fluid Interface

In this section we generalize some of the results of (2.5) to the transition zone set up by a point source embedded in an isotropic elastic medium, with a fluid elastic spherical scatterer. Density and elastic parameters are smoothly varying functions of radius (although discontinuous across the fluid/solid boundary). Many special techniques have been developed for finding frequency dependent corrections to ray theory, and such general solutions are commonly stated as asymptotic series in inverse powers of frequency. (See e.g. Seckler and Keller, 1959 a, b; Yanovskaya, 1968; Babich, 1961; together with the discussion in Bennett and Chessell (1969), in which such methods are compared with the known and exact solution for a specific inhomogeneous problem.) The first term in such expansions

is identifiable as the product of geometrical spreading (which is independent of frequency) and a phase integral carried along the ray path from source to receiver.

However, we see in sections (2.2) - (2.5) above, for several source-scatterer-receiver geometries, that the ray spreading term itself requires modification in the transition zone. In this section we find the modification in transition zones, to geometrical spreading, for spherically symmetric media. We neglect those additional terms which arise in a more complete discussion of P/SV/upgoing/downgoing interactions in continuously varying media - which terms typically are of lower order in frequency than the modified geometrical spreading term. Our method involves some of the results of Chapter 3, together with a generalization of the Hankel functions used in (2.2) - (2.5) above. We restrict our discussion to media with subcritical velocity gradients, that is, media in which a ray bottoms at every depth. A new method is also developed for evaluating amplitudes in the shadow region.

The Expansion of Source Potential, and Potential-Displacement Relation

It is shown below in Chapter 3 that the assignment "P-wave component" of displacement in smoothly varying inhomogeneous media may usefully be discussed by the form

$$f(r)^{-1} \text{ grad} \left[\frac{\phi(\underset{\sim}{r},t)}{\sqrt{\rho(r)}} f(r) \right]$$

where f is a known function of radius and $\phi(\underset{\sim}{r},t)$ is a potential which satisfies

$$\nabla^2\phi(\underset{\sim}{r},t) - \frac{\rho(r)}{\lambda(r) + 2\mu(r)} \frac{\partial^2\phi}{\partial t^2}(\underset{\sim}{r},t) + \varepsilon_p(r)\ \phi(\underset{\sim}{r},t) = A(\underset{\sim}{r},t).$$

$\varepsilon_p(r)$ is known, and $A(\underset{\sim}{r},t)$ is an expression of the coupling between $\phi(\underset{\sim}{r},t)$ and a similar SV-wave potential. We discuss a steady state point source of P-waves $\propto e^{-i\omega t}$, at distance b from the center of the fluid scatterer (see Figure 16). Since we are here assuming the neglect of continuous scattering, and neglect of terms which are of at least one lower order in frequency than geometrical spreading, we may approximate to an uncoupled Helmholtz equation

$\nabla^2\phi(\underset{\sim}{r},t) + h^2(r)\ \phi(\underset{\sim}{r},t) = 0$, with $h^2 = \frac{\omega^2\rho}{\lambda+2\mu}$ and P-wave displacement $\underset{\sim}{u} = \frac{1}{\sqrt{\rho(r)}}$ grad $\phi(\underset{\sim}{r})$. This approximation is discussed further in section (3.4a), below.

The source potential of our homogeneous solutions above is in the form $\frac{e^{ihR}}{ihR}$, with R as the straight-line source receiver distance, and constant wave number h. If such a source ϕ_i is placed in the heterogeneous medium, we may thus characterize it as the solution to

$$\nabla^2\phi_i + \left(h(r)\right)^2 \phi_i = \frac{\delta(r-b)\ \delta(\Delta)}{2\pi r^2\ \sin\Delta} \times \left(\frac{-4\pi}{ih(b)}\right) \quad , \text{ together}$$

with a radiation condition expressing amplitude decay with distance away from the source.

In Appendix II we follow some of the methods of Friedman (1951) and Seckler and Keller (1959b) to obtain an exact series for ϕ_i in the form

$$\phi_i(r,\Delta) = \sum_{n=0}^{\infty} \left(n + \tfrac{1}{2}\right)\ g_n^{(1)}(r_>) \left[\ g_n^{(1)}(r_<) + g_n^{(2)}(r_<)\right]\ P_n(\cos\ \Delta)$$

where

$r_> = \max(r,b)$, $r_< = \min(r,b)$, and the $g_n^{(\ell)}(r)(\ell=1,2;n=0,1,2,....)$

are analogous to spherical Hankels $h_n^{(\ell)}(hr)$. We use the approximation (cf Debye methods for Hankel functions)

$$g_n^{(1)}_{(2)}(r) \approx \frac{e^{\mp i\pi/4}}{\left(h(b)\right)^{1/2}} \cdot \frac{1}{r} \cdot \frac{1}{\left[h^2(r) - \left(\frac{n+\frac{1}{2}}{r}\right)^2\right]^{\frac{1}{4}}} \times$$

$$\exp \pm i \int_{r_o}^{r} \left[\ h^2(\xi) - \left(\frac{n+\frac{1}{2}}{\xi}\right)^2\ \right]^{\frac{1}{2}} d\xi \qquad (2.6.1)$$

in the region above the radius r_o - which radius is the deepest penetration of the ray with ray parameter $p \equiv \frac{n+\frac{1}{2}}{\omega}$, so r_o depends on n.

By writing the boundary conditions of continuous stresses and radial displacement on the solid/fluid interface at r = a in terms of our weakly coupled potentials for P and SV, we may obtain the formula for scattered potential of PcP as

$$\phi_s(r,\Delta) \approx -\frac{1}{2}\int_0^\infty 2\nu g^{(1)}_{\nu-\frac{1}{2}}(b)\; g^{(1)}_{\nu-\frac{1}{2}}(r) \qquad X$$

$$\left[\; 1 + \frac{\Omega g^{(2)}_{\nu-\frac{1}{2}}(a)}{\Omega g^{(1)}_{\nu-\frac{1}{2}}(a)} \;\right] \quad Q^{(2)}_{\nu-\frac{1}{2}}(\cos\Delta)\,d\nu \qquad (2.6.2)$$

where the operator Ω is equivalent to the Ω_5 of equation (2.5.2), but now operating on $g^{(\ell)}_n(a)$ instead of $h^{(\ell)}_n(ha)$.

For a discussion of amplitudes within the transition zone, we again use

$$\phi_s = -\frac{1}{2}\left[a_1(r,\Delta) + a_2(r,\Delta)\right] \qquad \text{where}$$

$$a_1(r,\Delta) \equiv \int_0^{h(a)a} 2\nu g^{(1)}_{\nu-\frac{1}{2}}(b)\; g^{(1)}_{\nu-\frac{1}{2}}(r)\; Q^{(2)}_{\nu-\frac{1}{2}}(\cos\Delta)\; d\nu \qquad \text{and}$$

$$a_2(r,\Delta) \equiv \int_0^{h(a)a} 2\nu g^{(1)}_{\nu-\frac{1}{2}}(b)\; g^{(1)}_{\nu-\frac{1}{2}}(r)\; \frac{\Omega g^{(2)}_{\nu-\frac{1}{2}}(a)}{\Omega g^{(1)}_{\nu-\frac{1}{2}}(a)}\; Q^{(2)}_{\nu-\frac{1}{2}}(\cos\Delta)\; d\nu \;+$$

$$\int_{h(a)a}^{\infty} 2\nu g^{(1)}_{\nu-\frac{1}{2}}(b)\; g^{(1)}_{\nu-\frac{1}{2}}(r)\left[\, 1 + \frac{\Omega g^{(2)}_{\nu-\frac{1}{2}}(a)}{\Omega g^{(1)}_{\nu-\frac{1}{2}}(a)}\,\right] Q^{(2)}_{\nu-\frac{1}{2}}(\cos\Delta)\; d\nu \;.$$

Evaluation of the Scattered (PcP) Potential

For the approximation of $a_1(r,\Delta)$, equation (2.6.1) is available. We see

$$a_1(r,\Delta) = \int_0^{h(a)a} \frac{2\nu}{h(b)}\cdot\frac{1}{rb}\cdot\frac{1}{\left[h^2(r)-\left(\frac{\nu}{r}\right)^2\right]^{\frac{1}{4}}}\; X \qquad (2.6.3)$$

$$\frac{1}{\left[h^2(b)-\left(\frac{\nu}{b}\right)^2\right]^{\frac{1}{4}}}\cdot\frac{1}{\left(2\pi\nu\,\sin\Delta\right)^{\frac{1}{2}}}\; e^{i\Phi(\nu)}\; d\nu$$

where

$$\Phi(\nu) \equiv \int_{r_o(\nu)}^{r} \left[h^2(\xi) - \left(\frac{\nu}{\xi}\right)^2 \right]^{\frac{1}{2}} d\xi \quad +$$

(2.6.3 Continued)

$$\int_{r_o(\nu)}^{b} \left[h^2(\xi) - \left(\frac{\nu}{\xi}\right)^2 \right]^{\frac{1}{2}} d\xi + \nu\Delta - \frac{3\pi}{4}$$

Then, to examine the saddlepoint of (2.6.3) we obtain

$$\frac{d\Phi}{d\nu} = -\nu \left\{ \int_{r_o(\nu)}^{r} \left[h^2(\xi) - \left(\frac{\nu}{\xi}\right)^2 \right]^{-\frac{1}{2}} \frac{d\xi}{\xi^2} \quad + \right.$$

(2.6.4)

$$\left. \int_{r_o(\nu)}^{b} \left[h^2(\xi) - \left(\frac{\nu}{\xi}\right)^2 \right]^{-\frac{1}{2}} \frac{d\xi}{\xi^2} \right\} + \Delta$$

But the angular separation may be expressed by

$$\Delta = \omega p \left\{ \int_{r_o(\omega p)}^{r} \left[h^2(\xi) - \frac{\omega^2 p^2}{\xi^2} \right]^{-\frac{1}{2}} \frac{d\xi}{\xi^2} + \int_{r_o(\omega p)}^{b} \left[h^2(\xi) - \frac{\omega^2 p^2}{\xi^2} \right]^{-\frac{1}{2}} \frac{d\xi}{\xi^2} \right\}$$

(see e.g. Bullen, (1963), equation 7.7.2), where p is the ray parameter for the direct wave from source $(b,0)$ to receiver (r,Δ). Hence $\Phi(\nu)$ is stationary when $\nu = \omega p$, and standard techniques are available for evaluation of formula (2.6.3). However, to apply them we need to differentiate $\frac{d\Phi}{d\nu}$ again, and this presents certain manipulative difficulties since the integrands of (2.6.4) are singular at a limit of the integration which itself depends on ν. In Appendix III it is shown that

$$\left. \frac{d^2\Phi}{d\nu^2} \right|_{\nu=\omega p} = -1 \Big/ \left[\omega \frac{\partial^2 T}{\partial \Delta^2} \right] \quad , \text{ where T is the travel}$$

time from source to (r,Δ) along the direct ray. From (2.6.3) we find

$$\Phi(\omega p) = \int_{\text{source}}^{\text{receiver}} h(s)\, ds - \frac{3\pi}{4} \quad , \text{ where s is an element of}$$

length along the direct ray, and by crossing half the saddle we have

$$a_1(r,\Delta) \approx \frac{1}{irbh(b)} \left[\frac{\omega p}{\sin \Delta \; h(b) \; h(r) \; \cos i(b) \; \cos i(r)} \cdot \left(-\omega \frac{\partial^2 T}{\partial \Delta^2} \right) \right]^{\frac{1}{2}} X$$

$$e^{i \int_{\text{source}}^{\text{receiver}} h(s)\, ds}$$

$$X \left\{ 1 + e^{-i\pi/4} \sqrt{2} \int_0^{\left[-\pi\omega \frac{\partial^2 T}{\partial \Delta^2} \right]^{\frac{1}{2}} h(a)a - \omega p} e^{i\pi/2\beta^2} \, d\beta \right\}$$

Using (2.6.1) to evaluate $a_2(r,\Delta)$, we find

$$a_2(r,\Delta) \approx \frac{e^{-i\pi/4}}{ih(b)br} \sqrt{\omega p} \; \frac{e^{i \int_{\text{source}}^{\text{receiver}} h(s) ds}}{\sqrt{h(b)h(r)\pi/2 \sin\Delta \; h(b)h(r) \cos i(b) \cos i(r)}}$$

$$X \quad \left[h(a)a \right]^{\frac{1}{3}} \quad C_p(\omega)$$

where now

$$C_p(\omega) = \frac{1}{\left(h(a)a\right)^{\frac{1}{3}}}\left\{ \int_0^{h(a)a} \frac{\Omega g^{(2)}_{\nu-\frac{1}{2}}(a)\, d\nu}{\Omega g^{(1)}_{\nu-\frac{1}{2}}(a)} + \int_{h(a)a}^{\infty} \left[1 + \frac{\Omega g^{(2)}_{\nu-\frac{1}{2}}(a)}{\Omega g^{(1)}_{\nu-\frac{1}{2}}(a)} \right] d\nu. \right.$$

Using the geometrical spreading methods of Bullen (1963), or by the method of Appendix II and the evaluation above for $a_1(r,\Delta)$, we know

$$\phi_i(r,\Delta) = \frac{1}{ibrh(b)} \left[\frac{\omega p}{\sin\Delta\ h(b)\ h(r)\ \cos i(b)\ \cos i(r)} \cdot \left(-\omega \frac{\partial^2 T}{\partial \Delta^2}\right)\right]^{\frac{1}{2}}$$

$$X\ e^{i\int_{\text{source}}^{\text{receiver}} h(s)ds} X \left(1 + 0\left(\frac{1}{\omega}\right)\right)$$

and so finally we have

$$\phi = \phi_i + \phi_s = \frac{1}{2}\left\{ 1 - e^{-i\pi/4}\sqrt{2}\int_0^{\left[\frac{h(a)a-\omega p}{-\pi\omega\,\frac{\partial^2 T}{\partial\Delta^2}}\right]^{1/2}} e^{i\pi/2\tau^2}\,d\tau \right.$$

$$\left. - e^{-i\pi/4}\left(\frac{2}{-\pi\omega\,\frac{\partial^2 T}{\partial\Delta^2}}\right)^{1/2}\left(h(a)a\right)^{1/3} C_p(\omega) + 0\left(\frac{1}{\omega}\right)\right\} x\ \phi_i \qquad (2.6.5)$$

(The factor $\frac{1}{2}\{\ \}$ is the correction to geometrical spreading. If we approximate the Fresnel integral within the transition zone, we obtain the standard form (e.g. (2.5.5)), but now generalized to radially heterogeneous media.)

The methods used above to obtain a formula for ϕ make frequent reference to the "direct ray between source and receiver," but for a receiver slightly beyond the shadow boundary there is no such ray. Equation (2.6.5) is then useful only for the lit region (up to and including the geometrical shadow boundary), although it still has meaning just within the shadow, in the sense that if the velocity profile $\alpha(r)$ in the mantle is continued (in some smooth way) below the radius $r = a$, then all the terms in the right hand

side of equation (2.6.4) have meaning. The value of ν which makes ϕ stationary is still ωp, where now p is the ray parameter for a ray which is travelling in the extended profile, and bottoms below r = a. All the symbols in equation (2.6.5) can now be defined, but we must acknowledge that this procedure is not very useful, since it is difficult to justify any particular choice of mantle extension below r = a. However, we are able to give below a separate discussion of the shadow region - back to and including the geometrical shadow boundary - and also find a numerical method for the evaluation of $C_p(\omega)$.

It follows from (2.6.5) that the shadow boundary, defined as the distance $\Delta_{\frac{1}{2}}$ at which amplitudes are one-half that given by ray theory for the direct wave, satisfies

$$\omega p(\Delta_{\frac{1}{2}}) - h(a)a = \left(h(a)a\right)^{1/3} \left[\text{Re } C_p(\omega) + \text{Im } C_p(\omega) \right] \quad .$$

An alternative derivation of part of the solution (2.6.5) is given in Appendix V; the method there is to use Fresnel-Kirchhoff theory, and (2.6.5) is reproduced without the term involving $C_p(\omega)$. However, although the shifts are dependent on $C_p(\omega)$, we see below that there is an important and practical application of (2.6.5) which

does not require evaluation of the $C_p(\omega)$ term.

Diffracted Arrivals within the Shadow

Even though diffracted first arrivals within the core shadow zone are small, the large surface area of the Earth within this zone has yielded considerable data on amplitudes and amplitude decay rates (Gutenberg, 1960; Sacks, 1966, 1967; Alexander and Phinney, 1966). We may show by the methods of Friedman (1951) and Nussenzweig (1965) that the total P-wave potential within the shadow is

$$\phi(r,\Delta) = -\int_0^\infty \nu\, g^{(1)}_{\nu-\frac{1}{2}}(b)\, g^{(1)}_{\nu-\frac{1}{2}}(r)\, \frac{\Omega g^{(2)}_{\nu-\frac{1}{2}}(a)}{\Omega g^{(1)}_{\nu-\frac{1}{2}}(a)}\, Q^{(2)}_{\nu-\frac{1}{2}}(\cos\Delta)\, d\nu \qquad (2.6.6)$$

(cf equation (2.6.2) for PcP), where the operator Ω is equivalent to the Ω_5 of equation (2.5.2). And $\phi(r,\Delta)$ is evaluated by summation of the residue series of this integral, which series is determined by the zeros $\{\nu_j\}$ of $\Omega g^{(1)}_{\nu-\frac{1}{2}}(a)$ as ν varies in the complex order plane near the value $h(a)a$. Thus we find (using the formula 2.6.1)

$$\phi(r,\Delta) = \frac{e^{3i\pi/4}}{h(b)br}\left(\frac{2\pi\ h(a)a}{h(b)\ h(r)\ \cos i\ (b)\ \cos i(r)\ \sin\Delta}\right)^{1/2}\cdot$$

$$\sum_j R_j \exp\left[-i\,\delta_j\left(h(a)a\right)^{1/3}\left(\Delta-\Delta_1-\Delta_2\right)\right]\cdot \exp i\,\Phi_{DIFF} \qquad (2.6.7)$$

where (see Figure 19)

Φ_{DIFF} = phase along the diffraction path from (b,0) to (r,Δ)

$$= \int_S^{C_1} h(s)\,ds + h(a)a\ (\Delta-\Delta_1-\Delta_2) + \int_{C_1}^{P} h(s)\,ds$$

$$R_j = \Omega g^{(2)}_{\nu-\frac{1}{2}}(a) \Big/ \frac{d}{d\nu}\ \Omega g^{(1)}_{\nu-\frac{1}{2}}(a)\ \Big|_{\nu\,=\,\nu_j}$$

and δ_j is related to ν_j by $\nu_j = h(a)a + \delta_j\left(h(a)a\right)^{1/3}$.

It remains to calculate the δ_j for specific models, and we give here a generalization of the successful method, set out in Section (2.5), for a model with individually homogeneous mantle and core.

The definition of $\Omega g^{(1)}_{\nu-\frac{1}{2}}(a)$ is different from the definition of $\Omega_5 h^{(1)}_{\nu-\frac{1}{2}}(ha)$ (see (2.5.2)) in just two respects. (i) We replace the spherical Hankel functions by $g^{(\ell)}_{\nu-\frac{1}{2}}(a)$, $g^{(\ell)}_{\nu-\frac{1}{2},S}(a)$, $g^{(\ell)}_{\nu-\frac{1}{2},K}(a)$ (where the latter two are the radial functions for mantle S and core P-wave velocity structures), and (ii) the effect of intrinsic coupling adds to each of the constituent functions $p^{(\ell)} - u'^{(2)}$ in (2.5.2) an unknown term which is one order lower in frequency. Since (see Appendix VI), for ν near $h(a)a$,

$$a \frac{d}{dr} g^{(1)}_{\nu-\frac{1}{2}}(r) \Big|_{r=a} = g^{(1)}_{\nu-\frac{1}{2}}(a). \quad 0\left\{\left(h(a)a\right)^{\frac{2}{3}}\right\}, \text{ and each of}$$

$g^{(1)}_{\nu-\frac{1}{2}}$ and $g^{(1)'}_{\nu-\frac{1}{2}}$ may be written as an asymptotic series in ascending powers of $\left(\frac{2}{h(a)a}\right)^{\frac{2}{3}}$, it follows that we may write $\Omega g^{(1)}_{\nu-\frac{1}{2}}(a)$ as an asymptotic series in ascending powers of $\left(\frac{2}{h(a)a}\right)^{1/3}$. We find the first three terms of this series are contained in

$$\Omega g^{(1)}_{\nu-\frac{1}{2}}(a) = g^{(1)}_{\nu-\frac{1}{2},S}(a)\left[\left(k^2(a)a^2-2\nu^2\right)^2 \; g^{(1)}_{\nu-\frac{1}{2}}(a)\right.$$

$$-\left(4\nu^2a^2R_1 + \frac{k^4(a)a^4\rho'}{\rho R_2}\right) g^{(1)'}_{\nu-\frac{1}{2}}(a)$$

$$\left. + g^{(1)}_{\nu-\frac{1}{2}}(a) \cdot 0\left\{\left(\frac{2}{h(a)a}\right)^{-9/3}\right\}\right] \text{ where} \qquad (2.6.8a)$$

$$R_1 = i\,k(a)\left(1 - \frac{\nu^2}{k^2(a)a^2}\right)^{1/2} \qquad R_2 = -\,i\,h'(a)\left(1 - \frac{\nu^2}{h'^2(a)a^2}\right)^{1/2}.$$

In Appendix VI we provide a study of $g^{(1)}_{\nu-\frac{1}{2}}(a)$ as ν varies in the complex order plane near $h(a)a$, and from the formulae (VI.9) we have

$$\Omega g^{(1)}_{\nu-\frac{1}{2}}(a) = \left(\frac{\pi}{2h(b)(1-x(a))}\right)^{1/2} g^{(1)}_{\nu-\frac{1}{2},S}(a)\left[k^2(a)\,a^2-2h^2(a)a^2\right]^2 \; X$$

$$\left[\frac{2(1-x(a))}{h(a)a}\right]^{1/3} 2e^{-i\pi/3}\left[G(z) + 0\left(\frac{2(1-x(a))}{h(a)a}\right)\right]$$

where $x(r)$ is the normalized velocity gradient $\frac{r}{\alpha}\frac{d\alpha}{dr}$,

z is given by $\nu = h(a)\, a \left[1 + \frac{z\, e^{i\pi/3}}{2} \left(\frac{2(1-x(a))}{h(a)a} \right)^{2/3} \right]$,

$$G(z) \equiv Ai(-z) + \left(\frac{2(1-x(a))}{h(a)a} \right)^{1/3} N_1\, e^{7i\pi/6}\, Ai'(-z) -$$

$$\left(\frac{2(1-x(a))}{h(a)a} \right)^{2/3} \left\{ \left(\frac{1}{15} + N_2 \right) z e^{i\pi/3}\, Ai(-z) + \left(\frac{1}{60} + N_3 \right) z^2 e^{4i\pi/3} Ai'(-z) \right\}$$

(2.6.8b)

with model constants (evaluated at the core-mantle boundary, $r = a$)

$$N_1 = \left[\frac{4\beta^3}{\alpha^3} \left(1 - \frac{\beta^2}{\alpha^2} \right)^{1/2} + \frac{\alpha'\rho'}{\alpha\rho} \left(1 - \frac{\alpha'^2}{\alpha^2} \right)^{-1/2} \right] \left(1 - \frac{2\beta^2}{\alpha^2} \right)^{-2}$$

$$N_2 = \frac{4\beta^2}{\alpha^2 \left(1 - \frac{2\beta^2}{\alpha^2} \right)} - \frac{x}{30(1-x)} - \frac{y}{30(1-x)^2}$$

where $y(r) = \frac{r^2}{\alpha} \frac{d^2\alpha}{dr^2}$, and

$$N_3 = -\frac{2x}{15(1-x)} - \frac{2y}{15(1-x)^2}$$

We assume that the problem of finding zeros, in the ν-plane, of $\Omega g^{(1)}_{\nu-\frac{1}{2}}(a)$ reduces to finding zeros $\{z_j\}$, in the complex z-plane, of $G(z)$. And then we may use equation (2.6.7) with

$\delta_j = z_j\, e^{i\pi/3}\{1-x(a)\}^{2/3}/2^{1/3}$. The zeros of G(z) are simple to evaluate, if we use Newton's rule with trial zeros which are real (see (2.5) above), and we have calculated δ_1 and δ_2 for several Earth models.

Our results are displayed in Table 5, for three different models of the core mantle boundary (each model specified by $(\alpha,\beta,\rho,\alpha',\rho',\ a)$), and in each basic model we specify different choices for x and y (the first and second derivatives of velocity gradient at the bottom of the mantle). The calculation is done for the four periods 50 seconds, 20 seconds, 5 seconds, and 1 second, and it is apparent from Table 5 that δ_1 and δ_2 are quite sensitive to the choice of x, the first derivative of velocity. In Figure 20ab we show the real and imaginary parts of δ_1, plotted against frequency for several different choices of x, in the model with a Gutenberg-Bullard density jump.

We discuss below in (2.7) the significance of these numerical results, and conclude this section with some final remarks on our method of finding residue series for the shadow zone.

(i) A knowledge of the imaginary part of δ_1 alone is probably sufficient to give accurately the amplitude decay rate - since Im $\delta_2 \sim 3 \times$ Im δ_1, and then Im $\delta_{j+1} \sim 1 +$ Im δ_j, so the terms in equation (2.6.7) are essentially negligible for $j > 1$. The factors R_j may be evaluated (which permits a study of absolute amplitudes, rather than amplitude decay rates) by using the methods of Appendix VI

to discuss $g^{(2)}_{\nu-\frac{1}{2}}(a)$.

(ii) The constant N_1 is approximately 10 for realistic Earth models, and, since $\left(\frac{2}{h(a)a}\right)^{1/3} \leq \frac{1}{10}$ only for periods less than about 1 second, it follows that the behavior of G(z) is characterized by the quantity Ai'(-z). The zeros of Ai'(-z) are in fact appropriate to the "hard" boundary condition, $\phi' = 0$ on r = a. Some authors (e.g. Johnson, 1969) have made the assumption $\phi = 0$ on r = a, the "soft" boundary condition, which is equivalent to characterizing G(z) by the leading term, Ai(-z). The "soft" boundary condition is a valid approximation for hollow core models (as we have seen above in section (2.2) and Figure 5), for then N_1 is approximately $3\frac{1}{2}$.

(iii) Phinney and Alexander (1969) have given a discussion of the effect of a velocity gradient on diffracted P in the shadow zone. They have given values of Im δ_1 based on the assumption that the effect of a velocity gradient on zeros of $\Omega g^{(1)}_{\nu-\frac{1}{2}}(a)$ is merely to multiply $\{\nu_j - h(a)a\}$ by the factor $\left(1-x(a)\right)^{2/3}$, where the δ_j are calculated for the homogeneous case from a computer study of $\Omega_5 h^{(1)}_{\nu-\frac{1}{2}}(ha)$. We see from our method above that this scaling assumption is justified for either the "hard" or "soft" boundary condition. However, the gradient x(a) appears in G(z) outside the argument of the Airy functions. So the assumption is not justified for our case of a mixed boundary condition. It does provide a useful approximation and the values of δ_2 in our Table 5, for $x \neq 0$, $y = 0$,

can be found to within about 5% from the values for $x = 0$, $y = 0$.

(iv) SV-diffraction may be discussed with our method above, but this is of little interest since SH dominates S arrivals in the shadow zone (see Figures 14 and 15). It is simple to find the poles relevant to SH diffraction, and they are the zeros of

$$\left[a \frac{d}{dr} g^{(1)}_{\nu-\frac{1}{2},S}(r) \Big|_{r=a} - g^{(1)}_{\nu-\frac{1}{2},S}(a) \right] \equiv D(\nu) \text{ (say)}$$

near $\nu = k(a)a$. From (VI.9) it follows that $D(\nu)$ may be written as an asymptotic series in ascending powers of $\left[\frac{2(1-x(a))}{k(a)a}\right]^{2/3}$ (where now $x(r) = \frac{r}{\beta}\frac{d\beta}{dr}$), and that the series is strongly dominated by the first term $Ai'(-z)$, where z is given by

$$\nu = k(a)a \left[1 + \frac{z\, e^{i\pi/3}}{2} \left(\frac{2(1-x(a))}{k(a)a} \right)^{2/3} \right].$$

Hence we take $z_1 = 1.019$, $z_2 = 3.248$, $z_3 = ...$, which are the zeros of $Ai'(-z)$. Values of $\{z_j\}$ may be found which are slightly more accurate, by obtaining explicitly the second term in the expansion $D(\nu)$. This will permit a qualitative appreciation of large "curvature" in the velocity profile.

(v) By performing numerically the integration in equation (2.6.6) we may directly obtain amplitudes in the vicinity of the shadow boundary, and within the shadow. (N. B. equation (2.6.6) is valid for the whole forward scattering region, $\Delta > \Delta_1$.) We evaluate part of the integrand (which is needed only near $\nu = h(a)a$) by using methods developed above for $a_1(r,\Delta)$. Thus, expanding $\Phi(\nu)$ in (2.6.3) as a Taylor series and using Appendix III, we can show for ν varying near $h(a)a$ that

$$-\nu g^{(1)}_{\nu-\frac{1}{2}}(r)\; g^{(1)}_{\nu-\frac{1}{2}}(b)\; Q^{(2)}_{\nu-\frac{1}{2}}(\cos\Delta) \sim \frac{e^{i\pi/4}}{h(b)rb}\quad F_1(\text{ray geometry},\ \omega)\quad X$$

$$\exp i\left[\ \nu(\Delta-\Delta_1-\Delta_2) + \frac{(\nu-h(a)a)^2}{2}\left(\frac{1}{-\omega\,\frac{\partial^2 T}{\partial\Delta^2}}\right)\right] \tag{2.6.10}$$

where

$$F_1(\text{ray geometry},\omega) \equiv \left(\frac{h(a)a}{h(r)h(b)\cos i(r)\cos i(b)2\pi\sin\Delta}\right)^{1/2}$$

$$\exp i\left[\int_S^{C_1} h(s)ds + \int_{C_2}^{P} h(s)\,ds\right] .$$

The formula (2.6.10) is valid for all Δ between (but not including) the antipodal region (near $\Delta = \pi$) and back to and including the geometrical shadow boundary ($\Delta = \Delta_1 + \Delta_2$). F_1 may be found from a knowledge of the ray geometry in Figure 19, and $\frac{\partial^2 T}{\partial \Delta^2}$ is the ray theory value of $\frac{\partial p}{\partial \Delta}$ obtained in the limit as $\Delta \to \Delta_1 + \Delta_2$ from below. Unfortunately, we must not expect (2.6.10) to be useful within the lit region, since there the direct arrival bottoms at some radius $r_1 > a$, and it is inappropriate to discuss approximations only near $\nu = h(a)a$.

We have in (2.6.8) a formula for $\Omega g^{(1)}_{\nu-\frac{i}{2}}(a)$, and similar methods for $\Omega g^{(2)}_{\nu-\frac{i}{2}}(a)$ give the result

$$\frac{\Omega g^{(2)}_{\nu-\frac{i}{2}}(a)}{\Omega g^{(1)}_{\nu-\frac{i}{2}}(a)} \sim e^{2i\pi/3} \left\{ Ai(te^{-2i\pi/3}) + \frac{i N_1}{q} e^{-2i\pi/3} Ai'(te^{-2i\pi/3}) \right.$$

$$\left. - \frac{1}{q^2} \left[\left(\frac{1}{15} + N_2 \right) tAi(te^{-2i\pi/3}) + \left(\frac{1}{60} + N_3 \right) t^2 e^{-2i\pi/3} Ai'\left(te^{-2i\pi/3} \right) \right] \right\} X$$

$$\left\{ Ai(te^{2i\pi/3}) + \frac{i N_1}{q} e^{2i\pi/3} Ai'(te^{2i\pi/3}) \right.$$

$$\left. - \frac{1}{q^2} \left[\left(\frac{1}{15} + N_2 \right) tAi(te^{2i\pi/3}) + \left(\frac{1}{60} + N_3 \right) t^2 e^{2i\pi/3} Ai'(te^{2i\pi/3}) \right] \right\}^{-1}$$

(2.6.11)

where $\frac{1}{q} = \left(\frac{2(1-x(a))}{h(a)a} \right)^{1/3}$, $t = \frac{2(\nu - h(a)a)\ q^2}{h(a)a}$, and

N_1, N_2, N_3 are the model constants defined in (2.6.8).

With formulae (2.6.10) and (2.6.11) we may now compute the integral (2.6.6). The technique is essentially the same as our method in section (2.5), in which we obtained the P-P response in a medium with individually homogeneous mantle and core - instead of the Hankel functions of (2.5), we here use Airy functions. Hence we use below the terms "Hankel function method" and "Airy function method" in referring to these similar techniques. Note that the results of the Airy function method may be compared with ray theory right at the grazing distance $\Delta = \Delta_1 + \Delta_2$ by using the geometrical spreading formula

$$\Phi_{DIRECT}(r,\ \Delta_1 + \Delta_2) = \frac{e^{-i\pi/2}}{h(b)rb} \left(-2\pi\omega \frac{\partial^2 T}{\partial \Delta^2} \right)^{1/2} F_1\ (\text{ray geometry},\ \omega) \qquad (2.6.12)$$

which gives the potential for the direct P arrival (ignoring PcP). We expect that (2.6.6) will give just $\frac{1}{2}\ \Phi_{DIRECT}\ (r,\ \Delta_1 + \Delta_2)$ for sufficient high frequencies.

A simple numerical experiment to check the more general Airy function method is to use it for calculating $\phi(r, \Delta)$ in a model with a homogeneous mantle, and to compare these values with $\phi(r, \Delta)$ calculated by the Hankel function method (using IFLAG = 1 in the program described in Appendix IV) for the same model. The results of such an experiment, using the "model 1" of Phinney and Alexander (1966), are given for amplitudes in Figure 21, and for $\frac{\partial T}{\partial \Delta}$ (i.e. $\frac{1}{\omega}\frac{\partial}{\partial \Delta}$ phase$\left[\ \phi(r, \Delta)\right]$) in Figure 22. The computation is done for the two frequencies 0.1 Hz and 1 Hz, and we see that there is excellent agreement between the two methods. The amplitude curves for 1 Hz run together throughout the shadow region, as do the $\frac{\partial T}{\partial \Delta}$ curves for 1 Hz. For 0.1 Hz the amplitude curves run together just within the shadow region, and the $\frac{\partial T}{\partial \Delta}$ curves run together throughout the shadow. We may further note that the agreement of the two methods within the lit region is fortuitous, since the Airy function method would not be so accurate there in a medium for which $\frac{\partial^2 T}{\partial \Delta^2}$ varied more strongly with distance. (In such a medium we should use (2.6.5), with numerical integration of (2.6.11) for calculation of $C_p(\omega)$.) Within the shadow, the Airy function method is probably more accurate, since we may show that (2.6.10) and (2.6.11) neglect only terms in $0\left(\frac{2}{ha}\right)$, whereas we have used the Hankel function method with a HANKEL package which in fact obliges us to neglect terms in $0\left(\left[\frac{2}{ha}\right]\right)^{2/3}$.

(vi) Our formula (2.6.11) may be used for investigating the reflection coefficient for a solid-fluid spherical interface, at near grazing incidence. We may define this coefficient (following Scholte) by assuming that the primary downgoing wave $g^{(2)}_{\nu-\frac{1}{2}}(r)\ Q^{(2)}_{\nu-\frac{1}{2}}(\cos\Delta)$ gives rise to an upgoing wave (LL) $\dfrac{g^{(2)}_{\nu-\frac{1}{2}}(a)}{g^{(1)}_{\nu-\frac{1}{2}}(a)} \cdot g^{(1)}_{\nu-\frac{1}{2}}(r)\ Q^{(2)}_{\nu-\frac{1}{2}}(\cos\Delta)$ on reflection at the radius r = a. Then for the longitudinal-longitudinal reflection coefficient, we have (by the method following our (2.4.1))

$$(LL) = \frac{-g^{(1)}_{\nu-\frac{1}{2}}(a)}{g^{(2)}_{\nu-\frac{1}{2}}(a)} \cdot \frac{\Omega g^{(2)}_{\nu-\frac{1}{2}}(a)}{\Omega g^{(1)}_{\nu-\frac{1}{2}}(a)} \qquad (2.6.13)$$

We recall that wave functions with order $\nu - \frac{1}{2}$ are associated with rays having the ray parameter $\dfrac{r \sin i(r)}{\alpha(r)} = \dfrac{\nu}{\omega}$. So the phenomena of PcP reflection may be discussed by evaluating (2.6.13) with $\nu = h(a)a \sin i(a)$. SV waves within the mantle, and K waves within the core, are also generated, with respective angles of incidence j(a) and i'(a) (say) at the radius r = a.

Let us first evaluate (LL) within the lit zone, where i(a) is less than 90°. We have from a study of the Riccati equation for $g^{(\ell)'}_{\nu-\frac{1}{2}}(r) \Big/ g^{(\ell)}_{\nu-\frac{1}{2}}(r)$ the result

$$g^{(2)\,\prime}_{\nu-\frac{1}{2}}(a) \Big/ g^{(2)}_{\nu-\frac{1}{2}}(a) \sim \pm i\, h(a)\, \mathrm{cosi}(a),$$ and then from

formula (2.6.8a) we find after some reduction

$$(LL) \sim \frac{\beta^2/\alpha^2 \sin 2i \sin 2j + \frac{\rho'\alpha'}{\rho\alpha}\frac{\cos i}{\cos i'} - \cos^2 2j}{\beta^2/\alpha^2 \sin 2i \sin 2j + \frac{\rho'\alpha'}{\rho\alpha}\frac{\cos i}{\cos i'} + \cos^2 2j} \qquad (2.6.14)$$

which is exactly the coefficient of reflection for a plane wave incident upon the plane boundary between homogeneous solid and fluid half-spaces.

But to evaluate (LL) for near grazing angles of incidence, $i(a) \sim 90°$, we must use the results of Appendix VI and formula (2.6.11), giving approximately

$$(LL) \sim - \frac{\left[\mathrm{Ai}\left(t\, e^{-2i\pi/3} \right) + \frac{i\, N_1}{q}\, e^{-2i\pi/3}\, \mathrm{Ai}'\left(t\, e^{-2i\pi/3} \right) \right]}{\left[\mathrm{Ai}\left(t\, e^{2i\pi/3} \right) + \frac{i\, N_1}{q}\, e^{2i\pi/3}\, \mathrm{Ai}'\left(t\, e^{2i\pi/3} \right) \right]} \qquad (2.6.15).$$

where t, N_1, q are defined in (2.6.11).

We may now assess the approximation (2.6.14) for near grazing angles, and see that at i(a) = 90°, this plane wave/plane boundary approximation gives (LL) $\sim$ - 1. The same value is returned by (2.6.15), with t = 0, only if $N_1/q \ll 1$. But we have already noted (see (ii) above) that N_1 is approximately 10 for realistic Earth models, and $N_1/q \sim 1$ for periods as short as 1 second. We see from the second terms in the numerator and denominator of (2.6.15) that, very roughly, (LL) $\sim e^{-i\pi/3}$ for periods greater than two or three seconds. Such a phase change then leads to amplitudes of (P + PcP) which are very different from the amplitudes calculated with the phase reversal predicted by (2.6.14), and hence, for geophysical problems, the plane boundary approximation is completely inadequate at near grazing incidence.

A summary of the more important techniques developed in this section is now provided by calculating the total potential $\phi(r,\Delta)$ for 2 second P waves in an inhomogeneous Earth model. Our results are given in Table 6 for seven degrees into the lit zone, and in Table 7 for seven degrees into the shadow. The particular Earth

model is specified by

(a) values of $p = p(\Delta)$ within the lit zone. The eight values we use are listed in Table 6: they are an approximation to CIT208, described by Johnson (1969),

(b) a geometrical shadow boundary distance of 97°, and a surface source,

(c) velocities, densities and radius for the core mantle boundary, We take α = 13.68 km/sec, β = 7.3 km/sec, ρ = 5.6 gm/cc, α' = 8.1 km/sec, ρ' = 10.0 gm/cc, $\frac{d\alpha}{dr} = -0.2\frac{\alpha}{r}$, and a = 3481 km.

In the lit zone we may find $\frac{\partial^2 T}{\partial \Delta^2}$ as a function of distance. Values of this quantity are listed in Table 6, and for interest we also tabulate the time interval between ray arrivals PcP and P. By numerically integrating (2.6.11) for 2 second waves, we find $C_p(\pi) = (0.3797, 0.0086)$. Then for the half amplitude distance (i.e. the distance Δ at which $|\phi|$ is one half the value given by ray theory) we may obtain from (2.6.5) the result

$$p(\Delta_{\frac{1}{2}}) - 4.440 = 0.020 \text{ sec/degree},$$

indicating a shadow boundary shift of about 1.2° into the lit zone.

Using formula (2.6.5) it is simple to calculate the correction factor $\sum' \{\ \}$ which multiplies the geometrical ray term ϕ_i to give $\phi(r,\Delta)$. From the phase correction $\delta\Phi$ we may calculate (by a method

discussed below in some detail) the apparent $\frac{\partial T}{\partial \Delta}$ for 2 second waves. Values of the correction factor, and of the apparent $\frac{\partial T}{\partial \Delta}$, are given in Table 6.

In the shadow zone, we find $\phi(r,\Delta)$ by numerically integrating (2.6.6), using the method described above in note (v). The source normalization used in our computation gives for the direct wave at the geometrical shadow boundary (see (2.6.12)) a value 2.259, with zero phase, and the correction factor F listed in Table 7 is related to ϕ by

$$\phi(r,\Delta) = 2.259\ F \exp i\left[h(a)a\ (\Delta - 97\pi/180)\right].$$

Also given in Table 7 are values of $\ell n\ |\phi|$ and the apparent $\frac{\partial T}{\partial \Delta}$.

Our results in Tables 6 and 7 are encouragingly consistent at the geometrical shadow boundary distance of 97°. The correction factors in each table should here be equal, and we see that their amplitudes (0.425 and 0.404) differ by only 5%. There is some difference in their phase, but note that the rate of change of correction phase is almost continuous from lit zone to shadow (0.163 radians/degree at 96½°, and 0.161 at 97½°).

The numerical techniques described in this section may prove extremely powerful in discriminating between models of the bottom

of the mantle - and they may find application in studying regions of the upper mantle in which the velocity gradients are high. Our methods for studying the grazing incidence spherical reflection coefficient can also be used for the time domain problem discussed by Knopoff and Gilbert (1961) who make an approximation (in the Laplace transform plane) which corresponds to the assumption of a plane wave reflection coefficient, and who use scattering poles appropriate to the soft boundary condition.

In the following section we develop some applications of our new theoretical results.

2.7 Relevance of our Theory, and Applications to Seismic Data

The results of Section (2.5) show explicitly that, in a very simple Earth model, the amplitude of transition and shadow region body waves is quite strongly dependent on frequency. And in Section (2.6) we see that there is a frequency dependent correction to geometrical spreading for such regions in a more general class of models. We confine our discussion of these results to some qualitative remarks on amplitude, and introduce a quantitative study of the phase of body waves.

P-Wave Amplitudes in the Shadow of the Earth's Core

Sacks (1966) has given estimates of amplitude decay rate within the shadow, for the periods 25 and 2.5 seconds, and his results may be expressed in our notation (see Section (2.6), Table 5 and Figure 20) as Im $\delta_1(25) = 0.82$, Im $\delta_1(2.5) = 1.02$. We see in Figure 20b that both these points fit a theoretical curve for $\delta_1(T)$ in the model for which $x = -0.2$, and from Sacks' data we would conclude that 25 second and 2.5 second waves "see" the same average velocity gradient - and hence, the bottom (c. 100 kilometers) of the mantle has a constant velocity gradient $\frac{d\alpha}{dr} = -0.2\,\frac{\alpha}{r}$.

However, Alexander and Phinney (1966) and Phinney and Alexander (1969) give observed amplitude decay rates which differ from Sacks

in that (i) Im $\delta_1(T)$ varies for different regions of core surface, and (ii) even for data taken from one region of core surface, Im$\delta_1(T)$ does not increase with frequency $\frac{1}{T}$ in the way that all our theoretical curves (Figure 20b) would predict. We may draw conclusions from their data in the following way: the velocity gradient throughout most of the lower mantle is quite reliably known to be $\frac{d\alpha}{dr} = -0.28\,\frac{\alpha}{r}$ (see e.g. Hales, Cleary and Roberts, 1968), and so diffracted waves of 50 seconds period will "see" an averaged gradient that must be near $x = -0.28$ (since this wavelength is several hundred kilometers). From Figure 20b we thus expect Im $\delta_1(50) \sim 0.83$. Phinney and Alexander (1969) show two sets of Im $\delta_1(T)$ (obtained from two different events, but sampling approximately the same core surface region) which have Im $\delta_1(50) \sim 0.8$, and these sets show a slight <u>decrease</u> with increasing frequency to about Im $\delta_1(10) \sim 0.75$. The implication from our Figure 20b is then that 10 second waves are "seeing" a different average velocity gradient $x \sim +0.1$, and hence the velocity gradient must be changing rapidly as the core boundary is approached, indicating a low velocity zone.

The necessary resolution of theory with data must await a careful study of amplitude decay rates at even shorter periods - perhaps even 2 second and 1 second data may be used quantitatively, especially since amplitudes near the shadow boundary itself are now theoretically understood.

S-Wave Polarization

Theory

Within the transition region and the shadow zone of a simple Earth model (individually homogeneous mantle and core), we see in section (2.5) that there are considerable differences between the different body wave types. And in particular, we see from a comparison of Figures 14 and 15 that core diffraction will act as a polarizing mechanism for S-waves. SV waves decay with distance about three times as fast as SH waves, in this model, and the different decay rates are evident even 5° within the lit region. Hence, we should expect that a seismogram written at the geometrical shadow boundary, or beyond, would contain diffracted S only as SH. This conclusion may reasonably be maintained even for models with a radially heterogeneous mantle, since we have seen that it is the particular boundary conditions at the interface which are responsible for the particular observed departures from ray theory, and radial heterogeneity merely changes the location of geometrical shadow boundaries.

Observation

Gutenberg and Richter (1935, p. 331) state that S "is very large in the few degrees about 95°, but beginning about 99° it decreases with distance." They note that, although in several records S arrives chiefly as SH, the sharp polarization appears to depend on the mechanism of the shock. Also, "at distances beyond 105°.....the diffracted S appears to be recorded more frequently than diffracted P." Lehmann (1953) also describes 18 records of diffracted S in Europe for the Chilean earthquake of December 1, 1928, and notes that this

phase appears on N-component records, whereas SKS and SKKS were much larger on E-components. The azimuth from Europe is approximately WSW, and so the polarization is SH. Cleary, Porra and Reed (1967) describe twelve records of diffracted S at Canberra, for distances between 99° and 130°. Even though these authors have assumed that SV cannot theoretically be diffracted at all, one can see from their Figure 1 (which is three sets of the two horizontal components, each set from a different event) that SV is indeed insignificant relative to SH.

Conclusion

Thus, although fault-plane studies and calculation of radiation patterns must complement the discussion of any particular record, we may conclude from the number of published observations that our theoretical expectation is verified; diffracted S is polarized towards SH.

The Phase of Transition Region Body Waves

In equation (2.6.5) above we obtain a term which, in the transition region, corrects the simple ray theory of geometrical spreading. This new factor has a small imaginary part which is an implied function of distance Δ (since $p = p(\Delta)$), and so the apparent phase velocity measured by an array in the distance range 90° - 105° must be frequency dependent. If the phase of our correction factor is $\delta\Phi$, then an array measurement of the quantity $\frac{\partial T}{\partial \Delta}$ will be greater than the infinite frequency (or, ray theory) value p by an amount

$$\delta p = \frac{1}{\omega} \frac{\partial}{\partial \Delta} \delta \Phi \qquad (2.7.1)$$

This equation is obtained and studied by Johnson (1969), who also shows that the dispersion is large enough to affect array measurements. Johnson's methods of correction are based on the necessarily separate theories for lit and shadow regions, and hence they fail for the crucial region of grazing incidence. But it is in precisely this region that the correction is most important, since P and PcP cannot be separated in the time domain. (For example, the time difference is given as one second at 90° by Herrin et al (1968)). In order to see effects of ignoring the difference between $\frac{\partial T}{\partial \Delta}$ (obtained by measuring the phase velocity of a certain frequency component as it travels across an array) and the ray parameter p, we study the following simple Earth model, in which the known velocity structure is compared with the Herglotz-Wiechert inversion of uncorrected $\frac{\partial T}{\partial \Delta}$ values:

Numerical discussion of dispersion effect.

Suppose that a point source of 10 second P waves is established in the simple Earth model of Section (2.5). This mantle is homogeneous, with velocity 13.6 km/sec. The $\frac{\partial T}{\partial \Delta}$ values at different distances have been found for such a model from the rate of change of phase

(and the phase is computed from the exact displacement formula in Table 2, using the FORTRAN program described in Appendix IV). These $\frac{\partial T}{\partial \Delta}$ values are plotted in Figure 23 for the range $105.5° \leq \Delta \leq 124.5°$, together with

a) the known ray parameter, $p = \frac{6350}{13.6} \sin i \times \frac{\pi}{180}$ sec/degree

b) an approximation (discussed below) to $\frac{\partial T}{\partial \Delta}$ (10 sec.),

and c) the computed values of $\frac{\partial T}{\partial \Delta}$ for 1 second waves.

A method for the inversion of such $\frac{\partial T}{\partial \Delta}$ values is developed in Appendix VII from a suggestion due to Jeffreys (1966), who discusses the perturbation of velocities due to a perturbation in the p-Δ relation, and a brief slide rule calculation leads to the results:

For the 10 second "ray" emerging at $\left\{\begin{array}{l} 108.5° \\ 109.5 \\ 110.5 \\ 111.5 \\ 112.5 \\ 113.5 \end{array}\right.$, the deepest point

along the "ray" has radius $\left\{\begin{array}{l} 3710 \text{ km} \\ 3691 \\ 3672 \\ 3651 \\ 3630 \\ 3608 \end{array}\right\}$

and at this depth the "velocity is $\left\{\begin{array}{l} 13.600 \text{ km/sec} \\ 13.595 \\ 13.585 \\ 13.574 \\ 13.561 \\ 13.545 \end{array}\right\}$.

Hence, for a model in which the velocity is in fact 13.6, we note

(i) that the inversion of $\frac{\partial T}{\partial \Delta}$ (10 sec) leads to a zone of slightly low velocity, with gradient

$$\frac{\partial \alpha}{\partial r} \sim - 0.05 \text{ km/sec/100 km}$$

at the bottom of the mantle,

(ii) that this small velocity gradient completely changes the ray pattern. For example, the ray emerging at 113.5° has its turning point at radius 3608 km if we invert the $\frac{\partial T}{\partial \Delta}$ (10 sec) curve, and about 3480 km if we invert the p curve. If we have some independent method which indicates that 113.5° is the distance of emergence of the grazing ray, then the $\frac{\partial T}{\partial \Delta}$ curve for 10 second data would give a core radius over 120 km too large - even though the dispersion is at most 4%. Sacks' (1966) estimate for a core radius of 3550 km may suffer from just this effect, since he obtains a grazing ray distance of 96° (determined by studying amplitudes at different frequencies) and then uses Jeffreys' solution giving depth of penetration of rays at various epicentral distances. Sack's estimate is over 70 km greater than the "standard" radius of 3473 km, determined originally by Jeffreys from P and ScS travel times.

(iii) If we extrapolate the calculated "velocity" profile down to the known core radius of our model, 3480 km, we obtain an erroneous velocity of 13.48 km/sec for the bottom of the mantle.

Of course, the observed $\frac{\partial T}{\partial \Delta} - \Delta$ relation for P-waves in the Earth is typically obtained with data from short period instruments, and the more relevant $\frac{\partial T}{\partial \Delta}$ (1 second) curve of Figure 21 shows better agreement with ray theory. But even this 1 second curve would give an incorrect core radius (see note (ii) above). Also the observations for S waves may be expected to be worse than the 10 second P wave $\frac{\partial T}{\partial \Delta}$.

It is apparent from the above numerical discussion that, in order to obtain the ray parameter p as a function of distance, we should like to be able to correct the observed $\frac{\partial T}{\partial \Delta}$ values which are associated with a given frequency. We have seen that this correction is small (although its cumulative effect can be significant), so trial-and-error guesses for $p=p(\Delta)$ are adequate. Given such a trial solution, the approximate $\frac{\partial T}{\partial \Delta}$ at a given frequency ω may be found by the following methods:

(A) In the transition zone we use equation (2.7.1), with $\delta\Phi$ obtained from the phase of the bracket { } in equation (2.6.5). It may be shown that the $C_p(\omega)$ term contributes merely a (small and) almost constant phase to $\delta\Phi$, and so this complicated term may be neglected in the differentiation (2.7.1), yielding

$$\delta p \sim \frac{1}{\omega} \frac{\partial}{\partial \Delta} \left[\text{Phase} \left\{ 1 - e^{-i\pi/4} \sqrt{2} \int_0^{\frac{h(a)a-\omega p}{}} \left(-\pi\omega \frac{\partial^2 T}{\partial \Delta^2} \right)^{1/2} e^{i\pi/2\tau^2} \, d\tau \right\} \right] \tag{2.7.2}$$

The formula is to be used for the transition region, starting at the distance for which P and PcP cannot be distinguished.

This method of calculating $\frac{\partial T}{\partial \Delta} = p + \delta p(\omega)$ has been used for the model discussed above, in which exact values of $\frac{\partial T}{\partial \Delta}$ (10 sec) are available. The resulting approximation is displayed in

Figure 23, and we see that (2.7.2) is indeed adequate for the transition region.

Further confirmation of the approximation is given by Figure 24, which is for SH waves in the same Earth model (see Table 4). Figure 24 displays computed $\frac{\partial T}{\partial \Delta}$ (33 sec) and $\frac{\partial T}{\partial \Delta}$ (5 sec), together with the approximation obtained from (2.7.2) for the 33 second curve, and also the ray parameter. These four quantities are plotted against distance, and we may note the agreement between the exact and approximate 33 second curve. (The agreement, however, is not quite so good as in Figure 21, as $|C_{SH}| >> |C_P|$.) Also note the disparity between these curves and the ray parameter.

A particular simple formula for δp can be found from (2.7.2) at the distance corresponding to the grazing ray (113.54° in Figures 23 and 24). At this distance we have

$$\delta p(\omega) = \left(\frac{-1}{\pi \omega} \frac{\partial^2 T}{\partial \Delta^2} \right)^{1/2} \qquad (2.7.3)$$

The resulting value of $\frac{\partial T}{\partial \Delta}$ at 113.54° for 10 and 1 sec. P waves is shown in Figure 23, and for 33 second and 5 second SH waves in Figure 24. All these values agree quite well with the exact values, and with the values obtained more directly from equation (2.7.2)

We thus note for the transition region (i) that $\delta p \to 0$ as $\omega \to \infty$. This is another demonstration that simple ray theory is arbitrarily good at sufficiently high frequencies.

(ii) δp is significant, since e.g. $\frac{\partial^2 T}{\partial \Delta^2} = 200$ sec/rad.^{2} in the simple model of section (2.5). So $\delta p \sim 0.055$ and 0.078 sec/deg. for 1 second and 2 second waves, respectively. But the precision of the measured $\frac{\partial T}{\partial \Delta}$ values may be reduced to between 0.025 and 0.050 sec/deg. (Johnson, 1969, p. 987) for P waves. The longer period of S waves gives, for example, $\delta p \sim 0.25$ sec/deg. at a period of 20 seconds.

(iii) The formulae (2.7.2) and (2.7.3) are independent of the boundary condition at r = a, This might be expected, since although different boundary conditions give different phase shifts at any given location, the rate of change of phase shift is primarily a geometrical property (and we may find it from the result of Appendix V). It may also be possible to use this correction δp for discontinuities within the Earth other than the core mantle boundary.

(iv) The explicit dependence on travel time curvature indicates δp is strongly influenced by the gradient of velocity near the bottom of the mantle. But note that if this curvature is very small, so that δp from (2.7.3) is negligible, it follows that P and PcP cannot be distinguished over larger distances. And then the accumulation of δp from (2.7.2) may be significant over these larger distances.

(B) In the shadow region. We see from the residue series (2.6.7) (which is dominated in the shadow region by the first term) that

$$\delta p(\omega) \sim \frac{1}{\omega} \text{ Re } \delta_1 . \quad \{h(a)a\}^{1/3} \qquad (2.7.4)$$

where δ_1 is a complex number specifying the zero of $\Omega g^{(1)}_{\nu-\frac{1}{2}}(a)$ nearest $\nu = h(a)a$. Re δ_1 is shown for several models in Table 5 and Figure 20a.

We thus note for the shadow region (i) that $\delta p(\omega) \to 0$ as $\omega \to \infty$. But $\delta p(\omega) \not\to 0$ as Δ increases. (We exclude here a discussion of the focussing effect as the source antipodes at $\Delta = 180°$ is approached.) So $\frac{\partial T}{\partial \Delta}$ tends asymptotically, with increasing distance, to a value which lies above the core grazing ray parameter. This asymptotic value, calculated from (2.7.4), is shown for the four different computed $\frac{\partial T}{\partial \Delta}$ curves in Figures 23 and 24, and the agreement within the shadow is very good.

(ii). It is unfortunate that the dispersion implied by (2.7.4) would be difficult to observe directly by the standard method, of calculating Fourier phase spectra for different seismograms written in the shadow zone along the same great circle path from the same seismic event. To appreciate this difficulty, let us calculate the change in phase $\delta\Phi$ due to dispersion over 20° within the shadow, for four different Fourier components. Since $\delta\Phi = \omega\, \delta p(\omega) \times 20 \times \frac{\pi}{180}$ we find (from (2.7.4) and Figure 20a, for the model with no velocity gradient) that $\delta\Phi$ for period $\begin{pmatrix} 50 \text{ secs} \\ 30 \\ 10 \\ 2 \end{pmatrix}$ is $\begin{pmatrix} 0.61 \text{ radians} \\ 0.75 \\ 1.17 \\ 2.37 \end{pmatrix}$, implying a phase delay $\frac{\delta\Phi}{\omega}$ of $\begin{pmatrix} 4.8 \text{ secs} \\ 4.0 \\ 1.9 \\ 0.7 \end{pmatrix}$. The value of $\delta\Phi$ for the 2 second period is probably not recoverable from seismic data, because of the high attenuation (by diffraction) of such a short period signal. The larger time delays associated with phases of longer period are bracketed by 3.4 ± 1.5 seconds, so it would be difficult to separate the dispersive effect from the effect of an erroneous choice of digitization origin time. The seismologist who lacked

a dispersion theory, and who obtained such values of $\delta\Phi$, might interpret them as being due to his having chosen an origin time for digitization which is about 3.4 seconds too early for synchronization with the arrival 20° within the shadow. If he based his choice of origin time on a standard Earth model, he might think either that the velocity at the bottom of the mantle should be about 0.4 km/sec lower than the standard value, or that he is observing some crustal or upper mantle travel time anomaly. Clearly, a more correct approach is to accept that phase delays may be, atleast partly, due to dispersion.

Our discussion of $\delta\Phi$ above is concerned with the resulting effect on measured phase velocities. However, we may also investigate the consequences of group delay, since for the group arrival time T we have

$$\frac{\partial T}{\partial \Delta} = p + \frac{\partial}{\partial \omega}\frac{\partial}{\partial \Delta}\delta\Phi \qquad (2.7.5)$$

The group delay, $\frac{\partial}{\partial \omega}\ \delta\Phi$, is found to be approximately half the phase delay, and so may still be big enough to introduce a significant delay in the arrival of P on a diffraction record.

Conclusion

In this chapter we have been able to extend the theory of body wave diffraction by the Earth's core. Emphasis has been given to the theory of arrivals near the geometrical shadow boundary, and we have found that an intuitive appreciation of reflection, based on a study of plane waves and plane boundaries, does not suffice for the spherical problem. We have also been able to obtain new theoretical methods for studying the deep shadow, in models with individually homogeneous mantle and core. And we have generalized all our methods to investigate the shadow boundary and deep shadow in radially heterogeneous models.

We have found that diffraction effects on seismic data are quite small, but their consistent biasing may introduce significant errors if the data is not corrected before inversion. Methods of correction are found, both for the lit region and the shadow region, which are simple in application to core diffraction studies, and which may be useful in regions of the upper mantle.

Chapter 3

Elastic Wave Propagation in Spherically Symmetric Inhomogeneous Media: Potential Methods

3.1 Introduction

It is well known that the vector wave equation of elastic displacement in a spherically symmetric, isotropic Earth model has three approximate high frequency solutions, referred to in the geophysical literature as P, SV and SH waves. The P + SV motion, and SH motion, are independent solutions, and P and SV are approximately independent in those regions of the model for which the gradients of physical properties are not too large. Further, in such slowly varying regions of the model, downgoing and upgoing waves of the same mode type are also approximately independent.

These approximations have led to extensive and highly successful ray theory methods for studying properties of the Earth (see for example, Bullen's, 1963 text). However, some data clearly require a more precise theory, not only because ray theory may actually be inadequate for certain problems, but also because we do not know how much confidence to place in ray theory in some borderline problems for which it may in fact be perfectly adequate.

For example, we might wish to know if mode coupling is especially significant near the bottom point along a P wave ray. Or, how are the amplitudes of PKPPKP precursors related to velocity profile.

The potential approach to P + SV coupling problems, in general inhomogeneous isotropic media, has really received very little attention. The methods reviewed by Ewing et al (1957, Chapter 7), which assume a specific dependence of physical properties with Cartesian depth, are useful only if the medium is weakly heterogeneous. In a series of papers, Hook (1959, 1961, 1962a,b, 1965) and Alverson, Gair and Hook (1963) have studied the separation of the elastic wave equation, for general media in which properties vary with Cartesian depth. (Such media are sometimes called "transversely homogeneous.") We find below that this work, which is widely referenced by other authors studying inhomogeneous media, contains a basic physical error which (a) leads to incorrect equations for (P + SV) when they are coupled, and (b) does not permit discov ery of the general solution in media for which P and SV decoupling is possible. However, Hook's equations, which have recently been generalized by Singh and Ben-Menahem (1969a,b) to study spherically symmetric media, may be modified with some manipulative effort to give a correct theory.

Zavadskii (1965a,b,c) has used potentials in very restricted types of inhomogeneous elastic media, to find solutions by methods which may be applicable in more general inhomogeneity. For example, in one problem (Zavadskii, 1965a) he is able to give the general P potential as a linear sum of four independent Whittaker functions, and the coupled SV potential is then a linear sum of the same four functions, with coefficients simply related to the coefficients appearing in the P potential.

There is some interest in discussing special media for which P and SV can decouple, since the method of Epstein (see Brekhovskikh's (1960) text, Chapter III) may then be used to evaluate the reflection and transmission coefficients for a transition layer. But in this chapter we emphasize a discussion of the P-SV coupling problem, and establish a framework in which we can see how the coupling occurs. In Section (3.2) we examine the choice of scalar fields, or dependent variables, for which we may most usefully develop potentials. In Section (3.3) we rearrange the vector equation, for elastic motion in spherically symmetric isotropic media, into a system of coupled equations, in which two of the unknowns are potentials for our choice of P and SV components of displacement. And in (3.4) we investigate several properties of the general coupled system of equations, and indicate

(as one of their consequences) that strong restrictions may now be placed on the kinds of transition zone, within the Earth's upper mantle, which can generate observable reflections. It seems that the extent of velocity gradient anomaly must be limited to within about 4 km, in order to explain the short-period reflection data.

3.2 A discussion of the choice of dependent variables

The displacement equation of elastic motion may be found by substituting for the stress tensor $\underset{\sim}{\underset{=}{\sigma}}(\underset{\sim}{x})$ in the conservation of momentum equation,

$$\rho(\underset{\sim}{x}) \frac{\partial^2 \underset{\sim}{u}}{\partial t^2} = \nabla \cdot \underset{\sim}{\underset{=}{\sigma}} + \rho \underset{\sim}{F} \qquad (3.2.1)$$

where $\underset{\sim}{F}(\underset{\sim}{x})$ is the applied force per unit mass, acting within the medium at $\underset{\sim}{x}$. We expect (from studies of displacement in locally homogeneous solids) that for general media there are two types of body wave solutions, one related to the velocity $\alpha(\underset{\sim}{x}) \equiv \left(\frac{\lambda(\underset{\sim}{x}) + 2\mu(\underset{\sim}{x})}{\rho(\underset{\sim}{x})} \right)^{1/2}$ and one to the velocity $\beta(\underset{\sim}{x}) \equiv \left(\frac{\mu(\underset{\sim}{x})}{\rho(\underset{\sim}{x})} \right)^{1/2}$. This expectation is in fact confirmed by the work of Karal and Keller (1959), and we wish here to associate a potential with each of the two types of solution.

Our basic motivation for using potentials is that we hope to develop wave equations which are approximately, or exactly, in the canonical form

$$\nabla^2 \Phi(\underset{\sim}{x},t) = \frac{1}{v^2(\underset{\sim}{x})} \frac{\partial^2 \Phi(\underset{\sim}{x},t)}{\partial t^2} \qquad (3.2.2)$$

Then with such potentials, we may immediately tap the accumulated store of known properties for canonical wave solutions.

We must expect that the choice of potentials, and the division of displacement into a P component and an S component, are somewhat arbitrary and artificial procedures in heterogeneous media, because there is a complete failure of almost all the familiar properties which define P and S in homogeneous media. Thus, in our problem, a longitudinal wave is not necessarily irrotational, a transverse wave is not necessarily solenoidal, and in general none of these four types of motion can alone satisfy the displacement equation. Somehow we must also reconcile the fact that a P wave within the (inhomogeneous) Earth is intuitively thought of as longitudinal, and S as transverse, whereas the only useful decomposition theorem for general vector fields is that providing irrotational and solenoidal components (with respectively a scalar and a vector potential).

A reconciliation of this last problem provides the key to obtaining our final choice of potentials, and in the remainder of this section we use intuitive methods to examine the approximate longitudinal and transverse ray solutions, in order to develop constraints on potentials which approximately satisfy (3.2.2). The constraints are found to arise from a study of the proportionality functions which relate cross sectional area of ray tubes to the wide choice of dependent variables, for which some form of ray

approximation is appropriate.

An elegant way to study the longitudinal and two transverse components of body wave displacement is to set up a system of "ray coordinates," in which these three components of motion are each parallel to a coordinate axis. Thus, for a point source A within a spherically symmetric medium, we follow Yosiyama (1933, 1941) and use coordinates (p,τ,ϕ) which we define (in that part of the medium which is reached by geometrical rays from the source), for the point B, as follows:

p is the ray parameter for the ray connecting A to B, assuming Snell's law and some specified velocity profile $v = v(r)$.

τ is the travel time integral, $\int_A^B \frac{ds}{v}$, taken along p = constant.

ϕ is the azimuthal coordinate of B from A in the spherical polar system (r,θ,ϕ), with $\theta = 0$ on A.

An intuitive guess that (p,τ,ϕ) form an orthogonal set is easily proved correct, since it is simple to obtain the formula for a distance element as

$$ds = \left[h_p^2 \, dp^2 + h_\tau^2 \, d\tau^2 + h_\phi^2 \, d\phi^2 \right]^{\frac{1}{2}}$$

We also see that h_τ is the velocity v.

The exact equations of motion in this coordinate system may be found from Love (1944, p.90), and we also use the constitutive relations of Love (op. cit., p. 54). Noting that this reference uses h_x which are the reciprocals of our more modern definition, we have

$$\rho\frac{\partial^2 u_p}{\partial t^2} = \frac{1}{h_p h_\tau h_\phi}\left[\frac{\partial}{\partial p}\left(h_\tau h_\phi \sigma_{pp}\right) + \frac{\partial}{\partial \tau}\left(h_\phi h_p \sigma_{p\tau}\right) + \frac{\partial}{\partial \phi}\left(h_p h_\tau \sigma_{\phi p}\right)\right]$$

$$+ \frac{\sigma_{p\tau}}{h_p h_\tau}\frac{\partial}{\partial \tau} h_p + \frac{\sigma_{\phi p}}{h_\phi h_p}\frac{\partial}{\partial \phi} h_p - \frac{\sigma_{\tau\tau}}{h_p h_\tau}\frac{\partial}{\partial p}\ h_\tau - \frac{\sigma_{\phi\phi}}{h_\phi h_p}\frac{\partial h_\phi}{\partial p} \qquad (3.2.3)$$

with similar equations (3.2.4) and (3.2.5) for $\rho\frac{\partial^2 u_\tau}{\partial t^2}$, $\rho\frac{\partial^2 u_\phi}{\partial t^2}$ obtained by cyclic permutation of suffices. Examples of the stress-displacement relations are

$$\sigma_{pp} = (\lambda + 2\mu)\left[\frac{1}{h_p}\frac{\partial u_p}{\partial p} + \frac{u_\tau}{h_p h_\tau}\frac{\partial h_p}{\partial \tau} + \frac{u_\phi}{h_\phi h_p}\frac{\partial h_p}{\partial \phi}\right] \qquad (3.2.6)$$

$$+ \lambda\left[\frac{1}{h_\tau}\frac{\partial u_\tau}{\partial \tau} + \frac{u_\phi}{h_\tau h_\phi}\frac{\partial h_\tau}{\partial \phi} + \frac{u_p}{h_p h_\tau}\frac{\partial h_\tau}{\partial p}\right]$$

$$+ \lambda\left[\frac{1}{h_\phi}\frac{\partial u_\phi}{\partial \phi} + \frac{u_p}{h_\phi h_p}\frac{\partial h_\phi}{\partial p} + \frac{u_\tau}{h_\tau h_\phi}\frac{\partial h_\phi}{\partial \tau}\right]$$

$$\sigma_{\tau\phi} = \mu\left[\frac{h_\phi}{h_\tau}\frac{\partial}{\partial \tau}\left(\frac{u_\phi}{h_\phi}\right) + \frac{h_\tau}{h_\phi}\frac{\partial}{\partial \phi}\left(\frac{u_\tau}{h_\tau}\right)\right] \qquad (3.2.7)$$

For waves with high frequency content, we expect spatial derivatives perpendicular to the ray path to be small relative to the derivative along the ray path, i.e. we assume

(i) that terms in $h_p \frac{\partial}{\partial p}$, $h_\phi \frac{\partial}{\partial \phi}$ are negligible in relation to $h_\tau \frac{\partial}{\partial \tau}$.

Further intuitive assumptions must be made before the ray theory formulae are obtained from our equations of motion, and two of them are

(ii) that u_p, u_τ, u_ϕ are independent, and

(iii) that the time dependence at $B(p,\tau,\phi)$ is proportional to the source time dependence $T(t)$ (say), but delayed by an amount τ.

With these three assumptions, we can show how (3.2.3), (3.2.3) and (3.2.4) give the ray theory for respectively SV, P, and SH waves. Consider, for example, SV:

In (3.2.3) we are to substitute for the stress components, and these are approximated by taking $u_\tau = u_\phi = 0$ (see assumption (ii)), and by neglecting terms which do not contain at least one $\frac{\partial}{\partial\tau}$ operation on u_p (see assumption (i)). Thus, the needed stress components are simply

$$\sigma_{pp} = \sigma_{\phi p} = \sigma_{\tau\tau} = \sigma_{\phi\phi} = 0, \text{ and } \sigma_{p\tau} = \mu \frac{h_p}{h_\tau} \frac{\partial}{\partial\tau}\left(\frac{u_p}{h_p}\right)$$

From (3.2.3) we can show

$$\rho \frac{\partial^2 u_p}{\partial t^2} = \frac{1}{h_p h_\tau h_\phi} \frac{\partial}{\partial\tau}\left[\mu \frac{h_p h_\phi}{h_\tau} \frac{\partial u_p}{\partial\tau}\right] \qquad (3.2.8)$$

and assumption (iii) implies that we expect a solution in the form

$$u_p(p,\tau,\phi,t) = T(t-\tau)\, U(p,\tau,\phi)$$

where T(t) is the source time function. From (3.2.8) we find

$$\left(\rho - \frac{\mu}{h_\tau^2}\right) \ddot{T}\, U = \frac{1}{h_p h_\tau h_\phi} \frac{\partial}{\partial \tau}\left(\mu \frac{h_p h_\phi}{h_\tau}\right) \left[T \frac{\partial U}{\partial \tau} - \dot{T}\, U \right]$$

$$+ \frac{\mu}{h_\tau^2} \left[T \frac{\partial^2 U}{\partial \tau^2} - 2\, \dot{T} \frac{\partial U}{\partial \tau} \right] \qquad (3.2.9)$$

Since from our definition of ray coordinates it follows that $h_\tau = \beta$, the left hand side of (3.2.9) is zero. If we make the final assumption

(iv) that the time variation of source properties is sufficiently rapid, i.e.

$$\left| \frac{\dot{T}}{T} \right| >> \left| \frac{1}{U} \frac{\partial U}{\partial \tau} \right| \text{ and } \left| 2 \frac{1}{\frac{\partial U}{\partial \tau}} \frac{\partial^2 U}{\partial \tau^2} \right|$$

then

$$U \frac{\partial}{\partial \tau}\left(\mu \frac{h_p h_\phi}{\beta}\right) + 2 \frac{\partial U}{\partial \tau} \mu \frac{h_p h_\phi}{\beta} = 0,$$

and the ray approximation for transverse SV displacement at B is obtained as

$$u_p(B) \propto T(t-\tau)\sqrt{\frac{\beta}{\mu h_p h_\phi}}\Bigg|_B, \quad u_\tau = u_\phi = 0 \tag{3.2.10}$$

Note that $h_p h_\phi$ has the physical interpretation of being proportional to the cross-sectional area at B of a tube of S rays emanating from the source at A. So (3.2.10) is the geometrical spreading formula, weighted by a function of time and a function of radius. We could have obtained these functions from Bullen's (1963) energy formula, together with an approximation for the energy in SV. But our method above is instructive in emphasizing the assumptions (i) - (iv).

Results corresponding to (3.2.10) may be proved for the longitudinal P approximation. The same four assumptions are required, and

$$u_\tau(B) \propto T(t-\tau) \sqrt{\frac{\alpha}{(\lambda + 2\mu)\, h_p h_\phi}}\Bigg|_B \qquad (3.2.11)$$

For SH, we find that assumption (ii) may be dropped if the source has azimuthal symmetry, since we can show equations (3.2.3-5) have an exact solution $\underset{\sim}{u} = (0,0,u_\phi(p,\tau,t))$. Then approximately

$$u_\phi(B) \propto T(t-\tau) \sqrt{\frac{\beta}{\mu\, h_p h_\phi}}\Bigg|_B \qquad (3.2.12)$$

Now, suppose that Φ is some potential field due to a point source in the elastic medium, and that Φ approximately satisfies (3.2.2). This equation may be written out as a sum of differential operations in our ray coordinate system for the velocity profile v(r), and it can then be shown that

$$\Phi \propto T_\Phi(t-\tau) \sqrt{\frac{v}{h_p h_\phi}} \qquad (3.2.13)$$

where T_Φ is the potential source time function.

We are now in a position to provide necessary constraints on some of the potentials, weighted by functions of radius, which are suggested by Hook (1959, 1961). For example, suppose, for the SV wave due to an azimuthally symmetric point source, that we attempt to find a canonical potential χ in the form

$$\underset{\sim}{u}_{SV} = \frac{1}{f_{SV}(r)} \quad \text{curl curl} \left(r\, g_{SV}(r)\, \chi,\ 0,\ 0 \right)$$

(Here we are using spherical polar coordinates.) The radial component of the left hand side is (from (3.2.10)) proportional to

$$T(t-\tau) \sqrt{\frac{\beta}{\mu\, h_p h_\phi}} \quad \sin i \qquad (3.2.14)$$

where i is the angle between radial vector and ray path. The radial component of the right hand side is exactly

$$-\frac{g_{SV}}{f_{SV}}\ r \sin\theta\ \frac{\partial}{\partial\theta}\ \sin\theta\ \frac{\partial\chi}{\partial\theta} \sim -\frac{g_{SV}}{r f_{SV}}\ \frac{\partial^2\chi}{\partial\theta^2}$$

$$\sim -\frac{g_{SV}}{f_{SV}}\ \frac{r \sin^2 i}{h_\tau^2}\ \frac{\partial^2\chi}{\partial\tau^2} \quad \text{(since spatial changes of } \chi \text{ are principally along the ray direction)}$$

which, since $\frac{r \sin i}{h_\tau}$ is constant along a ray, is approximately proportional to

$$\frac{g_{SV}}{f_{SV}} \frac{\sin i}{h_\tau} \ddot{T}_\chi \sqrt{\frac{\beta}{h_p h_\phi}}$$

(from (3.2.13), with the potential χ, $v = \beta = h_\tau$, and time factor T_χ)

By a comparison with (3.2.14) we obtain the constraints

(a) $\ddot{T}_\chi(t-\tau) \propto T(t-\tau)$, which relates the source time functions of potential and displacement, and is satisfied most simply by $T_\chi = e^{i\omega t}$. If T(t) is to be a step function, then we may take $T_\chi(t) = 0$ $(t \leq 0)$, $= \frac{1}{2} t^2$ $(t \geq 0)$.

(b) $\frac{g_{SV}(r)}{f_{SV}(r)} \propto \frac{h_\tau}{\sqrt{\mu}} = \frac{1}{\sqrt{\rho(r)}}$, which we interpret below as allowing a free choice for f_{SV}, and then $g_{SV} = f_{SV}\, \rho^{-1/2}$.

To investigate P waves, we try the form

$\underset{\sim}{u}_P = \frac{1}{f_P(r)}$ grad $\{g_P(r)\ \Phi\}$ and obtain constraints for all possible canonical potentials as

(c) $\dot{T}_\Phi(t-\tau) \propto T(t-\tau)$ and

(d) $\frac{g_p(r)}{f_p(r)} \propto \frac{1}{\sqrt{\rho(r)}}$. We find below in (3.3) the reason for similarity between (d) and (b).

To investigate SH waves, we try

$\underset{\sim}{u}_{SH} = \frac{1}{f_{SH}(r)}$ curl $(r\, g_{SH}(r)\, \psi, 0, 0)$ and find

(e) $\dot{T}_\psi(t-\tau) \propto T(t-\tau)$,

(f) $\frac{g_{SH}}{f_{SH}} \propto \frac{1}{\sqrt{\mu}}$ (which differs from the P-SV constraints).

In the above discussion we have been able to relate geometrical spreading properties of longitudinal and transverse components of displacement to the spreading properties of canonical potentials. In the following section we abandon any reliance on the intuitive methods used above, and develop a choice of potentials for P, SV and SH which is partly suggested by the constraints (b), (d), and (f).

3.3 Wave Equations for Potentials

The use of potentials to study elastic displacement in inhomogeneous media requires a preliminary investigation, to check that our choice of potentials can cover all possible displacement solutions. In Appendix VIII we show that the general solution for displacement $\underset{\sim}{u}$ in a spherically symmetric, self-gravitating, non-rotating, elastic isotropic Earth may be written as

$$\underset{\sim}{u}(\underset{\sim}{r},t) = \frac{1}{f(r)} \left[\text{grad } \Phi(\underset{\sim}{r}, t) + \text{curl curl } \{ r\, \chi(\underset{\sim}{r}, t),0,0 \} \right]$$

$$+ \text{ curl } \{r\Psi(r,t),0,0\} \qquad (3.3.1)$$

where $f(r)$ is any specified twice continuously differentiable function of radius; Φ, χ and Ψ are potentials, and (Φ,χ) are independent of Ψ.

Toroidal motion

The wave equation for Ψ may be found from the substitution of (3.3.1), with $(\Phi,\chi) = (0,0)$, into equation (VIII.2). We note that Ψ is not influenced by the gravitational terms. Introducing the scaling factor $\mu^{\frac{1}{2}}$ (suggested by (f) in section (3.2)), we find for $T = \mu^{\frac{1}{2}} \Psi$ that

$$\underset{\sim}{u} = \text{curl}\left(\frac{rT}{\mu^{\frac{1}{2}}}, 0, 0\right) = \frac{1}{\mu^{\frac{1}{2}}}\left(0, \frac{1}{\sin\theta}\frac{\partial T}{\partial \phi}, -\frac{\partial T}{\partial \theta}\right)$$

$$= \underset{\sim}{M} \text{ (say), with}$$

$$\nabla^2 T - \frac{\rho}{\mu}\frac{\partial^2 T}{\partial t^2} + \varepsilon_T(r)\, T = 0 \qquad (3.3.2)$$

where $\varepsilon_T \equiv \frac{1}{4}\left(\frac{\mu'}{\mu}\right)^2 - \frac{1}{2}\frac{\mu''}{\mu} - \frac{2\mu'}{r\mu}$

Clearly this motion is toroidal, or SH (since $M_r = 0$), and (3.3.2) may be studied by the well known methods set out (for example) in Brekhovskikh's (1960) text.

Spheroidal motion, neglecting self-gravitation

The wave equations for (Φ,χ) may be found from the substitution of (3.3.1), with $\Psi = 0$, into (VIII.2), and we neglect here the gravitation terms. Introducing the scaling factor $\rho^{1/2}/f$ (suggested by (b) and (d) in section (3.2)), we define new potentials

$$(P,S) = \frac{\rho^{1/2}}{f}(\Phi,\chi)$$

so that $\underset{\sim}{u} = \underset{\sim}{L} + \underset{\sim}{N}$, where $\underset{\sim}{L} = \frac{1}{f}\,\text{grad}\,\frac{f}{\rho^{\frac{1}{2}}}\,P$, $\underset{\sim}{N} = \frac{1}{f}\,\text{curl}\,\text{curl}\left(\frac{rf}{\rho^{\frac{1}{2}}}\,S,0,0\right)$.

(3.3.3)

It follows from Appendix VIII that the applied force/unit mass may be written as

$$\frac{1}{f}\,\text{grad}\,\frac{f}{\rho^{\frac{1}{2}}}\,D(\underset{\sim}{r},t) + \frac{1}{f}\,\text{curl}\,\text{curl}\left(\frac{rf}{\rho^{\frac{1}{2}}}\,F(\underset{\sim}{r},t),\ 0,\ 0\right).$$

Then if A, B, C are introduced by

$$A \equiv \frac{\rho D}{\lambda+2\mu} + \nabla^2 P - \frac{\rho}{\lambda+2\mu}\frac{\partial^2 P}{\partial t^2} - \pi_o(r)\,\frac{\partial P}{\partial r} + \varepsilon_P(r)\,P \qquad (3.3.4)$$

$$C \equiv \frac{\rho F}{\mu} + \nabla^2 S - \frac{\rho}{\mu}\frac{\partial^2 S}{\partial t^2} - \sigma_o(r)\,\frac{\partial S}{\partial r} + \varepsilon_S(r)\,S \qquad (3.3.5)$$

$$B \equiv \frac{1}{\sin\theta}\frac{\partial}{\partial\theta}\sin\theta\,\frac{\partial C}{\partial\theta} + \frac{1}{\sin^2\theta}\frac{\partial^2 C}{\partial\phi^2} = r^2\,\nabla_T^2\,C \quad \text{(say)} \qquad (3.3.6)$$

(with π_o, σ_o, ε_P, ε_S given in Appendix IX) we find

$$\pi_o \rho \frac{\partial^2 P}{\partial t^2} + \pi_1 \frac{\partial P}{\partial r} + \pi_2 P + \frac{\lambda+2\mu}{r} \frac{\partial A}{\partial r} + \pi_3 A - \frac{\mu B}{r} + \pi_4 D = 0 \qquad (3.3.7)$$

and

$$\sigma_o \rho \frac{\partial^2 S}{\partial t^2} + \sigma_1 \frac{\partial S}{\partial r} + \sigma_2 S + \mu \frac{\partial C}{\partial r} + \left(\frac{\mu}{r} + \sigma_3 \right) C + \frac{\lambda+2\mu}{r} A + \sigma_4 F = 0 \qquad (3.3.8)$$

The twelve functions of radius ε_P, ε_S, π_o —— π_4, σ_o —— σ_4 are dependent on our specifiable function f(r), and they are all zero in homogeneous regions. Defining $g(r) = f'/f$, these twelve terms are listed in Appendix IX.

We may regard (3.3.4 - 8) as five equations in the unknowns (P,S,A,B,C,), with source functions D and F. Equation (3.3.7) is simply the radial component of the vector wave equation for displacement, and (3.3.8) is either an integral over θ of the θ component of this vector equation, or an integral over ϕ of the ϕ component. (We lose no generality by neglecting the arbitrary additional function of radius and time implied by these integrations, since it can only change S (and C) by an additional function of radius and time. And this does not change the resulting value of $\underset{\sim}{N}$ obtained in (3.3.3)). In the following section we establish some of the properties of our system of coupled equations, and see how P and S decouple at high frequencies.

3.4 Properties of the coupled potential equations

We show first how certain special sources excite solutions of the coupled system (3.3.4-8) which are identifiable at high frequencies as P and SV. A critical review of Hook's method is then given, and we conclude with a summary of some applications of our potential equations.

(a) High frequency decoupling of P and SV waves

By eliminating C from equation (3.3.7), and A from equation (3.3.8), we can obtain two fourth order equations for potentials P and S in the form

$$(\lambda + 2\mu)r\,\nabla^2\left[\frac{\rho D}{\lambda+2\mu} + \nabla^2 P - \frac{\rho\partial^2 P}{\lambda+2\mu\ \partial t^2}\right]$$

$$+ (\lambda+2\mu)r\left[\frac{\lambda+3\mu}{\mu}\,g + 2\left(\frac{\lambda'+2\mu'}{\lambda+2\mu}\right) - \frac{2\mu'}{\mu} - \frac{2\rho'}{\rho}\right]\frac{\partial}{\partial r}\left[\frac{\rho D}{\lambda+2\mu} + \nabla^2 P - \frac{\rho}{\lambda+2\mu}\,\frac{\partial^2 P}{\partial t^2}\right]$$

$$+ L(P) + a(r)D = -\,r^2\nabla_T^2\left[\sigma_o\rho\left(\frac{\partial^2 S}{\partial t^2} - F\right) + \sigma_1\,\frac{\partial S}{\partial r} + \sigma_2 S\right]$$

(3.4.1)

$$\mu r \nabla^2 \left[\frac{\rho F}{\mu} + \nabla^2 S - \frac{\rho}{\mu} \frac{\partial^2 S}{\partial t^2} \right]$$

$$+ \mu r \left[\frac{\lambda+3\mu}{\lambda+2\mu} g + \frac{2\mu'}{\mu} - \frac{2\mu'}{\lambda+2\mu} - \frac{2\rho'}{\rho} \right] \frac{\partial}{\partial r} \left[\frac{\rho F}{\mu} + \nabla^2 S - \frac{\rho}{\mu} \frac{\partial^2 S}{\partial t^2} \right]$$

$$+ N(S) + c(r)\ F = \pi_o \rho \left(\frac{\partial^2 P}{\partial t^2} - D \right) + \pi_1 \frac{\partial P}{\partial r} + \pi_2 P$$

(3.4.2)

where L and N are differential operators with terms up to second order. (Only the fourth and third order terms on the left hand side of these equations are needed explicitly, in our study here of high frequency decoupling.)

Now suppose that we choose the radial scaling function f(r) so that $\pi_o = 0$, and consider the point source with potentials

$$D = \frac{\delta(r-b)\ \delta(\theta)\ e^{-i\omega t}}{2\pi r^2 \sin\theta} \quad , \qquad F = 0 \qquad (3.4.3)$$

First, we match orders of discontinuity in the source region: it follows from (3.4.1) that the source discontinuity in the fourth and third order terms is at most a delta function (since $L(P) + a(r)\ D$ has at most a delta function discontinuity there), and hence that

$\nabla^2 P$ has a delta function discontinuity $-\frac{\rho D}{\lambda+2\mu}$ at the source. This last result then suggests a particular solution (or, particular integral) of the coupled system, valid throughout the region in which our potential P propagates as a wave: namely, that

$$\frac{\rho D}{\lambda+2\mu} + \nabla^2 P - \frac{\rho}{\lambda+2\mu}\frac{\partial^2 P}{\partial t^2} = 0(1).P \qquad (3.4.4a)$$

From (3.4.1) we see that our potential P is coupled to a potential S which is two orders in frequency down from P, i.e. since $\sigma_o \neq 0$ we have

$$S = 0(\omega^{-2})\ P \qquad (3.4.4b)$$

and from (3.4.2) we must then require cancellation of the fourth order terms in S (since $\pi_1 \neq 0$, $\pi_o = 0$), giving an eikonal equation for the S-potential phase.

The equations (3.4.4 a,b) have been obtained essentially by inspection, and hence are sufficient for a solution (P,S) to the coupled system. In Appendix X we give a proof that necessarily the right hand sides of (3.4.4a,b) are at most 0(1)P and $0(\omega^{-2})P$ (respectively), for the source-generated solution (P,S). In Appendix X we also show that the turning point formulae of Appendix VI are still appropriate for partial waves of the solution P to the coupled fourth order equations (3.4.1-2).

We may now claim that potentials P and S represent respectively P and SV waves, since they have the appropriate phases, and potential P has the correct geometrical property at sufficiently high frequencies (we may prove this from 3.4.4a). From the formulae (3.3.3), we see that the derived SV wave displacement is one order in frequency down from the derived P-wave displacement. The force potentials (3.4.3) then represent a P-wave source. Clearly, an SV-wave source can be discussed by the above method, with $\sigma_o = 0$ and force potentials

$$D = 0 \qquad F = \frac{\delta(r-b)\ \delta(\theta)\ e^{-i\omega t}}{2\pi r^2 \sin\theta} \qquad (3.4.5)$$

(b) Comparison with Hook's method

The development of potentials for P and SV in media varying along one Cartesian axis has been discussed by Hook (1959, 1961, 1962 a,b, 1965) and Alverson, Gair and Hook (1963), and the same methods extended to spherically symmetric media by Singh and Ben-Menahem (1969ab). The approach of these authors is superficially similar to our work, but implies conclusions which depart from our results in several respects.

Hook's method is essentially a search for displacement solutions which are of the form

$$\underset{\sim}{L}_o = \frac{1}{f_1(r)} \text{ grad } \Phi, \qquad \underset{\sim}{N}_o = \frac{1}{f_2(r)} \text{ curl curl } (r\chi, 0, 0) \qquad (3.4.6)$$

with two arbitrary scaling functions f_1 and f_2, instead of our single function f, and the above papers focus on the model constraints necessary for the existence of non-trivial uncoupled solutions $\underset{\sim}{u} = \underset{\sim}{L}_o$, $\underset{\sim}{u} = \underset{\sim}{N}_o$, in the absence of source terms. [Note that, for these solutions in such special media, our potential representation (3.3.3) is equivalent to (3.4.6): for $\underset{\sim}{u} = \underset{\sim}{L}_o$ we take S = 0 and $f = f_1$, and for $\underset{\sim}{u} = \underset{\sim}{N}_o$ take P = 0 and $f = f_2$.] Such model constraints are successfully found (see e.g. Singh and Ben-Menahem (1969a)), and are simple

to obtain in our notation by inspection of the coupled system (3.3.4-3.3.8): if $\underset{\sim}{u} = \underset{\sim}{L}_o$ is to be a solution then our S = 0. So C, B and A are zero and we require

$$\rho\pi_o \frac{\partial^2 P}{\partial t^2} + \pi_1 \frac{\partial P}{\partial r} + \pi_2 P = 0 \qquad \text{with } f_1 P = \rho^{\frac{1}{2}} \Phi, \text{ and}$$

$$\nabla^2 P - \frac{\rho}{\lambda+2\mu} \frac{\partial^2 P}{\partial t^2} - \pi_o \frac{\partial P}{\partial r} + \varepsilon_P P = 0$$

If P represents a non-trivial wave, we must require π_o, π_1 and π_2 to be zero. So $\pi_o = 0$ defines the choice of f_1, and then $\pi_1 = 0$, $\pi_2 = 0$ are the required necessary model constraints. (See Appendix IX for the definition of these functions.) Similarly, if $\underset{\sim}{u} = \underset{\sim}{N}_o$ is a non-trivial solution, then $\sigma_o = 0$ defines the choice of f_2 (and $f_2 \neq f_1$), and $\sigma_1 = 0$ and $\sigma_2 = 0$ are the required necessary constraints. Finally, it can be shown that if $\underset{\sim}{u} = \underset{\sim}{L}_o$ is a non-trivial solution, then so is $\underset{\sim}{u} = \underset{\sim}{N}_o$.

The special nature of these solutions is revealed by examining the representation (3.4.6), and we can see how

(i) these potentials are unnecessarily general, in that Hook and his co-workers have not given a proof that their representation (with two arbitrarily chosen scaling functions) is possible for every displacement solution. Thus, with a specified choice of (f_1, f_2), and a particular displacement solution $\underset{\sim}{u}_1$, we do not know if (Φ,χ) exist such that

$$\underset{\sim}{u}_1 = \frac{1}{f_1} \text{ grad } \Phi + \frac{1}{f_2} \text{ curl curl } (r\chi, 0, 0).$$

[We have supplied the necessary proof in Appendix VIII for our representation (3.3.3), which potentials are a subset of the set of potentials in (3.4.6) for different choices of f, f_1 and f_2.] Hence, we must regard as suspect those equations given by Hook (1961) which couple Φ and χ in his general media. We can also see

(ii) that Hook's application of (3.4.6) is too narrow, since, in the absence of source terms, P and SV are in general coupled even in those special media for which decoupling is possible. This fact, which we see by inspection of (3.4.1) and (3.4.2) with either π_o, π_1, π_2 all zero or σ_o, σ_1, σ_2 all zero, does follow from the analysis of Alverson, Gair and Hook (1963), who write the equations of motion ~~as~~

as $A\underset{\sim}{u} = \underset{\sim}{0}$ (where A is a matrix differential operator acting on displacement components),

transform to potentials ϕ_1, ϕ_2, ϕ_3 (ϕ_3 gives the SH motion) by $\underset{\sim}{u} = B\underset{\sim}{\phi}$ for some matrix differential operator B (given essentially by (3.4.6) when $\phi_3 = 0$), and

try to find B such that

$A\underset{\sim}{u} = AB\underset{\sim}{\phi} = CD\underset{\sim}{\phi}$ in which D is diagonal. (The condition that D can be found is a model constraint, and reduces to the requirement that π_0, π_1 and π_2 can all be zero.) Alverson et al discuss only the uncoupled equations $D\underset{\sim}{\phi} = \underset{\sim}{0}$ (i.e. $d_{11}\phi_1 = 0$, $d_{22}\phi_2 = 0$, say), but in general these are not the only significant solutions to $CD\underset{\sim}{\phi} = \underset{\sim}{0}$, since $CD\underset{\sim}{\phi}$ is of the form

$$\frac{\rho}{f_1} \text{ grad } (d_{11}\phi_1) + \frac{\rho}{f_2} \text{ curl curl } (r\, d_{22}\phi_2, 0, 0)$$

and ϕ_1 is in general still coupled to ϕ_2.

(iii) Hook and his co-workers have not considered the effect of a source term. Using our method of analysis in (a) above, it may be seen that (for media in which non-trivial solutions $\underset{\sim}{u} = \underset{\sim}{L}_0$, $\underset{\sim}{u} = \underset{\sim}{N}_0$ exist), the source-generated potentials P and S are indeed decoupled if the applied force/unit mass is expressible as

$$\underset{\sim}{F} = \frac{1}{f_1} \text{ grad } \left(\frac{f_1 D}{\rho^{\frac{1}{2}}} \right) + \frac{1}{f_2} \text{ curl curl } \left(\frac{r f_2}{\rho^{\frac{1}{2}}} \; F, \; 0, \; 0 \right) \qquad (3.4.7)$$

where f_1 is chosen so that $\pi_0 = 0$, and f_2 so that $\sigma_o = 0$. We note further that such force potentials can always be found if the force is confined to a homogeneous part of the medium.

(iv) Singh and Ben-Menahem (1969b) have recently used Hook's method to explain the geophysical observation that P and SV are substantially decoupled in the Earth. Their work implies that these waves are independent, because in special models potentials can be chosen which satisfy uncoupled wave equations like (3.3.2) for the SH potential, and they show by example that the Jeffreys-Bullen Earth is at most depths similar to such a special model. This study may be criticized directly because their special model is still split up into several layers, and indirectly because of our remark (ii) above, concerning coupling in the special media. (It would however be interesting to evaluate the functions $\pi_1(r)$ and $\pi_2(r)$ for Earth models which best satisfy modern data, to see at which depths most mode conversion may be expected to take place.)

Our work in (a) above implies rather that P and S are sufficiently independent to explain the geophysical observation (of independence), and satisfy a wave equation (3.4.4) like

that for the SH potential, merely because the effect of heterogeneity near a confined source can be made negligible. Thus, suppose that the source is non-zero only near the radius r = b. It follows from Appendix VII that the applied force/unit mass may in the frequency domain be written as

$$\underset{\sim}{F} = \frac{1}{f_2(r)} \left[\text{grad } D_1 + \text{curl curl } (rF_1, 0, 0) \right] e^{-i\omega t} \tag{3.4.8}$$

for some force potentials D_1, F_1. And since the force is zero away from r = b, we can have

$$\frac{1}{f_2(r)} \text{ grad } D_1 \sim \frac{1}{f_1(r)} \text{ grad } \left[D_1 \frac{f_1(b)}{f_2(b)} \right]$$

(or a similar result with F_1).

Using new force potentials

$$D = \frac{\rho^{\frac{1}{2}}(r)}{f_1(r)} \frac{f_1(b)}{f_2(b)} D_1 e^{-i\omega t} \sim \frac{\rho^{\frac{1}{2}}(r)}{f_2(b)} D_1 e^{-i\omega t} \quad \text{and}$$

$$F = \frac{\rho^{\frac{1}{2}}(r)}{f_2(r)} F_1 e^{-i\omega t}$$

we may use the methods of (a) above, with D as a P-wave source (coupled to a smaller SV displacement) and F as an independent SV-wave source (coupled to a smaller P displacement).

(c) Brief summary of applications and extensions

(i) A conclusion of our study of coupled potentials in (a) above is that, at high frequencies, P and S separately satisfy wave equations like (3.4.4a), which are essentially in the canonical form (3.2.2). This basic result is the assumption needed in Chapter 2, to generalize the theory for an Earth model with individually homogeneous mantle and core to the theory for general radial heterogeneity. [We prove in Appendix X that the WKBJ and turning point results, obtained in Chapter 2 from the canonical equation (3.2.2), may also be derived from our coupled equations (3.4.1) and (3.4.2).] And so Chapter 2 is justified as a major application of our choice for coupled potentials.

(ii) The general form of the coupled equations (3.3.4)-(3.3.8) permits specialization to the detailed study of specified forms of radial heterogeneity. The many logarithmic derivatives $\left(\frac{d}{dx} \ell n\, F = \frac{F'}{F} \right)$ appearing in Appendix IX suggest that power laws

$$\begin{pmatrix} \rho \\ \lambda \\ \mu \end{pmatrix} \propto \begin{pmatrix} r^a \\ r^b \\ r^c \end{pmatrix}$$

may be particularly suitable, for then such derivatives are constants. Zavadskii (1965a) discusses a similar elastic medium which is transversely homogeneous, i.e. the logarithmic depth derivative of

ρ, λ, and μ are constant, and in which also the squares of the two velocities are proportional to depth. He obtains the equations corresponding to our (3.4.1-3.4.2), but without the option of a varying scale factor f, and is able to reduce them to two Whittaker equations. The solution is then given by two coupled potentials, each a linear combination of the same four Whittaker functions.

(iii) The numerical study of such a special inhomogeneous medium is sometimes able to give us considerable insight into seismological problems. A practical example here is the relevance of theory and numerical details, given by Brekhovskikh (1960), to the problem of describing postulated upper mantle transitions in the Earth. The theory here indicates that regions of anomalous velocity gradient must be confined to within at most 4 kilometers, in order to generate observable PKPPKP precursors.

Several steps are needed to obtain this result.

First, we note from Engdahl and Flinn (1969) that the apparent slowness $\frac{dT}{d\Delta}$ for the precursors (near $\Delta = 65°$) is about 2.9 seconds/degree, which implies that the angle of incidence i (say) at a transition zone near 650 km is about 16° to the vertical. An S wave with the same slowness has at this depth an angle of incidence j (say) about 9°.

Second, in Appendix XI we find formulae giving the reflection and transmission coefficients between two slightly different

welded homogeneous half-spaces, for an incident P wave. [This Appendix gives two methods for obtaining the coefficients, first by studying the boundary condition and second from the intrinsic coupling contained in the wave equations of displacement in heterogeneous media.] Suppose that this wave is incident from below at 16° to the vertical, and that the upper medium has a density 5% smaller, a longitudinal velocity 10% smaller, and a shear velocity about 20% smaller than corresponding parameters in the lower medium. [These velocity values are somewhat less than the total change across the major transition region suggested at 650 km depth by Anderson and Julian (1969): the density jump is found not to be particularly important in our argument, in contrast to the suggestion of Teng and Tung (1969).] From our Appendix XI formulae, we conclude that in this extreme case of a step discontinuity the reflection coefficient for P waves (i.e. P(up) → P(down)) and the conversion coefficient for SV waves (i.e. P(up) → SV(down)) are both about -0.057.

Third, in order to obtain an upper limit for reflection coefficients (P(up) → P(down)) in different models of the transition region, we make the strong assumption that mode conversion is negligible. (We see from the calculation in Appendix XI that this is indeed a strong assumption. However, we may expect that the conclusions of the order of magnitude argument which it permits

are not significantly changed, since we are interested in obtaining only an upper bound for the P-P reflection amplitude.) We may also reasonably assume that the PKP wave incident at the transition has a horizontal phase velocity centered at one dominant value, and that the transition itself is transversely homogeneous. It follows from our results in (a) above that the longitudinal wave system may then be discussed by a potential P satisfying

$$\nabla^2 P + h^2(z)\, P = 0 \qquad (3.4.9)$$

where the wave number h is a function of depth z, and we take z_o to be the depth to the center of the transition region.

Brekhovskikh (1960) gives an extended account of the Epstein (1930) method of studying (3.4.9), which permits the calculation of reflection coefficients (for different angles of incidence) from a transition region described by the velocity profile

$$\frac{\alpha(z)}{\alpha(\infty)} = \left[1 - \frac{N\, e^{-m(z-z_o)}}{1 + e^{-m(z-z_o)}} \right]^{-\frac{1}{2}} \qquad (3.4.10)$$

(N.B. our z increases downwards) where N and m are real constants. This profile is a smooth transition between the two values $\alpha(\infty)$ and $\alpha(-\infty) = \alpha(\infty)(1-N)^{-1/2}$ (from bottom to top), and for our study of the 650 km (= z_o) transition in the Earth we are interested in finding reflection coefficients for the value $(1-N)^{1/2} = 1.1$, which represents a 10% change in velocity. We take the effective thickness ℓ of the transition zone to be given by $\ell = \frac{3.52}{m}$ km, since at depths $z_o - \frac{1}{2}\ell$, $z_o + \frac{1}{2}\ell$ we can show the velocities are less than 1% different from respectively their upper and lower limiting values, $\alpha(-\infty)$ and $\alpha(\infty)$.

Brekhovskikh gives for the modulus of the reflection coefficient the exact formula

$$R = \frac{\sinh\left\{\frac{2\pi^2}{\lambda m}\left[\cos i - \sqrt{\cos^2 i - N}\right]\right\}}{\sinh\left\{\frac{2\pi^2}{\lambda m}\left[\cos i + \sqrt{\cos^2 i - N}\right]\right\}}$$

where i is the angle of incidence at $z = +\infty$ (taken as 16° in our application) and λ is the wavelength $2\pi\alpha(\infty)/\omega$. Brekhovskikh also plots values of R against i for different ratios ℓ/λ in this case of $N = -0.21$ (his Figure 76). These are just the values needed to discuss our geophysical problem. They are not in fact particularly sensitive to the angle of incidence in the range $0 \leq i \leq 30°$, and

we note the values

$$R = 4.5 \times 10^{-2},\ \ 2.5 \times 10^{-2},\ \ 1.8 \times 10^{-3},\ 1.0 \times 10^{-5},$$

$$3.2 \times 10^{-10},\ \ 7.9 \times 10^{-24}$$

for ratio values

$$\frac{\ell}{\lambda} = 0.1,\ \ 0.2,\ \ 0.5,\ \ 1,\ \ 2,\ \ 5$$

Note that the approximation we have obtained in Appendix XI is $R = 5.7 \times 10^{-2}$ in the limiting case $\frac{\ell}{\lambda} = 0$ - which result fits in well with the above sequence.

Fourth, we quote Adams' (1968) remarks that "Amplitudes observed for the clearer reflections range from a few percent up to 20 percent and in one case 40 percent of the main phase," that "At times there are clear pulse-like early arrivals," and that the more common "emergent forerunner is usually of short period (one second or less)," and note also (from our formula 2.6.14) that the main phase (reflected essentially from the Earth's surface) has a reflection coefficient of nearly one. Adams' remarks concern horizons less deep than 650 km, and Engdahl and Flinn (1969) have pointed out that some of the arrivals picked as precursors by Adams are probably the phase SKKKP. However, the brief summary of "a few percent ... of the main phase" and an "emergent forerunner .....(one second...)"

is all we need, and seems to be unchanged by more recent studies (Whitcomb, personal communication, 1969).

Fifth, and finally, it is clear from the comparison of theory and observation that transition zones must be highly localized. For, a wave with the predominant period of two seconds (say), incident upon the transition with wavelength about 20 km, is reflected back down with more than 2.5% of its incident amplitude only if the transition width is less than about 4 km. To obtain this final upper bound we have made highly conservative estimates throughout our theoretical development (except in neglecting a focusing effect of curvature of the transition; this should change our conclusion only if such curvature is substantially different from the curvature of that horizon which produces the main PKPPKP phase), in the postulated size of the jump in parameters across the transition, and in our observational summary. The less conservative assumptions of a one second incident wave, reflected back down with more than 4% of its incident amplitude, imply a transition width of less than about 1 km.

The reason why our somewhat crude assumptions can lead to such a definite result is that the fall off in the reflection coefficient R is extremely rapid as $\frac{\ell}{\lambda}$ increases. As a corollary we may remark that the continuous scattering, due to the large vertical extent of small velocity gradients in the Earth, is essentially negligible, and presumably that anelasticity has a

more important effect on the total transmission coefficient along a ray path.

It is of considerable importance to determine if the localized transition required above to explain reflection observations may have the nature of a discontinuity in velocity gradient, rather than in the velocity itself (i.e., a second-order discontinuity rather than a first). The general methods set out in Chapter 2 (Section 6) above may be appropriate for an accurate discussion of such modelling, but we can profitably enter here a brief summary of the solution found by Rayleigh in his study of waves propagating along inhomogeneous strings. (See Rayleigh, 1945, Vol. I, §148.) Brekhovskikh (1960) quotes this solution in the context of light-wave propagation in media of varying refractive index, and gives a numerical discussion. We use seismological terminology, rather than the mechanical and optical parameters of these references, and the "profile" is

$$\alpha(z) = \alpha_1 \qquad z \leq z_o - L/2$$

$$\alpha(z) = \alpha_1 + (\alpha_2-\alpha_1)\left[\frac{z-z_o}{L} + \frac{1}{2}\right] \qquad z_o - L/2 \leq z \leq z_o + L/2$$

$$\alpha(z) = \alpha_2 \qquad z_o + L/2 \leq z.$$

Brekhovskikh's numerical work is for the case of a wave incident in the first medium, with $\alpha_1 = 0.8\ \alpha_2$. So the second medium has a higher velocity (and the total jump of 20% is almost certainly larger than those jumps which may occur in realistic Earth models). If the incident wavelength is λ, then R, the reflection coefficient modulus for normal incidence, is given in general by

$$R = \frac{\left|\sinh\left[\mu \ln (\alpha_1/\alpha_2)\right]\right|}{\left\{\sinh^2\left[\mu \ln (\alpha_1/\alpha_2)\right] + 4\mu^2\right\}^{\frac{1}{2}}} \quad \text{if} \quad \frac{L}{\lambda} < \frac{\alpha_2-\alpha_1}{4\pi\alpha_1} \ ,$$

where

$$\mu = \left\{\frac{1}{4} - \left[\frac{2\pi L\ \alpha_1}{\lambda(\alpha_2-\alpha_1)}\right]^2\right\}^{1/2}$$

or by

$$R = \frac{\left|\sin\left[m \ln (\alpha_1/\alpha_2)\right]\right|}{\left\{\sin^2\left[m \ln (\alpha_1/\alpha_2)\right] + 4m^2\right\}^{1/2}} \quad \text{if} \quad \frac{L}{\lambda} > \frac{\alpha_2-\alpha_1}{4\pi\alpha_1} \ ,$$

where

$$m = \left\{\left[\frac{2\pi L\ \alpha_1}{\lambda(\alpha_2-\alpha_1)}\right]^2 - \frac{1}{4}\right\}^{\frac{1}{2}} \ .$$

[Note: the boundary conditions assumed here are those originating in Rayleigh's problem. We may expect the general features of the seismological reflection to be the same.] The following brief description of R can be given, in the case $\alpha_1 = 0.8\ \alpha_2$:

R = 0 for certain specific values $\frac{L}{\lambda} = 0.56, 1.11, 1.66, \ldots\ldots$ given by solutions of $m\ \ell n\ (\alpha_1/\alpha_2) = \nu\pi$, where ν is an integer. In the range $0 \leq \frac{L}{\lambda} \leq 0.56$, R falls almost linearly from 12% to zero. In the range $0.56 \leq \frac{L}{\lambda} \leq 1.11$, R rises from zero to a maximum of 2.5% and falls back to zero. In the range $1.11 \leq \frac{L}{\lambda} \leq 1.66$, R rises from zero to a maximum of 1.6%, and falls back to zero. The maxima occur about half way between the zeros.

It is again apparent that the observations impose some severe restrictions on this model of transition zones, if it is to explain the PKPPKP precursor amplitude data. [Note, the above numerical work is obtained for reflection from a medium of greater velocity, rather than a lesser. However, R falls into about the same range of values if we evaluate reflection from the lesser velocity medium, since $|\ \ell n\ (\alpha_1/\alpha_2)\ | = |\ -\ell n\ (\alpha_2/\alpha_1)|$.] Thus, if the data do indeed indicate that the reflection coefficient is more than 2.5%, then $L/\lambda \leq 0.45$ is required by the model. The upper limit here then implies for observation of a one second wave that the transition

is less than about 4 kilometers - even in this case of a 20% jump in velocity.

The zeros and maxima in the reflection coefficient suggest that for different frequencies there is destructive and constructive interference, between reflections reverberating between upper and lower velocity gradient discontinuities. Hence, for a similar transition, but in which one of the two second-order discontinuities is smoothed out, we may reasonably expect a reflection coefficient lying between the extrema (maxima and zeros) calculated for our pair of discontinuities. (See Archambeau, Flinn and Lambert, 1969, for the development of Earth models with such one-sided transitions.) That is, a modified reflection coefficient obtained approximately as

$$R = 9.5 \times 10^{-2} \quad , \; 3 \times 10^{-2}, \quad 1 \times 10^{-2}$$

for the ratio values

$$\frac{L}{\lambda} = 0.2 \quad , \quad 0.5 \; , \quad 1.0,$$

and here we make the interpretation of L/λ as the gradient in the transition region. Then $L/\lambda = 0.5$ gives for a 10 km wavelength the gradient

$\frac{d\alpha}{dz} \sim \frac{\alpha_2-\alpha_1}{L} \sim 2$ km/sec, per 5 km. Yet even this large second-order discontinuity (plus about 5 km of anomalous gradient) has a reflection coefficient of only 3% (which perhaps may just be large enough to explain the observations).

In conclusion, we may emphasize that it is the short period reflection data from transitions which provide our strongest restrictions on the localized nature of these regions. The search for such data, difficult though they are to find, must become one of the more important projects in seismology - since each confirmed reflection horizon must be a narrower region, of larger velocity anomaly, than has previously been supposed. We also note that the present lack of reflection data, from the major 350-400 km "discontinuity" (described by, for example, Johnson, 1967), merely implies that the anomalous region is spread over more than about 20 kilometers. Some of the conservative estimates we have been obliged to make in the above discussion should be improved by obtaining special solutions for our basic coupling equations (3.3.4)-(3.3.8), rather than by discussing approximations to them.

(iv) An extension of our method for obtaining useful potentials can be given, to examine the displacement $\underset{\sim}{u}$ in an elastic isotropic medium with general heterogeneity. For, the equation of motion is

$$\rho \frac{\partial^2 \underset{\sim}{u}}{\partial t^2} = \rho \underset{\sim}{F} + \nabla \cdot \underline{\underline{\sigma}}$$

where $\underset{\sim}{F}$ is the applied force/unit mass, the Cartesian tensor $\underline{\underline{\sigma}}$ has components

$$\sigma_{ij} = \lambda \, \delta_{ij} \, u_{\ell,\ell} + \mu \left[u_{i,j} + u_{j,k} \right]$$

and ρ, λ and μ are all functions of position. We may then seek solutions in the form

$$\underset{\sim}{u} = \frac{1}{f(\underset{\sim}{r})} \left[\text{grad} \left(\frac{f}{\rho^{\frac{1}{2}}} \phi \right) + \text{curl} \left(\frac{f}{\rho^{\frac{1}{2}}} \underset{\sim}{A} \right) \right]$$

and generalize the discussion given in (3.4a) above to discuss the choices of f which, for special sources, lead to decoupled equations in ϕ and $\underset{\sim}{A}$ in the high frequency limit.

(d) Conclusions

We have been able to find a system of potentials by which we may study all elastic displacements in a spherically symmetric, isotropic, Earth model. Properties of P, SV and SH waves may be identified by individual potentials, and it is found that well-known methods of solution for canonical wave problems are available for an examination of high-frequency elastic waves in the Earth.

Such solutions have frequency-dependent amplitudes for the waves scattered by transition regions. We find in (3.4c) above that those transition regions in the Earth, which are experimentally identifiable as reflection horizons for short periods, must be much more localized than has hitherto been generally supposed.

Our new method of potentials permits a shadow boundary solution method (presented in sections 2.2-2.5) to be generalized to study elastic waves in realistic models of the Earth's core/mantle transition. The conclusions of this study are given at the end of Chapter 2 above: they include a quantitative appreciation of Johnson's (1969) caveat, that the body wave phases which bottom near the core/mantle interface have a significantly dispersed horizontal phase velocity. It is expected that our numerical methods, developed in Chapter 2 for the evaluation of waves which travel close to the core shadow boundary, may find applications in many other wave propagation problems.

REFERENCES

Abramowitz, M., and I. A. Stegun, Handbook of Mathematical Functions, U. S. Natl. Bur. Stan., 1964.

Adams, R. D., Early Reflections of P'P' as an Indication of Upper Mantle Structure, Bull. Seism. Soc. Am., 58, 1933-1947, 1968.

Alexander, Shelton S., and Robert A. Phinney, A Study of the Core-Mantle Boundary Using P Waves Diffracted by the Earth's Core, J. Geophys. Res., 71, 5943-5958, 1966.

Alverson, R. C., F. C. Gair, and Joseph F. Hook, Uncoupled Equations of Motion in Non-Homogeneous Elastic Media, Bull. Seism. Soc. Am., 53, 1023-1030, 1963.

Anderson, Don L., and Bruce R. Julian, Shear Velocities and Elastic Parameters of the Mantle, J. Geophys. Res., 74, 3281-3286, 1969.

Archambeau, C. B., E. A. Flinn, and D. G. Lambert, Fine Structure of the Upper Mantle, J. Geophys. Res., 74, 5825-5865, 1969.

Babich, V. M., Fundamental Solutions of the Dynamical Equations of Elasticity for Nonhomogeneous Media, Appl. Math. and Mech., 49-60, 1961.

Baker, B. B., and E. T. Copson, The Mathematical Theory of Huygens' Principle, Oxford, Clarendon Press, 1939.

Ben-Menahem, Ari, Mode-Ray Duality, Bull. Seism. Soc. Am., 54, 1315-1321, 1964.

Bennett, J. A., and C. I. Chessell, Discussion of Paper by S. S. Rao and H. Unz, 'Asymptotic Solutions of Waves in Inhomogeneous Plasma with Longitudinal Magnetic Field,' J. Geophys. Res., 74, 1886-1890, 1969.

Berry, Leslie A., Computation of Hankel Functions, U. S. Natl. Bur. Stan. Tech. Note 216, 1964.

Berry, M. J., and G. F. West, Reflected and Head Wave Amplitudes in a Medium of Several Layers, Geophysical Monograph 10, The Earth Beneath Continents (American Geophysical Union), 464-481, 1966.

Born, Max, and Emil Wolf, Principles of Optics, Pergamon Press, 1959.

Brekhovskikh, Leonid M., Waves in Layered Media, Academic Press, 1960.

Bremmer, H., Terrestrial Radio Waves, Elsevier Publishing Co, New York, 1949.

Bremmer, H., The W.K.B. Approximation as the First Term of a Geometric-Optical Series, Comm. Pure and Appl. Math., 4, 105-116, 1951.

Brune, J. N., and J. Dorman, Seismic Waves and Earth Structure in the Canadian Shield, Bull. Seism. Soc. Am., 53, 167-210, 1963.

Budden, K. G., Radio Waves in the Ionosphere, Cambridge University Press, 1961.

Bullen, K. E., An Introduction to the Theory of Seismology, 3rd edition, Cambridge University Press, 1963.

Červený, Vlastislav, On the Dynamical Properties of Reflected and Head Waves in the n-layered Earth's Crust, Geophys. J. Roy. Astr. Soc., 11, 139-147, 1966.

Chapman, Christopher H., Seismic Wave Diffraction Theory, Ph.D. Thesis, University of Cambridge, August 1969.

Chekin, B. S., The Effect on a Head Wave of Small Inhomogeneities in a Refracting Medium, Izv. Phys. of the Earth, 3, 143-147, 1965.

Cleary, J., K. Porra, and L. Read, Diffracted S, Nature, 216, 905-906, 1967.

Duwalo, George, and J. A. Jacobs, Effects of a Liquid Core on the Propagation of Seismic Waves, Can. J. Phys., 37, 109-128, 1959.

Engdahl, Eric R., and Edward A. Flinn, Remark on the Paper "Early Reflections of P'P' as an Indication of Upper Mantle Structure," by R. D. Adams, Bull. Seism. Soc. Am., 54, 1415-1417, 1969.

Epstein, P. S., Reflection of Waves in an Inhomogeneous Absorbing Medium, Proc. Natl. Acad. Sci. U. S. A., 16, 627-637, 1930.

Erdélyi, A. (editor), Higher Transcendental Functions, Bateman Manuscript Project, 3 vols, McGraw-Hill, 1953.

Ewing, W. Maurice, Wenceslas S. Jardetzky, and Frank Press, Elastic Waves in Layered Media, McGraw-Hill, 1957.

Fock, V. A., The Field of a Plane Wave near the Surface of a Conducting Body, J. Phys. U. S. S. R., 10, 399-409, 1946.

Friedman, Bernard, Propagation in a Non-homogeneous Atmosphere, Comm. Pure and Appl. Math., 4, 317-350, 1951.

Gerver, M., and V. Markushevich, Determination of a Seismic Wave Velocity from the Travel Time Curve, Geophys. J. Roy. Astr. Soc., 11, 165-173, 1966.

Gilbert, Freeman, and Leon Knopoff, Scattering of Impulsive Waves by a Rigid Cylinder, J. Acoust. Soc. Am., 31, 1169-1175, 1959.

Goodier, J. N., and R. E. D. Bishop, A Note on Critical Reflections of Elastic Waves at Free Surfaces, J. Appl. Phys., 23, 124-126, 1952.

Gutenberg, B., and C. F. Richter, On Seismic Waves (Second Paper), Ger. Beit. zur Geoph., 45, 280-360, 1935.

Gutenberg, B., The Shadow of the Earth's Core, J. Geophys. Res., 65, 1013-1020, 1960.

Hales, A. L., J. R. Cleary, and J. L. Roberts, Velocity Distribution in the Lower Mantle, Bull. Seism. Soc. Am., 58, 1975-1989, 1968.

Haskell, N. A., The Dispersion of Surface Waves on Multilayered Media, Bull. Seism. Soc. Am., 43, 17-34, 1953.

Haskell, Norman A., Crustal Reflection of Plane SH Waves, J. Geophys. Res., 65, 4147-4150, 1960.

Haskell, Norman A., Crustal Reflection of Plane P and SV waves, J. Geophys. Res., 67, 4751-4767, 1962.

Herrin, E., W. Tucker, J. Taggart, D. Gordon, and J. Lobdell, Estimation of P Travel Times, Bull. Seism. Soc. Am., 58, 1273-1291, 1968.

Hill, David P., Head Waves from a Medium with a Small Negative Velocity Gradient, Work in preparation, 1970.

Hille, E., Analytic Function Theory, Vol. II, Blaisdell Publishing Co., 1962.

Hook, Joseph Frederick, On the Theory of Propagation of Seismic Waves in Inhomogeneous Isotropic Elastic Media, Ph.D. Thesis, U.C.L.A., 1959.

Hook, Joseph F., Separation of the Vector Wave Equation of Elasticity for Certain Types of Inhomogeneous, Isotropic Media, J. Acoust. Soc. Am., 33, 302-313, 1961.

Hook, Joseph F., Generalization of a Method of Potentials for the Vector Wave Equation of Elasticity for Inhomogeneous Media, J. Acoust. Soc. Am., 34, 354-355, 1962a.

Hook, Joseph F., Contributions to a Theory of Separability of the Vector Wave Equation of Elasticity for Inhomogeneous Media, J. Acoust. Soc. Am., 34, 946-953, 1962b.

Hook, Joseph F., Determination of Inhomogeneous Media for which the Vector Wave Equation of Elasticity is Separable, Bull. Seism. Soc. Am., 55, 975-987, 1965.

Hudson, J. A., The Total Internal Reflection of SH waves, Geoph. J. Roy. Astr. Soc., 6, 509-531, 1962.

Jeffreys, H., On Compressional Waves in Two Superposed Layers, Proc. Camb. Phil. Soc., 33, 472-481, 1926.

Jeffreys, Sir Harold, Research Note: Small Changes in Seismic Distributions of Velocity, Geophys. J. Roy. Astr. Soc., 12, 113, 1966.

Johnson, Lane R., Array Measurements of P Velocities in the Upper Mantle, J. Geophys. Res., 72, 6309-6325, 1967.

Johnson, Lane R., Array Measurements of P Velocities in the Lower Mantle, Bull. Seism. Soc. Am., 59, 973-1008, 1969.

Julian, Bruce R., and Don L. Anderson, Travel Times, Apparent Velocities and Amplitudes of Body Waves, Bull. Seism. Soc. Am., 58, 339-366, 1968.

Karal, Frank C., Jr., and Joseph B. Keller, Elastic Wave Propagation in Homogeneous and Inhomogeneous Media, J. Acoust. Soc. Am., 31, 694-705, 1959.

Knopoff, L., A. Matrix Method for Elastic Wave Problems, Bull. Seism. Soc. Am., 54, 431-438, 1964.

Knopoff, Leon, and Freeman Gilbert, Diffraction of Elastic Waves by the Core of the Earth, Bull. Seism. Soc. Am., 51, 35-49, 1961.

Lehmann, I., On the Shadow of the Earth's Core, Bull. Seism. Soc. Am., 43, 291-306, 1953.

Love, A. E. H., A Treatise on the Mathematical Theory of Elasticity, 4th Edition, Dover Publications, 1944.

Miklowitz, Julius, Elastic Wave Propagation, Applied Mechanics Surveys, Spartan Books, Washington, D. C., pp 809-839, 1966.

Morse, Philip M., and Herman Feshbach, Methods of Theoretical Physics, Vols. I and II, McGraw-Hill, 1953.

Nagase, Masahumi, Diffraction of Elastic Waves by a Spherical Surface, J. Phys. Soc. Japan, 11, 279-301, 1956.

Nussenzweig, H. M., High-Frequency Scattering by an Impenetrable Sphere, Research Report No. EM-203, Division of Electromagnetic Research, Courant Institute, N.Y.U., 1965, Also, Ann. Phys. (N.Y.), 34, 23 +, 1965.

Officer, C. B., Introduction to the Theory of Sound Transmission, McGraw-Hill, 1958.

Phinney, Robert A., and Shelton S. Alexander, P Wave Diffraction Theory and the Structure of the Core Mantle Boundary, J. Geophys. Res., 71, 5959-5975, 1966.

Phinney, Robert A., and Lawrence M. Cathles, Diffraction of P by the Core: A Study of Long-Period Amplitudes near the Edge of the Shadow, J. Geophys. Res., 74, 1556-1574, 1969.

Phinney, Robert A., and Shelton S. Alexander, The Effect of a Velocity Gradient at the Base of the Mantle on Diffracted P Waves in the Shadow, J. Geophys. Res., 74, 4967-4971, 1969.

Rayleigh, Baron, The Theory of Sound, Second American Edition, Dover Publications, 1945.

Rice, S. O., Diffraction of Plane Radio Waves by a Parabolic Cylinder, Bell System Tech. J., 33, 417-504, 1954.

Robin, L., Fonctions Sphériques de Legendre et Fonctions Sphéroidales, Tome II, Gautier-Villars, Paris, 1958.

Robinson, A., Wave Propagation in a Heterogeneous Elastic Medium, J. Math. and Phys., 36, 210-222, 1957.

Rubinow, S. I., and Joseph B. Keller, Shift of the Shadow Boundary and Scattering Cross Section of an Opaque Object, J. Appl. Phys., 32, 814-820, 1961.

Rubinow, S. I., and T. T. Wu, First Correction to the Geometric-Optics Scattering Cross Section from Cylinders and Spheres, J. Appl. Phys., 27, 1032-1039, 1956.

Sacks, S., Diffracted Wave Studies of the Earth's Core: 1. Amplitude, Core Size, and Rigidity, J. Geophys. Res., 71, 1173-1181, 1966.

Sacks, I. Selwyn, Diffracted P-Wave Studies of the Earth's Core: 2. Lower Mantle Velocity, Core Size, Lower Mantle Structure, J. Geophys. Res., 72, 2589-2594, 1967.

Scholte, J. G. J., On Seismic Waves in a Spherical Earth, Koninkl. Ned. Meteorol. Inst. Publ. 65, 1-55, 1956.

Seckler, Bernard D., and J. B. Keller, Geometrical Theory of Diffraction in Inhomogeneous Media, J. Acoust. Soc. Am., 31, 192-205, 1959a.

Seckler, Bernard D., and J. B. Keller, Asymptotic Theory of Diffraction in Inhomogeneous Media, J. Acoust. Soc. Am., 31, 206-216, 1959b.

Shenderov, E. L., Diffraction of a Cylindrical Sound Wave by a Cylinder, Sov. Phys. Acoust., 7, 293-296, 1962.

Singh, Jit Sarva, and Ari Ben-Menahem, Decoupling of the Vector Wave Equation of Elasticity for Radially Heterogeneous Media, J. Acoust. Soc. Am., 46, 655-660, 1969.

Singh, Jit Sarva, and Ari Ben-Menahem, Asymptotic Theory of Body Waves in a Radially Heterogeneous Earth, Bull. Seism. Soc. Am., 59, 2039-2059, 1969.

Teng, T. L., and F. T. Wu, A Two-Dimensional Ultrasonic Model Study of Compressional and Shear-Wave Diffraction Patterns Produced by a Circular Cavity, Bull. Seism. Soc. Am., 58, 171-178, 1968.

Teng, T. L., and James P. Tung, PKPPKP and Upper Mantle Discontinuities, Trans. Am. Geophys. U., 50, 644, 1969.

Thomson, William T., Transmission of Elastic Waves through a Stratified Solid Medium, J. Appl. Phys., 21, 89-93, 1950.

Vlaar, N. J., Ray Theory in an Anisotropic Inhomogeneous Elastic Medium, Bull. Seism. Soc. Am., 58, 2053-2072, 1968.

Wait, James R., and Alyce M. Conda, Diffraction of Electromagnetic Waves by Smooth Obstacles for Grazing Angles, J. Res. Nat. Bur. Stand.-D, 63D, 181-197, 1959.

Watson, G. N., The Diffraction of Electric Waves by the Earth, Proc. Roy. Soc. Lond., XCV, Series A, 83-99, 1919.

Watson, G. N., A Treatise on the Theory of Bessel Functions, Cambridge University Press, 1958.

Whitcomb, James H., and Don L. Anderson, Upper Mantle P'P' Reflections, Manuscript submitted to J. Geophys. Res., 1970.

Yanovskaya, T. B., Lecture notes on Approximate Methods in Elastic Wave Theory, Department of Applied Mathematics and Theoretical Physics, Cambridge University, 1967.

Yosiyama, Ryoiti, Elastic Waves from a Point in an Isotropic, Heterogeneous Sphere, Part I, Bull. Earthq. Res. Inst., 11, 1-13, 1933.

Yosiyama, Ryoiti, Elastic Waves from a Point in an Isotropic Heterogeneous Sphere, Part III, Bull. Earthq. Res. Inst., 19, 185-205, 1941.

Zavadskii, V. Yu., Concerning Wave Motion in an Elastic Layer-wise Inhomogeneous Medium with Power Law Variations in Density and Lamé Parameters, Sov. Phys. Acoust., 10, 94-96, 1965a.

Zavadskii, V. Yu., Displacement Potentials in an Elastic Layered-Inhomogeneous Medium, Sov. Phys. Acoust., 10, 246-249, 1965b.

Zavadskii, V. Yu., Asymptotic Approximations in the Dynamics of an Elastic Layered Inhomogeneous Medium, Sov. Phys. Acoust., 11, 141-146, 1965c.

Appendix I

Formulae for P-S and S-P Scattering

We discuss here our simplest model of diffraction - a steady state plane wave of unit displacement, incident from the left on a circular cylindrical cavity. See Section (2.2).

a) P-S (See Figure 1(b))

With equations (2.2.2) and (2.2.3) we may use the Poisson sum formula to obtain ψ_s, the potential for scattered SV waves, as

$$\psi_s = -\frac{1}{2} \sum_{m=-\infty}^{\infty} \mathcal{B}(r, 2m\pi + \theta) \qquad \text{where}$$

$$\mathcal{B}(r,\theta) = \int_{-\infty}^{\infty} e^{i\nu\left(\theta + \frac{\pi}{2}\right)} H_\nu^{(1)}(kr) \frac{\Omega_2 J_\nu(ha)}{\Omega_1 H_\nu^{(1)}(ha)} d\nu .$$

We can show that $\mathcal{B}(r,-\theta) = -\mathcal{B}(r,-2\pi+\theta)$ and so

$$\psi_s = -\frac{1}{2}\left[\left\{ \sum_{m=1}^{\infty} \left(\mathcal{B}(r,2m\pi+\theta) - \mathcal{B}(r,2m\pi-\theta) \right) \right\} + \mathcal{B}(r,\theta) - \mathcal{B}(r,-\theta) \right]$$

All but one of these terms are negligible, and we have

$$\psi_s = + \frac{1}{2} \mathcal{B}(r,-\theta) \quad \text{near the upper PS boundary.}$$

Contributions to the integral $\mathcal{B}(r,-\theta)$ must come from near $\nu = kr \sin i$ (see Figure 2), i.e. from near $\nu = ha$, if (r,θ) is near the PS boundary (see Figure 1(b)). So we approximate the integrand in this region.

$$e^{i\nu\left(-\theta+\frac{\pi}{2}\right)} H_\nu^{(1)}(kr) \sim \left(\frac{2}{\pi}\right)^{\frac{1}{2}} e^{i\nu\left(i_c - \frac{\pi}{2}\right)} \frac{1}{\left(k^2r^2 - \nu^2\right)^{\frac{1}{4}}} e^{i\Phi_1}$$

where

$$\Phi_1 = \left(k^2r^2 - \nu^2\right)^{\frac{1}{2}} - \frac{\pi}{4} + \nu\left[\sin^{-1}\frac{\nu}{kr} - \theta + \frac{\pi}{2} - i_c\right] ,$$

and i_c is the critical angle of incidence at $r = a$. Then

$$e^{i\nu\left(-\theta+\frac{\pi}{2}\right)} H_\nu^{(1)}(kr) \sim \left(\frac{2}{\pi kX}\right)^{\frac{1}{2}} e^{i\left(kX-\frac{\pi}{4}\right)} e^{i\nu\left(i_c - \frac{\pi}{2}\right)} ,$$

where X is a Cartesian coordinate along $\theta = \frac{\pi}{2} - i_c$. See Figure 1b. The asymptotic expression is valid if $\nu \sim kr\sin i$ and

$kX \left| i - \left(\theta + i_c - \frac{\pi}{2}\right) \right| << 1$, i.e. for (r,θ) sufficiently

near the PS geometrical shadow boundary.

Finally, then, we have

$$\psi_s \sim \left(\frac{1}{2\pi kX}\right)^{\frac{1}{2}} e^{i\left(kX - \frac{\pi}{4}\right)} (ha)^{\frac{1}{3}} C_{PS}(\omega), \text{ where}$$

$$C_{PS}(\omega) \equiv \frac{1}{(ha)^{\frac{1}{3}}} \int_{-\infty}^{\infty} e^{i\nu\left(i_c - \frac{\pi}{2}\right)} \frac{\Omega_2 J_\nu(ha)}{\Omega_1 H_\nu^{(1)}(ha)} \, d\nu \ .$$

b) S-P (see Figure 1(c)).

The derivation here is exactly parallel to the case of P-S scattering, and we find the SP potential

$$\phi_s = -\left(\frac{1}{2\pi hX}\right)^{\frac{1}{2}} e^{i\left(hX - \frac{\pi}{4}\right)} (ha)^{\frac{1}{3}} C_{SP}(\omega), \text{ where}$$

$$C_{SP}(\omega) \equiv \frac{1}{(ha)^{\frac{1}{3}}} \int_{-\infty}^{\infty} e^{i\nu\left(i_c - \frac{\pi}{2}\right)} \frac{\Omega_4 J_\nu(ka)}{\Omega_3 H_\nu^{(1)}(ka)} \, d\nu \ .$$

The sign difference between ψ_s and ϕ_s above is due to the sign difference in our choice of source potentials for the two problems.

Appendix II

Expansion of the Point Source in a Smoothly Varying Spherically-Symmetric Medium

We wish to find the expansion, in an infinite series of spherical waves, for the solution to

$$\nabla^2\phi_i + h^2(r)\phi_i = \frac{\delta(r-b)\ \delta(\Delta)}{2\pi r^2 \sin\Delta} \quad x \quad \left(-\frac{4\pi}{ih(b)}\right)$$

(see Figure 1b for parameters r,Δ,b).

The angular functions are separable and lead to the same equation as the homogeneous case, with Legendre function solutions. So we try the form

$$\phi_i(r,\Delta) = \sum_{n=0}^{\infty} a(r,n)\ P_n(\cos\Delta) \qquad \text{(II.1)}$$

Then $a(r,n) = \left(n+\frac{1}{2}\right)\int_0^{\pi}\phi_i(r,\Delta)\ P_n(\cos\Delta)\sin\Delta\ d\Delta$, and substitution of (II.1) in the Helmholtz equation yields

$$\frac{d^2}{dr^2}\left[ra(r,n)\right] + \left[h^2(r) - \frac{n(n+1)}{r^2}\right] ra(r,n) = \frac{-\delta(r-b)(2n+1)}{i\ h(b)\ r} \qquad \text{(II.2)}$$

after an appeal to the orthogonality of Legendre functions.

Following Seckler and Keller (1959b) and Friedman (1951) we introduce three particular solutions of the homogeneous equation related to (II.2). Let $f_n(r)$ be that solution for $a(r,n)$ which is regular at the singularity r=0, and for large values of r let $g_n^{(1)}(r)$ and $g_n^{(2)}(r)$ be respectively, the outgoing and ingoing solution. (We may assume that outside some very large radius the medium is homogeneous.) Apart from a normalization, the three solutions are then completely defined, and we may take

$$\begin{aligned} a(r,n) &= c_1\, g_n^{(1)}(r) && b \le r \\ &= c_2\, f_n(r) && 0 \le r \le b. \end{aligned} \qquad \text{(II.3)}$$

The constants c_1, c_2 are determined from noting that (II.2) implies both

$$c_1\, g_n^{(1)}(b) - c_2\, f_n(b) = 0 \qquad \text{and}$$

$$c_1 \left[g_n^{(1)}(b) + b\, g_n^{(1)\prime}(b) \right] - c_2 \left[f_n(b) + b f_n'(b) \right] = - \frac{2n+1}{ih(b)b} ,$$

so

$$c_1 = \frac{2n+1}{ih(b)b^2} \frac{f_n(b)}{W(b)} , \quad c_2 = \frac{2n+1}{ih(b)b^2} \frac{g_n^{(1)}(b)}{W(b)}$$

where $W(r) \equiv g_n^{(1)}(r)\, f_n'(r) - g_n^{(1)'}(r)\, f_n(r)$ is the Wronskian of these two solutions.

Since $\left[r^2 W\right]' = \left[r g_n^{(1)}(r)\right]\left[r f_n(r)\right]'' - \left[r g_n^{(1)}(r)\right]''\left[r f_n(r)\right]$

$$= 0, \qquad W(r) \propto \frac{1}{r^2} \ .$$

The constant of proportionality depends on the normalization we choose for the basic solutions. Apart from this constant factor, we also know (for media in which rays do not become trapped in a duct) that the $g_n^{(\ell)}(r)$ may be given approximately by WKBJ solutions, i.e.

$$r\, g_n^{(2)}(r) \approx \frac{K^{(2)}}{\left[h^2(r) - \left(\frac{n+\frac{1}{2}}{r}\right)^2\right]^{1/4}} \exp \pm i \int_{r_o}^{r} \left[h^2(\xi) - \left(\frac{n+\frac{1}{2}}{\xi}\right)^2\right]^{1/2} d\xi \qquad (II.4)$$

where $K^{(1)}$, $K^{(2)}$ are constants and r_o is that radius at which the integrand vanishes (see Morse and Feshbach (1953), p. 1101).

Defining

$$p \equiv \frac{n + \frac{1}{2}}{\omega} \quad , \quad \text{we have} \quad p = \frac{r_o}{v(r_o)}$$

where $v(r)$ is the velocity from which wave-number $h(r) \equiv \omega/v(r)$ is derived. Hence, r_o has a physical interpretation as the radius to the deepest point along the ray with ray parameter p.

Our normalization for $g_n^{(\ell)}(r)$ is made after comparison with the Debye approximation to spherical Hankel functions. This approximation is

$$h_n^{(1)}(hr) \approx \frac{\exp \pm i\left[\left(h^2r^2-\left(n+\frac{1}{2}\right)^2\right)^{\frac{1}{2}} + \left(n+\frac{1}{2}\right)\sin^{-1}\left(\frac{n+\frac{1}{2}}{hr}\right) - \left(n+\frac{1}{2}\right)\frac{\pi}{2} - \frac{\pi}{4}\right]}{(hr)^{\frac{1}{2}}\left[h^2r^2 - \left(n+\frac{1}{2}\right)^2\right]^{\frac{1}{4}}}$$

and so may be written as

$$r\, h_n^{(1)}(hr) \approx \frac{e^{\mp i\pi/4}}{h^{\frac{1}{2}}} \cdot \frac{1}{\left[h^2-\left(\frac{n+\frac{1}{2}}{r}\right)^2\right]^{\frac{1}{4}}} \exp \pm i\int_{r_o}^{r}\left[h^2-\left(\frac{n+\frac{1}{2}}{\xi}\right)^2\right]^{\frac{1}{2}} d\xi$$

(in which h is constant).

We then take the normalization for $g_n^{(\ell)}(r)$ which allows equation (II.4) to be written as

$$g_n^{(1)}(r) \approx \frac{e^{\mp i\frac{\pi}{4}}}{\left(h(b)\right)^{\frac{1}{2}}} \cdot \frac{1}{r} \cdot \frac{1}{\left[h^2(r) - \left(\frac{n+\frac{1}{2}}{r}\right)^2\right]^{\frac{1}{4}}} \cdot \exp \pm i \int_{r_o}^{r} \left[h^2(\xi) - \left(\frac{n+\frac{1}{2}}{\xi}\right)^2\right]^{\frac{1}{2}} d\xi$$

in the region for which $h(r) \cdot r > n + \frac{1}{2}$ (i.e. above the depth of deepest penetration of the ray with parameter p). In homogeneous media, the $g_n^{(\ell)}(r)$ are spherical Hankel functions $h_n^{(\ell)}(hr)$.

Similarly, from WKBJ theory we have

$$r\, f_n(r) \approx \frac{K}{\left[\left(\frac{n+\frac{1}{2}}{r}\right)^2 - h^2(r)\right]^{\frac{1}{4}}} \exp + \int_{r_o}^{r} \left[\left(\frac{n+\frac{1}{2}}{\xi}\right)^2 - h^2(\xi)\right]^{\frac{1}{2}} d\xi$$

in the region for which $h(r)\, r < n + \frac{1}{2}$. We take

$$K = \frac{1}{2\left(h(b)\right)^{\frac{1}{2}}} \quad , \quad \text{for then in homogeneous media}$$

$f_n(r)$ is the spherical Bessel function $j_n(hr)$.

The three functions $f_n(r)$, $g_n^{(\ell)}(r)$ are solutions in all ranges of radius, and it is of interest to find the connection formula between them. From Morse and Feshbach (1953, pp. 1097-1101) we see that the same relation is satisfied as that for spherical Hankel/Bessel functions, i.e. the connection formula has the simple form

$$f_n(r) = \frac{1}{2}\left[g_n^{(1)}(r) + g_n^{(2)}(r) \right] \qquad \text{(II.5)}$$

With the normalization above, it is now possible to evaluate the Wronskian. We find

$$W(r) = -\frac{i}{r^2 h(b)} \quad , \text{ exactly.}$$

So from equations (II.1), (II.3), (II.5) we finally obtain

$$\phi_i(r,\Delta) = \sum_{n=0}^{\infty} \left(n + \frac{1}{2}\right) g_n^{(1)}(r_>) \left[g_n^{(1)}(r_<) + g_n^{(2)}(r_<) \right] \qquad \text{(II.6)}$$

where

$$r_> = \max(r,b), \qquad r_< = \min(r,b).$$

The formula used in section (2.5) for expanding the point source in a homogeneous medium is a special case of equation (II.6).

Appendix III

A Proof that $\left.\frac{d^2\Phi}{d\nu^2}\right|_{\nu = \omega p} = -\frac{1}{\omega \frac{d^2T}{d\Delta^2}}$,

where Φ is the Phase Function of Section (2.6).

From equation (2.6.4), we have

$$\frac{d\Phi}{d\nu} = -\nu\left\{\int_{r_o(\nu)}^{r} \frac{d\xi}{\xi^2\left[h^2(\xi) - \frac{\nu^2}{\xi^2}\right]^{\frac{1}{2}}} + \int_{r_o(\nu)}^{b} \frac{d\xi}{\xi^2\left[h^2(\xi) - \frac{\nu^2}{\xi^2}\right]^{\frac{1}{2}}}\right\} + \Delta,$$

where $r_o(\nu) = \nu/h\left(r_o(\nu)\right)$, and hence is a singularity of the integrands. We consider only those media in which the velocity gradient is sub-critical, i.e. $\frac{dv}{dr} < \frac{v}{r}$. It is then permissible to transform from ξ to η, where

$$\eta = \frac{\xi\, h(\xi)}{\omega} \quad . \qquad \text{Then} \qquad d\xi = \frac{\omega}{h(\xi)\,(1-\zeta)}$$

where $\zeta = -\frac{\xi}{h(\xi)} \cdot \frac{d\, h(\xi)}{d\xi}$, and so

$$\frac{d\Phi}{d\nu} = -\nu \left\{ \int_{\frac{\nu}{\omega}}^{h(r)\cdot r/\omega} \frac{d\eta}{\eta\left[\omega^2\eta^2-\nu^2\right]^{\frac{1}{2}}(1-\zeta)} + \int_{\frac{\nu}{\omega}}^{h(b)\cdot b/\omega} \frac{d\eta}{\eta\left[\omega^2\eta^2-\nu^2\right]^{\frac{1}{2}}(1-\zeta)} \right\} + \Delta$$

This formula may be integrated by parts, and

$$\frac{d\Phi}{d\nu} = -\left[\left(\frac{1}{1-\zeta}\right)\cos^{-1}\left(\frac{\nu}{\omega\eta}\right)\right]_{\frac{\nu}{\omega}}^{h(r)r/\omega} - \left[\left(\frac{1}{1-\zeta}\right)\cos^{-1}\left(\frac{\nu}{\omega\eta}\right)\right]_{\frac{\nu}{\omega}}^{h(b)b/\omega}$$

$$+ \int_{\nu/\omega}^{h(r)r/\omega} \cos^{-1}\left(\frac{\nu}{\omega\eta}\right)\cdot\frac{d}{d\eta}\left(\frac{1}{1-\zeta}\right)d\eta + \int_{\nu/\omega}^{h(b)\ b/\omega} \cos^{-1}\left(\frac{\nu}{\omega\eta}\right)\cdot\frac{d}{d\eta}\left(\frac{1}{1-\zeta}\right)d\eta$$

These integrands have no singularity (unless at $\zeta = 1$. But this is ruled out by requiring sub-critical velocity gradients). They are zero at the lower limits of integration, and so by direct differentiation we may obtain

$$\frac{d^2\Phi}{d\nu^2} = \left(\frac{1}{1-\zeta}\right)_{\xi=r} \frac{1}{\left[h^2(r)r^2-\nu^2\right]^{\frac{1}{2}}} + \left(\frac{1}{1-\zeta}\right)_{\xi=b} \cdot \frac{1}{\left[h^2(b)b^2-\nu^2\right]^{\frac{1}{2}}}$$

$$- \int_{\nu/\omega}^{h(r)\ r/\omega} \frac{1}{\left[\omega^2\eta^2-\nu^2\right]^{\frac{1}{2}}} \frac{d}{d\eta}\left(\frac{1}{1-\zeta}\right)\ d\eta - \int_{\nu/\omega}^{h(b)b/\omega} \frac{1}{\left[\omega^2\eta^2-\nu^2\right]^{\frac{1}{2}}} \frac{d}{d\eta}\left(\frac{1}{1-\zeta}\right) d\eta\ .$$

Comparing Bullen (1963, p. 113), we see that

$$\left.\frac{d^2\Phi}{d\nu^2}\right|_{\nu=\omega p} = -\frac{1}{\omega} \cdot \frac{d\Delta}{dp}\ .$$ But $p = \frac{dT}{d\Delta}$ where T is the travel

time, and so finally we have

$$\left.\frac{d^2\Phi}{d\nu^2}\right|_{\nu=\omega p} = -1\Big/\left[\omega \frac{d^2T}{d\Delta^2}\right]\ .$$

Appendix IV

Description of the Program EXACT

EXACT is a FORTRAN 4 computer program, written for an IBM 360/75 system, which evaluates complex path integrations in the ν-plane of certain functions F(IFLAG, ν), discussed in Section (2.5).

Purpose

For correct choice of the path, this integral is the exact solution at the point $P(r,\Delta)$ to one of six elasticity problems (specified by IFLAG = 1,...,6). With IFLAG = 1,2 and 3 these solutions are for the exact total potential in respectively, P-P, SV-SV, SH-SH scattering due to a source potential at point $S(b,0)$. For IFLAG = 4,5 and 6 the solutions are an exact total component of displacement for the problems listed in Tables 2, 3 and 4, respectively.

Usage

A problem of the above type is specified by an Earth model $(\alpha,\beta,\alpha',\rho,\rho'$, a), IFLAG, a frequency, a set of (up to 6) source radii b, one station radius r, a set of (up to 30) station distances Δ, and a description of the complex path Γ (up to 5 line segments).

Choice of path Γ.

A discussion of this type of path integral is given by Phinney and Cathles (1969), in which it is pointed out that the solution at (r,Δ) for a range of Δ may be found numerically using the same complex path Γ. Thus the integrand has to be changed for different Δ, and the integrand has two saddles or none according as (r,Δ) is in the lit zone or the shadow. But we do not attempt to make Γ follow a steepest descent path. The advantage of fixing Γ in each problem is seen by observing that the integrand may be split into three factors, dependent respectively on source/station radii, on the Earth model, and on Δ. For example, we have

$$F(1,\nu) = \left[-\nu h^{(1)}_{\nu-\frac{1}{2}}(hb)\ h^{(1)}_{\nu-\frac{1}{2}}(hr) \right] \times \left[\frac{\Omega_5 h^{(2)}_{\nu-\frac{1}{2}}(ha)}{\Omega_5 h^{(1)}_{\nu-\frac{1}{2}}(ha)} \right] \times \left[Q^{(2)}_{\nu-\frac{1}{2}}(\cos\Delta) \right] .$$

The evaluation of the first two factors is much more time consuming than evaluation of $Q^{(2)}_{\nu}$. So the program stores values of the first two factors, and these values may be re-used in each integration for different Δ, since Γ is fixed.

For the solutions given in Chapter 2, Γ is composed of three line segments. See Figure 17. For P-wave problems, Γ is $A \to (ha,0) \to B \to C$ where B is chosen to be near the direct P-wave saddle point for the smallest Δ in the range discussed. The integrands decay exponentially along directions $(ha,0) \to A$, $B \to C$; A and C are chosen sufficiently far from the real axis to include all the

significant contributions of the integrand. Thus, for P-wave problems Γ is essentially the path described by Phinney and Cathles (1969). For SH problems we use E → (ka,0) → F → G in the same way as for P-wave problems. For SV there is the additional complication (see Section (2.5)) due to the poles near (h'a,0). So for the low frequency (f = 0.03 Hz) we use D → (h'a,0) → F → G, and for the high frequency (f = 0.2 Hz) we use E → (ka,0) → F → G. A choice of different paths has in fact shown the "head-wave" effect to be negligibly small (~ 1%), and we mention it because this is the only case in which our program returns solutions varying by more than 0.2% for a different choice of paths.

Method

The Hankel package of SHARE numbers 1355-1359, 1361 is used, after correction of three errors. The functions $Q^{(2)}_{\nu-\frac{1}{2}}(\cos\Delta)$ are evaluated by converting formulae in Robin (1958, pages 237 and 240) into a power series in $\frac{1}{\nu}$, and retaining $0\left(\frac{1}{\nu_3}\right)$.

A considerable reduction in core space is achieved by integrating the different line segments separately. For example, with a P-wave problem, the three factors mentioned above are first evaluated at (say) 51 points along A → (ha,0) (see Figure 17; these have to be stored some for each b, some for each Δ). A Simpson integration scheme then selects values corresponding to each (b,Δ) combination,

and stores the integrals along this first line segment. The second line segment is then treated, and note that the values of the three factors mentioned above need to be stored only along one line segment, and only before segment integration. The third line segment is integrated, and the final solution is a sum of the three line segments corresponding to one (b,Δ) combination.

A simple on-line plotting option is available for each segment, to monitor the choice of end points and also the spacing of points at which the integrand is evaluated. (Up to 101 points may be taken on each segment.) The fact that both real and imaginary parts of the integrand are well-behaved numerically is our justification for using a Simpson's rule with even spacing. Any integration method which varies the spacing will required much more computer time, since for example, the model factor

$$\left[\frac{\Omega_5 h^{(2)}_{\nu-\frac{1}{2}}(ha)}{\Omega_5 h^{(1)}_{\nu-\frac{1}{2}}(ha)} \right]$$

would have to be re-calculated for each Δ, and separately for real and imaginary integrations.

Appendix V

The Fresnel-Kirchhoff Method in Radially Heterogeneous Media

We take the elasticity problem posed in section (2.6), and use methods of geometrical ray theory to obtain a similar solution.

Our basic formula is a standard integral theorem for the potential at $P(r,\Delta)$:

$$\phi(P) = -\frac{1}{4\pi} \iint_S \left[\phi(Q) \frac{\partial}{\partial n} G(Q,P) - G(Q,P) \frac{\partial \phi}{\partial n}(Q) \right]_{Q \text{ on} S} dS \qquad (V.1)$$

where S is any closed surface surrounding P, n is the outward normal on S, and $G(Q,P)$ is a Greens function. The normalization of G in equation(V.1) is such that ray theory approximation gives

$$G(Q,P) \sim \frac{e^{i\Phi(Q,P)}}{R(Q,P)} \qquad \text{where we define}$$

$$\Phi(A,B) \equiv \int_A^B h(s)ds \qquad \text{(integrating along the direct ray from A to B)}$$

$$R(A,B) \equiv \frac{r_A r_B \left[\sin(\Delta_A - \Delta_B)\, h(r_A)\, h(r_B) \cos i(r_A) \cos i(r_B) \right]^{\frac{1}{2}}}{\left[\omega p \left(-\omega \frac{\partial^2 T}{\partial \Delta^2} \right) \right]^{\frac{1}{2}}} \qquad (V.2)$$

in which p (the ray parameter), $i(r_A)$ and $i(r_B)$ (angles of incidence), and T(travel time) refer to the direct ray from A to B. Note that in a homogeneous medium R(Q,P) = distance between Q and P, and the formula for G is exact.

We chose the surface $S = A + B + C$ where (see Figure 18a) A is part of the plane normal to SP which passes through 0 (the turning point) - namely that part between some arbitrarily large radius and radius r = a; B is the hemisphere of core surface on the P side of A, and C is the hemisphere which contains P and forms a closed surface together with A and B.

The contribution from C to the integral (V.1) is negligible.

We take Kirchhoff's boundary conditions on A and B, i.e.

on A:

$$\phi(Q) = \phi_i(Q), \quad \left.\frac{\partial\phi}{\partial n}\right|_Q = \left.\frac{\partial\phi_i}{\partial n}\right|_Q \quad \left(\text{note: } \phi_i(Q) = \frac{1}{ih(b)}\, G(S,Q)\right)$$

on B: $\phi(Q) = 0$, $\left.\frac{\partial\phi}{\partial n}\right|_Q = 0$ (see Born and Wolf (1959, p. 378)),

and neglect $\frac{1}{R}$ in comparison to h to obtain

$$\phi(P) = -\frac{1}{4\pi} \iint_A \frac{e^{i\Phi(S,Q)} e^{i\Phi(Q,P)} \left[\sin i(r_Q;S,Q) + \sin i(r_Q;Q,P)\right] ih(r_Q)\, dS}{i\, h(b)\, R(S,Q)\, R(Q,P)}$$

As the element dS(Q) ranges over A, the only factors in this integrand which change rapidly are the phase functions. So we take all other factors outside the integration (using their values when Q is at 0, see Figure 18a), giving

$$\phi(P) = - \frac{h(y)\ e^{i\int_S^P h(s)\ ds}}{2\pi h(b)\ R(S,0)\ R(0,P)} \iint_A e^{i\delta\Phi(Q)} dS \qquad (V.3),$$

where $\delta\Phi(Q)$ is the difference in phase between the sum of ray paths $(S \to Q)$ and $(Q \to P)$, and the ray path $(S \to P)$.

We thus need to evaluate $\delta\Phi(Q)$ as some function of two parameters (u,v), say, which specify the position of Q on the "aperture" plane A. Our choice of these parameters is guided by the Fresnel method for a screen in homogeneous media (see e.g. Baker and Copson (1939)); thus, the integration of exp i $\delta\Phi(Q)$ has contributions only from the vicinity of the point 0, about which point $\delta\Phi$ is first expressed as some second order formula $\lambda(u(Q) - u(0))^2 + \mu(v(Q) - v(0))^2$.

Our parameterization of the aperture plane is shown in Figure 18b, as viewed from the source side, near 0. The horizontal axis is simply Cartesian distance z from the vertical plane through S and P. The vertical axis is given by the ray parameter q of the ray $(S \to Q)$.

$\delta\Phi(Q)$ has a component $\delta_z\Phi$ (say) due to the fact that Q is not in the same vertical plane as SP. If the angular distance from S to Q is $\Delta_1 + \delta\Delta_1$, and from Q to P is $\Delta_2 + \delta\Delta_2$, then it follows from a

formula for travel time (Bullen, 1963, p. 112) that $\delta_z \Phi = \omega p(\delta\Delta_1 + \delta\Delta_2)$, where we use p as the ray parameter for (S → P). But $\delta\Delta_i = (z^2 \cot \Delta_i)/2y^2$, where y is the radius to 0, so we have obtained one component of $\delta\Phi(Q)$.

The remaining component, due to the vertical difference between 0 and Q, may be obtained graphically as follows:

Suppose Q is a fixed point, and P is varied (with constant radius) around that position P(Q) which has the same ray parameter as (S → Q). Let us examine the p-Δ diagram, Figure 18c, for both the rays S → P and Q → P as P varies. The ray parameter for the S → P path is a function of distance (Δ) governed by the Earth model. But the ray parameter for Q → P is $\left.\frac{h\ r \sin i(r)}{\omega}\right|_{r=r_Q}$, and this has the almost constant value q as P varies for fixed Q. Note that the travel time difference for arrivals at P (from S) via the two paths is given by the area between the two curves in Figure 18c, i.e. $\frac{(q-p)^2}{2}\left(-\frac{\partial\Delta}{\partial p}\right)$, and the corresponding component of $\delta\Phi$ is ωx travel time distance.

The formulae used for the integration of (V.3) are thus

$$\delta\Phi(Q) = \omega p \frac{z^2}{2y^2}\left(\cot \Delta_1 + \cot \Delta_2\right) + \frac{\omega(q-p)^2}{2}\left(-\frac{\partial\Delta}{\partial p}\right) \qquad \text{and}$$

$$dS = \frac{dz\ dq\ \omega}{h(y)[1-\zeta(y)]} \quad \text{where } \zeta \text{ is the normalized velocity gradient,}$$

$\frac{r}{v}\frac{dv}{dr}$. Then

$$\phi(P) = \frac{-h(y)e^{i\int_S^P h(s)ds}}{2\pi h(b)\ R(S,O)\ R(O,P)}\ \frac{\omega}{h(y)(1-\zeta(y))}\ X$$

$$\int_{z=-\infty}^{\infty}\ \int_{\omega q=h(a)a}^{\infty} \exp\, i\left[\omega p\,\frac{z^2}{2y^2}\left(\cot\Delta_1+\cot\Delta_2\right)+\frac{\omega(q-p)^2}{2}\left(-\frac{\partial\Delta}{\partial p}\right)\right]dzdq\ .$$

Set

$\frac{\omega(q-p)^2}{2}\left(-\frac{\partial\Delta}{\partial p}\right)=\frac{\pi}{2}\tau^2$, and note that $\int_{-\infty}^{\infty} e^{i\pi/2\alpha^2}\,d\alpha = e^{i\pi/4}\sqrt{2}$,

and $\frac{\partial\Delta}{\partial p} = \left(\frac{\partial^2 T}{\partial\Delta^2}\right)^{-1}$. We then obtain

$$\phi(P) = \frac{y}{ih(b)\ R(S,O)\ R(O,P)[1-\zeta(y)]}\left[\frac{1}{\omega p\left(\cot\Delta_1+\cot\Delta_2\right)}\left(-\omega\frac{\partial^2 T}{\partial\Delta^2}\right)\right]^{\frac{1}{2}}\ X$$

$$\frac{1}{2}\left\{1-e^{-i\pi/4}\sqrt{2}\int_0^{\frac{h(a)a-\omega p}{\left[-\pi\omega\frac{\partial^2 T}{\partial\Delta^2}\right]^{\frac{1}{2}}}} e^{i\pi/2\tau^2}\,d\tau\right\}\ X\ e^{i\int_{\text{source}}^{\text{receiver}} h(s)ds}$$

(V.4)

This is a useful form for $\phi(P)$, but we can obtain better similarity with section (2.6). For, noting from (V.2) that

$$R(S,O) = b\left[\frac{\sin\Delta_1\, h(b)\cos i(b)}{h(y)(1-\zeta(y))}\right]^{\frac{1}{2}}$$

$$R(O,P) = r\left[\frac{\sin\Delta_2\, h(r)\cos i(r)}{h(y)(1-\zeta(y))}\right]^{\frac{1}{2}} \quad \text{and also that}$$

$\left(\cot\Delta_1 + \cot\Delta_2\right)\sin\Delta_1\sin\Delta_2 = \sin\Delta$, we have from (V.4) the result

$$\phi(P) = \frac{1}{i\, br\, h(b)}\left[\frac{\omega p}{\sin\Delta\, h(b)\, h(r)\cos i(b)\cos i(r)}\left(-\omega\frac{\partial^2 T}{\partial\Delta^2}\right)\right]^{\frac{1}{2}} X$$

$$\frac{1}{2}\left\{1 - e^{-i\pi/4\sqrt{2}}\int_0^{\frac{h(a)a-\omega p}{\left[-\pi\omega\frac{\partial^2 T}{\partial\Delta^2}\right]^{\frac{1}{2}}}} e^{i\pi/2\tau^2}\, d\tau\right\} X\, e^{i\int_{\text{source}}^{\text{receiver}} h(s)ds} \qquad (V.5)$$

which is part of the solution (2.6.5). Since in this Appendix we use the Kirchhoff boundary conditions $\phi(Q) = 0$, $\left.\frac{\partial\phi}{\partial n}\right|_Q = 0$ on the surface $\mathcal{B}$, equation (V.5) does not contain the integral of reflection coefficients which is a feature of (2.6.5).

If the medium is homogeneous, and if further r = b, then (V.5) does reduce to the Fresnel formula quoted by Phinney and Cathles (1969).

Appendix VI

Asymptotic Expansion about Turning Points

We study the function $g^{(1)}_{\nu-\frac{1}{2}}(r)$, introduced in Section (2.6), and obtain first a method of evaluation for r varying in the region $|r - R| \sim R|\nu|^{-2/3}$, where we define the turning point radius R to be the solution of

$$\nu = h(R)R \qquad \text{(VI.1)}$$

We restrict our discussion to media for which a ray bottoms at every depth, and then equation (VI.1) defines just one value R, which is a function of ν.

If we take $b(r) = r^{+1/2}\, g^{(1)}_{\nu-\frac{1}{2}}(r)$, then

$$\frac{d^2b}{dr^2} + \frac{1}{r}\frac{db}{dr} + \left[h^2(r) - \frac{\nu^2}{r^2} \right] b = 0.$$

We need to evaluate several physical variables (e.g. the gradient of velocity $\alpha(r)$) at the turning point radius R, and it is convenient to use the notation of capital letters to represent values at r = R. Thus, we use

$$H = h(R), \quad X = x(R) \quad \text{where} \quad x = \frac{r}{\alpha(r)}\frac{d\alpha}{dr} = -\frac{r}{h(r)}\frac{d\,h(r)}{dr} \quad ,$$

and $Y = y(R)$ where $y = \frac{r^2}{\alpha(r)} \frac{d^2\alpha}{dr^2}$. We also define a variable u by $u = \frac{1}{Q}(\nu - Hr)$, where $Q = q(R)$ and $\frac{1}{q(R)} = \left(\frac{2(1-x)}{h(r)r} \right)^{1/3}$.

Note that capitals are independent of r, but do depend on ν.

Since $\frac{d}{dr} = -\frac{H}{Q}\frac{d}{du}$ (for a fixed value of ν), we have for $c(u) \equiv b(r)$ the result

$$\frac{1}{Q^2}\frac{d^2c}{du^2} - \frac{1}{QHr}\frac{dc}{du} + \left[\frac{h^2(r)}{H^2} - \frac{\nu^2}{H^2r^2} \right] c = 0$$

In order to study solutions of this equation near the value $u = 0$, we expand the coefficients as a power series in $\frac{1}{Q^2}$, to obtain

$$\frac{1}{Q^2}\frac{d^2c}{du^2} - \frac{1}{Q^4.2(1-X)} \left[1 + \frac{0(u)}{Q^2} \right] \frac{dc}{du}$$

$$+ \left[-\frac{u}{Q^2} + \frac{u^2(3X^2-3-Y)}{Q^4 4(1-X)^2} + \frac{0(u^3)}{Q^6} \right] c = 0$$

(VI.2)

Now we assume the asymptotic form

$$c(u) = \sum_{n=o}^{\infty} \frac{1}{Q^{2n}} f_n(u), \text{ valid for } u = 0(1).$$

Upon substitution for $c(u)$ into (VI.2), it follows that we require

$$f_o''(u) - uf_o(u) = 0$$

$$f_1''(u) - uf_1(u) = -\frac{1}{2(1-X)} \left[f_o'(u) + \left(\frac{3(1+X)}{2} + \frac{Y}{2(1-X)} \right) u^2 f_o(u) \right]$$

(VI.3)

and so on for $f_n(u)$, with $n > 1$.

Clearly, $f_o(u)$ is some combination of Airy functions, and the combination may be found by taking an arbitrarily large value of ν (so that $f_o(u)$ dominates the expansion for $c(u)$) and comparing the resultant $g^{(1)}_{\nu-\frac{1}{2}}(r) \sim \frac{1}{r^{1/2}} f_o(u)$ with the approximation given in Appendix II:

$$g^{(1)}_{\nu-\frac{1}{2}}(r) \sim \frac{e^{-i\pi/4}}{(h(b))^{\frac{1}{2}}} \frac{1}{r} \frac{1}{\left[h^2(r)-\frac{\nu^2}{r^2}\right]^{\frac{1}{4}}} \exp i \int_R^r \left[h^2(\xi) - \frac{\nu^2}{\xi^2}\right]^{\frac{1}{2}} d\xi$$

(VI.4)

for r just greater than R. Expanding the phase integrand about $\xi = R$, we have

$h^2(\xi) - \frac{\nu^2}{\xi^2} \sim \left(\xi - \frac{\nu}{H}\right) \frac{2H^3}{\nu}(1-X)$. This approximation may be integrated, and from (VI.4) we obtain

$$g^{(1)}_{\nu-\frac{1}{2}}(r) \sim \frac{e^{-i\pi/4}}{r^{\frac{1}{2}}} \left[2\, h(b)(1-X)\right]^{-\frac{1}{2}} \left(\frac{2(1-X)}{\nu}\right)^{1/3} \frac{\exp i\frac{2}{3}(-u)^{3/2}}{(-u)^{1/4}}.$$

The Airy function which has the corresponding phase property is

$$Ai(ue^{2i\pi/3}) \sim \frac{1}{2} \frac{e^{i\pi/12}}{\sqrt{\pi}} \frac{\exp i\frac{2}{3}(-u)^{3/2}}{(-u)^{1/4}}, \text{ and hence we obtain}$$

$f_o(u)$ as

$$f_o(u) = 2\, e^{-i\pi/3} \left(\frac{\pi}{2h(b)(1-X)}\right)^{\frac{1}{2}} \left(\frac{2(1-X)}{\nu}\right)^{1/3} Ai(ue^{2i\pi/3})$$

Then $f_1(u)$ may be determined from equation (VI.3), and we achieve the result

$$g^{(1)}_{\nu-\frac{1}{2}}(r) = \frac{2e^{-i\pi/3}}{r^{\frac{1}{2}}}\left(\frac{\pi}{2h(b)(1-X)}\right)^{\frac{1}{2}}\left(\frac{2(1-X)}{\nu}\right)^{\frac{1}{3}}\Bigg[\mathrm{Ai}(ue^{2i\pi/3}) +$$

$$\left(\frac{2(1-X)}{\nu}\right)^{2/3}\Bigg\{\left(\frac{2-3X}{20(1-X)} - \frac{Y}{20(1-X)^2}\right)\ u\ \mathrm{Ai}(ue^{2i\pi/3}) +$$

$$\left(\frac{3(1+X)}{20(1-X)} + \frac{Y}{20(1-X)^2}\right)\ u^2\ e^{2i\pi/3}\ \mathrm{Ai}'(ue^{2i\pi/3})\Bigg\} + O\left\{\left(\frac{2(1-X)}{\nu}\right)^{4/3}\right\}\Bigg]$$

where

$$u = \left(\frac{2(1-X)}{\nu}\right)^{\frac{1}{3}} H(R-r) \qquad \text{(VI.5)}$$

We note (i) that X, Y, R, H are all functions of ν, but not of r. (ii) The intrinsic coupling in an inhomogeneous medium (P-SV coupling, up-downgoing P to P coupling) merely adds terms to equation (VI.2) which are $O\left(\frac{1}{Q^5}\right)$ (for a proof, we use the coupled equations developed in Chapter 3). And so even the second term in our expansion for $g^{(1)}_{\nu-\frac{1}{2}}(r)$ is not affected by intrinsic coupling.

(iii) From equation (VI.5) we find

$$\frac{d}{dr}\, g^{(1)}_{\nu-\frac{1}{2}}(r) = -\frac{2e^{i\pi/3}H}{r^{\frac{1}{2}}}\left(\frac{\pi}{2h(b)(1-X)}\right)^{1/2}\left(\frac{2(1-X)}{\nu}\right)^{2/3}\Bigg[\, Ai'(ue^{2i\pi/3}) +$$

$$\left(\frac{2(1-X)}{\nu}\right)^{2/3}\Bigg\{\left(\frac{3(1+X)u^3}{20(1-X)} + \frac{Yu^3}{20(1-X)^2} + \frac{7-3X}{20(1-X)} - \frac{Y}{20(1-X)^2}\right) e^{-2i\pi/3}Ai(ue^{2i\pi/3})$$

$$+ \left(\frac{8+3X}{20(1-X)} + \frac{Y}{20(1-X)^2}\right)\, uAi'(ue^{2i\pi/3}) + O\left\{\left(\frac{2(1-X)}{\nu}\right)^{4/3}\right\}\Bigg] \qquad \text{(VI.6)}$$

(iv) The results (VI.5) and (VI.6) reduce to standard expansions for spherical Hankel functions, if we take $X = Y = 0$. (See Abramowitz and Stegun (1964), § 9.3.23).

(v) The formulae above have been obtained for any fixed choice of ν, as r varies near the turning point radius R. Since $u = O(1)$, our formulae are valid in the region $|r - R| \sim R|\nu|^{-2/3}$.

But provided we maintain $u = O(1)$, it is clear that our results may also be used for a fixed choice of r, $r = r_1$ (say), as ν varies such that R is near r_1. The expansions (VI.5) and (VI.6) are then useful only if we can evaluate

$$u(\nu) = \left(\frac{2\{1 - X(R(\nu))\}}{\nu} \right)^{1/3} \left(\nu - H\{R(\nu)\}\, r_1 \right)$$

as ν varies in the complex order plane near the value $\nu = h(r_1)r_1$. A simple and sufficiently accurate formula for $u(\nu)$ is provided by the Taylor series expansion, since we can show

$$u(\nu) = (\nu - h(r_1)r_1) \left.\frac{du}{d\nu}\right|_{\nu=h(r_1)r_1} + \frac{\{\nu - h(r_1)r_1\}^2}{2} \left.\frac{d^2u}{d\nu^2}\right|_{\nu=h(r_1)r_1} + O\left[\left(\frac{1}{h(r_1)r_1}\right)^{4/3}\right]$$

(VI.7)

We find after some algebraic reduction, that

$$u = t - \frac{t^2}{6} \left(\frac{2(1-x(r_1))}{h(r_1)r_1}\right)^{2/3} \left[\frac{1}{1-x(r_1)} - \frac{y(r_1)}{2(1-x(r_1))^2}\right] + O\left[\left(\frac{1}{h(r_1)r_1}\right)^{4/3}\right]$$

(VI.8)

where we define

$$t \equiv \left(\frac{2(1-x(r_1))}{h(r_1)r_1} \right)^{1/3} \left[\frac{\nu - h(r_1)r_1}{1-x(r_1)} \right] = 0(1).$$

Since $h(r_1)r_1 >> 30$ for almost all seismic body wave problems, the first two terms in equation (VI.8) are sufficiently accurate to determine u. The expansions (VI.5) and (VI.6) may now be written in terms of t, and ν and t are equivalent independent variables (satisfying a linear relation). Our final asymptotic expressions are then

$$g^{(1)}_{\nu-\frac{1}{2}}(r_1) = \frac{2e^{-i\pi/3}}{r_1^{1/2}} \left(\frac{\pi}{2h(b)(1-x_1)} \right)^{\frac{1}{2}} \left(\frac{2(1-x_1)}{h_1 r_1} \right)^{\frac{1}{3}} \left[Ai(t\, e^{2i\pi/3}) + \right.$$

$$\left(\frac{2(1-x_1)}{h_1 r_1} \right)^{2/3} \left\{ \left(\frac{3x_1-2}{30(1-x_1)} + \frac{y_1}{30(1-x_1)^2} \right) t\, Ai(t\, e^{2i\pi/3}) \right.$$

$$\left. \left. + \left(\frac{9x_1-1}{60(1-x_1)} + \frac{2y_1}{15(1-x_1)^2} \right) t^2 e^{2i\pi/3} Ai'(t\, e^{2i\pi/3}) \right\} + 0\left\{ \left(\frac{2(1-x_1)}{h_1 r_1} \right)^{1/3} \right\} \right]$$

and

$$\frac{d}{dr}\, g^{(1)}_{\nu-\frac{1}{2}}(r)\Big|_{r=r_1} = -\frac{2e^{i\pi/3}h_1}{r_1^{\frac{1}{2}}}\left(\frac{\pi}{2h(b)(1-x_1)}\right)^{1/2}\left(\frac{2(1-x_1)}{h_1 r_1}\right)^{2/3}\Bigg[\mathrm{Ai}'(t\,e^{2i\pi/3}) +$$

$$\left(\frac{2(1-x_1)}{h_1 r_1}\right)^{2/3}\Bigg\{\left(\frac{(9x_1-1)t^3}{60(1-x_1)} + \frac{2y_1 t^3}{15(1-x_1)^2} + \frac{7-3x_1}{20(1-x_1)} - \frac{y_1}{20(1-x_1)^2}\right) e^{-2i\pi/3}$$

$$\times\ \mathrm{Ai}(te^{2i\pi/3})$$

$$+\ \left(\frac{2-3x_1}{30(1-x_1)} - \frac{y_1}{30(1-x_1)^2}\right)\ t\,\mathrm{Ai}'(te^{2i\pi/3}) + O\left\{\left(\frac{2(1-x_1)}{h_1 r_1}\right)^{4/3}\right\}\Bigg] \qquad \text{(VI.9)}$$

The suffix 1 denotes evaluation at $r = r_1$, and we recall the definitions

$x = \frac{r}{\alpha}\frac{d\alpha}{dr}$, $y = \frac{r^2}{\alpha}\frac{d^2\alpha}{dr^2}$ for velocity profile $\alpha(r)$, and

$$\nu = h_1 r_1\left[1 + \frac{t}{2}\left(\frac{2(1-x_1)}{h_1 r_1}\right)^{2/3}\right].$$

Appendix VII

Inversion of Perturbed $\frac{dT}{d\Delta}$ data

Statement of Inversion Problem

We wish to invert $\frac{dT}{d\Delta}$ values (given as a function of Δ) to obtain the velocity profile $V(r)$, when $\frac{dT}{d\Delta} - p(\Delta) = \delta p(\Delta)$ is small, and the profile $v(r)$ corresponding to $p(\Delta)$ is known.

Solution Method (due to Jeffreys, 1966)

Let r be the turning point radius for the ray with emergence at distance Δ in the known structure $v(r)$, and let $r + \delta r$ be this radius, for emergence at Δ, in $V(r)$. Then from Wiechert-Herglotz inversion in each model we have

$$\int_0^{\Delta} \left[\cosh^{-1}\left(\frac{p_1 + \delta p_1}{\eta + \delta\eta}\right) - \cosh^{-1}\left(\frac{p}{\eta}\right) \right] d\Delta_1 = \pi \ln\left(\frac{r}{r+\delta r}\right),$$

where $p_1 = p(\Delta_1)$ and $\eta = p(\Delta)$. Jeffreys (1966) points out that for small perturbations δp_1, the integrand here may adequately be approximated by the first order terms, which are

$$\frac{\eta\ \delta p_1 - p_1\ \delta\eta}{\eta[p_1^2 - \eta^2]}$$

Application

This method is particularly simple to use when v(r) is a constant (since the integrals of the first order terms may be found explicitly). Thus, to invert the 10 second values of $\frac{dT}{d\Delta}$ in Figure 22 we take

$$v = 13.6 \text{ km/sec, for which } p(\Delta) = \frac{6350}{13.6} \sin\left(\frac{\pi-\Delta}{2}\right) \text{ sec/radian,}$$

and $\frac{dT}{d\Delta}$ (10 sec) = p for $\Delta \leq 108.5° \times \frac{\pi}{180} \equiv \Delta_o$(say)

$$= p + \frac{0.18}{5} (\Delta-\Delta_o) \times \left(\frac{180}{\pi}\right)^2 \text{ for } \Delta_o \leq \Delta \leq 113.5° \times \frac{\pi}{180}$$

Our solution method gives $r + \delta r = r \exp\left[- I_1 - I_2\right]$ where

$$I_1 = - \frac{1}{\pi} \int_0^{\Delta} \frac{p_1 \delta\eta\ d\Delta_1}{\eta(p_1{}^2-\eta^2)} \quad , \quad I_2 = \frac{1}{\pi} \int_0^{\Delta} \frac{\delta p_1\ d\Delta_1}{(p_1{}^2-\eta^2)}$$

Clearly, $\delta r = 0$ for distances not greater than Δ_o(=108.5°). For $\Delta_o < \Delta \leqslant 113.5°$ we find that $I_1 = -\frac{\delta\eta}{\eta}$, and for I_2 we use

$$\delta p_1 = \frac{.18}{5} \times \left(\frac{180}{\pi}\right)^2 (\Delta_1 - \Delta_o)$$

$$\left(p_1^2 - \eta^2\right)^{\frac{1}{2}} = \frac{6350}{13.6}\left(\cos^2\frac{\Delta_1}{2} - \cos^2\frac{\Delta}{2}\right)^{1/2} \sim \frac{6350}{13.6}\left[(\Delta-\Delta_1)\frac{\sin\Delta}{2}\right]^{\frac{1}{2}}.$$

So

$$I_2 = \frac{1}{\pi}\left(\frac{13.6}{6350}\right)\left(\frac{.18}{5}\right)\left(\frac{180}{\pi}\right)^2\left(\frac{2}{\sin\Delta}\right)^{\frac{1}{2}}\int_{\Delta_o}^{\Delta}\frac{(\Delta_1-\Delta_o)}{(\Delta-\Delta_1)^{1/2}}\,d\Delta_1$$

$$= 0.000362\,(\Delta-\Delta_o)^{3/2} \quad \text{for } (\Delta - \Delta_o) \text{ in degrees.}$$

Since I_1 and I_2 are small, we may find δr from

$$\frac{\delta r}{r} = -I_1 - I_2. \text{ and then}$$

$$V(r + \delta r) = \frac{r + \delta r}{\eta + \delta\eta} = 13.6\left[1 + \frac{\delta r}{r} - \frac{\delta\eta}{\eta}\right] = 13.6\left[1 - I_2\right].$$

The generation of $V(r + \delta r)$ from the above formulae is shown in Table 8.

Appendix VIII

Potentials for Elastic Solutions in Spherically Symmetric Media

We wish to prove that, if $\underset{\sim}{u}$ is the elastic displacement solution due to a known body force $\underset{\sim}{F}$ in a spherically symmetric, self-gravitating, non-rotating Earth, and if f is any sufficiently smooth known function of radius, then there exist scalar fields Φ, χ, and Ψ such that $\underset{\sim}{u}$ may be written as $\underset{\sim}{u}(\underset{\sim}{r},t) = \underset{\sim}{u}_1 + \underset{\sim}{u}_2$, where

$$\underset{\sim}{u}_1 = \frac{1}{f(r)} \left[\text{grad } \Phi(\underset{\sim}{r},t) + \text{curl curl } (r\chi\ (\underset{\sim}{r},t),\ 0,\ 0) \right] \qquad \text{and}$$

$$\underset{\sim}{u}_2 = \text{curl } (r\Psi\ (\underset{\sim}{r},t),\ 0,\ 0).$$

Further, $\underset{\sim}{u}_1$ is the solution for a certain body force $\underset{\sim}{F}_1$, and $\underset{\sim}{u}_2$ is the solution for a certain body force $\underset{\sim}{F}_2$ (where $\underset{\sim}{F}_1$ and $\underset{\sim}{F}_2$ may be constructed from $\underset{\sim}{F}$).

(This representation of $\underset{\sim}{u}$ is used in Chapter 3 above, and it is found that certain useful choices of f(r) may be made, which allow Φ and χ to be interpreted as weakly coupled potentials for P and SV motion.)

Proof: The equations of motion are

$$\rho \underset{\sim}{F} = \rho \frac{\partial^2 \underset{\sim}{u}}{\partial t^2} + \rho \text{ grad}(\underset{\sim}{g}\cdot\underset{\sim}{u}) - \rho \underset{\sim}{g} \text{ div } \underset{\sim}{u} - \rho \text{ grad } \psi - (\lambda + 2\mu) \text{ grad div } \underset{\sim}{u}$$

$$+ \mu \text{ curl curl } \underset{\sim}{u} - (\text{grad } \lambda) \text{ div } \underset{\sim}{u} - \text{grad}(\underset{\sim}{u}\cdot\nabla\mu) + (\underset{\sim}{u}\cdot\nabla) \nabla\mu - (\nabla\mu\cdot\nabla)\underset{\sim}{u}$$

$$\nabla^2\psi = 4\pi G(\rho \text{ div } \underset{\sim}{u} + \underset{\sim}{u}\cdot\text{grad } \rho) \qquad \text{(VIII.2)}$$

where $\underset{\sim}{F}(\underset{\sim}{r},t)$ is a specified source term, ψ is the perturbation in gravitational potential, g is the gravitational acceleration, G is the gravitational constant, ρ, λ and μ are functions of radius r.

The first step in our proof is to write (VIII.2) as an equation for the vector $\underset{\sim}{v} = f(r)\underset{\sim}{u}$, where f is specified. [We should note that strong physical assumptions are made in taking (VIII.2) to be valid in the source region, if the source is highly localized. For example, this equation does not allow for any perturbations in $\lambda(r)$, $\mu(r)$, though perturbations might be expected for material in the neighborhood of a point source. However, some justification of the above linear equation is obtained from model experiments, in which good agreement (see e.g. our Table 1) is found between the observed displacements due to a point source, and the theoretical consequences of equation (VIII.2).] Term by term we have for $\underset{\sim}{v}$

$$\rho \frac{\partial^2 \underset{\sim}{u}}{\partial t^2} = \frac{\rho}{f} \frac{\partial^2 \underset{\sim}{v}}{\partial t^2}$$

$$\rho \text{ grad}(\underset{\sim}{g} \cdot \underset{\sim}{u}) = - \rho \text{ grad } \left(\frac{g}{f} v_r \right) \qquad \left(\underset{\sim}{g} = (-g, 0, 0) \right)$$

$$-\rho \underset{\sim}{g} \text{ div } \underset{\sim}{u} = \left(\frac{\rho g}{f}, 0, 0 \right) \left[\text{ div } \underset{\sim}{v} - \frac{f'}{f} v_r \right]$$

$$- (\lambda + 2\mu) \text{ grad div } \underset{\sim}{u} = (\lambda + 2\mu) \text{ grad } \left[\frac{f'}{f^2} v_r \right]$$

$$- (\lambda + 2\mu) \left(\text{grad } \frac{1}{f} \right) \text{ div } \underset{\sim}{v} - \frac{\lambda + 2\mu}{f} \text{ grad div } \underset{\sim}{v}$$

$$\mu \text{ curl curl } \underset{\sim}{u} = \frac{\mu f'}{f^2} \left[(-\text{div } \underset{\sim}{v}, 0, 0) + \frac{2}{r} \frac{\partial}{\partial r} (r \underset{\sim}{v}) - \text{grad } (v_r) \right]$$

$$+ \mu \left(\frac{f'}{f^2} \right)' (0, v_\theta, v_\phi) + \frac{\mu}{f} \text{ curl curl } \underset{\sim}{v}$$

$$- (\text{grad } \lambda) \text{ div } \underset{\sim}{u} = - \left(\frac{\lambda'}{f}, 0, 0 \right) \left[\text{ div } \underset{\sim}{v} - \frac{f'}{f} v_r \right]$$

$$- \text{grad } (\underset{\sim}{u} \cdot \nabla \mu) + (\underset{\sim}{u} \cdot \nabla) \nabla \mu - (\nabla \mu \cdot \nabla) \underset{\sim}{u}$$

$$= - \frac{\mu'}{f} \left[2 \left(\frac{\partial v_r}{\partial r} - \frac{f' v_r}{f} \right), \frac{\partial v_\theta}{\partial r} - \frac{v_\theta}{r} + \frac{1}{r} \frac{\partial v_r}{\partial \theta} - \frac{f'}{f} v_\theta, \right.$$

$$\left. \frac{\partial v_\phi}{\partial r} - \frac{v_\phi}{r} + \frac{1}{r \sin\theta} \frac{\partial v_r}{\partial \phi} - \frac{f'}{f} v_\phi \right]$$

(See Morse and Feshbach, 1953, p. 33) (VIII.3)

The second step is to use the Helmholtz theorem and represent $\underset{\sim}{v}$ by potentials as $\underset{\sim}{v} = \text{grad } \Phi + \text{curl } \underset{\sim}{A}$, in which we may choose the value of div $\underset{\sim}{A}$. Then note that $v_r = \frac{\partial \Phi}{\partial r} + \frac{1}{r\sin\theta}\left(\frac{\partial}{\partial \theta}(\sin\theta\, A_\phi) - \frac{\partial A_\theta}{\partial \phi}\right)$, and div $\underset{\sim}{v} = \nabla^2\Phi$. So v_r and $\nabla^2\Phi$ are independent of A_r. We also use $f(r)\underset{\sim}{F} = \text{grad } D + \text{curl } \underset{\sim}{E}$.

The third step is to substitute for $\underset{\sim}{v}$ and $\underset{\sim}{F}$ into (VIII.2), using (VIII.3), and to manipulate the resulting four scalar equations into two groups. These are

(i) 3 scalar equations involving Φ, $\text{curl}_r \underset{\sim}{A}$, ψ, and D, $\text{curl}_r \underset{\sim}{E}$ (but independent of A_r, div $\underset{\sim}{A}$, E_r, div $\underset{\sim}{E}$), and

(ii) 1 scalar equation involving A_r, div $\underset{\sim}{A}$, E_r, div $\underset{\sim}{E}$ (independent of Φ, $\text{curl}_r \underset{\sim}{A}$, ψ, and D, $\text{curl}_r \underset{\sim}{E}$).

This grouping of equations is obtained as follows:

The Poisson equation for gravitational potential is

$$\nabla^2\psi = 4\pi G\left(\frac{\rho}{f}\,\text{div}\,\underset{\sim}{v} - \frac{f'}{f^2}\rho v_r + \frac{\rho'}{f} v_r\right) \qquad \text{(a)}$$

Since v_r, div $\underset{\sim}{v}$ are independent of A_r, <u>(a) is one equation of group (i).</u>

The vector equation in (VIII.2) is

$$\rho \operatorname{grad} D + \rho \operatorname{curl} \underset{\sim}{E} = \rho \frac{\partial^2}{\partial t^2} \left[\operatorname{grad} \Phi + \operatorname{curl} \underset{\sim}{A} \right] + \left[\rho g + (\lambda+\mu) \frac{f'}{f} - \lambda', 0, 0 \right] \nabla^2 \Phi$$

$$- \rho f \operatorname{grad} \left(\frac{g}{f} v_r \right) + (\lambda+2\mu) f \operatorname{grad} \left(\frac{f'}{f^2} v_r \right) - \mu \frac{f'}{f} \operatorname{grad} v_r - \rho f \operatorname{grad} \psi$$

$$- \left(\frac{\rho g f'}{f} - \frac{\lambda' f'}{f}, 0, 0 \right) v_r + \frac{2\mu f'}{rf} \frac{\partial}{\partial r} (r \underset{\sim}{v}) + \mu f \left(\frac{f'}{f^2} \right)' (0, v_\theta, v_\phi)$$

$$- \mu' \left[2 \left(\frac{\partial v_r}{\partial r} - \frac{f'}{f} v_r \right), \frac{\partial v_\theta}{\partial r} - \frac{v_\theta}{r} + \frac{1}{r} \frac{\partial v_r}{\partial \theta} - \frac{f'}{f} v_\theta, \frac{\partial v_\phi}{\partial r} - \frac{v_\phi}{r} \right.$$

$$\left. + \frac{1}{r \sin\theta} \frac{\partial v_r}{\partial \phi} - \frac{f'}{f} v_\phi \right]$$

$$- (\lambda + 2\mu) \operatorname{grad} (\nabla^2 \Phi) + \mu \operatorname{curl} \operatorname{curl} \operatorname{curl} \underset{\sim}{A}.$$

(VIII.4)

Let the r-component of equation (VIII.4) be labelled "equation (b)." Then, since we may show $r \operatorname{curl}_r \operatorname{curl} \underset{\sim}{B} = \frac{1}{r} \frac{\partial}{\partial r} (r^2 \operatorname{div} \underset{\sim}{B}) - \nabla^2 (r B_r)$ for any $\underset{\sim}{B}$, we have

$$\operatorname{curl}_r \operatorname{curl} \operatorname{curl} \underset{\sim}{A} = - \frac{1}{r} \nabla^2 (r \operatorname{curl}_r \underset{\sim}{A}),$$

(VIII.5)

So, clearly <u>(b) is another equation of group (i).</u>

Perform on vector equation (VIII.4) the operation

$$L(\sim) \equiv \nabla\cdot(\sim) - \frac{1}{r^2}\frac{\partial}{\partial r} r^2 \, (\sim)_r = \frac{1}{r\sin\theta}\frac{\partial}{\partial\theta}\sin\theta \, (\sim)_\theta + \frac{1}{r\sin\theta}\frac{\partial}{\partial\phi}(\sim)_\phi$$

to obtain equation (c). Then, checking term by term, the independence of A_r is obvious down to

$$L\left[\frac{2\mu}{r}\frac{f'}{f}\frac{\partial}{\partial r}(r\underset{\sim}{y})\right] = \frac{2\mu}{r^2}\frac{f'}{f}\frac{\partial}{\partial r}\left[\frac{r}{\sin\theta}\frac{\partial}{\partial\theta}(\sin\theta\, v_\theta) + \frac{r}{\sin\theta}\frac{\partial v_\phi}{\partial_\phi}\right]$$

$$= \frac{2\mu}{r^2}\frac{f'}{f}\frac{\partial}{\partial r}\left[r^2\nabla^2\Phi - \frac{\partial}{\partial r}(r^2 v_r)\right] - \text{independent of } A_r.$$

A similar method works for $L\left[\mu f\left(\frac{f'}{f^2}\right)' (0, v_\theta, v_\phi)\right]$, and for the terms which multiply μ'. The final term we must check is

$$L\left[\mu \operatorname{curl}\operatorname{curl}\operatorname{curl}\underset{\sim}{A}\right] = \mu' \operatorname{curl}_r \operatorname{curl}\operatorname{curl}\underset{\sim}{A} -$$

$$\frac{1}{r^2}\frac{\partial}{\partial r}\left\{\mu r^2\left[\operatorname{curl}_r \operatorname{curl}\operatorname{curl}\underset{\sim}{A}\right]\right\},$$

and this too is independent of A_r (by VIII.5). So <u>equation (c) is another equation of group (i).</u>

Perform on vector equation (VIII.4) the operation

$$M(\sim) \equiv \text{curl}_r(\sim) = \frac{1}{r\sin\theta}\frac{\partial}{\partial\theta}\left[\sin\theta\ (\sim)_\phi\right] - \frac{1}{r\sin\theta}\frac{\partial}{\partial\phi}\ (\sim)_\theta$$

to obtain equation (d). We note that M (function of radius only x grad (scalar)) = 0. Then the left hand side of (d) is a function of (E_r, div $\underset{\sim}{E}$) only (by the vector identity leading to our (VIII.5)). Let us check in detail those terms in the right hand side of (d) for which the dependence only on (A_r, div $\underset{\sim}{A}$, E_r, div $\underset{\sim}{E}$) is not obvious. We have

$$M\left[\frac{2\mu f'}{rf}\frac{\partial}{\partial r}(r\underset{\sim}{y})\right] = \frac{2\mu}{r^2}\frac{f'}{f}\frac{\partial}{\partial r}\left[r^2\ \text{curl}_r\ (\text{grad}\ \Phi + \text{curl}\ \underset{\sim}{A})\right]$$

which depends only on (A_r, div $\underset{\sim}{A}$). The point here is that r curl_r commutes with functions of radius, and with radial derivatives, and r $\text{curl}_r\underset{\sim}{y}$ depends only on (A_r, div $\underset{\sim}{A}$). The only other term we should look at is

$$M\left[\mu\ \text{curl curl curl}\ \underset{\sim}{A}\right] = \mu\ \text{curl}_r\ \text{curl curl curl}\ \underset{\sim}{A}$$

$$= -\frac{\mu}{r}\ \nabla^2(r\ \text{curl}_r\ \text{curl}\ \underset{\sim}{A}) \qquad \text{(cf. VIII.5)}$$

but curl_r curl $\underset{\sim}{A}$ depends only on (A_r, div $\underset{\sim}{A}$). We may conclude that <u>(d) is our group (ii) equation.</u>

The fourth step in our proof is a discussion (cf. Scholte (1956) for homogeneous media) of properties of our two groups of equations.

In the first group (of three equations), the quantities D, $\text{curl}_r \underset{\sim}{E}$ generate unknowns Φ, $\text{curl}_r \underset{\sim}{A}$ and ψ. But these are independent of A_r. So, for this displacement solution ($\underset{\sim}{u}_1$, say) $A_r = 0$. With the choice $\text{div}\, \underset{\sim}{A} = 0$ we have

$$\frac{1}{r}\left[\frac{1}{\sin\theta}\frac{\partial}{\partial\theta}(\sin\theta\, A_\theta) + \frac{1}{\sin\theta}\frac{\partial A_\phi}{\partial\phi}\right] = 0.$$

But this is the condition that there exists a scalar function χ(say) such that

$$A_\theta = \frac{1}{\sin\theta}\frac{\partial\chi}{\partial\phi} \quad , \quad A_\phi = -\frac{\partial\chi}{\partial\theta} \quad . \quad \text{So } \underset{\sim}{A} = \text{curl}\,(r\chi,0,0)$$

and the solution to group (i) may be expressed in the form

$$\underset{\sim}{u} = \frac{1}{f(r)}\left[\text{grad}\,\Phi + \text{curl curl}\,(r\chi,0,0)\right] \quad . \qquad \text{(VIII.6)}$$

The second group consists of an equation for the quantities (A_r, $\text{div}\, \underset{\sim}{A}$), and we may choose $\Phi = \text{curl}_r \underset{\sim}{A} = 0$, $\psi = 0$ without changing this equation. So for this solution ($\underset{\sim}{u}_2$, say) we have $(f\, \underset{\sim}{u}_2)_r = 0$ and $\text{div}\,(f\, \underset{\sim}{u}_2) = 0$. Hence $(\underset{\sim}{u}_2)_r = 0$ and $\text{div}\, \underset{\sim}{u}_2 = 0$. So, there exists a scalar function $\underset{\sim}{\Psi}$(say) such that

$$\underset{\sim}{u}_2 = \text{curl } (r\Psi,0,0) \qquad \text{(VIII.7)}$$

(Note that we have now a specific choice of div $\underset{\sim}{A}$.)

The independence of potential forms (VIII.6) and VIII.7) may be emphasized by noting that $\underset{\sim}{u}_1$ is generated by that body force $\underset{\sim}{F}_1$ (with related potentials $f\underset{\sim}{F}_1$ = grad D_1 + curl $\underset{\sim}{E}_1$, say) for which

$$D_1 = D, \quad \text{curl}_r \underset{\sim}{E}_1 = \text{curl}_r \underset{\sim}{E}, \quad (\underset{\sim}{E}_1)_r = 0, \quad \text{div } \underset{\sim}{E}_1 = 0 \qquad \text{(VIII.8)}$$

and $\underset{\sim}{u}_2$ is generated by that body force $\underset{\sim}{F}_2$ (with related potentials $f\underset{\sim}{F}_2$ = grad D_2 + curl $\underset{\sim}{E}_2$, say) for which

$$D_2 = 0 \quad \text{curl}_r \underset{\sim}{E}_2 = 0, \quad (\underset{\sim}{E}_2)_r = E_r, \quad \text{div } \underset{\sim}{E}_2 = \text{div } \underset{\sim}{E}$$

(VIII.9).

It is simple to show that $\underset{\sim}{F}_1$ and $\underset{\sim}{F}_2$ exist (since we may construct solutions to (VIII.8), (VIII.9) with given D, $\underset{\sim}{E}$), and, finally, we also note that scalar fields F_1 and E_2 exist such that

$$\underset{\sim}{F}_1 = \frac{1}{f(r)} \left[\text{grad } D_1 + \text{curl curl } (rF_1,0,0) \right]$$

$$\underset{\sim}{F}_2 = \text{curl } (rE_2,0,0).$$

Appendix IX

A List of Functions Defined in Section (3.3)

$$g = f'/f$$

$$\varepsilon_p = \frac{\lambda+\mu}{\lambda+2\mu} g' - \frac{\lambda+\mu}{2(\lambda+2\mu)} \frac{\rho' g}{\rho} + \frac{\mu' g}{\lambda+2\mu} + \frac{2g}{r} + \frac{3}{4}\left(\frac{\rho'}{\rho}\right)^2$$

$$- \frac{1}{2}\frac{\rho''}{\rho} - \frac{\rho'}{r\rho} - \frac{\mu'\rho'}{(\lambda+2\mu)\rho} - \frac{2\mu'}{r(\lambda+2\mu)}$$

$$\pi_o = \frac{\rho'}{\rho} - \frac{2\mu'}{\lambda+2\mu} - \frac{\lambda+\mu}{\lambda+2\mu} g$$

$$\pi_1 = 2\mu g' - \frac{2\mu g}{r} + \frac{2\mu'}{r} - 2\mu'' + \left(\frac{2\mu'}{\mu} - g\right)\left[2\mu' + (\lambda+\mu)g\right] \frac{\mu}{\lambda+2\mu}$$

$$\pi_2 = \mu g'' - \frac{4\mu' g}{r} - \mu'' g - \frac{2\mu'}{r^2} + \frac{2\mu''}{r} +$$

$$\left(\frac{2\mu'}{\mu} - g\right)\left[(\lambda+\mu)\, g' + 2(\lambda+2\mu)\frac{g}{r} + \mu' g - \frac{2\mu'}{r}\right] \frac{\mu}{\lambda+2\mu} - \frac{\rho'}{2\rho} \pi_1$$

$$\pi_3 = \lambda' + \mu g - \frac{(\lambda+2\mu)}{2}\frac{\rho'}{\rho}$$

$$\pi_4 = -\rho\,\pi_o$$

$$\varepsilon_S = -\frac{\lambda+\mu}{\mu}g' + \frac{\lambda+\mu}{2\mu}\frac{\rho' g}{\rho} - \frac{\lambda' g}{\mu} + \frac{\lambda+3\mu}{r\mu}g + \frac{3}{4}\left(\frac{\rho'}{\rho}\right)^2$$

$$-\frac{1}{2}\frac{\rho''}{\rho} - \frac{\rho'}{r\rho} - \frac{\mu'\rho'}{\mu\rho} - \frac{2\mu'}{r\mu}$$

$$\sigma_o = \frac{\rho'}{\rho} - \frac{2\mu'}{\mu} + \frac{\lambda+\mu}{\mu}g$$

$$\sigma_1 = 2(\lambda+2\mu)g' + 2(\lambda'+\mu')\,g - \frac{2\mu'}{r} - 2\mu'' +$$

$$\left(\frac{2\mu'}{\mu} - \frac{\lambda+2\mu}{\mu}g\right)\left[-(\lambda+\mu)\,g + 2\mu' + \frac{2\mu}{r}\right]$$

$$\sigma_2 = (\lambda+2\mu)\,g'' + \frac{2(\lambda+2\mu)g'}{r} + 2(\lambda'+\mu')g' + \lambda''\,g + \frac{2(\lambda'-\mu')g}{r} - \frac{4\mu'}{r^2}$$

$$+\left(\frac{2\mu'}{\mu} - \frac{\lambda+2\mu}{\mu}g\right)\left[-(\lambda+\mu)g' + \frac{2\mu g}{r} - \lambda' g + \frac{2\mu}{r^2}\right] - \left(\frac{1}{r} + \frac{\rho'}{2\rho}\right)\sigma_1$$

$$\sigma_3 = - \mu' + (\lambda+2\mu) g - \frac{\mu \rho'}{2\rho}$$

$$\sigma_4 = - \rho \sigma_o$$

Appendix X

Some Properties of the source-generated potentials described in Section (3.4)(a).

We prove the necessity of equations (3.4.4a,b), and show that the results of Appendices II and VI still apply. The source term is taken (see 3.4.3) as

$$\underset{\sim}{F} = \frac{1}{f(r)} \operatorname{grad}\left[\frac{f_1(r)}{\rho^{1/3}(r)} \; D \right] \quad \text{where} \quad D = \frac{\delta(r-b)\; \delta(\theta)\; e^{-i\omega t}}{2\pi r^2 \sin\theta}$$

and $f(r)$ is chosen so that $\pi_o(r) = 0$.

First, to amplify the discussion given in (3.4)(a) we follow the method of Luneburg (described, e.g., by Karal and Keller (1959)), and consider a solution (A,B,C,P,S) where each of the five unknowns is in the form

$$V = e^{i\omega(\tau_V - t)} \sum_{m=0}^{\infty} (i\omega)^{-m} v_m \qquad \text{(X.1)}$$

where the phase τ_V and the v_m are functions of position only.

Consider integers ℓ and n defined by

$$\frac{\rho D}{\lambda+2\mu} + \nabla^2 P - \frac{\rho}{\lambda+2\mu}\frac{\partial^2 P}{\partial t^2} = O(\omega^{\ell})P \quad (=A)$$

$$\nabla^2 S - \frac{\rho}{\mu}\frac{\partial^2 S}{\partial t^2} = O(\omega^{n})S \quad \left(= C + \sigma_o \frac{\partial S}{\partial r}\right) \qquad (X.2)$$

Clearly we have $\ell \leq 2$, $n \leq 2$.

Suppose $\ell = 2$. By comparing the highest powers of frequency in equation (3.4.1), we see that $S = O(1)P$ (i.e. that the leading terms in the expansion X.1 for P and S are of the same order). From (3.4.2) we see that $n \leq 0$, and hence from X.2 that $C = O(\omega)S$.

Now examine equation (3.3.7): the terms in P are $O(\omega)P$ (since $\pi_o = 0$), the terms in A, $\frac{\partial A}{\partial r}$ are $O(\omega^3)P$ (from X.2 with $\ell = 2$) and those in B are $O(\omega^3)S$ (from 3.3.6 and our last result for C), which equal $O(\omega^3)P$. So for this equation the terms in P are two orders in frequency down from those in A and B.

It is therefore possible to obtain the first two terms in our expansion X.1 for each of A,B,C, and S (by comparing the highest two powers of frequency in the four equations 3.3.5-3.3.8), independent of the source term D. Hence the two leading terms of the derived displacement $\underset{\sim}{N}$ (see 3.3.3) are independent of the applied force $\underset{\sim}{F}$. Clearly this solution is not generated by the

source, but is one of the solutions to the homogeneous equations (3.4.1) and (3.4.2) with D = 0, F = 0. Hence, we reject the case $\ell = 2$.

Suppose $\ell = 1$. Then similarly we find $S = 0(\omega^{-1})P$ and still $C = 0(\omega)S$. In (3.3.7) the terms in P are one order in frequency down from those in A and B, and then the first term in displacement $\underset{\sim}{N}$ is independent of $\underset{\sim}{F}$. Hence we reject $\ell = 1$.

So $\ell \leq 0$, and from (3.4.1) S is at most $0(\omega^{-2}P)$. These results are two of our desired properties.

Second, we briefly discuss the turning point method of our Appendix VI, in which (3.4.4a) was taken to be valid in the turning point region. This assumption is questionable, since it is obtained above with heavy reliance on wave properties. (Note also that the expansion (X.1) is not useful at the turning point radius, for a partial wave of V, since this radius is then a caustic and the geometrical optics approximation for the first term is unbounded.)

We study the expansions

$$\begin{pmatrix} P \\ S \end{pmatrix} = \sum_{n=0}^{\infty} \begin{pmatrix} a(r,n) \\ c(r,n) \end{pmatrix} P_n(\cos\theta)$$

(cf Appendix II. The P_n are Legendre polynomials) and introduce a partial wave $g_n^{(1)}(r)$ as the outgoing solution for $a(r,n)$ so that $a(r,n) = c_1\, g_n^{(1)}(r)$ for $b \le r$. In the region in which $g_n^{(1)}(r)$ travels as a wave, the result $\ell \le 0$ in (X.2) is sufficient to establish the WKBJ formula - which is thus seen to be unchanged by the weak coupling to an SV mode.

Suppose that throughout the medium $g_n^{(1)}(r)$ is coupled to the S-function $d(r,n)$. (In fact, $c(r,n) = c_1\, d(r,n)$ for $b \le r$.) We now give a brief outline to establish that the concluding formulae of Appendix VI are still valid near the turning point $r = R$ of $g_{\nu-\frac{1}{2}}^{(1)}(r)$:

Define $b(r)$, R, Q, H, X, Y, u, and $c(u)$ by the formulae given in Appendix VI. Then equation (3.4.1) may be written as

$$B_1(R)\, H^4 \left[\frac{1}{Q^2} \frac{d^2}{du^2} e(u) + \left(\frac{-u}{Q} + \frac{u^2(3X-3-Y)}{4Q^4(1-X)} \right) e(u) \right]$$

$$+(B_1(R) + RB_2(R))\, H^4 \left[-\frac{1}{2Q^4(1-X)} \frac{d}{du} \left(\frac{1}{Q^2} \frac{d^2c}{du^2} - \frac{uc}{Q^2} \right) \right]$$

$$+ O(Q^4)\, c(u) = O(Q^6)\, O(\omega^2)\, d(R,\nu-\tfrac{1}{2}) \qquad (X.3)$$

where e(u) is the expression on the left hand side of equation (VI.2),

$$B_1(r) = \lambda+2\mu \text{ and } B_2(r) = (\lambda+2\mu)\left[\frac{\lambda+3\mu}{\mu} g+2\left(\frac{\lambda'+2\mu'}{\lambda+2\mu}\right) - \frac{2\mu'}{\mu} - \frac{2\rho'}{\rho}\right]$$

The highest order term on the right hand side of (3.4.2) is $0(Q^2)$ c(u), and hence $d(r, \nu - \frac{l}{2})$ (travelling as a wave and satisfying the eikonal equation) is such that $0(\omega^3)$ $d(R, \nu - \frac{l}{2}) = 0(Q^2)$ c(u). So the right hand side of X.3 is $0(Q^5)$ c(u), and we see that c(u) can be expanded in the form

$$f_o(u) + \frac{1}{Q^2} f_1(u) + \sum_{n=3}^{\infty} \frac{f_n(u)}{Q^n} .$$ Thus, comparing coefficients for Q^8 in X.3 we have $(f_o'' - uf_o)'' - u(f_o'' - uf_o) = 0$ and for Q^6

$$(f_1'' - uf_1)'' - u(f_1'' - uf_1) + \left[\frac{-f_o'}{2(1-X)} + \frac{u^2(3X - 3 - Y)}{4(1-X)} f_o\right]''$$

$$- u\left[\frac{-f_o'}{2(1-X)} + \frac{u^2(3X-3-Y)}{4(1-X)}\right] - \left(1 + \frac{RB_2}{B_1}\right)\frac{(f_o'' - uf_o)'}{2(1-X)} = 0$$

It is then seen that we have essentially the same formulae for f_o and f_1 which were obtained as VI.3, and we have proved our desired result: that the turning point expansion of $g_n^{(1)}(r)$ satisfying (3.4.1) or (3.4.4a) have the same first two terms. It is of interest also to note that the next term for c(u), $\frac{f_3(u)}{Q^3}$, depends on $d(r, \nu - \frac{1}{2})$, and hence that the mode coupling effect on $g_n^{(1)}(r)$ is still one order in frequency down from the main term, even at the turning point.

Appendix XI

The Reflection and Transmission Coefficients, Between Two Slightly Different Welded Homogeneous Elastic Half-Spaces, for an Incident P-Wave.

The derivation below is done in two ways, first by a study of the boundary condition, and second from the equations of motion. The numerical result referred to in (3.4) above is obtained here in the final paragraph.

Take Cartesian coordinates with $z = 0$ as the boundary between the media, z increasing into the first medium, and consider an incident plane P wave in the first medium, propagating perpendicular to the y-axis and in the direction of increasing x.

We use the standard potential representation for this problem, displacement = grad ϕ + curl $(0,0,\psi)$, use suffices to label quantities in the two media, and solve for the system

$$\phi_1^i = P^i \exp i \left[\omega t - H_1 x \sin i_1 + H_1 z \cos i_1 \right] \qquad \text{incident P}$$

$$\phi_1^r = P^r \exp i \left[\omega t - H_1 x \sin i_1 - H_1 z \cos i_1 \right] \qquad \text{reflected P}$$

$$\phi_2^t = P^t \exp i \left[\omega t - H_2 x \sin i_2 + H_2 z \cos i_2 \right] \qquad \text{transmitted P}$$

$\psi_1^r = S^r \exp i [\, \omega t - K_1 x \sin j_1 - K_1 z \cos i_1 \,]$ reflected SV

$\psi_2^t = S^t \exp i [\, \omega t - K_2 x \sin j_2 + K_2 z \cos j_2 \,]$ transmitted SV.

i.e. we wish to obtain P^r, P^t, S^r, S^t in terms of P^i and the difference in properties between the two media. For this purpose we use the continuity of two displacement and two stress components across the boundary, finding

$$\omega q \left(P^i + P^r\right) - K_1 \cos j_1 \, S^r = \omega q \, P^t + K_2 \cos j_2 \, S^t$$

$$\rho_1 \cos 2j_1 \left(P^i + P^r\right) + \rho_1 \sin 2j_1 \, S^r = \rho_2 \cos 2j_2 \, P^t - \rho_2 \sin 2j_2 \, S^t$$

$$H_1 \cos i_1 \left(P^i - P^r\right) - \omega q \, S^r = H_2 \cos i_2 \, P^t - \omega q \, S^t$$

$$\mu_1 H_1^2 \sin 2i_1 \left(P^i - P^r\right) + \mu_1 K_1^2 \cos 2j_1 \, S^r =$$

$$\mu_2 H_2^2 \sin 2i_2 \, P^t + \mu_2 K_2^2 \cos 2j_2 \, S^t.$$

where

$$H_1 \sin i_1 = K_1 \sin j_1 = \omega q.$$

If $\Delta\rho$, $\Delta\alpha$, and $\Delta\beta$ are the increments in density, longitudinal velocity, and shear wave velocity (from the first to the second medium), and if we take mean angles $i = \frac{i_1+i_2}{2}$, $j = \frac{j_1+j_2}{2}$, then we can show that to first order the solution is

$$P^r = \left[\frac{\Delta\rho}{\rho} \left(\cos 2j - \frac{1}{2}\right) + \frac{\Delta\alpha}{\alpha} \left(\frac{1}{2\cos^2 i}\right) - \frac{\Delta\beta}{\beta} \left(4 \sin^2 j\right) \right] P^i$$

$$P^t = \left[1 + \frac{\Delta\rho}{\rho} \left(\frac{-1}{2}\right) + \frac{\Delta\alpha}{\alpha} \left(\frac{1}{2\cos^2 i}\right) \right] P^i$$

$$S^r = \frac{\sin j}{2 \cos j \sin i} \left[\sin \left(i + 2j\right) \frac{\Delta\rho}{\rho} + 4 \sin j \cos\left(i + j\right) \frac{\Delta\beta}{\beta} \right] P^i$$

$$S^t = \frac{\sin i}{2 \cos j \sin i} \left[\sin \left(i - 2j\right) \frac{\Delta\rho}{\rho} - 4 \sin j \cos \left(i - j\right) \frac{\Delta\beta}{\beta} \right] P^i$$

(XI.1)

These formulae break down only if $i \sim 90°$, that is, for propagation nearly parallel to the boundary. [Numerical work for the application required in Chapter 3 is given following our equation (XI.9).]

The reflection/transmission coefficients obtained above are derived from the study of boundary conditions. It is of some interest to obtain them also directly from the equations of motion in continuous media. We here outline the steps by which this may be done, acknowledging the work of Chapman (1969), who obtains the equations (XI.8) below by a slightly different and less direct method:

We study an elastic medium in which density and velocities α and β vary in the z direction of a set of Cartesian axes, and discuss the steady-state wave system P-SV which moves with velocity c in the x direction. Having thus specified the horizontal wave number, ω/c, the vertical wave numbers are then

$$\pm\left(\frac{\omega^2}{\alpha^2}-\frac{\omega^2}{c^2}\right) \equiv \pm\,\omega q_\alpha \qquad \text{(say)}$$

$$\pm\left(\frac{\omega^2}{\beta^2}-\frac{\omega^2}{c^2}\right) \equiv \pm\,\omega q_\beta \qquad \text{(XI.2)}$$

Suppressing the factor $e^{i\omega(t-x/c)}$, we can show that the wave equation may be written in the canonical matrix form

$$\frac{d}{dz}\,\underset{\sim}{u} = \underline{\underline{M}}\,\underset{\sim}{u} \quad \text{(XI.3) where} \quad \underset{\sim}{u} \equiv \begin{pmatrix} u_x \\ -\sigma_{zz} \\ u_z \\ \sigma_{zx} \end{pmatrix} \quad \text{and}$$

$$\underline{\underline{M}} \equiv \begin{bmatrix} 0 & 0 & \frac{i}{c} & \frac{1}{\mu} \\ 0 & 0 & \rho\omega^2 & \frac{-i\omega}{c} \\ \frac{i\omega\lambda}{c(\lambda+2\mu)} & \frac{-1}{\lambda+2\mu} & 0 & 0 \\ -\rho\omega^2 + \frac{4\mu(\lambda+\mu)\omega^2}{c^2(\lambda+2\mu)} & \frac{-i\omega\lambda}{c(\lambda+2\mu)} & 0 & 0 \end{bmatrix}$$

(which has the eigenvalues $\pm i\omega q_\alpha$, $\pm i\omega q_\beta$).

In this plane strain problem, u_x and u_z are two components of displacement, and σ_{zz} and σ_{zx} are two of the components of the stress tensor. There are close analogies here with some equations arising in the study of radio wave propagation in the ionosphere (see Budden, 1961).

For a homogeneous medium, $\underline{\underline{M}}$ is constant, and it is clear that the solutions of equation (XI.3) are essentially the eigenvectors of $\underline{\underline{M}}$, multiplied by a phase factor derived from the corresponding

eigenvalues and path length. This suggests that for our inhomogeneous problem we try solutions in the form of a sum of coupled eigenvectors, i.e.

$$u = W_2(z)\begin{pmatrix} \frac{-i\omega}{c} \\ \omega^2\mu R \\ -i\omega q_\alpha \\ -\frac{2\mu\omega^2}{c} q_\alpha \end{pmatrix} + W_2(z)\begin{pmatrix} \frac{-i\omega}{c} \\ \omega^2\mu R \\ i\omega q_\alpha \\ \frac{2\mu\omega^2}{c} q_\alpha \end{pmatrix} + W_3(z)\begin{pmatrix} i\omega q_\beta \\ \frac{2\mu\omega^2}{c} q_\beta \\ \frac{-i\omega}{c} \\ \omega^2\mu R \end{pmatrix}$$

$$+ W_4(z)\begin{pmatrix} -i\omega q_\beta \\ \frac{-2\mu\omega^2}{c} q_\beta \\ \frac{-i\omega}{c} \\ \omega^2\mu R \end{pmatrix} \qquad \text{(XI.4)}$$

where $R \equiv \frac{1}{\beta^2} - \frac{1}{c^2}$, and the W_i contain phase factors. [Note: these eigenvectors of $\underline{\underline{M}}$ may be found directly, but a simple way to write them straight down can be found from discussion of potentials in a homogeneous medium.] It is found that if the W_i are scaled by a function of depth, according to the scheme

$$V_{\substack{1\\2}} = \sqrt{\rho q_\alpha}\ W_{\substack{1\\2}},\ V_{\substack{3\\4}} = \sqrt{\rho q_\beta}\ W_{\substack{3\\4}} \tag{XI.5}$$

then substitution of (XI.4) and (XI.5) into (XI.3) gives for V_i the matrix equation

$$\frac{d\underset{\sim}{V}}{dz} + \begin{pmatrix} i\omega q_\alpha & 0 & 0 & 0 \\ 0 & -i\omega q_\alpha & 0 & 0 \\ 0 & 0 & i\omega q_\beta & 0 \\ 0 & 0 & 0 & -i\omega q_\beta \end{pmatrix} = \begin{pmatrix} 0 & -\delta_3 & \delta_1 & \delta_2 \\ -\delta_3 & 0 & -\delta_2 & -\delta_1 \\ -\delta_1 & -\delta_2 & 0 & -\delta_4 \\ -\delta_2 & \delta_1 & -\delta_4 & 0 \end{pmatrix} \underset{\sim}{V} \tag{XI.6}$$

where

$$\delta_{\substack{1\\2}} = \frac{1}{2c\left(q_\alpha q_\beta\right)^{1/2}}\left[\frac{\rho'}{\rho} - \frac{2\beta^2}{c^2}\frac{\mu'}{\mu} \mp 2q_\alpha\, q_\beta\, \beta^2 \frac{\mu'}{\mu}\right]$$

$$\delta_3 = \frac{\rho'}{2\rho} - \frac{q_\alpha'}{2q_\alpha} - \frac{2\beta^2}{c^2}\frac{\mu'}{\mu}\ ,\quad \delta_4 = \frac{\rho'}{2\rho} - \frac{q_\beta'}{2q_\beta} - \frac{2\beta^2}{c^2}\frac{\mu'}{\mu}$$

This equation for $\underset{\sim}{V}$ opens up many interesting interpretations of coupling in heterogeneous media. For example, the WKBJ solution is obtained by ignoring the gradient terms δ_i, and taking the right hand side of equation (XI.6) to be zero. Unfortunately, however, the δ_i have singularities at depths where either q_α or q_β are zero (or singularities at both depths) - corresponding to the WKBJ turning point, and the bottoming depth along a ray - and approximate methods of solution break down.

We can examine the continuous scattering process (away from depths such that q_α or q_β are zero), and obtain our equations (XI.1) in the following way: From (XI.6) we may identify V_1 approximately as the P-wave phase for an up-going wave (z increases upwards). If this wave is taken as incident, then (following Chapman, 1969) we introduce reflection and transmission coefficients by

$$V_2 = R_{PP}\, V_1, \quad V_3 = T_{PS}\, V_1, \quad V_4 = R_{PS}\, V_1 \qquad \text{(XI.7)}$$

These phase functions are respectively appropriate for reflection to a down-going P-wave, converted transmission to upgoing SV, and converted reflection to downgoing SV.

Substituting (XI.7) into (XI.6), and eliminating V_1, we obtain

$$\frac{d}{dz} R_{PP} = 2i\omega q_\alpha R_{PP} - \delta_3 (1-R_{PP}^2)-(\delta_2 + R_{PP}\delta_1) T_{PS} -(\delta_1 + R_{PP}\delta_2)R_{PS}$$

$$\frac{d}{dz} T_{PS} = i\omega(q_\alpha-q_\beta) T_{PS}-\delta_1(1 + T_{PS}^2) -(\delta_2-T_{PS}\delta_3) R_{PP}-(\delta_4 + T_{PS}\delta_2) R_{PS}$$

$$\frac{d}{dz} R_{PS} = i\omega(q_\alpha+q_\beta) R_{PS} + \delta_2(1-R_{PS}^2)+(\delta_1 + R_{PS}\delta_3) R_{PP}-(\delta_4 + R_{PS}\delta_1) T_{PS}$$

(XI.8)

[These coupled Riccati equations have been obtained by Chapman (1969), using the Budden (1961) approach of discussing a matrix transformation on $\underset{\sim}{u}$.]

Now we see that approximately

$$\frac{d}{dz} R_{PP} = 2i\omega q_\alpha R_{PP} - \delta_3$$

$$\frac{d}{dz} T_{PS} = i\omega(q_\alpha-q_\beta) T_{PS} - \delta_1$$

$$\frac{d}{dz} R_{PS} = i\omega(q_\alpha+q_\beta) R_{PS} + \delta_2 \text{ , with for example the solution}$$

$$R_{PP}(z) = e^{2i\omega\int^z q_\alpha dz'} \cdot \int_z^\infty \delta_3(z')\, e^{-2i\omega\int^{z'} q_\alpha dz''} dz'$$

This integral may be interpreted as the summed contribution of a stack of individually homogeneous layers of thickness dz', with density and velocity discontinuities of $\frac{d\rho}{dz'}\,dz'$, $\frac{d\alpha}{dz'}\,dz'$, and $\frac{d\beta}{dz'}\,dz'$ between the layers. The phase of the integrand is appropriate for such an interpretation, and so also is the amplitude, since we may show that if q_α and q_β are physically described by angles of incidence i and j, then $q_\alpha = \frac{\cos i}{\alpha}$, $q_\beta = \frac{\cos j}{\beta}$, and

$$\delta_3 = \left[\frac{\rho'}{\rho} \left(\cos 2j - \frac{1}{2} \right) + \frac{\alpha'}{\alpha} \left(\frac{1}{2 \cos^2 i} \right) - \frac{\beta'}{\beta} \left(4 \sin^2 j \right) \right] \tag{XI.9}$$

This is just our desired result, for a comparison of (XI.9) and (XI.1) shows that

$\delta_3 \cdot dz' = \frac{P^r}{P^i}$ (≡ the reflection coefficient between two slightly different homogeneous half spaces). Similar results may be shown for δ_1 and δ_2, and we have found that the same approximate formulae for reflection and conversion coefficients may be derived either from the boundary conditions or from the equations of motion. The type of approximation we find has in fact been widely studied in the case of simple boundary conditions - see Bremmer (1951) and Brekhovskikh (1960).

We now return to the results of our first derivation, and examining the reflected and transmitted amplitudes P^t, S^r, S^t as i tends to zero, we are able to see that $|S^r|$, $|S^t| << |P^r|$, i.e. that the SV waves are negligible for propagation nearly normal to the boundary. But for the application in section (3.4) we have $i = 16°$, $j = 9°$, $\frac{\Delta\rho}{\rho} = -\frac{1}{20}$, $\frac{\Delta\alpha}{\alpha} = -\frac{1}{10}$, $\frac{\Delta\beta}{\beta} = -\frac{1}{5}$. And then the P-P reflection coefficient, $\frac{P^r}{P^i}$, is -0.057, and the P-S conversion (reflection) coefficient, $\frac{S^r}{P^i}$, is -0.058. Note that these are the reflection and conversion coefficients for potentials. The corresponding coefficents for amplitudes are easily derived, and we find that the reflection coefficient P-P is still -0.057, but the conversion coefficient P-S is $-0.058 \times \alpha/\beta$. So in fact the reflected S wave amplitude is substantially greater than the reflected P wave amplitude.

LIST OF TABLES

Table 7. Amplitudes and $\frac{\partial T}{\partial \Delta}$, for 2 second core diffracted P waves, in a model with the geometrical shadow boundary at 97°, with

$$\left.\frac{\partial^2 T}{\partial \Delta^2}\right|_{\Delta = 97°} = -50 \text{ sec/radian}^2,$$

and velocity gradient $\frac{d\alpha}{dr} = -0.2\,\frac{\alpha}{r}$ at the bottom of the mantle. Our source normalization gives an amplitude of 2.259 for the direct ray arrival at 97°, with zero phase.

Table 8. Evaluation of the velocity profile $V(r + \delta r)$. See Appendix VII.

Table 1

Comparison of theoretical and experimental shadow shifts. Experimental data from Teng and Wu (1968).

Model (See Figure 9)	Geophysical Problem	Observed Shift	Calculated Shift
II	31 sec P-wave	$s_P \sim -0.3$ cm	$s_P \sim -0.2$ cm
I	12 sec P-wave	$s_P \sim +1.1$ cm	$s_P \sim +0.8$ cm
I	5 sec P-wave	$s_P \sim 1.1$ cm	$s_P \sim 0.9$ cm
II	48 sec SV-wave	$s_{SV} \sim 8.7$ cm	$s_{SV} \sim 9.2$ cm
II	32 sec SV-wave	$s_{SV} \sim 7.7$ cm	$s_{SV} \sim 6.1$ cm

MODEL I: a = 24 inches, b = 34.5 inches, R_1 = 63.0 cm. Two P-wave sources, frequency 500 and 200 kc/sec

MODEL II: a = 6 inches, one P-wave source, b = 13.4, R_1 = 30.5 cm, frequency 300 kc/sec. Two SV-wave sources. b = 12.5 inches, R_1 = 27.8 cm, frequency = 300, 200 kc/sec.

Table 2

Formulae for P-P scattering from a point source by a spherical fluid core.

See Figure 13 for plots of the amplitude of vertical displacement, $|u_r|$, at frequencies 0.1 and 1.0 Hz.

P-Source Potential

$$\phi_{INC} = \frac{\exp ihR}{ihR}$$

Exact formula

$$u_r = -\int_0^{\infty} \nu h^{(1)}_{\nu-\frac{1}{2}}(hb).hh^{(1)\prime}_{\nu-\frac{1}{2}}(hr).\frac{\Omega_5 h^{(2)}_{\nu-\frac{1}{2}}(ha)}{\Omega_5 h^{(1)}_{\nu-\frac{1}{2}}(ha)} Q^{(2)}_{\nu-\frac{1}{2}}(\cos\Delta)\, d\nu$$

Simple Ray Theory for the Direct Wave

$$u_r = \cos i_r \cdot \frac{\exp ihR}{R} \quad \text{(lit zone)} \left(= \frac{e^{ihR}}{2r} \text{ if } r = b \right)$$

$$= 0 \quad \text{(shadow zone)} \quad (i_r = \text{angle of incidence})$$

Approximate formula in the Transition Region

$$u_r = \cos i_r \cdot \frac{\exp ihR}{R} \left\{ \frac{1}{2} - e^{-i\pi/4} \sqrt{\frac{R}{2\pi h R_1 R_2}} \left[h(a-y) + (ha)^{\frac{1}{3}} C_P(\omega) \right] \right\}$$

Table 3

Formulae for SV-SV scattering from a point source by a spherical fluid core. See Figure 14 for plots of a normalized amplitude of horizontal displacement, $|u_\theta/(-ikr)|$, at frequencies 0.03 and 0.2 Hz.

SV-Source Potential

$$\psi_{INC} = \frac{\exp ikR}{ikR}$$

Exact Formula

$$u_\theta = + \int_0^\infty \nu h^{(1)}_{\nu-\frac{1}{2}}(kb) \left[kh^{(1)\prime}_{\nu-\frac{1}{2}}(kr) + \underbrace{h^{(1)}_{\nu-\frac{1}{2}}(kr)}_{r} \right] \frac{\Omega_7 h^{(2)}_{\nu-\frac{1}{2}}(ka)}{\Omega_7 h^{(1)}_{\nu-\frac{1}{2}}(ka)} \frac{d}{d\Delta} Q^{(2)}_{\nu-\frac{1}{2}}(\cos\Delta)\, d\nu$$

Simple Ray Theory for the Direct Wave

$$u_\theta = (-ikr) \sin i_r \cos i_r \frac{e^{ikR}}{R} \quad \text{(lit zone)}$$

$$= 0 \quad \text{(shadow zone)}$$

Approximate formula in the Transition Region

$$u_\theta = (-ikr) \sin i_r \cos i_r \frac{e^{ikR}}{R} \left\{ \frac{1}{2} - e^{-i\pi/4} \sqrt{\frac{R}{2\pi k R_1 R_2}} \left[k(a-y) + (ka)^{\frac{i}{3}} C_{SV}(\omega) \right] \right\}$$

Table 4

Formulae for SH-SH scattering from a point source by a spherical fluid core (or cavity). See Figure 15 for plots of a normalized amplitude of horizontal displacement, $|u_\phi/r|$, at frequencies 0.03 and 0.02.

SH-Source Potential $\quad \chi_{INC} = \frac{\exp ikR}{ikR}$

Exact Formula $\quad u_\phi = -\int_0^\infty h^{(1)}_{\nu-\frac{1}{2}}(kb)\; h^{(1)}_{\nu-\frac{1}{2}}(kr) \left[\frac{kah^{(2)\prime}_{\nu-\frac{1}{2}}(ka) - h^{(2)}_{\nu-\frac{1}{2}}(ka)}{kah^{(1)\prime}_{\nu-\frac{1}{2}}(ka) - h^{(1)}_{\nu-\frac{1}{2}}(ka)} \right] \frac{d}{d\Delta}\; Q^{(2)}_{\nu-\frac{1}{2}}(\cos\Delta)\, d\nu$

Simple Ray Theory for the Direct Wave $\quad u_\phi = r \sin i_r \frac{e^{ikR}}{R}$ (lit zone)

$\quad = 0$ (shadow zone)

Approximate Formula in the Transition Region $\quad u_\phi = r \sin i_r \frac{e^{ikR}}{R} \left\{ \frac{1}{2} - e^{-i\pi/4} \sqrt{\frac{R}{2\pi k R_1 R_2}} \left[k(a-y) + (ka)^{\frac{1}{3}}\; C_{SH}(\omega) \right] \right\}$

Table 5

Values of the complex numbers δ_1 and δ_2 for different models of the core mantle boundary, given at different periods.

Model		x	y	δ_1(50 sec)	δ_2(50 sec)	δ_1(20)	δ_2(20)	δ_1(5)	δ_2(5)	δ_1(1 sec)	δ_2(1 sec)
Phinney and	(α = 13.6	-0.2	0.0	0.585	0.780	.625	.835	.705	.920	.820	1.060
Alexander	β = 7.5			1.500	2.450	1.520	2.485	1.555	2.535	1.615	2.600
(1966)	ρ = 5.5										
		0.0	0.0	0.525	0.695	.560	.745	.635	.825	.735	.950
"Model 1"	α' = 8.3										
				1.330	2.175	1.345	2.210	1.380	2.250	1.435	2.305
	ρ' = 9.5										
	a = 3480 km)										

Table 5 (continued)

Model	x	y	δ_1(50 sec) δ_2(50 sec)		δ_1(20) δ_2(20)		δ_1(5) δ_2(5)		δ_1(1 sec) δ_2(1 sec)	
Gutenberg-Bullard										
densities	-0.2	0.0	.605	.785	.655	.850	.740	.955	.860	1.110
(α = 13.6			1.510	2.450	1.530	2.490	1.570	2.545	1.635	2.615
β = 7.3	-0.2	-10.0	.615	.785	.660	.850	.745	.955	.865	1.120
ρ = 5.6			1.560	2.430	1.560	2.490	1.590	2.565	1.645	2.640
α' = 8.1										
ρ' = 10.0	0.0	0.0	.545	.710	.590	.760	.670	.855	.770	1.000
a = 3480 km)			1.340	2.175	1.360	2.210	1.395	2.261	1.455	2.330
	0.0	-10.0	.550	.705	.595	.765	.675	.865	.780	1.010
			1.420	2.180	1.400	2.225	1.420	2.285	1.465	2.355
	+0.2	0.0	.480	.620	.515	.670	.590	.755	.680	.880
			1.155	1.880	1.175	1.910	1.210	1.955	1.260	2.015
	+0.2	-10.0	.495	.610	.530	.670	.600	.765	.685	.895
			1.250	1.965	1.230	1.965	1.235	2.000	1.280	2.055

Table 5 (continued)

Model	x	y	δ_1(50 sec)	δ_2(50 sec)	δ_1(20)	δ_2(20)	δ_1(5)	δ_2(5)	δ_1(1 sec)	δ_2(1 sec)
	+0.2	-20.0					.610	.780	.690	.910
							1.190	2.090	1.250	2.120
	+0.2	-50.0							.700	.980
									1.040	2.150
	+0.4	0.0	.405	.525	.440	.565	.500	.640	.570	.750
			.960	1.565	.975	1.585	1.005	1.620	1.050	1.670

Table 5 (continued)

Model	x	y	δ_1(50 sec)	δ_2(50 sec)	δ_1(20)	δ_2(20)	δ_1(5)	δ_2(5)	δ_1(1 sec)	δ_2(1 sec)
Jeffreys-Bullen	-0.2	0.0	.615	.785	.665	.850	.755	.960	.870	1.125
densities.			1.510	2.445	1.535	2.485	1.580	2.545	1.645	2.620
(α = 13.6	0.0	0.0	.555	.705	.600	.765	.675	.865	.785	1.010
β = 7.3			1.340	2.175	1.360	2.210	1.405	2.265	1.465	2.330
ρ = 5.7	+0.2	0.0	.485	.625	.525	.675	.600	.760	.685	.890
α' = 8.1			1.160	1.880	1.180	1.910	1.215	1.955	1.270	2.020
ρ' = 9.4										
a = 3480 km)	+0.4	0.0	.410	.525	.445	.570	.505	.645	.580	.760
			.960	1.560	.975	1.585	1.010	1.625	1.060	1.680

Δ	p	$-\frac{\partial^2 T}{\partial \Delta^2}$	Time between PcP and P	Correction Factor Amplitude	Correction Factor Phase, $\delta\Phi$	$\frac{\partial T}{\partial \Delta} = p + \frac{1}{\omega}\frac{\partial}{\partial \Delta}\partial\Phi$
90°	4.650 sec/deg	154.5 sec/rad^2	0.65 sec	1.053	-0.135 rad	
						4.605 sec/deg
91	4.605	143.0	0.40	0.952	- .203	
						4.577
92	4.565	124.0	0.25	0.845	- .228	
						4.550
93	4.530	107.0	0.15	0.738	- .217	
						4.529
94	4.500	86.0	0.07	0.646	- .174	
						4.514
95	4.475	75.5	0.03	0.555	- .088	
						4.500
96	4.455	65.0	0.01	0.483	+ .021	
						4.499
97	4.440	50.0	0.0	0.425	+ .184	

Table 6: Corrections to ray theory, for 2 second P waves, in a model with specified ray parameter $p = p(\Delta)$, with the geometrical shadow boundary at 97°, and velocity gradient $\frac{d\alpha}{dr} = -0.2\,\frac{\alpha(r)}{r}$ at the bottom of the mantle.

Δ	Correction Factor, F			$\frac{\partial T}{\partial \Delta}$
	Amplitude	Phase	ℓn(Amplitude)	
97°	0.404	0.137 radians	-0.092	4.491 sec/deg
98	0.340	0.298	-0.264	4.490
99	0.286	0.454	-0.438	4.488
100	0.240	0.604	-0.613	4.487
101	0.201	0.752	-0.788	4.486
102	0.169	0.895	-0.964	4.485
103	0.142	1.035	-1.139	4.484
104	0.119	1.174	-1.313	

Table 7: Amplitudes and $\frac{\partial T}{\partial \Delta}$, for 2 second core diffracted P waves, in a model with the geometrical shadow boundary at 97°, with $\frac{\partial^2 T}{\partial \Delta^2}\Big|_{\Delta=97°} = -50$ sec/radian^2, and velocity gradient $\frac{d\alpha}{dr} = -0.2\,\frac{\alpha}{r}$ at the bottom of the mantle. Our source normalization gives an amplitude of 2.259 for the direct ray arrival at 97°, with zero phase.

Table 8

Evaluation of the velocity profile $V(r + \delta r)$. See Appendix VII.

Δ(in degrees)	I_1	I_2	r	δr	$V(r + \delta r)$	$r + \delta r$
108.5	0	0	3709.7	0	13.6	3709.7
109.5	-.007655	0.000362	3664.6	26.7	13.595	3691.3
110.5	-.01550	0.001022	3619.5	52.4	13.585	3671.9
111.5	-.02364	0.00188	3573.8	76.7	13.574	3650.5
112.5	-.03178	0.00290	3528.1	101.9	13.561	3630.0
113.5	-.04028	0.00405	3481.7	126.2	13.545	3607.9

FIGURE CAPTIONS

Figure 1a. Parameters for a plane wave, incident from the left on a cylindrical cavity.

Figure 1b,c. Parameters for a field point (r,θ) near (b) the PS boundary and (c) the SP boundary. See Appendix I.

Figure 2. Parameters for a geometrically reflected ray.

Figure 3. The complex integration path for evaluation of $C_P(\omega)$ $(z = ha)$, and $C_{SV}(\omega)$ $(z = ka)$.

Figure 4. The complex functions C_P, C_{SV} for scattering by a cylindrical cavity, plotted against frequency.

Figure 5. Comparison of solutions with different boundary conditions.

Figure 6. Shadow boundary shifts for P, SV and SH waves, scattered by a cylindrical cavity.

Figure 7. Parameters for a field point $P(r,\theta)$ near the shadow boundary, for a line or point source at $S(b,\pi)$.

Figure 8. The geometrical relation between line source and plane source shadow boundary shifts.

Figure 9. Parameters for the model experiments of Teng and Wu (1968).

Figure 10. The complex functions C_P, C_{SV} for scattering by a cylindrical fluid, plotted against frequency.

Figure 11. Location of shadow boundaries, plotted against frequency, for the three different wave types. Results are for a line source, and both cavity and fluid cylindrical scatterers.

Figure 12. The complex functions $C_P(\omega)$, $C_{SV}(\omega)$ for scattering by a spherical cavity, and for scattering by a fluid core.

Figure 13. Vertical component of P-wave displacement amplitude due to a P-wave source: comparison at two frequencies of different theories. See Table 2 for formulae.

Figure 14. Horizontal component of normalized SV-wave displacement amplitude, $\left| \frac{u_\theta}{-ikr} \right|$, due to a SV-wave source: comparison at two frequencies of different theories. See Table 3 for formulae.

Figure 15. Horizontal component of normalized SH wave displacement amplitude $\left| \frac{u_\phi}{r} \right|$, due to a SH-wave source: comparison at two frequencies of different theories. See Table 4 for formulae.

Figure 16. Parameters for a field point $P(r,\Delta)$ near the shadow boundary, for a point source at $(b,0)$ within a spherically symmetric medium.

Figure 17. Paths used for numerical integration in the complex order plane.

Figure 18a. Parameters for the Fresnel-Kirchhoff diffraction theory.

18b. Parameters in the aperture plane, near the turning point 0.

18c. p-Δ relations for the two rays $S \to P$, $Q \to P$ (for fixed Q, and P varying in Δ about the extension of $S \to Q$).

Figure 19. Parameters for a diffracted arrival.

Figure 20a. Real part of δ_1.

Figure 20b. Imaginary part of δ_1, where δ_1 parameterizes the location of the first pole ν_1 of $\Omega g^{(1)}_{\nu-\frac{1}{2}}(a)$ by $\nu_1 = h(a)a + \delta_1 (h(a)a)^{1/3}$, in the model $\alpha = 13.6$, $\beta = 7.3$, $\rho = 5.6$, $\alpha' = 8.1$, $\rho' = 10.0$, $a = 3480$. Results are plotted for four different linear velocity gradients at the bottom of the mantle:

$$x \equiv \frac{r}{\alpha}\frac{d\alpha}{dr}\bigg|_{r=a^+} = -0.2,\ 0.0,\ 0.2,\ 0.4.$$

Figure 21. P-wave potential amplitude due to a P-wave source in a homogeneous mantle, calculated at 0.1 Hz and 1.0 Hz by the Hankel function method and by the Airy function method.

Figure 22. $\frac{\partial T}{\partial \Delta}$ for P-wave potential due to a P-wave source in a homogeneous mantle, calculated at 0.1 Hz and 1.0 Hz by the Hankel function method and by the Airy function method.

Figure 23. $\frac{\partial T}{\partial \Delta}$ for the P-wave vertical displacement due to a P-wave source in a homogeneous mantle, calculated exactly at 0.1 Hz and 1.0 Hz by the Hankel function method, and calculated approximately by Fresnel, residue, and ray theories.

Figure 24. $\frac{\partial T}{\partial \Delta}$ for the SH-wave horizontal displacement due to a SH-wave source in a homogeneous mantle, calculated exactly at 0.03 Hz and 0.2 Hz by the Hankel function method, and calculated approximately by Fresnel, residue, and ray theories.

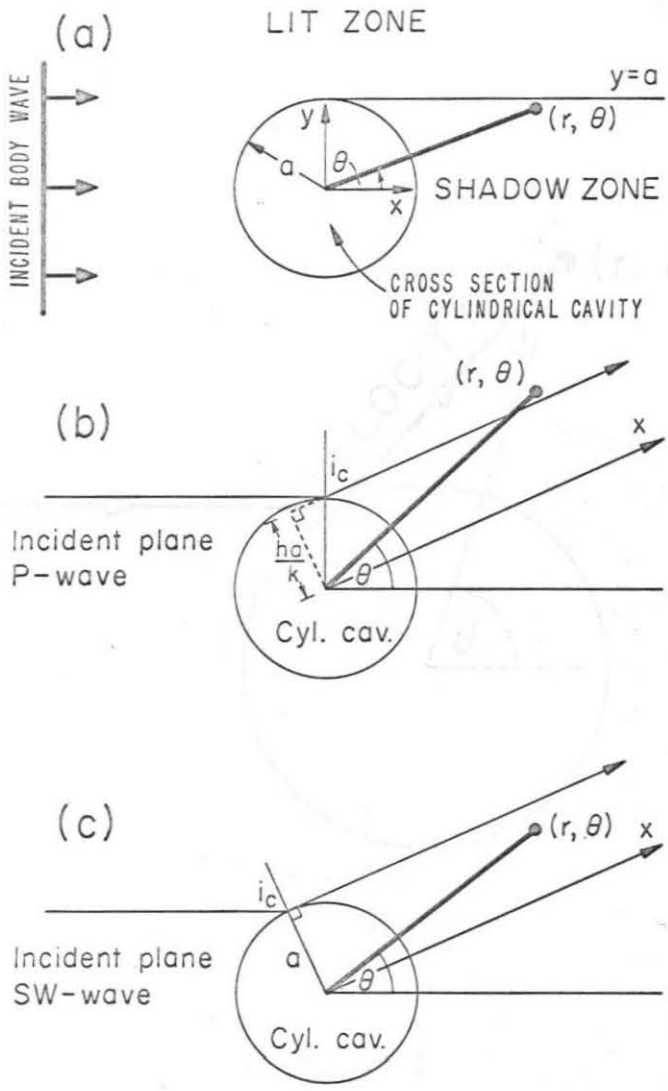
(a)
LIT ZONE
INCIDENT BODY WAVE
y=a
y
(r, θ)
a
θ
x
SHADOW ZONE
CROSS SECTION
OF CYLINDRICAL CAVITY
(b)
(r, θ)
x
i_c
Incident plane
P-wave
ka
k
θ
Cyl. cav.
(c)
(r, θ)
x
i_c
Incident plane
SW-wave
a
θ
Cyl. cav.

Figure 1

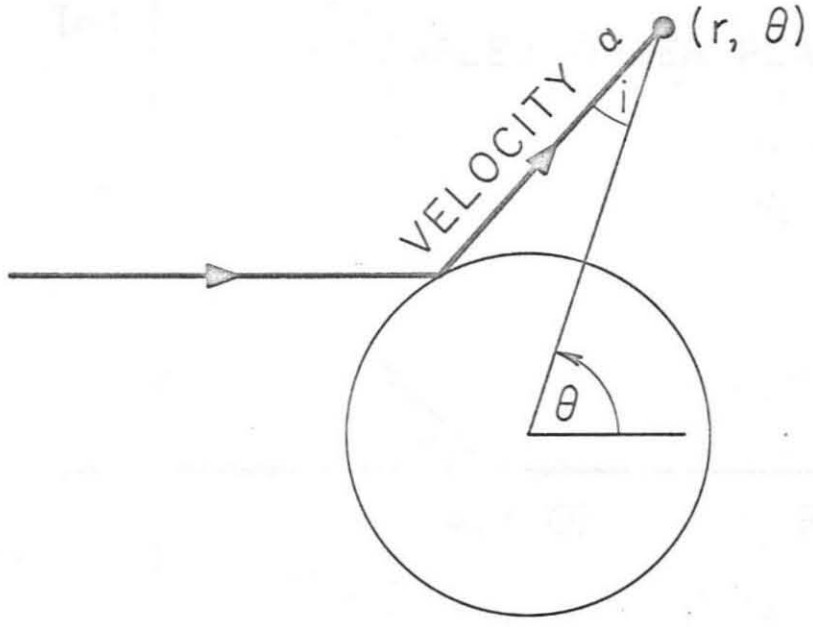

Figure 2

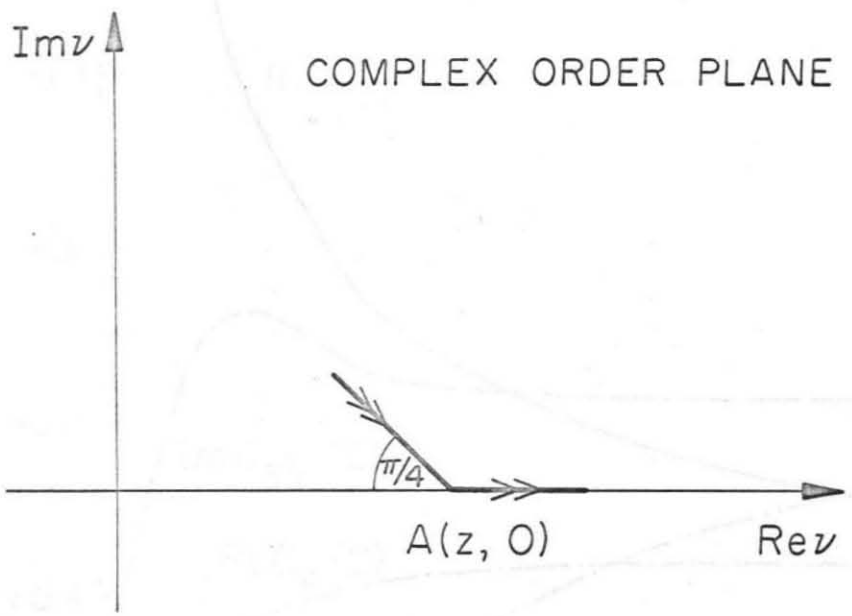

Figure 3

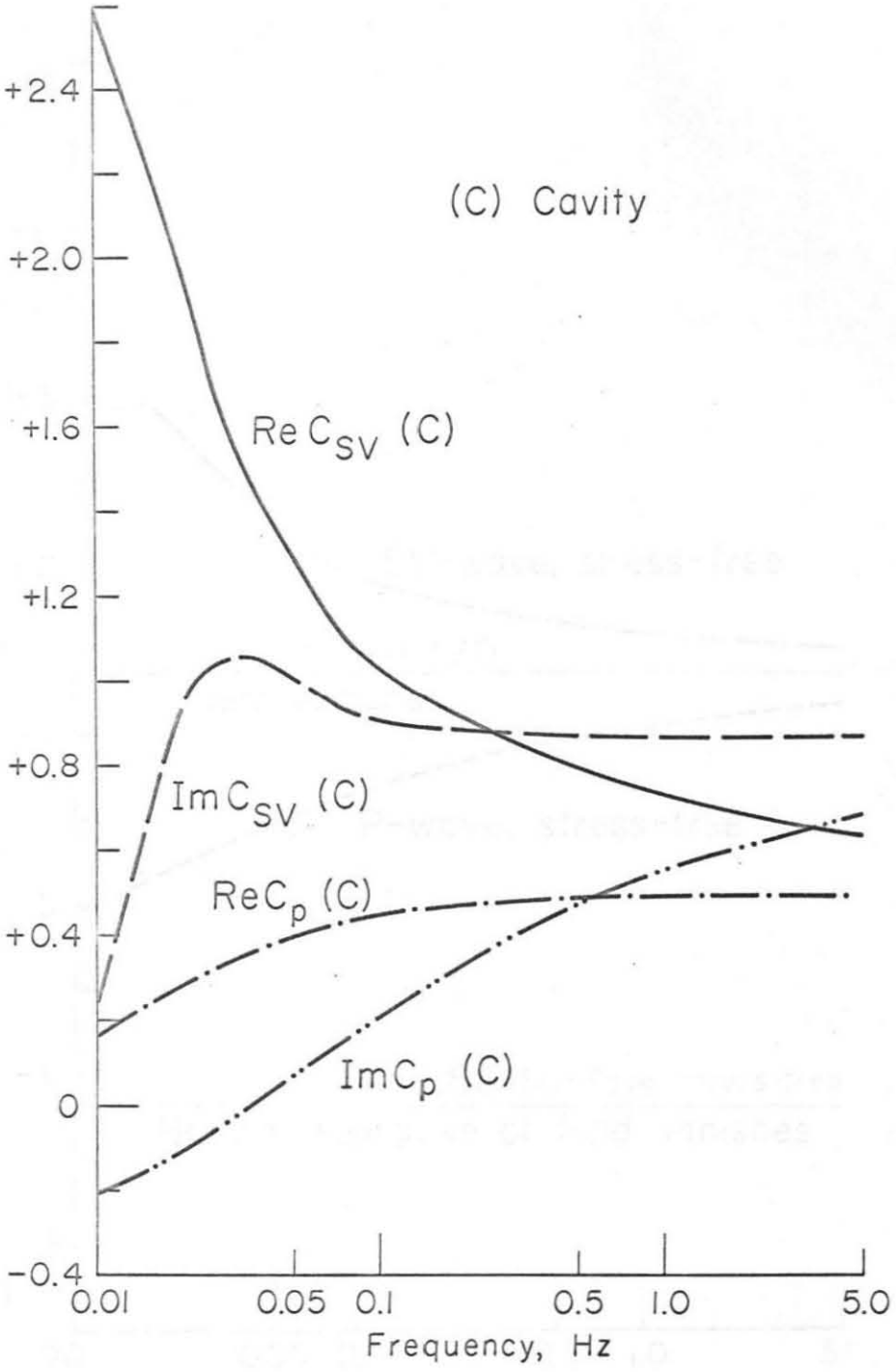
+2.4
+2.0
+1.6
+1.2
+0.8
+0.4
0
-0.4
(C) Cavity
Re C_{SV} (C)
Im C_{SV} (C)
Re C_p (C)
Im C_p (C)
0.01
0.05
0.1
0.5
1.0
5.0
Frequency, Hz

Figure 4

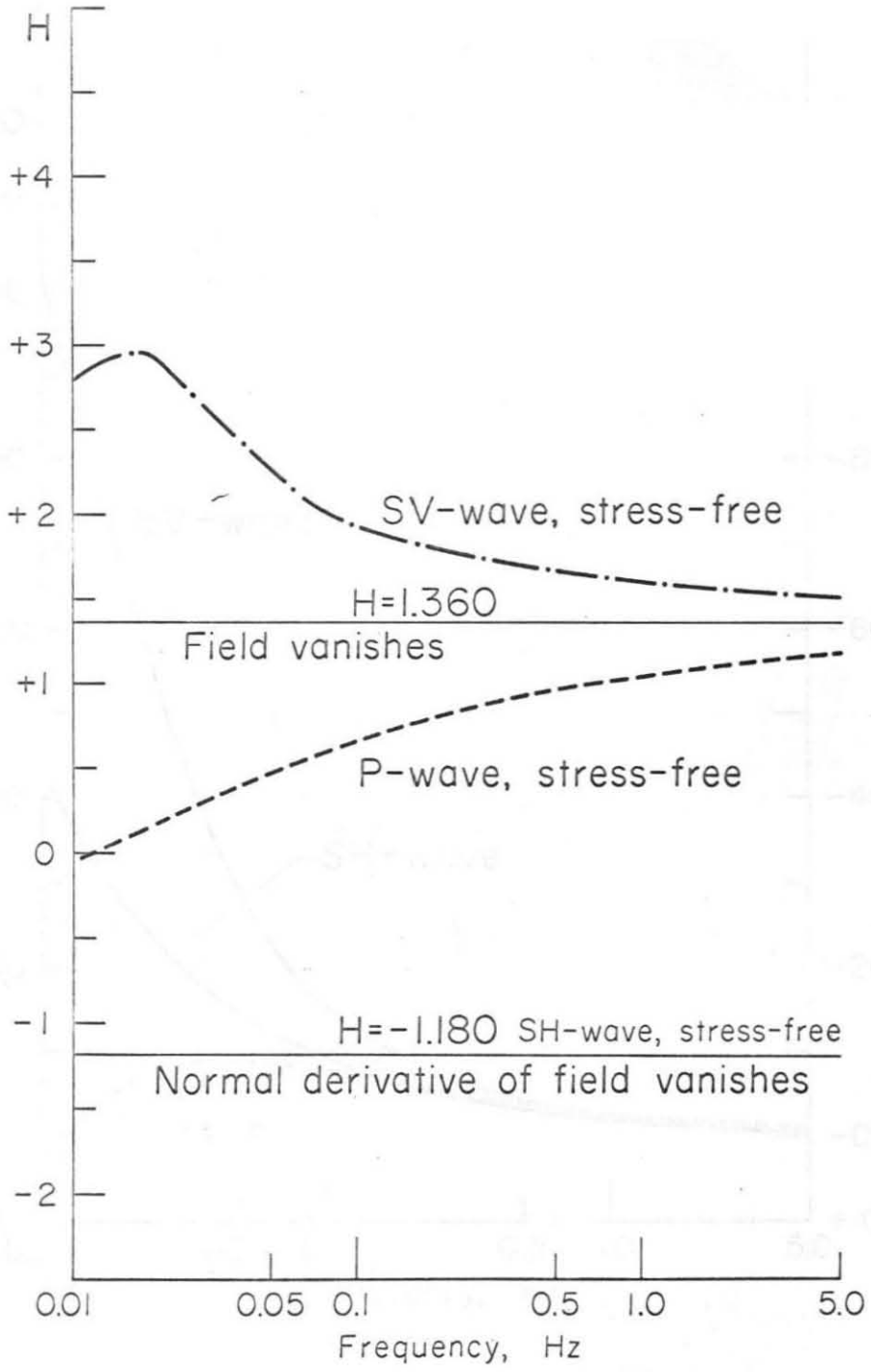
H
+4
+3
+2
+1
0
-1
-2
SV-wave, stress-free
H=1.360
Field vanishes
P-wave, stress-free
H=-1.180 SH-wave, stress-free
Normal derivative of field vanishes
0.01
0.05
0.1
0.5
1.0
5.0
Frequency, Hz

Figure 5

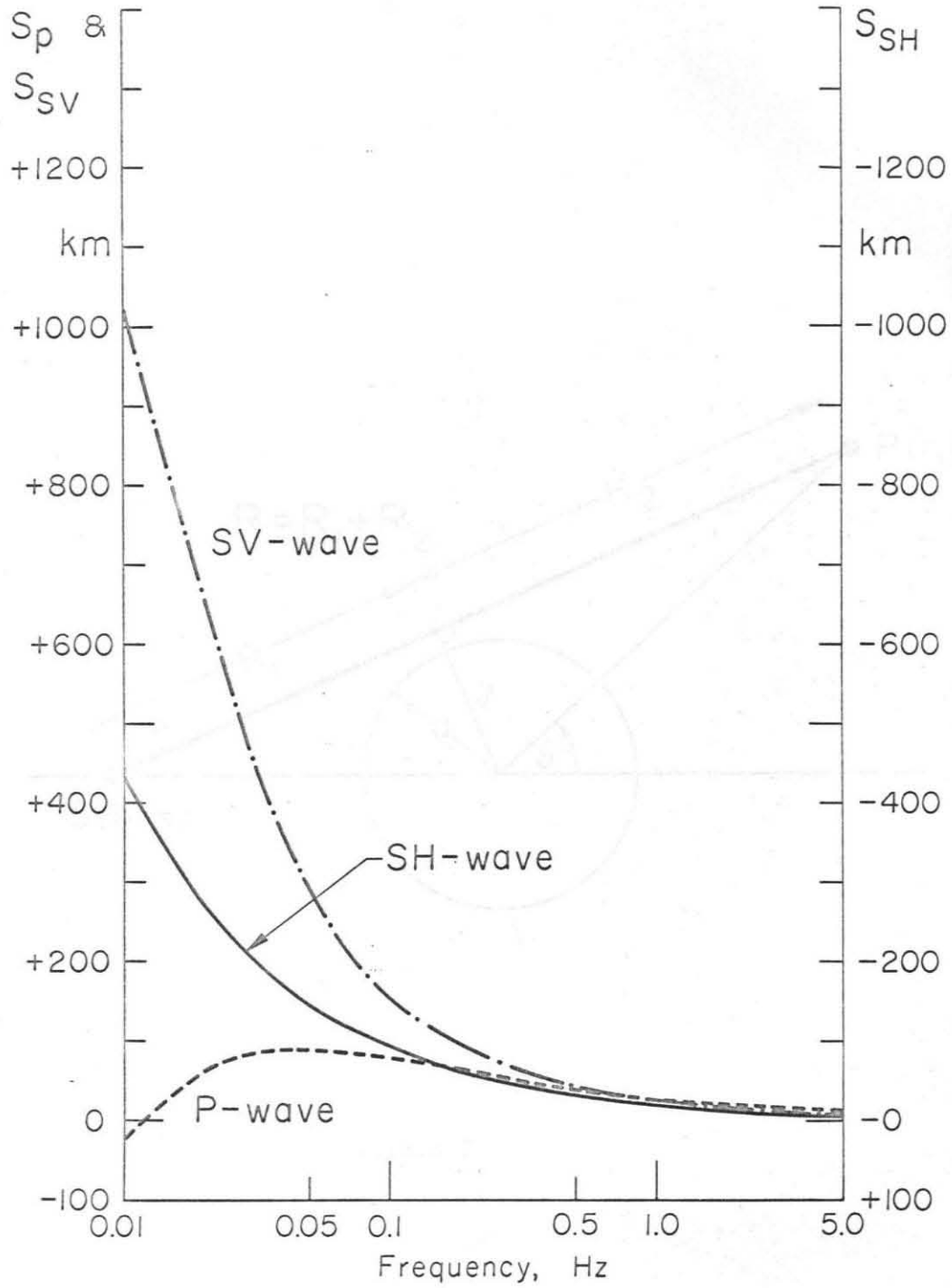
Sp &
SSV
+1200
km
+1000
+800
+600
+400
+200
0
-100
SSH
-1200
km
-1000
-800
-600
-400
-200
-0
+100
SV-wave
SH-wave
P-wave
0.01
0.05
0.1
0.5
1.0
5.0
Frequency, Hz

Figure 6

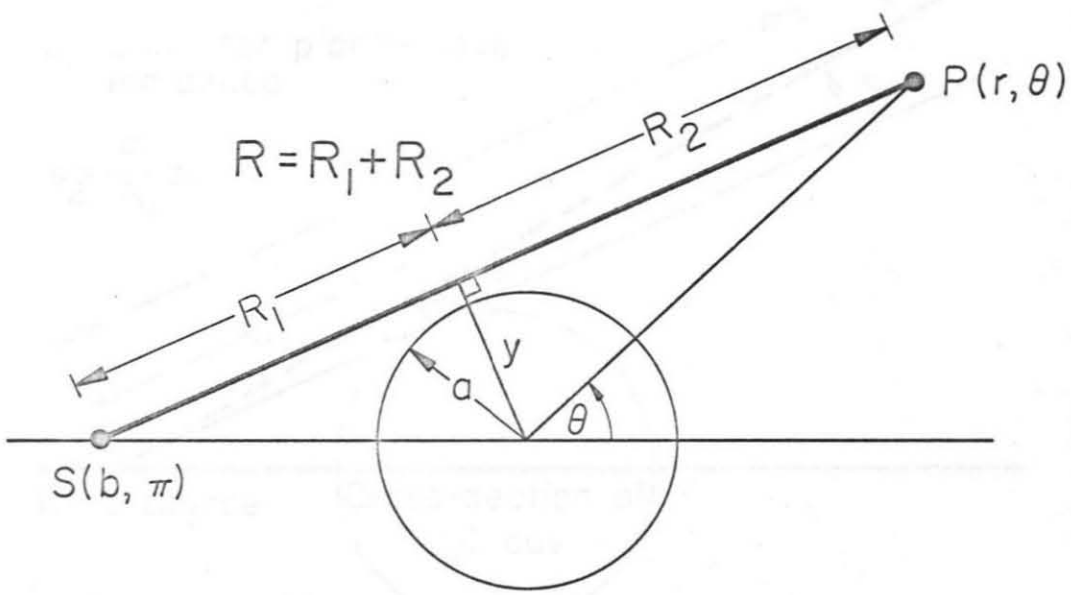

Figure 7

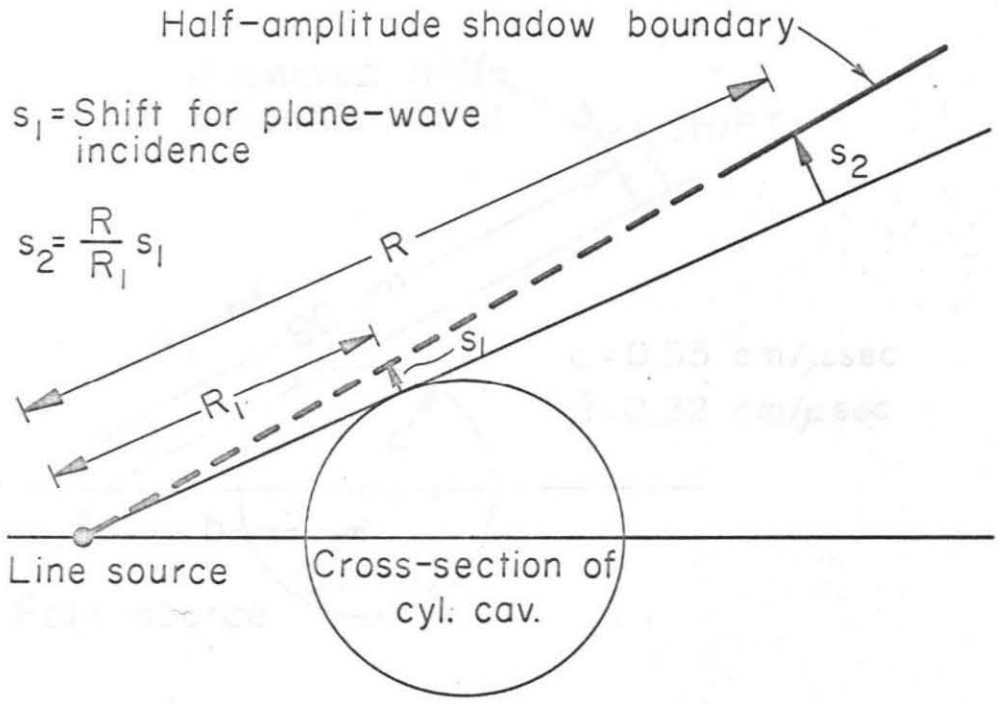
Half-amplitude shadow boundary
s_1 = Shift for plane-wave incidence
$s_2 = \frac{R}{R_1} s_1$
R
R_1
s_1
s_2
Line source
Cross-section of cyl. cav.

Figure 8

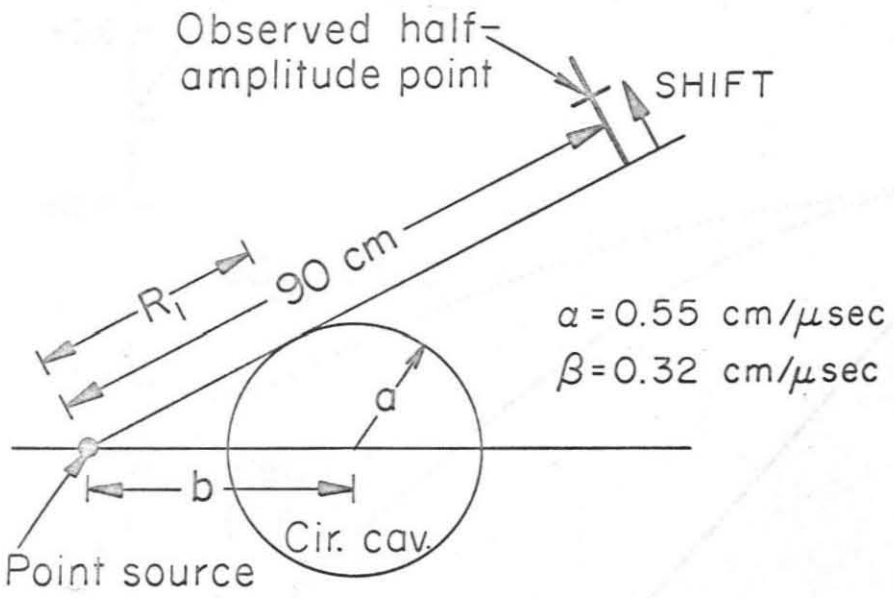
Observed half-
amplitude point
SHIFT
90 cm
R_1
$\alpha = 0.55$ cm/μsec
$\beta = 0.32$ cm/μsec
a
b
Cir. cav.
Point source

Figure 9

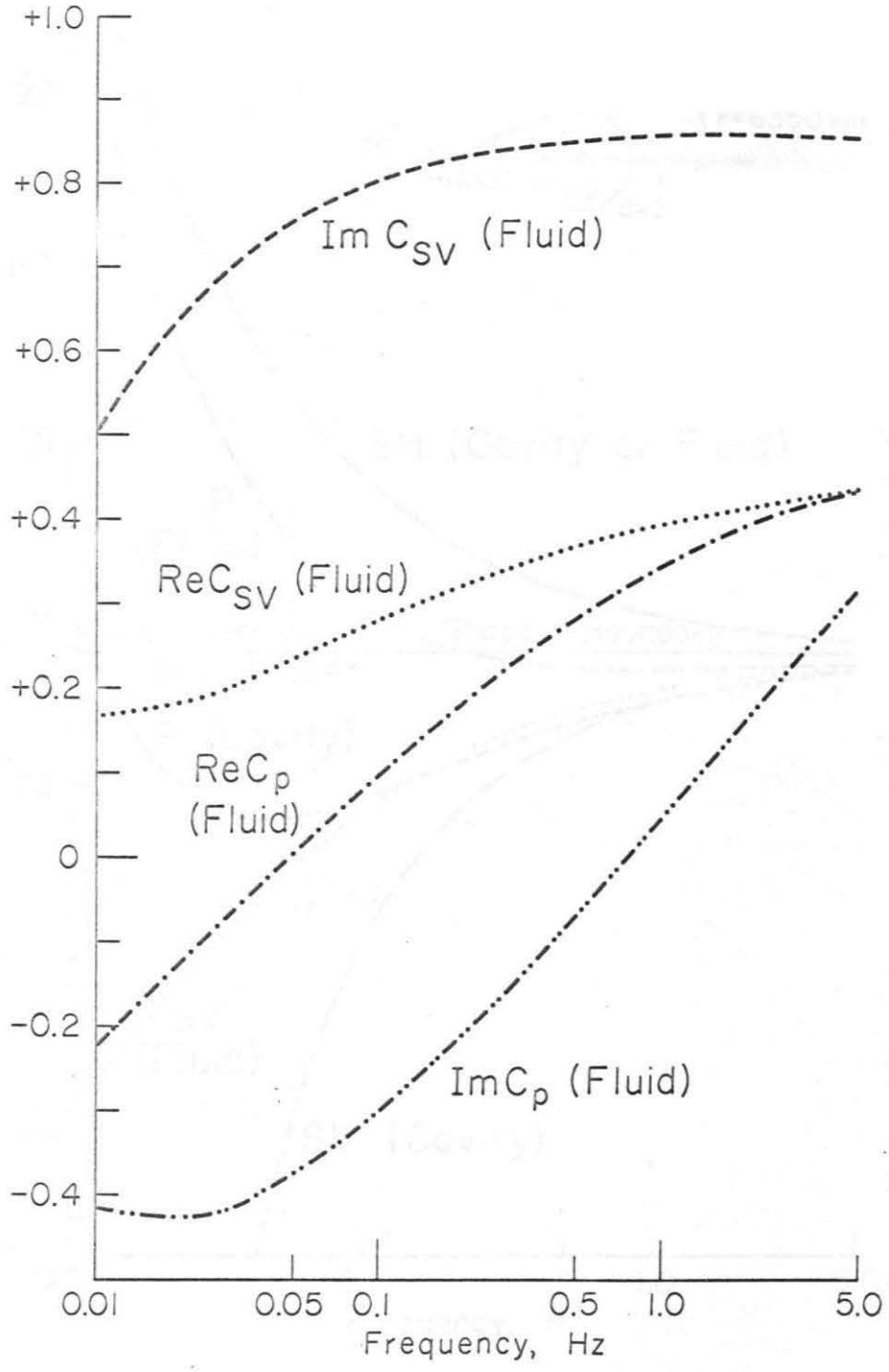
+1.0
+0.8
+0.6
+0.4
+0.2
0
-0.2
-0.4
Im C_{SV} (Fluid)
ReC_{SV} (Fluid)
ReC_p (Fluid)
ImC_p (Fluid)
0.01
0.05
0.1
0.5
1.0
5.0
Frequency, Hz

Figure 10

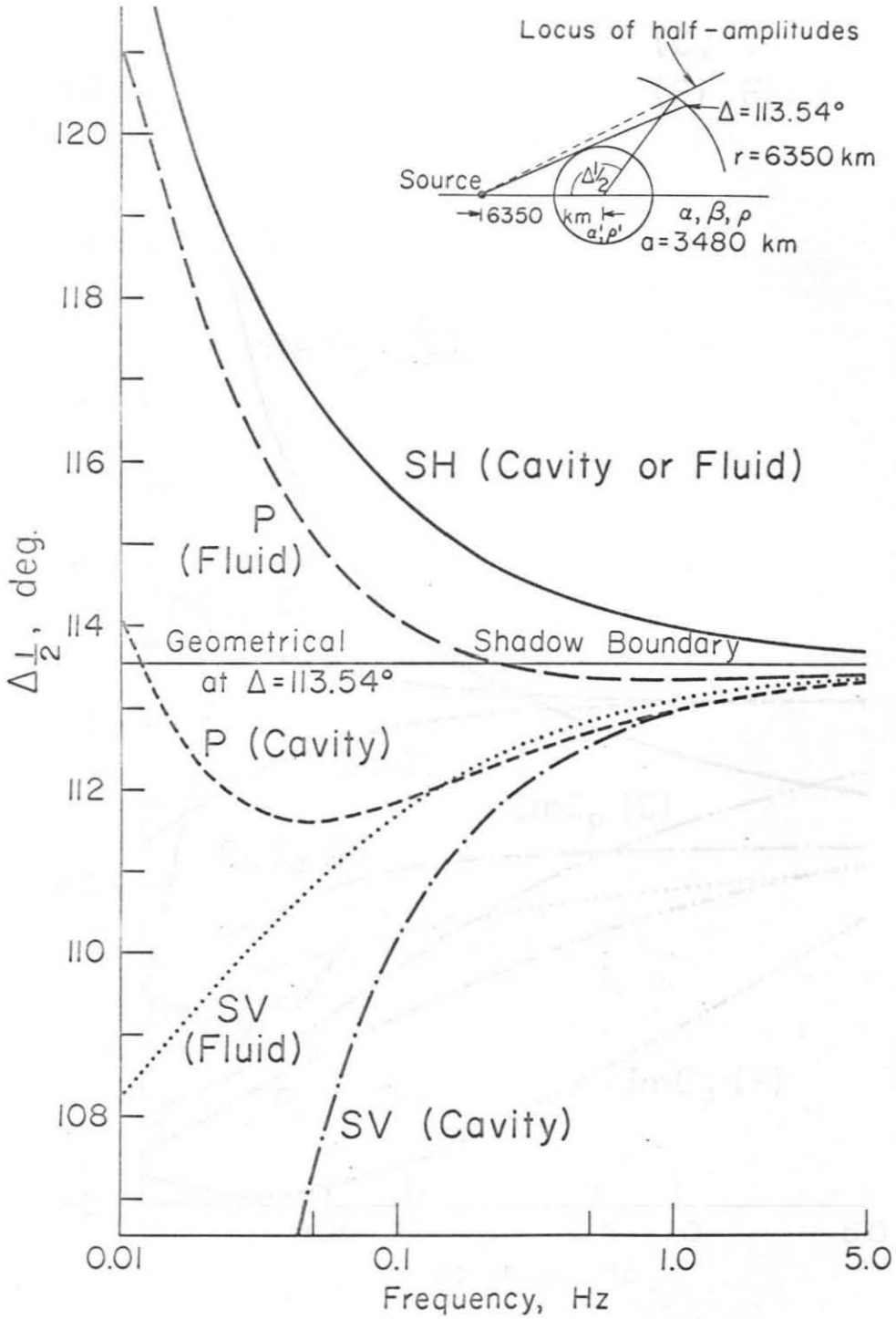
Locus of half-amplitudes
Δ=113.54°
r=6350 km
Source
Δ½
6350 km
α, β, ρ
a=3480 km
120
118
116
114
112
110
108
SH (Cavity or Fluid)
P
(Fluid)
Geometrical
Shadow Boundary
at Δ=113.54°
P (Cavity)
SV
(Fluid)
SV (Cavity)
Δ½, deg.
0.01
0.1
1.0
5.0
Frequency, Hz

Figure 11

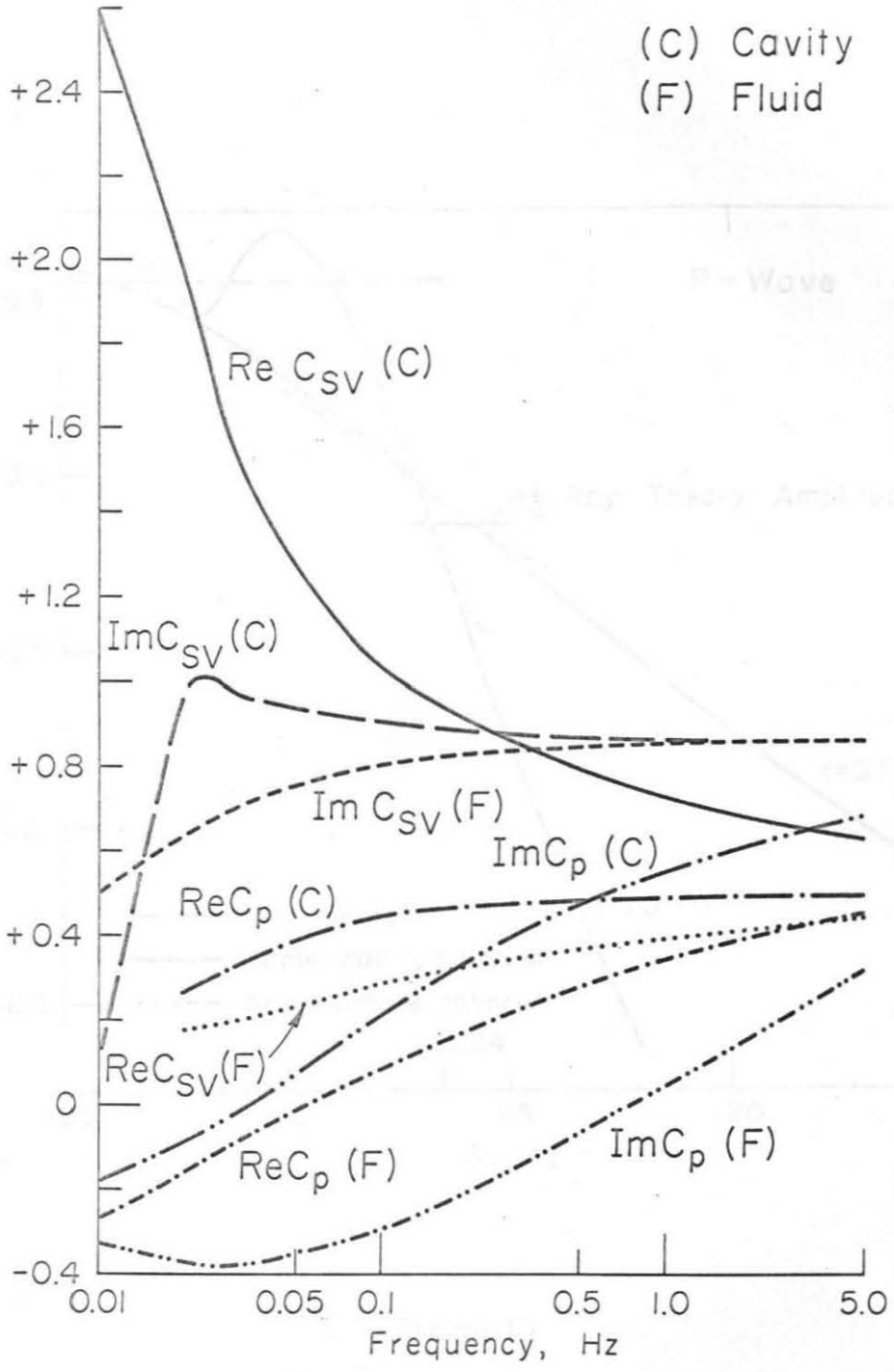
(C) Cavity
(F) Fluid
+2.4
+2.0
+1.6
+1.2
+0.8
+0.4
0
-0.4
Re C_{SV} (C)
Im C_{SV} (C)
Im C_{SV} (F)
Im C_p (C)
Re C_p (C)
Re C_{SV} (F)
Re C_p (F)
Im C_p (F)
0.01
0.05
0.1
0.5
1.0
5.0
Frequency, Hz

Figure 12

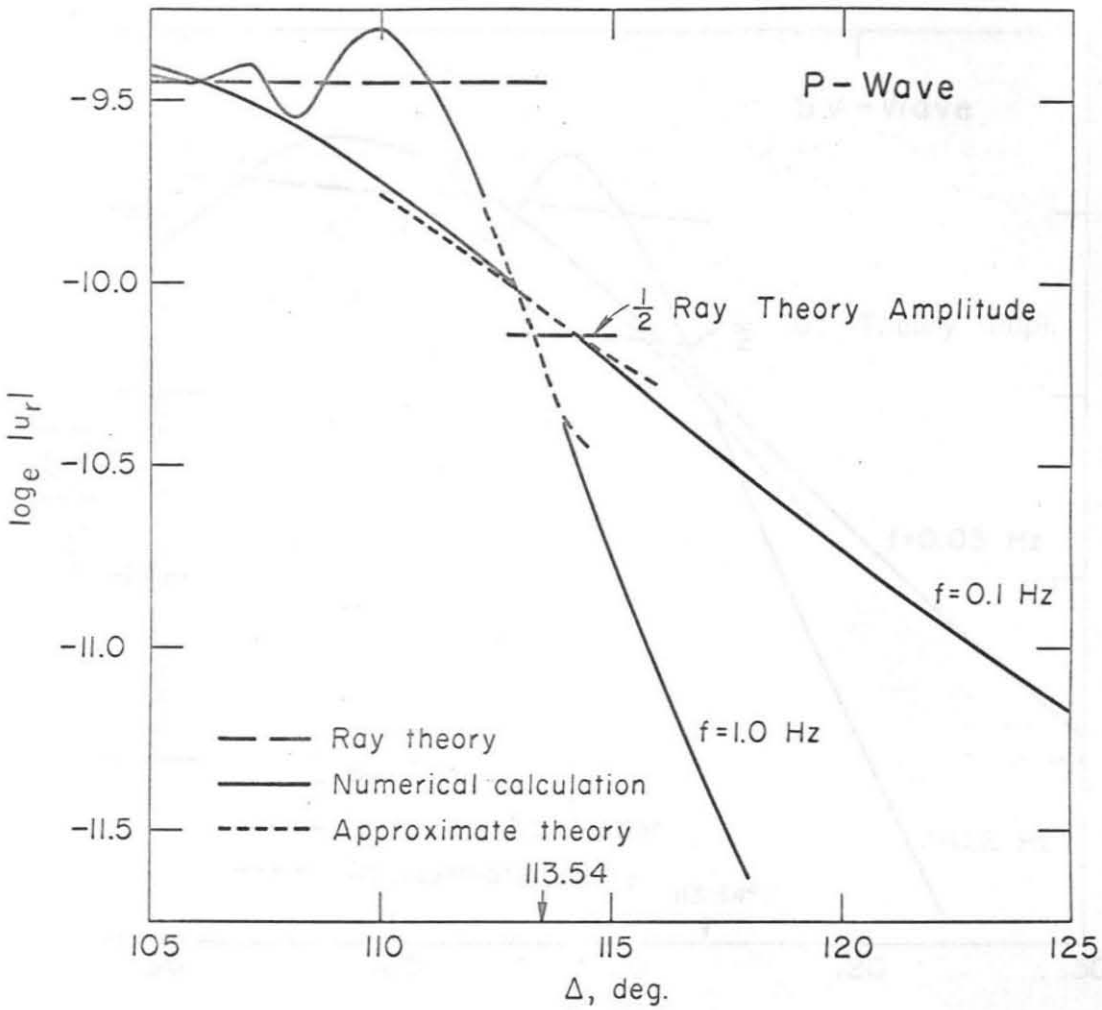
P-Wave
-9.5
-10.0
-10.5
-11.0
-11.5
$\log_e |u_r|$
$\frac{1}{2}$ Ray Theory Amplitude
f=0.1 Hz
f=1.0 Hz
Ray theory
Numerical calculation
Approximate theory
113.54
105
110
115
120
125
Δ, deg.

Figure 13

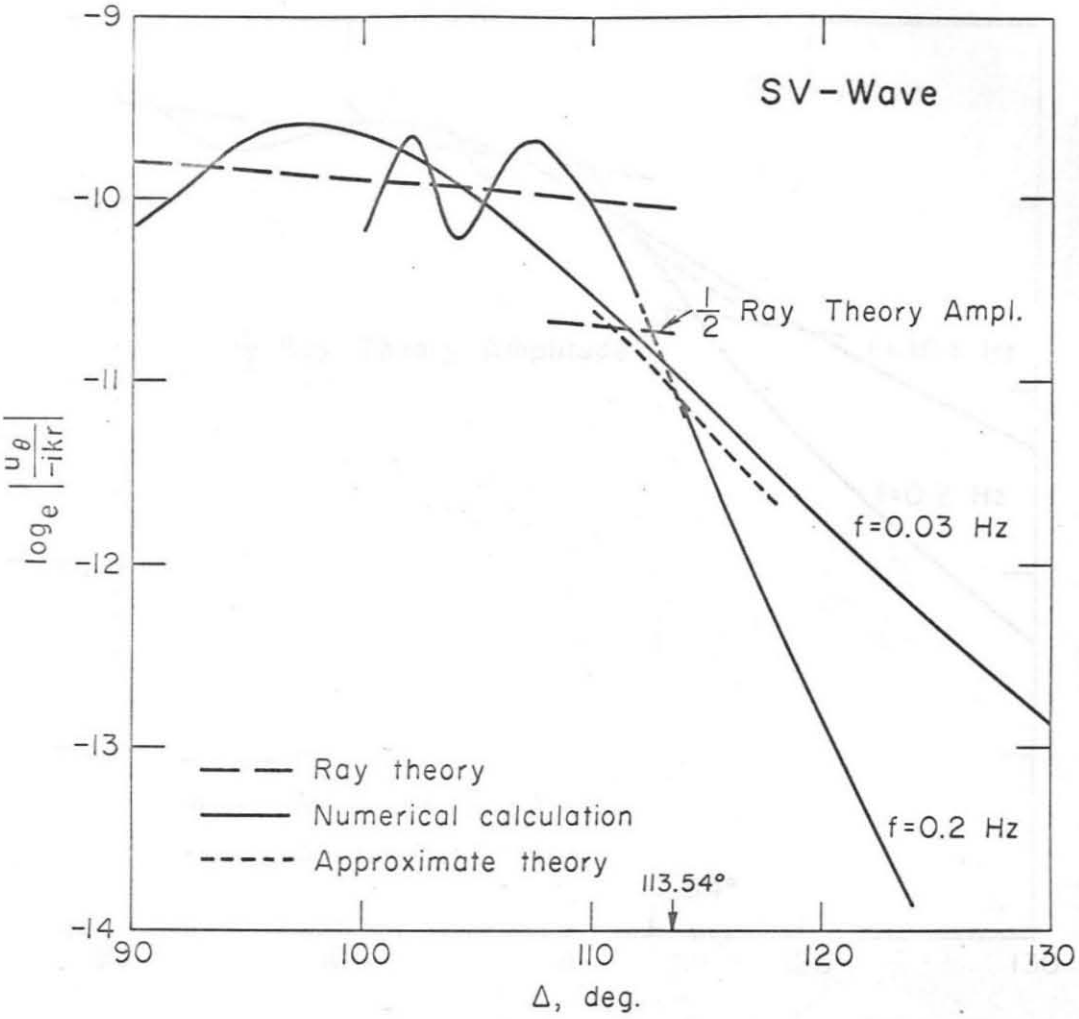
SV-Wave
1/2 Ray Theory Ampl.
f=0.03 Hz
f=0.2 Hz
Ray theory
Numerical calculation
Approximate theory
113.54°
-9
-10
-11
-12
-13
-14
90
100
110
120
130
Δ, deg.
log_e |u_θ / -ikr|

Figure 14

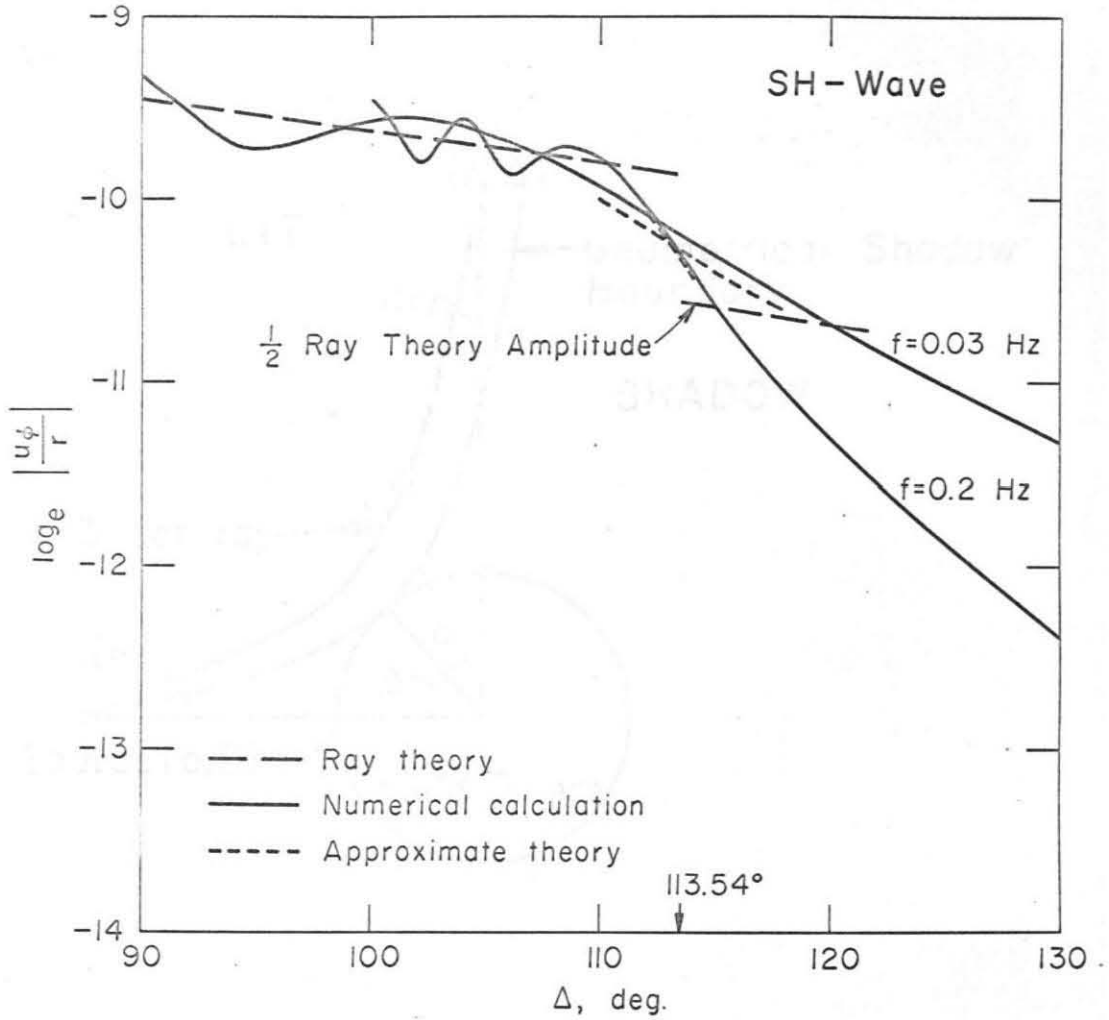
SH - Wave
½ Ray Theory Amplitude
f=0.03 Hz
f=0.2 Hz
Ray theory
Numerical calculation
Approximate theory
113.54°
log_e |u_φ / r|
Δ, deg.
-9
-10
-11
-12
-13
-14
90
100
110
120
130

Figure 15

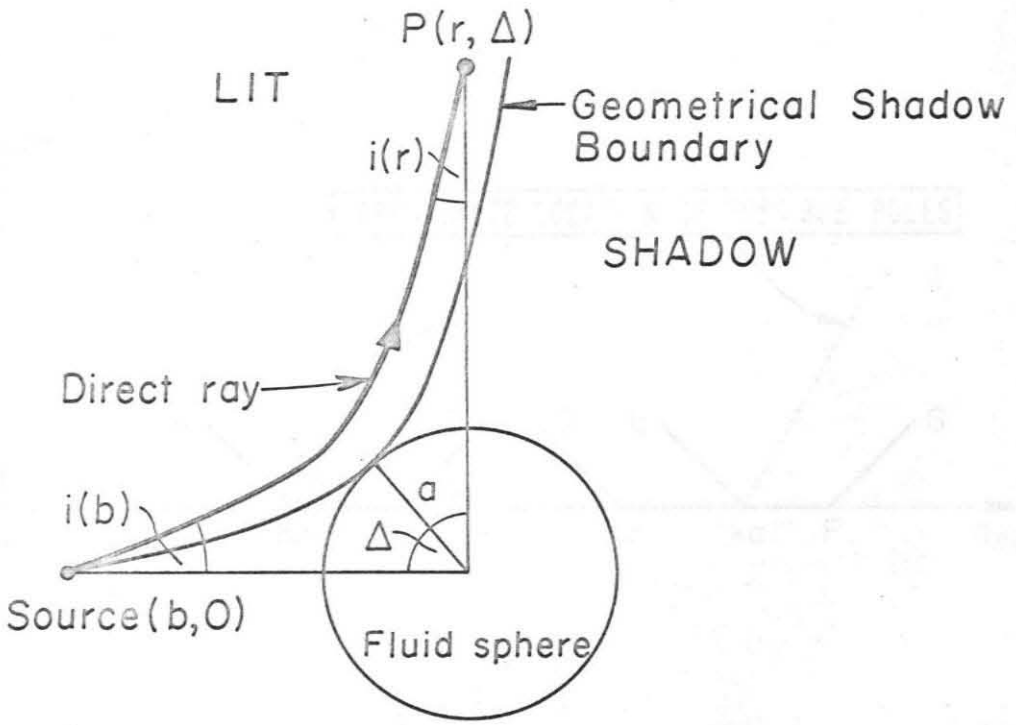
P(r, Δ)
LIT
Geometrical Shadow Boundary
i(r)
SHADOW
Direct ray
i(b)
a
Δ
Source(b,0)
Fluid sphere

Figure 16

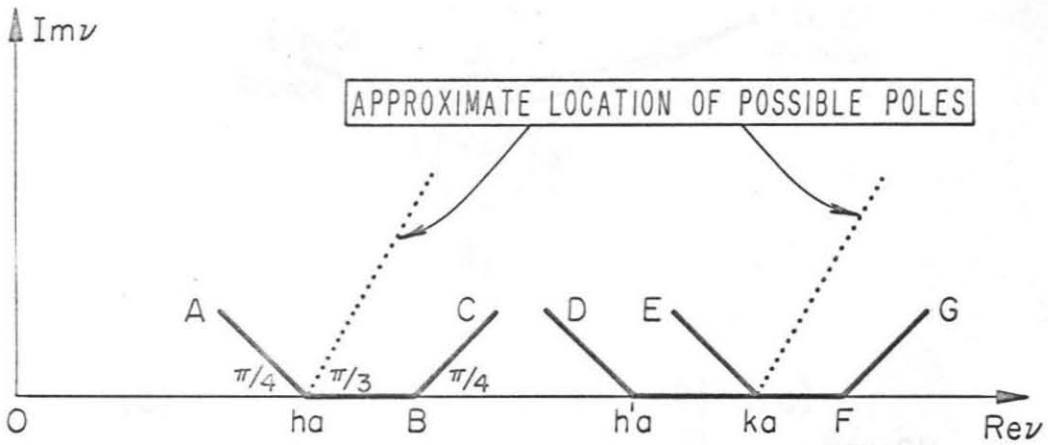
Im ν
APPROXIMATE LOCATION OF POSSIBLE POLES
A
C
D
E
G
π/4
π/3
π/4
O
ha
B
h'a
ka
F
Re ν

Figure 17

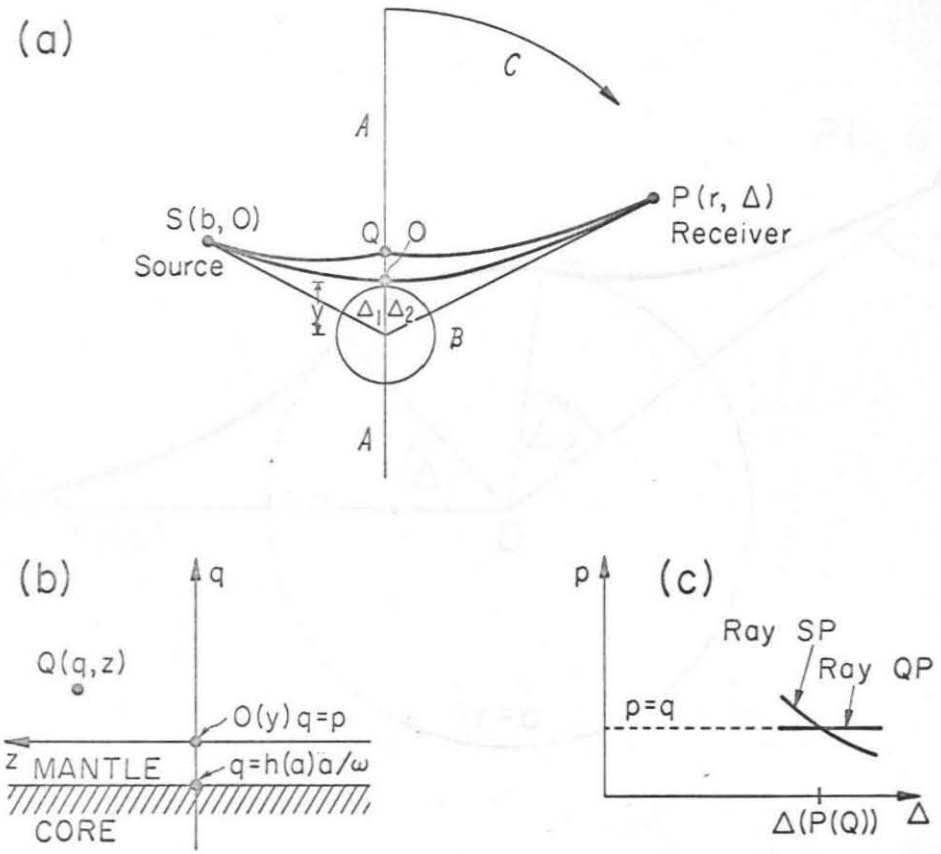
(a)
C
A
P(r, Δ)
Receiver
S(b, O)
Source
Q
O
Δ1
Δ2
B
A
(b)
q
Q(q,z)
O(y) q=p
z
MANTLE
q=h(a)a/ω
CORE
p
(c)
Ray SP
Ray QP
p=q
Δ(P(Q))
Δ

Figure 18

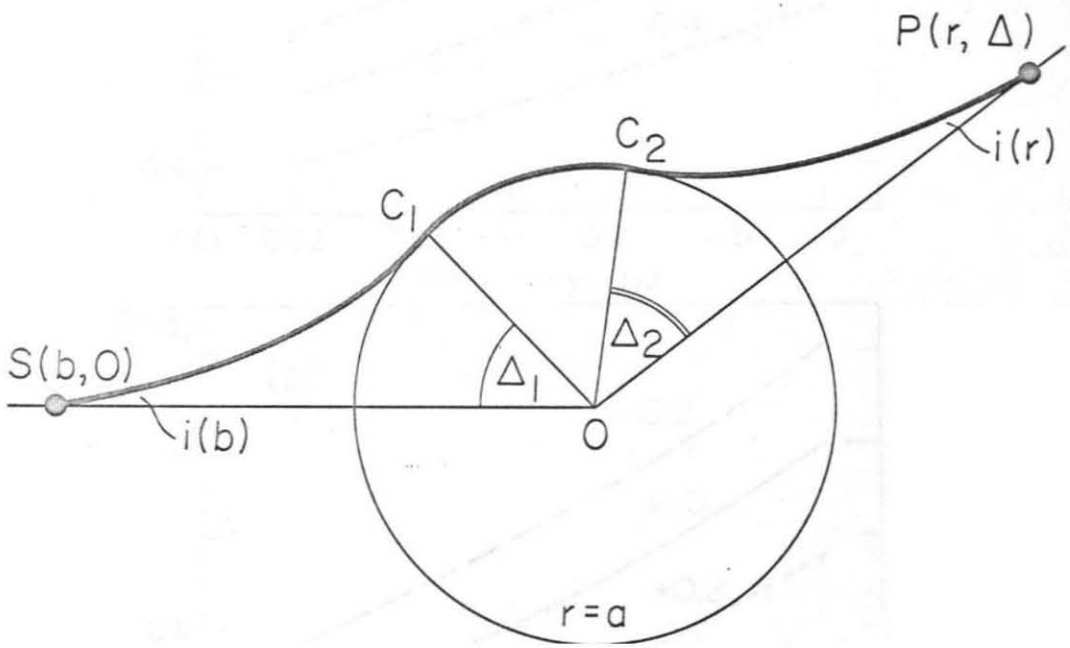

Figure 19

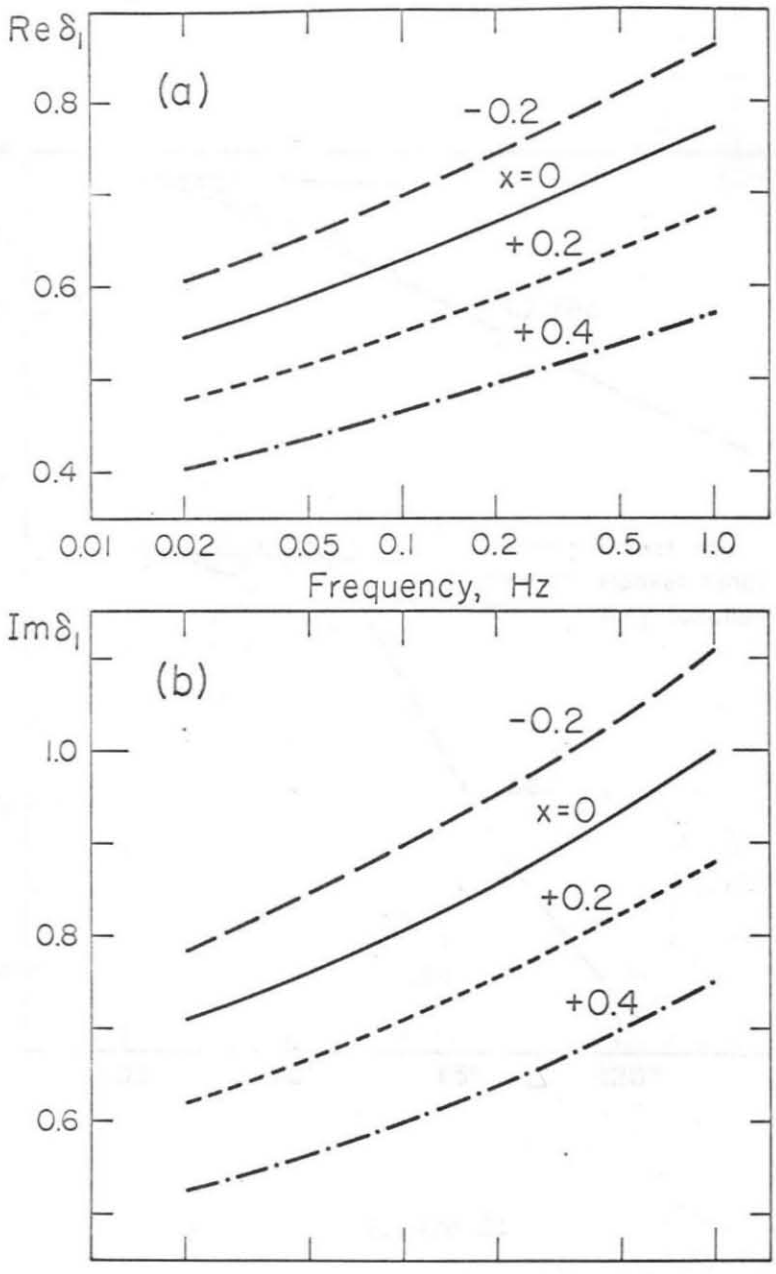
Re δ_1
(a)
0.8
0.6
0.4
-0.2
x=0
+0.2
+0.4
0.01
0.02
0.05
0.1
0.2
0.5
1.0
Frequency, Hz
Im δ_1
(b)
1.0
0.8
0.6
-0.2
x=0
+0.2
+0.4

Figure 20

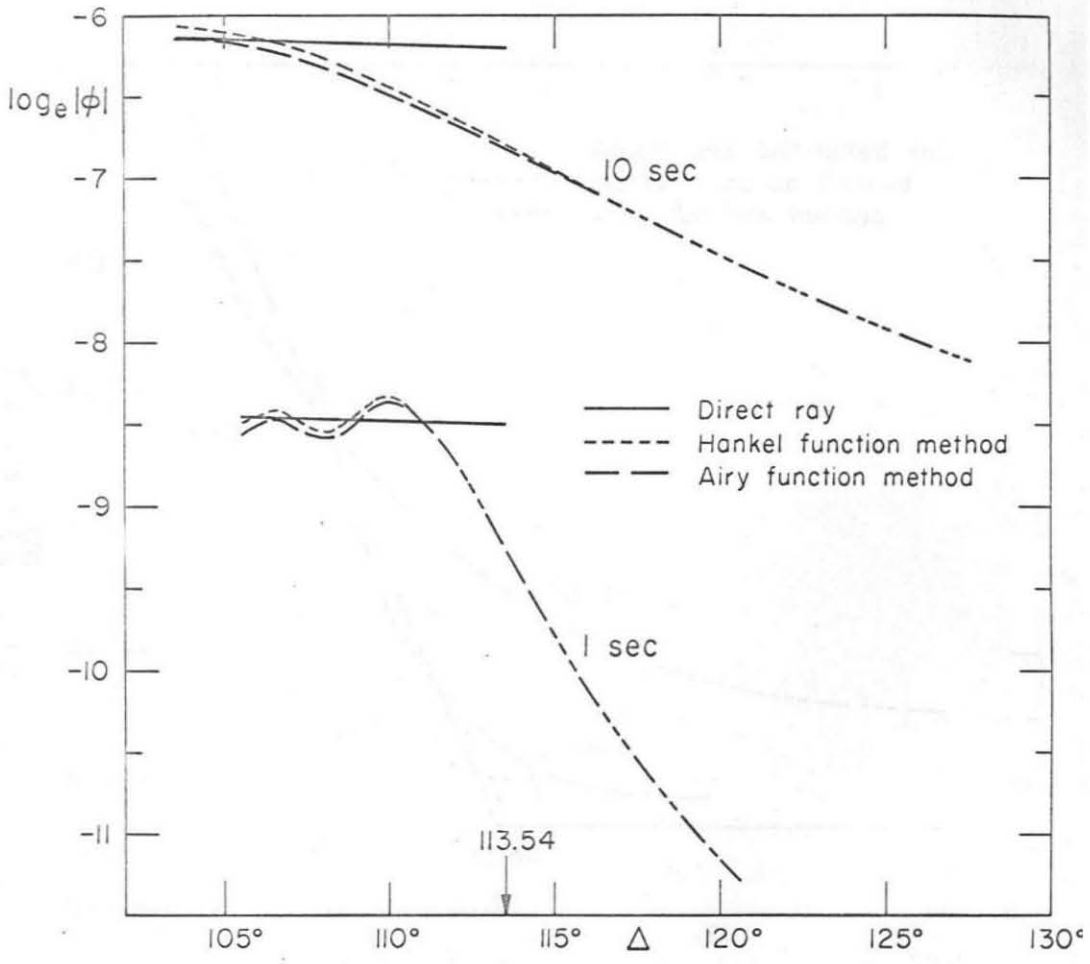
-6
$\log_e|\phi|$
-7
-8
-9
-10
-11
10 sec
1 sec
Direct ray
Hankel function method
Airy function method
113.54
105°
110°
115°
Δ
120°
125°
130°

Figure 21

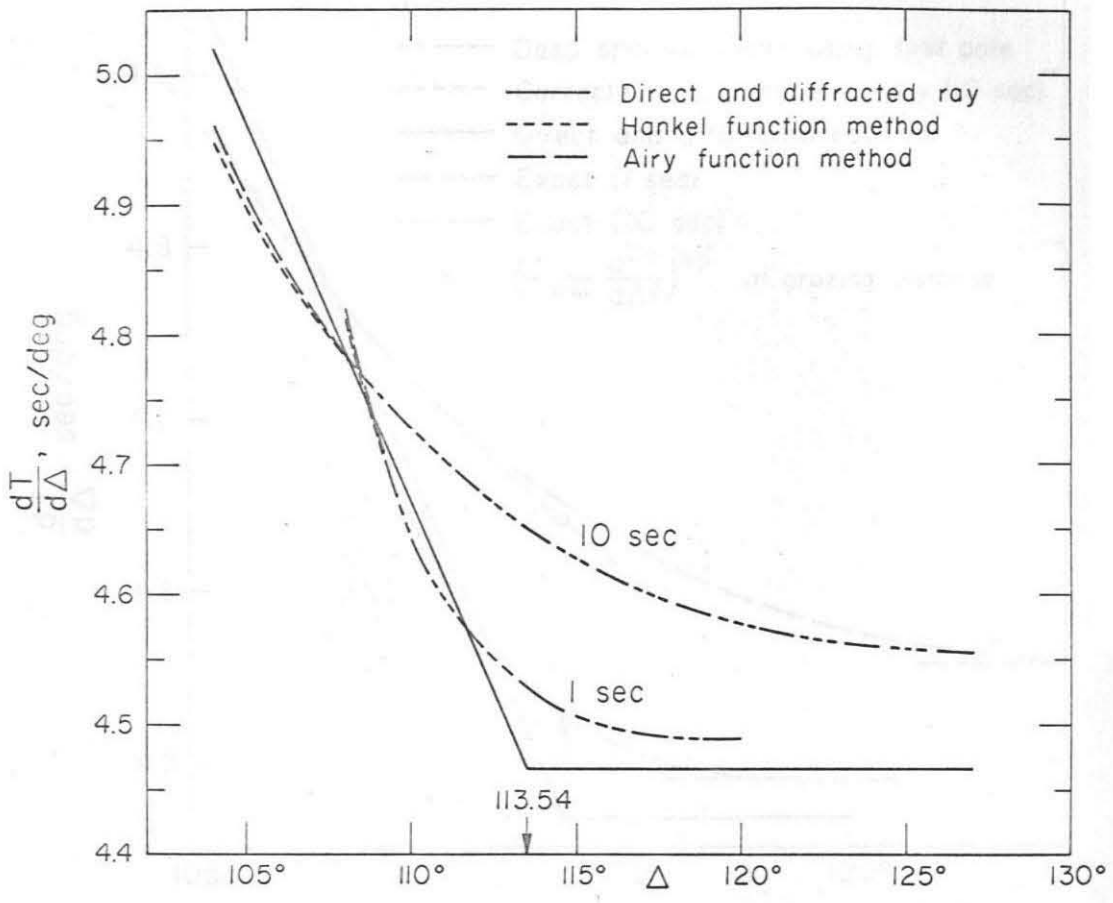
Direct and diffracted ray
Hankel function method
Airy function method
10 sec
1 sec
113.54
5.0
4.9
4.8
4.7
4.6
4.5
4.4
105°
110°
115°
120°
125°
130°
Δ
dT/dΔ, sec/deg

Figure 22

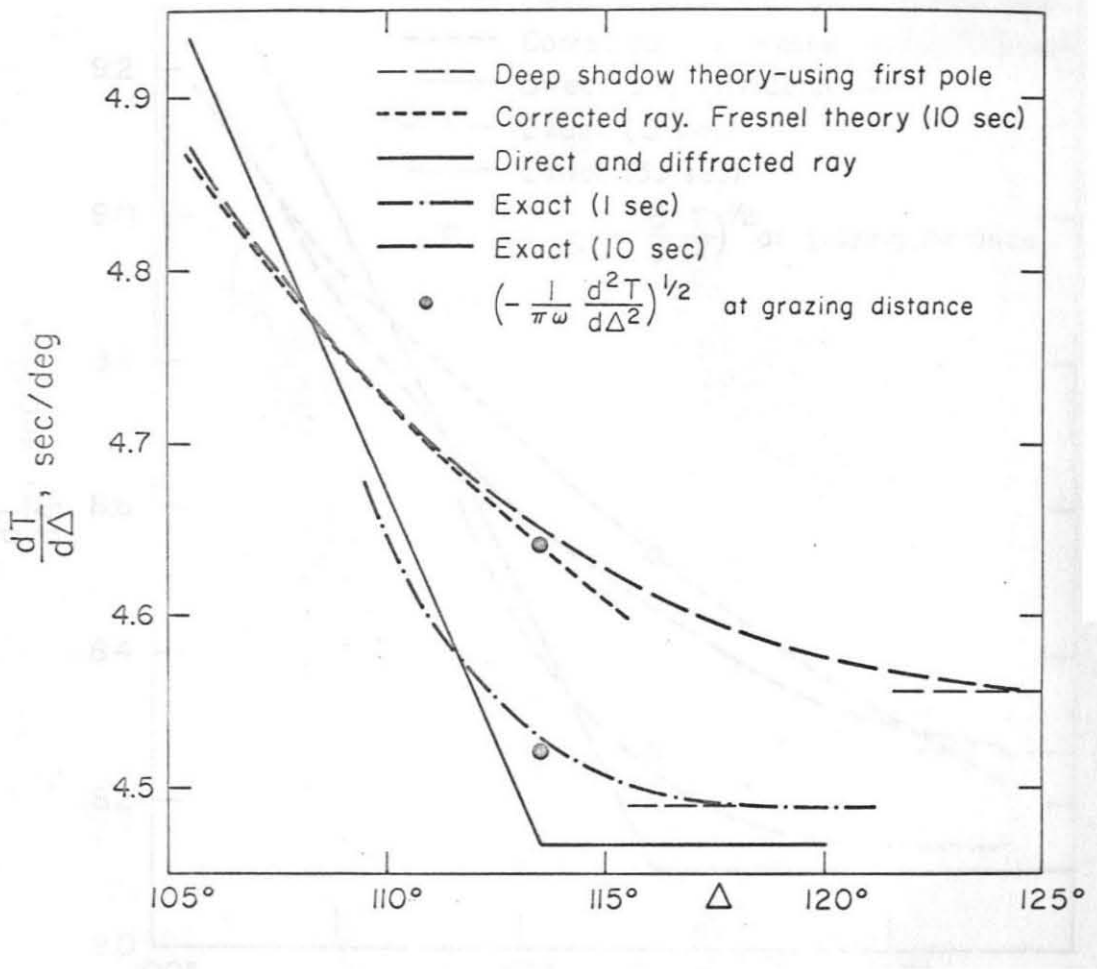
Deep shadow theory-using first pole
Corrected ray. Fresnel theory (10 sec)
Direct and diffracted ray
Exact (1 sec)
Exact (10 sec)
$\left(-\frac{1}{\pi\omega}\frac{d^2T}{d\Delta^2}\right)^{1/2}$ at grazing distance
$\frac{dT}{d\Delta}$, sec/deg
4.9
4.8
4.7
4.6
4.5
105°
110°
115°
Δ
120°
125°

Figure 23

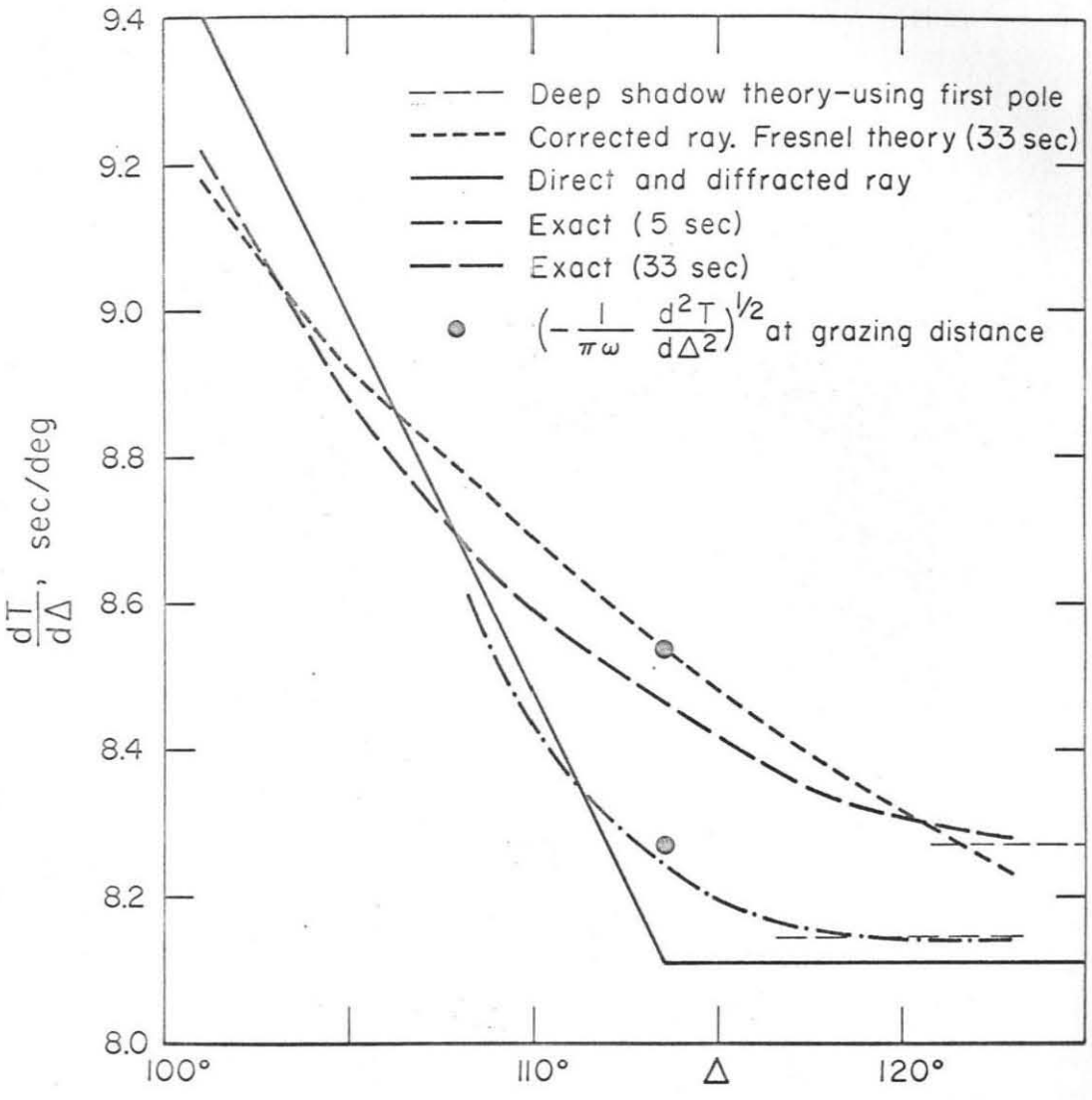
9.4
9.2
9.0
8.8
8.6
8.4
8.2
8.0
100°
110°
Δ
120°
dT/dΔ, sec/deg
Deep shadow theory–using first pole
Corrected ray. Fresnel theory (33 sec)
Direct and diffracted ray
Exact (5 sec)
Exact (33 sec)
$\left(-\frac{1}{\pi\omega}\frac{d^2T}{d\Delta^2}\right)^{1/2}$ at grazing distance

Figure 24